Development of Antiparasitic Agents from Natural Peptides and Peptidomimetics

YAZMIN SANTOS

Development of Antiparasitic Agents from Natural Peptides and Peptidomimetics

A Thesis Presented for the Degree of Doctor of Philosophy
The Department of Chemistry
Durham University, Ustinov College

Yazmin Santos

Supervised by Prof Steven Cobb and Prof. Paul Denny

2023

Author's Declaration

I declare that this thesis is a presentation of original work, and it is the work of the author unless otherwise stated. This work was conducted in the Department of Chemistry and Biosciences at Durham University and collaborative work was mentioned where applicable. The work has not been submitted for a degree in this or other university.

Abstract

Neglected Tropical Diseases (NTDs) affect hundreds of millions of people worldwide, resulting in significant mortality rates and devastating social and economic consequences. Current treatments for parasitic NTDs are far from ideal. Natural products have been, and continue to be, invaluable sources of inspiration in drug design and development, and they offer considerable potential in the field of NTDs.

A family of cyclic peptides, Chaiyaphumines, were isolated from *Xenorhabdus* bacteria, and they were found to show promising activity against *Trypanosoma brucei rhodesiense, Trypanosoma cruzi*, and *Plasmodium falciparum*, as well as low toxicity for mammalian L6 cells. In this work a versatile and efficient total synthesis of two natural Chaiyaphumines, and a series of amide analogues was developed. The improved synthetic process was also used to carry out an alanine scan on one of the most promising amide analogues.

Antimicrobial peptides (AMPs) have been studied previously as potential scaffolds for the development of new anti-leishmanials. Herein, the solid phase synthesis of two small libraries of AMPs (derived from the Temporin and Histatin families) has been carried out. The AMPs prepared were tested against *L. major* and *L. amazonensis* promastigotes, *L. mexicana*, promastigotes and axenic amastigotes. This was the first time a Histatin library of AMPs has been tested against three different types of leishmania parasites. Although the peptides prepared were found to have low biological activity, the information gathered adds to our understanding of the potential that AMPs could have in the development of new treatments for NTDs.

Finally, this thesis investigated the potential application of simple lipo-peptoids as a new source of NTD agents. Peptoids are a class of peptide-mimetics that given their easy of synthesis and enhanced proteolytic stability perhaps offer a better opportunity for the development of new anti-leishmanial therapeutics compared to peptides. A library of linear peptoids and lipo-peptoids was synthesised using a Ugi-4CR in a one-pot reaction. The

peptoid library prepared was then screened against both the promastigote and amastigote stages of the *Leishmania mexicana* parasite. From this library, seven peptoids showed antileishmanial activity against the axenic form of the parasite, with EC_{50}'s of less than 25 nM.

Acknowledgments

Firstly, I would like to thank my academic supervisor Professor Steven Cobb for all his advice and encouragement throughout my studies at Durham University. His investment of time and resources has been greatly appreciated and his insight into peptide chemistry invaluable. His kindness was appreciated not only in academia, but also personally during special circumstances such COVID-19 pandemic. I would also like to thank my co-supervisor, Professor Paul Denny, for providing advice and his expertise in the parasite biology.

Secondly, I would also like to extend my thanks to the rest of the members of the Cobb group. A special mention goes to Dr. Diana Gimenez-Ibanez who kindly took the time to train me on solid-phase peptide synthesis and many other skills, for which I am forever grateful. Also, to Hirunika Perera who trained me and taught me how to perform biological assays. Members of the O'Donogue group for their kindness and for being such good lab mates. I would also like to thank Juan Aguilar from NMR services for his support, Aileen Congreve from analytical services along with the departmental staff running the mass spectrometry – without them none of this would have been possible.

Finally, I also wish to show my appreciation towards my international family and friends, who have offered support and encouragement when I needed it the most. Especially to my parents and sister, who in their own way, made the effort to understand what chemistry means. I would like to express heartfelt gratitude to my Ustinov friends. Last, but not least, to my rock and now fiancé -who made Durham and any place in the world really- my home. Gracias.

Memorandum

The work within this thesis has been presented by the author at the following meetings:

Oral presentation at 7th International symposium-cum-training course on Molecular Medicine and Drug Research (MMDR-7), 4th - 7th November 2019, University of Karachi, Karachi, Pakistan.

Poster presentation at International Workshop (International Center for Chemical and Biological Sciences), 8th - 9th November 2019, University of Karachi, Karachi, Pakistan.

Poster presentation at the NTD network- Early career researcher Conference, 10th March 2022, Durham University

Poster presentation at 12th International peptide symposium (IPS) and 36th European Peptide Symposium (EPS), 28th August - 2nd September 2022, Barcelona, Spain.

Abbreviations

Anh	anhydride
AMP	Antimicrobial peptide
ATCUN	Amino-terminal Cu (II) and Ni (II)
Boc	*tert*-butoxycarbonyl
b.p.	Boiling point
Bu	Butyl
COSY	Correlation spectroscopy
DCM	Dichloromethane
DIC	*N, N'*-diisopropylcarbodiimide
DIPEA	*N, N'*-diisopropylethylamine
DMF	*N, N'*-dimethylformamide
DMSO	Dimethyl sulfoxide
DDI	Drug-drug interaction
EDG	Electron donating group
EI	Electron impact (ionisation)
ESI	Electrospray ionisation
Et	Ethyl
EtOAc	Ethyl acetate
EtOH	Ethanol
FDA	Food and Drug Administration
Fmoc	Fluorenylmethyloxycarbonyl chloride
GAS	Group A *Streptococcus*
h	Hour(s)
HMBC	Heteronuclear multiple-bond correlation spectroscopy
HPLC	High performance liquid chromatography
HRMS	High-resolution mass spectrometry

HSQC	Heteronuclear single-quantum correlation spectroscopy
HST	Histatin
IR	Infrared
LC-MS	Liquid chromatography – mass spectrometry
Me	Methyl
MeCN	Acetonitrile
MeOH	Methanol
MW.	Molecular weight
m/z	Mass to charge ratio
NMR	Nuclear magnetic resonance
NTA	Nitrilotriacetic acid
Ph	Phenyl
pK_a	Logarithmic acid dissociation constant
ppm	Parts per million
***i*-Pr**	Isopropyl
rt	Room temperature
rpm	Revolutions per minute
R_t	Retention time
R_f	Retention factor
SM	Starting material
S_N2	Bimolecular nucleophilic substitution
SPPS	Solid-phase peptide synthesis
ON	Overnight
***t*-Bu**	Tertiary butyl
TFA	Trifluoroacetic acid
THF	Tetrahydrofuran
TIPS	Triisopropylsilane
TLC	Thin layer chromatography

UV	Ultraviolet
v/v	Volumetric ratio
WT	Wild type

Contents

1. Introduction

1.1 Neglected tropical diseases

1.1.1 Overview

Neglected tropical diseases (NTDs) are a group of infectious diseases that have the unifying features of being poverty-related and significantly impacting some of the world's most impoverished areas. Many NTDs have been neglected for decades, initially as part of a general disregard for the developing world, and more recently due to the greater attention directed towards HIV/AIDS, tuberculosis, and malaria.[1]

NTDs are a diverse group of communicable diseases that prevail in the tropical and subtropical conditions of 149 countries.[2] Globally they affect more than one billion people and cost developing economies billions of dollars every year. Populations living in poverty without adequate sanitation and in close contact with infectious vectors and domestic animals and livestock are those worst affected.[3]

The collective term, 'neglected tropical diseases', implies two important shared characteristics. Firstly, these diseases predominate in the tropics, but their predilection for tropical conditions results principally from the fact that poverty is often found in the greatest concentration in remote rural communities, urban slums, and displaced populations near the equator. Thus, rather than thinking of them as tropical diseases, they could be considered as being primarily diseases of the 'bottom billion', i.e., the poorest one-sixth of the world's population,[4,5] amongst whom they cause massive suffering through acute illness, long-term disability, and early death.[6]

The parasitic and bacterial diseases identified as being neglected are among some of the most common infections in the estimated 2.7 billion people who live on less than $2 per day. These diseases occur primarily in rural areas and poor urban settings of low-income countries in Sub-Saharan Africa, Asia, and Latin America.[7] Concentrated almost

exclusively in impoverished populations, NTDs form a group, with more than 70% of affected countries in low-income or lower-middle-income economies (**Figure 1.1**).

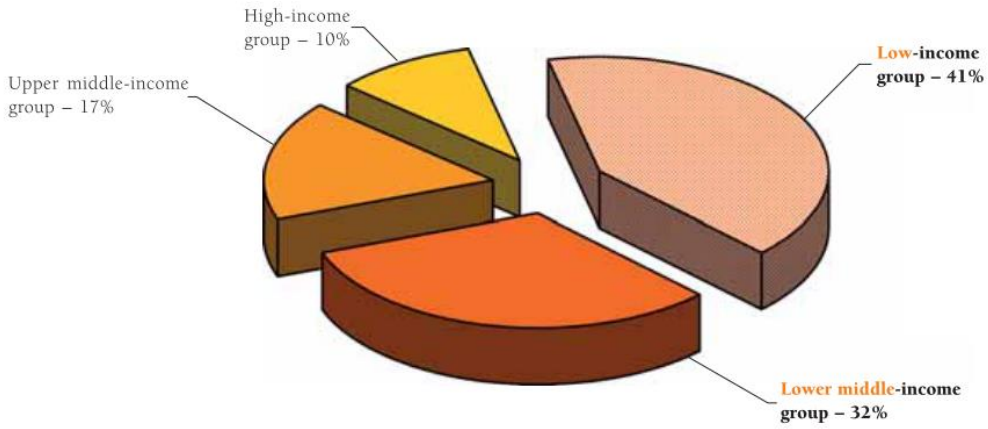

Figure 1.1. Countries affected by neglected tropical diseases, by income group, adapted from WHO.[7]

All low-income and underdeveloped countries are affected by at least five NTDs simultaneously, and many individuals who live in those countries are concurrently infected by more than one pathogen (**Figure 1.2**). Most of these infections are at least in part attributable to inadequate access to safe water, as well as lack of sanitation and appropriate housing. In addition, in conflict-affected countries, NTDs can pose a major health burden due to the collapse of disease-control programmes and surveillance systems. Patients often have poor access to health care, thereby prolonging suffering from preventable and treatable diseases.[7]

Therefore, the second common characteristic of NTDs is that many are preventable or even eradicable with existing, safe and cost-effective tools if only these could be made more widely available.[4,5] Moreover, NTDs are not transmitted easily and they are tied to specific geographical and environmental conditions. Thus, many NTDs do not pose an immediate threat to Western societies.[1]

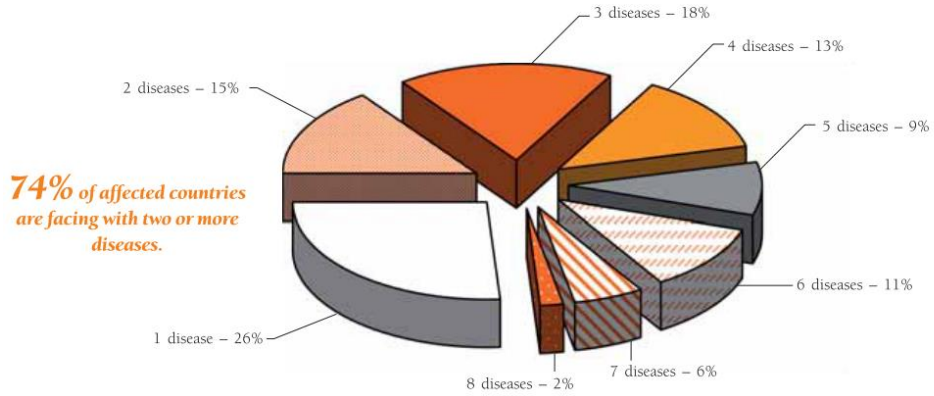

Figure 1.2 Overlapping neglected tropical diseases. Adapted from WHO.[7]

In September 2000, the international community through the United Nations declared an ambitious worldwide commitment to reduce extreme poverty, with a deadline of 2015.[8] This commitment was codified as the Millennium Development Goals.[9] These goals included broad targets to reduce child mortality and improve maternal health, as well as a very specific commitment to combat HIV/AIDS, malaria, and tuberculosis, the so-called 'big three'.

Consequently, attention to many other important causes of mortality and morbidity amongst populations living in impoverished areas, which had already been inadequate, declined further.[10] In the past decade, this situation has begun to change. In fact, now there is a specific department within the World Health Organization (WHO) tasked with addressing the problem of NTDs, an international alliance, known as the Global Network for Neglected Tropical Diseases Control, to raise the profile of and galvanise control efforts for NTDs, and a dedicated open-access journal, PLoS Neglected Tropical Diseases, first published in 2007. [1]

1.1.2 The WHO list of neglected tropical diseases

According to the Center for Disease Control and Prevention, ''A parasite is an organism that lives on or in a host organism and gets its food from or at the expense of its host''. The three main classes of parasites comprise protozoa, helminths, and ectoparasites.[11,12] Some of the most common parasitic diseases are caused by Plasmodium (malaria),

Entamoeba histolytica (amoebiasis), hookworms (ancylostomiasis), Leishmania (leishmaniasis), Trypanosoma (sleeping sickness), and Schistosoma (schistosomiasis). The latter four alone cause almost seven million disability-adjusted life years (DALYs). As part of a group of NTDs, the WHO is increasing its efforts to diminish suffering due to parasite infections.[13]

There is no precise definition as to which diseases constitute NTDs. The WHO officially listed 17 diseases back in 2010.[1] Subsequently, in 2017 the 10th meeting of the Strategic and Technical Advisory Group for Neglected Tropical Diseases received proposals for the addition of diseases and, in accordance with the required procedures, other diseases, such as chromoblastomycosis and other deep mycoses, scabies and other ectoparasites, and snakebite envenoming were added to the NTD portfolio.[2] The 4th NTD report published by WHO established the major NTD categories is presented in **Table 1.1**.

Table 1.1. The 20 neglected tropical diseases recognised by WHO. Adapted from Addisu *et al*.[14]

Infections by category				
Protozoan	**Helminth**	**Bacterial**	**Viral**	**Fungal**
Chagas disease Human African trypanosomiasis Leishmaniasis	*Taenia solium* (neuro) cysticercosis/ Taeniosis Dracunculiasis Echinococcus Foodborne trematodiases Lymphatic filariasis Onchocerciasis. Schistosomiasis Soil-transmitted helminthiases	Buruli ulcer Leprosy Trachoma Yaws	Dengue and chikungunya fevers Rabies	Mycetoma, chromoblastomycosis, deep mycosis

The WHO-recognised NTDs can be categorised further according to the class of the disease-causing agents (**Table 1.1**). Those NTDs caused by protozoan parasites include human African trypanosomiasis, also known as sleeping sickness. This is caused by two parasites of the genus *Trypanosoma*, *T. brucei gambiense* and *T. brucei rhodesiense*.[1] *Trypanosoma cruzi* represents another protozoan parasite that is responsible for Chagas disease, an infection that affects about 200,000 new people per year in the Americas. It is also one of the human parasitic conditions that is deeply concerning to the New World.[10] Leishmaniasis is caused by a myriad of species of protozoan parasites of the genus *Leishmania*. These parasites have been implicated in a range of disease conditions which can include self-healing ulcers and also a severe and fatal visceral form of the disease. Except for malaria and lymphatic filariasis, this group of parasites has been associated with the highest mortality and morbidity among human parasitic infections.[15]

As an overview, a major class of NTDs is caused by helminths, which include soil-transmitted helminths (STHs), schistosomiasis, lymphatic filariasis, onchocerciasis, and dracunculiasis. This group of infections has significant poverty-inducing impacts, but it should be noted that in most cases of infection death is an unlikely outcome.[16] Schistosomiasis, also known as bilharzia, represents another NTD caused by helminths with about 200 million people infected globally.[17] A psychological and socio-economic impact that can arise due to helminth infection is lymphatic filariasis, which is commonly known as elephantiasis. This is associated with enlargement of the limbs, genitals, or breasts.[18] Endemic areas harbour 20% of the global population, with over 120 million people in 83 countries infected. Of these, 40 million are disfigured by the disease.[1] Transmission is mediated by mosquitoes, with most infections acquired remaining asymptomatic for many years. Other helminth-caused NTDs include onchocerciasis (river blindness) and dracunculiasis, the manifestation, symptoms as well as the epidemiology of which are described elsewhere.[1]

Another class of NTDs which include trachoma, Buruli ulcer, and leprosy are caused by bacteria. Trachoma remains a public health concern in 44 countries and inflicts blindness or visual impairment in about 1.9 million people. Contact with eye and nose discharges from infected individuals transmits the disease-causing bacterium *Chlamydia trachomatis*. Inanimate objects such as towels and/or washcloths as well as eye-seeking flies can also facilitate transmission. The latest estimates (2018) indicate that 178 million people are residents in endemic districts and are thus at risk of trachoma blindness[19]

The literature on NTDs is complicated by the fact that both the terms ‘neglected tropical diseases’ and ‘neglected diseases’ are often used interchangeably. Moreover, the use by different stakeholders of the same term to encompass different diseases makes it difficult to set specific targets for control or to lobby for funding for NTDs as a group. Consequently, attention and funding are more aligned with the success of advocacy groups for individual diseases, with heavy reliance on pharmaceutical company donations, than to any

objective criteria such as disease burden, attributed deaths or the need for new drugs, diagnostics, and vaccines. [20]

The disability-adjusted life year (DALY), a metric used in the Global Burden of Disease Study in 2010, is a tool which may be used to assess and compare the relative impact of several diseases, locally and globally.[8] **Figure 1.3** shows the major NTDs as defined by WHO and their estimated DALYs.

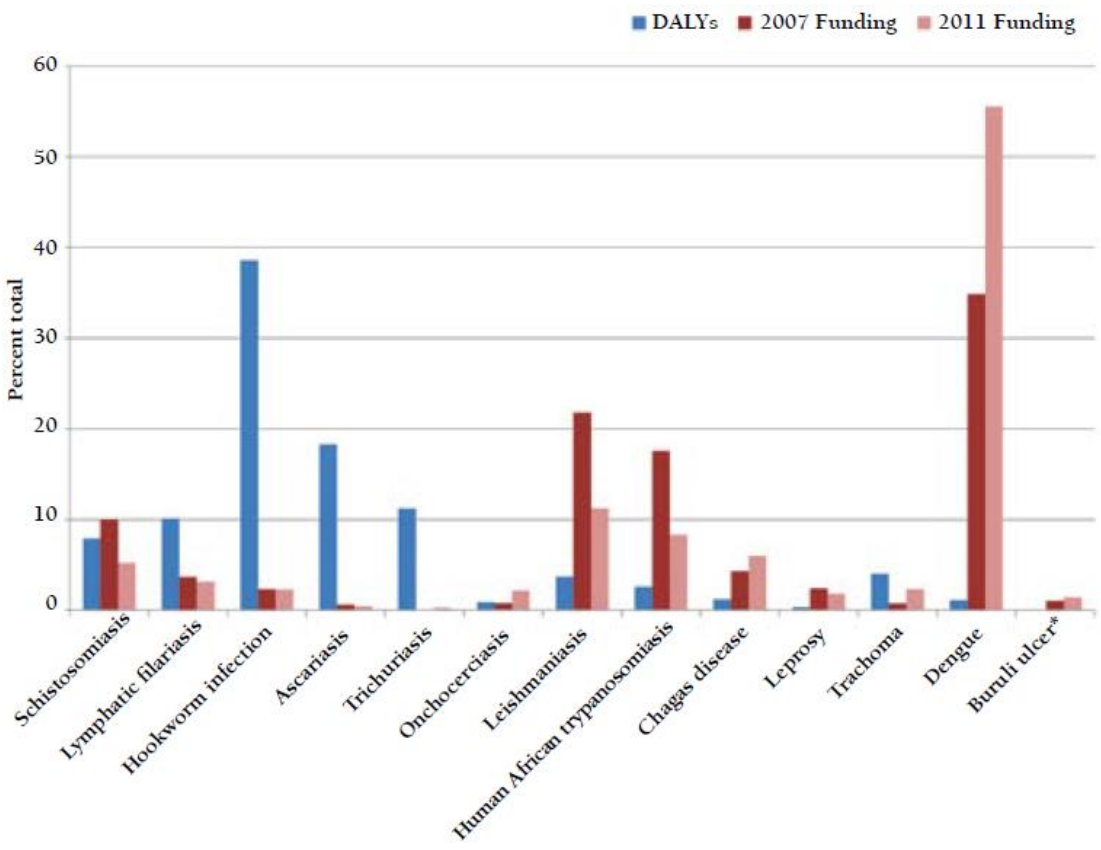

Figure 1.3. Misalignment of disease burden and funding. Discrepancies in disability-adjusted life years (DALY) and funding allocation for various neglected tropical diseases. Asterisk – DALY burden unknown. Adapted from Bhopal *et al*.[20]

However, additional aspects not considered by the DALY metrics are the important elements of social stigma for many of the NTDs and the indirect effects on family and community members,[21] loss of tourism, and health system overload, for example during outbreaks.[17] NTDs for which it is important to consider social stigma include leprosy, onchocerciasis, lymphatic filariasis, plague, Buruli ulcer, leishmaniasis, and Chagas

disease. Stigma is also an influential social determinant of the effectiveness of disease control through its effect on help-seeking and treatment adherence.[22]

Integrating NTDs into global health and development plans has shown significant progress since 2015 according to the latest NTD's WHO report.[14] These achievements result from the implementation of the five interventions recommended to overcome NTDs: (1) preventive chemotherapy; (2) innovative and intensified disease management; (3) vector ecology and management; (4) veterinary public health services; and (5) the provision of safe water, sanitation, and hygiene.

Of the five key interventions employed to tackle NTDs, preventive chemotherapy stands out, both in terms of its effectiveness as a strategy against certain NTDs and the resources going into it, the two things being related. However, each of the five interventions is vitally important, and, going forward, it is essential to ensure that each receives the attention it merits and the resources it requires. Vector ecology and management is particularly important, being woefully under-resourced despite its crucial importance, notably in response to outbreaks.[23]

1.1.3 Occurrence and geographical distribution of protozoan NTDs

Parasitic NTDs affect hundreds of millions of people worldwide and result in significant mortality rates and devastating social and economic consequences.[24] The regions in which the protozoan infections, such as Chagas disease (American trypanosomiasis), human African trypanosomiasis (HAT) (also known as 'sleeping sickness'), and Leishmaniasis, occur are highlighted in **Figure 1.4**. Chagas occur mainly in Central and South America. Sleeping sickness is prevalent in Africa. Leishmaniasis is endemic in about 90 countries across the globe.

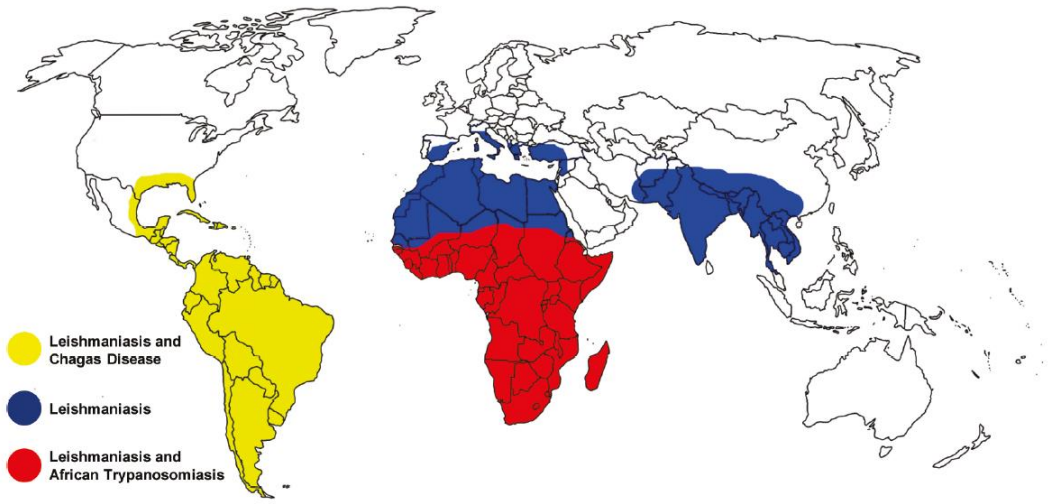

Figure 1.4. Geographic distribution of leishmaniasis, Chagas disease, and Human African Trypanosomiasis. The map was adapted from Cavalli *et al*.[25]

Chagas disease, also known as American trypanosomiasis, is a potentially life-threatening illness caused by the protozoan parasite *T. cruzi,* which was identified in the first decade of the 20th century. It is found mainly in 21 Latin American countries, where it is mostly vector-borne. The main vector involved in the transmission of the parasite to humans is a triatomine bug, also known as a 'kissing bug' (**Figure 1.5**). Chagas disease is clinically curable if treatment is initiated at an early stage. Therefore, universal access to prompt diagnosis and care is essential.[26]

Chagas disease is an anthropozoonosis originating from the American continent, which however has spread from its original boundaries through migration affecting around 6 million people worldwide.[27] Once acute infection resolves, patients can develop chronic disease, which in up to 30-40% of cases is characterised by cardiomyopathy, arrhythmias, mega viscera, and, more rarely, polyneuropathy and stroke[24]. After the initial infection, the majority of cases progress to an asymptomatic chronic phase, which can evolve into the chronic determinate form of the disease years later, with around 30% of patients presenting irreversible damage to the heart and nervous and digestive systems.[28]

Even after more than a century, many challenges remain unresolved, since epidemiological control and diagnostic, therapeutic, and prognostic methods must be improved. In particular, the efficacy and tolerability profile of therapeutic agents is far from ideal. Furthermore, the population affected is older and more complex (e.g., immunosuppressed patients and patients with cancer). Nevertheless, in recent years, our knowledge of Chagas disease has expanded, and the international networking needed to change the course of this deadly disease that began in the 21st century.[29]

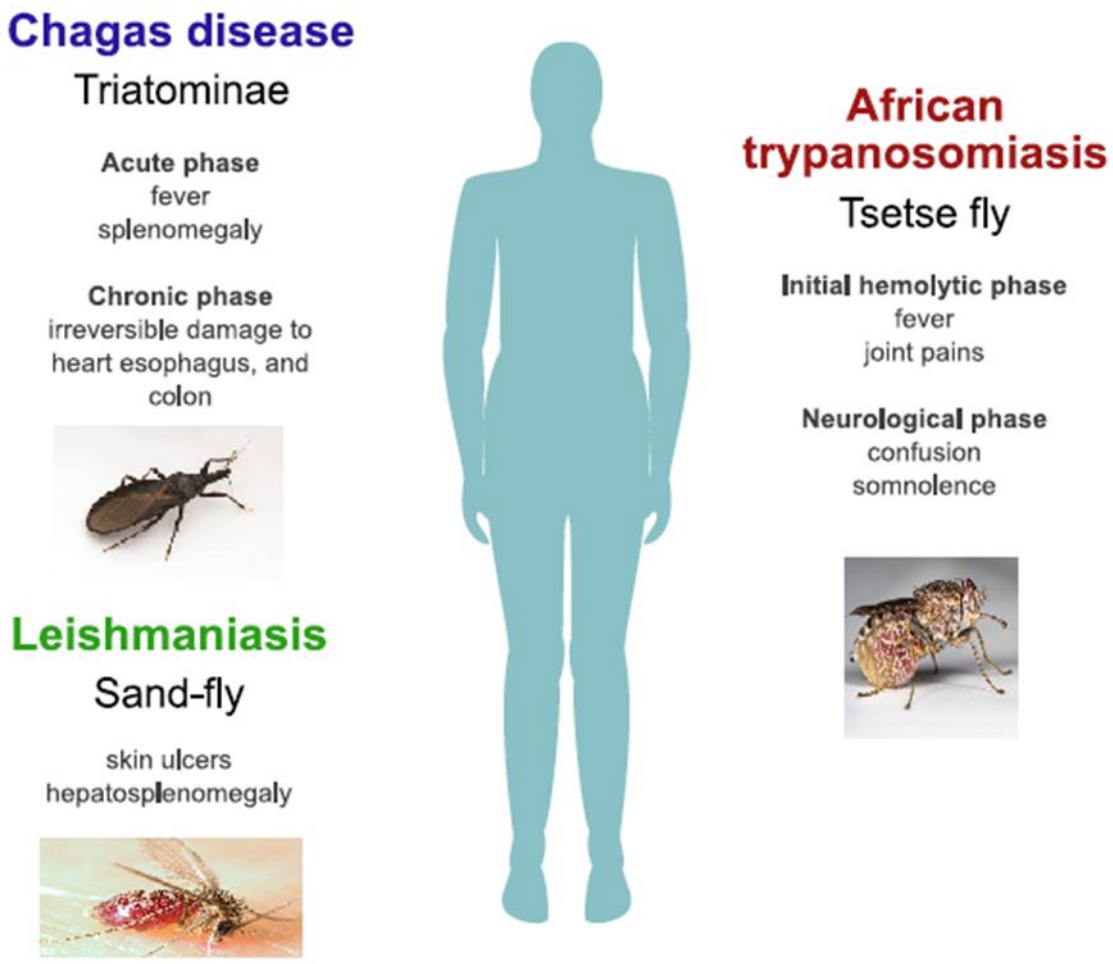

Figure 1.5. Summary of disease vectors and symptoms for the NTDs Chagas disease, African trypanosomiasis and leishmaniasis.

Another protozoan parasite of the genus Trypanosoma is responsible for the NTD human African trypanosomiasis. Commonly called sleeping sickness, this disease is transmitted

by vectors. Specifically, the bite of a tsetse fly (*Glossina spp*.) facilitates the entry of the parasites into the human host. The parasites further invade the central nervous system upon multiplication and subsequent crossing of the blood-brain barrier. At this stage, the more obvious symptoms of the disease are evident, i.e., changes in behaviour, confusion, sensory disturbances, and poor coordination. Another important symptom, which gives the disease its name, is the disruption of the sleep cycle, with victims usually sleeping uncontrollably during the day. The disease is usually fatal if not promptly diagnosed and treated. Of the two parasite species responsible for the disease, *T. brucei rhodesiense* and *T. brucei gambiense*, the latter accounts for 98% of reported cases. Due to sustained control efforts, the number of cases reported dropped below 10,000 (9,878) for the first time in 50 years. This decline in the number of cases has continued with 992 and 663 new cases reported in 2019 and 2020 respectively, the lowest level since the start of systematic geodata collection 80 years ago. The estimated population at risk is 55 million people for the period 2016–2020; with only 3 million people at moderate or higher risk.[30] The disease burden differs from one country to another, with variations in different localities of the same country. Moreover, the transmission may have stopped in some of these countries. However, it is still a challenge to assess the exact situation in some areas beset by social and political instabilities.[17]

Finally, leishmaniasis is caused by the protozoan *Leishmania* parasites, and transmission to humans is facilitated by the bite of infected female phlebotomine sandflies (**Figure 1.5**). The disease pathology takes three main forms: visceral leishmaniasis (VL, also known as kala-azar), cutaneous leishmaniasis (CL), and mucocutaneous leishmaniasis (MCL). *Leishmania* parasites are known to be transmitted by over 90 sandfly species.[18]

1.2 Leishmaniasis worldwide

Leishmaniasis is a global chronic disease that mainly affects the poor in Africa, Asia and Latin America, and is associated with malnutrition, migration, poor housing conditions, weak immune system and lack of resources.[31] Most cases are seen in South America, the

Mediterranean, and some areas of Asia and Africa. Fundamentally it is a zoonotic disease, with canids and rodents being the main reservoir, except for *Leishmania donovani* and *Leishmania tropica*, whose main reservoirs are humans, **Figure 1.6**).[32]

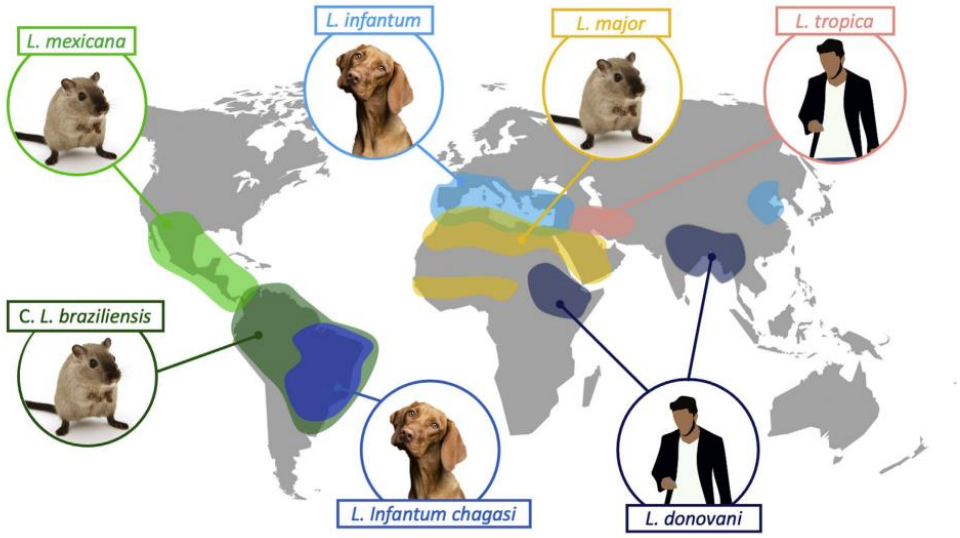

Figure 1.6. Geographical distribution of main Leishmania species with their respective fundamental reservoir adapter from Cerro *et al*.[32]

Leishmaniasis is caused by a protozoa parasite from over 20 different *Leishmania* species. There are three main forms of the disease: cutaneous (CL) (the most common), mucocutaneous (MCL), and visceral (VL) (the most severe). VL is a disseminated protozoan infection caused *by Leishmania donovani* and *Leishmania infantum*.[33] Exceptionally, dermatotropic species can visceralize and cause VL, particularly in immunosuppressed patients. Transmission occurs via the bite of phlebotome sand flies. Blood transfusion, intravenous drug use, organ transplantation, and congenital and laboratory accidents constitute exceptional modes of transmission. The zoonotic form, caused by *L. infantum*, occurs in the Mediterranean basin, China, the Middle East, and South America, and has dogs as the main reservoir. The anthroponotic form, caused by *L. donovani*, is prevalent in Eastern Africa, Bangladesh, India, and Nepal.[34] VL is fatal if left untreated in over 95% of cases. It is characterized by irregular bouts of fever, weight loss, enlargement of the spleen and liver, and anaemia. Most cases occur in Brazil, East

Africa and India. An estimated 50,000 to 90,000 new cases of VL occur worldwide annually, with only between 25 to 45% reported to WHO. In 2020, more than 90% of new cases reported to WHO occurred in 10 countries: Brazil, China, Ethiopia, Eritrea, India, Kenya, Somalia, South Sudan, Sudan and Yemen. [35]

MCL leads to the partial or total destruction of mucous membranes of the nose, mouth and throat. Over 90% of mucocutaneous leishmaniasis cases occur in Bolivia (the Plurinational State of), Brazil, Ethiopia and Peru. Finally, CL is the most common form of leishmaniasis and causes skin lesions, mainly ulcers, on exposed parts of the body, leaving life-long scars and serious disability or stigma. About 95% of CL cases occur in the Americas, the Mediterranean basin, the Middle East and Central Asia (**Figure 1.7**). In 2020 over 85% of new CL cases occurred in 10 countries: Afghanistan, Algeria, Brazil, Colombia, Iraq, Libya, Pakistan, Peru, the Syrian Arab Republic and Tunisia. It is estimated that between 600,000 to 1 million new cases occur worldwide annually.[35]

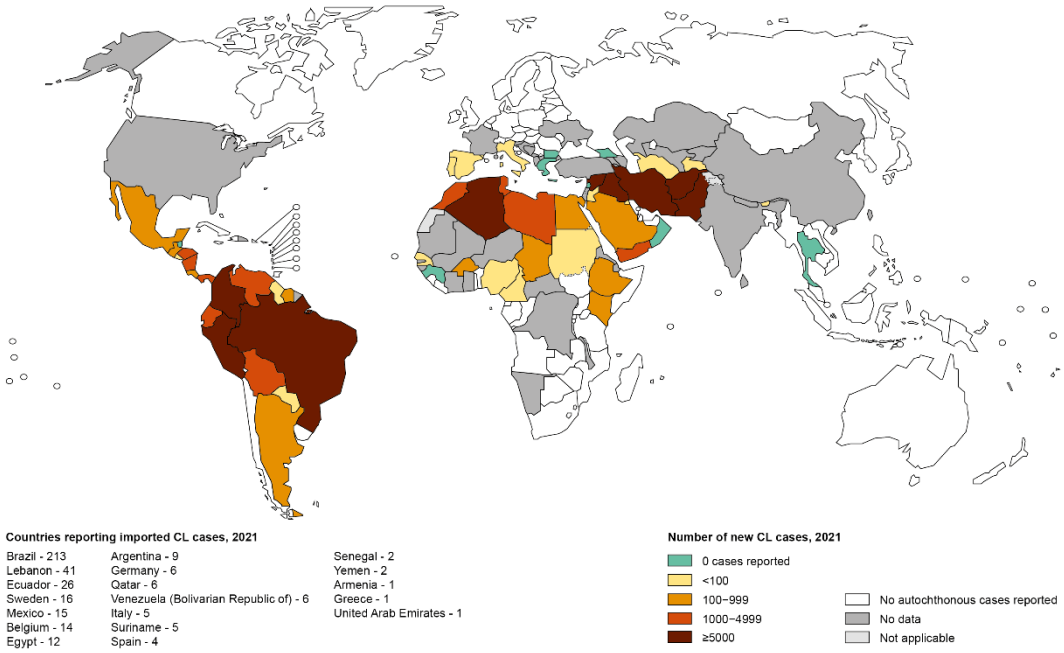

Figure 1.7. Status of endemicity of cutaneous leishmaniasis worldwide in 2021. Adapted from WHO.[36]

According to the World Health Organization (WHO), CL is the most common form of this disease. It usually produces ulcers on the exposed parts of the body, such as the face, arms and legs. There may be a large number of lesions – sometimes up to 200 – which can cause serious disability. When the ulcers heal, they invariably leave permanent scars, which are often the cause of serious social prejudice.[35]

1.2.1 Leishmania life cycle

Leishmaniasis is characterized by large clinical polymorphism and depending on the species of the *Leishmania* involved and the immune response triggered by the host, it can manifest in benign and self-limited clinical forms of cutaneous leishmaniasis, to the most serious forms such as mucosal leishmaniasis, mucocutaneous, diffuse cutaneous and visceral leishmaniasis. [31] This parasitic disease is found in parts of the tropics, subtropics, and southern Europe. It is classified as a neglected tropical disease (NTD). There are several different forms of these diseases in people.[1] VL is diagnosed by demonstrating the presence of *Leishmania* amastigotes in clinical specimens using direct microscopic examination or molecular analysis. Various treatments exist, although the evidence supporting the options available for cutaneous leishmaniasis is weak. Both the classical presentation of leishmaniasis and our management of the disease have changed in recent decades because of acquired immune deficiency caused by conditions such as HIV infection or the use of TNF inhibitors.[32]

In the Americas, leishmaniasis is a public health problem due to its morbidity and mortality and broad geographical distribution. Its complex cycle of transmission includes different species of parasites, reservoirs and vectors. They affect mainly the poorest and people with the most difficult accessing health services. In this region, leishmaniasis is caused by different protozoan species of the genus Leishmania and transmitted to animals and humans by insects of the family Psychodidae, maintained by the zoonotic cycle. In humans, they cause a set of clinical syndromes that can compromise the skin, mucosal membranes and viscera. The parasite is a protozoan belonging to the family

Trypanosomatidae. The genus Leishmania is divided into two subgenus *Leishmania* and *Viannia* and 15 of the 22 species pathogenic to humans have been identified in the Americas.[31] Particularly, *Leishmania mexicana* is the causative agent in Central America and Mexico of the cutaneous form of Leishmaniasis.

The infection with *L. mexicana* occurs (**Figure 1.8**) when an individual is bitten by an infected sandfly that injects promastigotes, which are carried in the salivary glands and expulsed by the proboscis, directly to the skin.[12] Promastigotes are elongated, flagellated and the infective form of the parasite that grows in the midgut of female sandflies. [37] The promastigotes are engulfed by phagocytic cells, such as macrophages and dendritic cells. The promastigotes are kept inside in a parasitophorous vacuole, where they transform into amastigotes and divide until they break the cell membrane. When an uninfected sandfly bites an infected mammal reservoir, the sand fly ingests the amastigotes, which transform back into promastigotes and divide in the midgut of the sandfly. There are no blood stages in the life cycle of *L. mexicana*.[12]

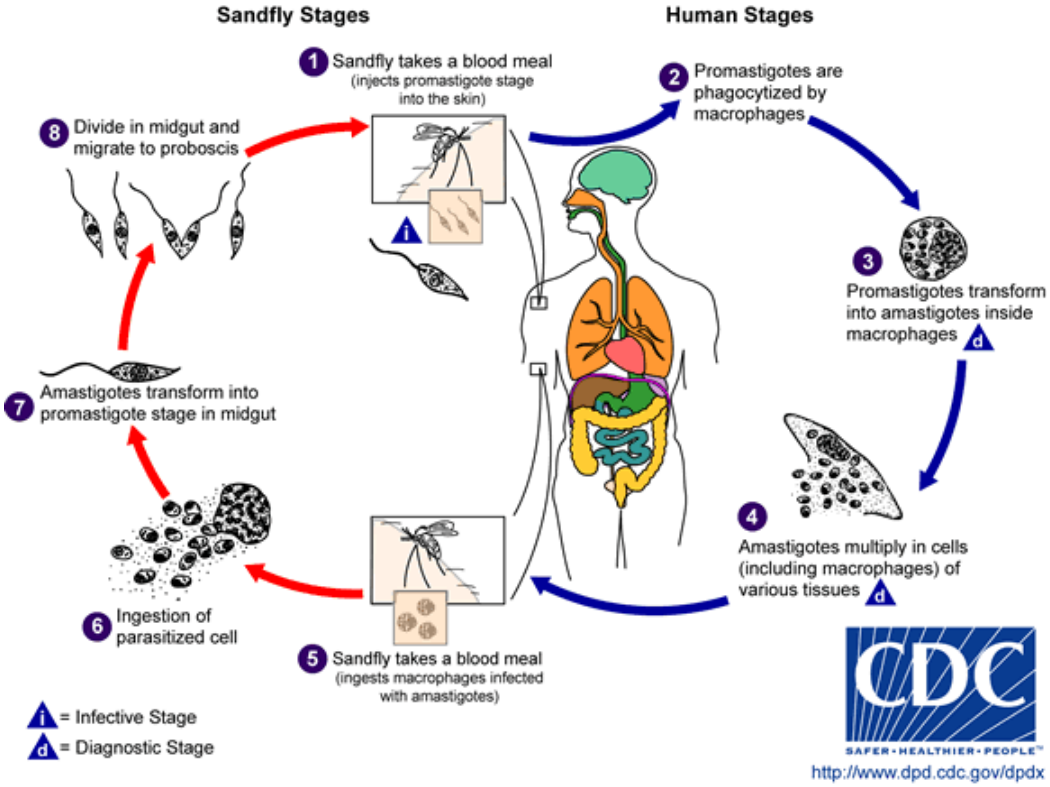

Figure 1. 8. *Leishmania* life cycle.

1.3 Limitations of current therapies and challenges in NTD drug discovery

Current clinically used drugs against NTDs are far from ideal. Some of the limitations associated with current chemotherapeutic agents include drug resistance, severe adverse side effects, lengthy treatment duration, unfavourable toxicity profiles, and complicated drug administration procedures. Moreover, the use of some drug regimens is jeopardised by their limited availability in the areas in which infections arise.[17,38]

The current antitrypanosomal drugs, such as Pentamidine (**3**), Melarsoprol (**4**), and Eflornithine (**5**) (**Figure 1.9**), are beset by several challenges ranging from limited effectiveness, the emergence of drug resistance, the complexity of administration, and numerous undesirable side effects.[39] The disease causative pathogen and the stage of disease progression are the two factors that are considered when selecting drug treatment regimens. Currently, antiparasitic drugs are donated to the WHO by pharmaceutical companies.[40] For first-stage *T. brucei gambiense* disease, Pentamidine (**3**) is the drug of choice for treatment. The administration is complicated, often requiring intravenous infusion in saline over 2 h, or intramuscular administration for a week. Although generally well tolerated, when administered via intramuscular injection, adverse events, including pain and swelling at the site of administration, abdominal pain, gastrointestinal problems, and hypoglycaemia, have been reported.[17,41]

Treatment with antitrypanosomal drugs is always recommended for acute and congenital Chagas disease, reactivated infections, and chronic disease in children younger than 18 years. Since the persistence of parasitosis and concomitant chronic inflammation underlie chronic chagasic cardiomyopathy, parasiticidal treatment is generally offered to patients with chronic Chagas disease in the indeterminate phase and to patients with mild-to-moderate disease.

Only two drugs, Benznidazole (**2**) and Nifurtimox (**1**) are licensed for the treatment of Chagas disease (**Figure 1.9**). Both have been the mainstay of parasiticidal treatment for almost 50 years, although their safety and efficacy profiles are far from ideal. Furthermore,

since the effectiveness of treatment seems to decrease with time from primary infection, early detection and intervention are crucial.[29]

Nifurtimox (**1**) was the first drug used and it is administered orally in three to four doses for 60–90 days.[42] Cure rates in the chronic indeterminate phase range from 86% in children younger than 14 years, to 7–8% in adults.[43,44] The most common adverse effects of Nifurtimox (**1**) are anorexia, weight loss, neurological disorders (irritability, insomnia, disorientation, mood changes, paresthesias, and peripheral neuropathy), digestive manifestations such as nausea and vomiting, and, occasionally, fever and rash.

Discovered in the 1970s, Benznidazole (**2**) is a 2-nitroimidazole pro-drug activated through the reduction of the nitro group by parasite nitroreductases, a process that generates reactive metabolites that ultimately disrupt parasite cell machinery and are responsible for the trypanocidal effect. [44] This nitro reduction can generate reactive oxygen species in humans, which are associated with the main toxicological findings, including carcinogenicity, teratogenicity, and genotoxicity (similar to other nitroimidazole-containing drugs). In the clinic, 20–25% of patients present dermatitis from hypersensitivity to the drug and this, together with digestive intolerance, is the main reason for treatment interruption.[45] Similarly, Nifurtimox (**1**) is a 5-nitrofuran derivative and is also activated via parasite nitro reduction producing reactive metabolites.[28] Nifurtimox (**1**) has an even higher frequency of adverse effects.[28,45]

Benznidazole (**2**) is generally preferred over Nifurtimox (**1**) because of its better tolerability profile, tissue penetration, and, possibly, efficacy. It is administered orally in two or three doses usually for 60 days. Higher doses of up to 15 mg/kg are recommended in cases of meningoencephalitis.[29] According to some reports, 30 days of treatment can be useful for chronically infected adults.[46] Benznidazole (**2**) has considerable activity during the acute and early phases of *T. cruzi* infection. In fact, the serological cure is achieved in up to 100% of patients with congenital disease[47,48] treated during the first year of life, and in 76% of patients with acute disease. In the chronic phase, cure rates are much lower. The most

common adverse effects involve hypersensitivity, mainly in the form of skin rash, digestive intolerance, and general symptoms such as anorexia, asthenia, headache, and sleeping disorders. Neuropathy and depression of the bone marrow are considered rare. Neither elevated serum drug levels nor high daily doses (>300 mg) have been associated with an increased frequency of adverse events.[49]

Chagas Desease

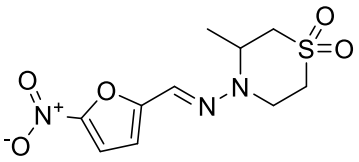

Nifurtimox, 1970
1

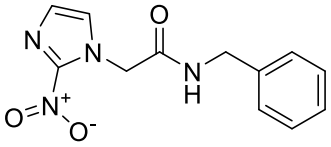

Benznidazole, 1974
2

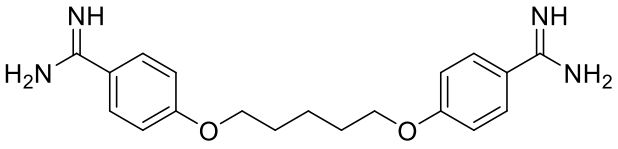

Pentamidine, 1939
3

African Tripanosomiasis

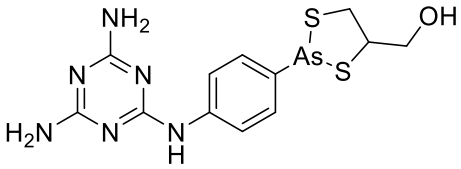

Melarsoprol, 1949
4

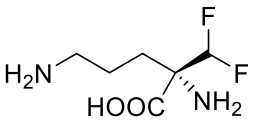

Eflornithine, 1991
5

Leishmaniasis

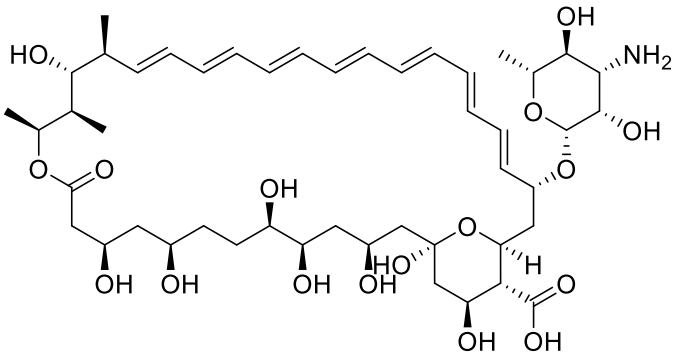

Amphotericin B, 1990
6

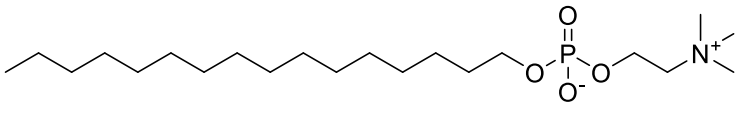

Miltefosine, 2002
7

Figure 1.9. Structures of commonly used therapies for Chagas disease, HAT and leishmaniasis.

The antimony-containing drugs, also known as pentavalent antimonials, are the drugs of choice for first-line treatment of Leishmaniasis where resistance has not been reported.[50] These include the generic sodium stibogluconate (pentostam) and the branded meglumine antimoniate (the structure of which remains a subject of debate). These have been in use for over five decades. Regrettably, *Leishmania* parasites have become increasingly resistant to the pentavalent antimonial drugs, and this has brought into question their use in disease-endemic areas.[51] Due to the fact that the antimonials (e.g. **4**) are administered intravenously or intramuscularly, they are not convenient for patients. They are also associated with side effects, which include chemical pancreatitis, elevations in serum aminotransferases, and electro-cardiographic abnormalities.[17]

In summary, even though NTDs affect more than one billion people worldwide, they have been largely neglected in terms of new drug development, mostly because they affect poor people in some of the poorest regions of the world. Currently available drugs for NTDs also worsen the present scenario, as they are decades old (dating back to the 1920s) and they have many limitations, including high toxicity and the emergence of drug resistance.[29]

1.4 Natural products as potential therapeutics in the area of NTDs

1.4.1 The role of Natural products in modern medicine

Natural products (NPs) have been, and continue to be, invaluable sources of inspiration in drug design and development. For example, in 2020 around 17% of all drugs approved by the US Federal Food and Drug Administration (FDA) were classified as NPs (**Figure 1.10**).[52] That is 1% higher compared to the ones approved in 2018.[53] Having evolved often over millennia to acquire specific ligand-protein binding motifs, NP structures cover a wide range of biologically relevant chemical space that cannot be explored efficiently by synthetic compounds in commercially available screening libraries.[54,55] Several studies in the early 2000s revealed that NPs favour the inclusion of aliphatic over aromatic rings, as well as more sp^3-hybridised bridgehead atoms and chiral centres rather than synthetic

small molecules.[56] As the clinical success of drug candidates is directly correlated to the molecules' three-dimensionality,[57] NPs clearly possess an advantageous structural foundation over synthetic small molecules in the development of drug candidates. However, the structural complexity, toxicity, and unfavourable pharmacokinetics often associated with NPs can limit their clinical potential, and, as such, structural modification is often required.[55] To this end, many leading chemists are not only targeting bioactive NPs, but also libraries of structurally-related compounds for biological evaluation.[58]

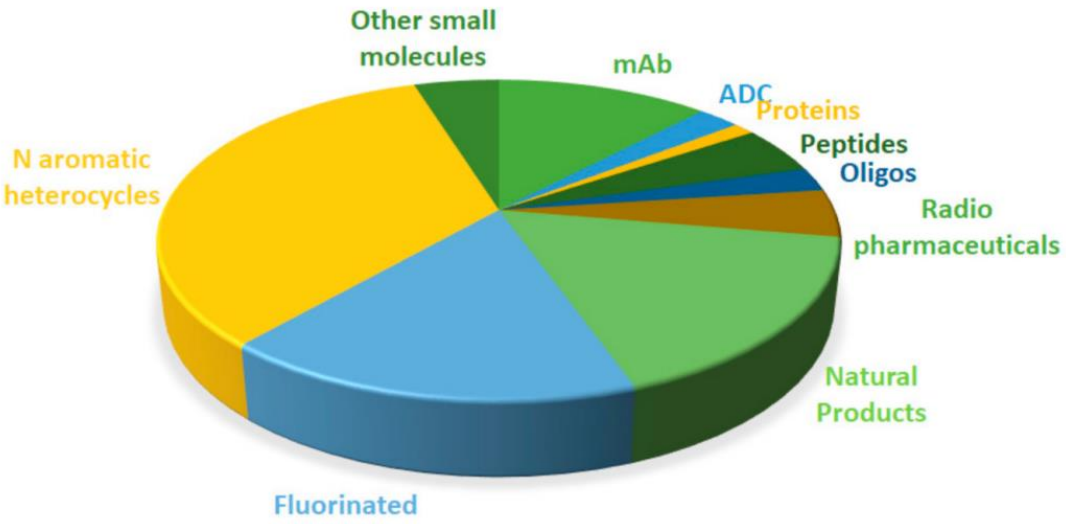

Figure 1.10. Drugs approved by the FDA in 2020 and classified based on their chemical structure.[52]

Many natural product-derived drugs have been essential for modern pharmaceutical care over the last 50 years, and these include quinine (**8**), vitamin A (**9**), penicillin G (**10**), morphine (**11**), paclitaxel, digoxin, vincristine, doxorubicin, cyclosporine among many other examples (**Figure 1.11**). [17]

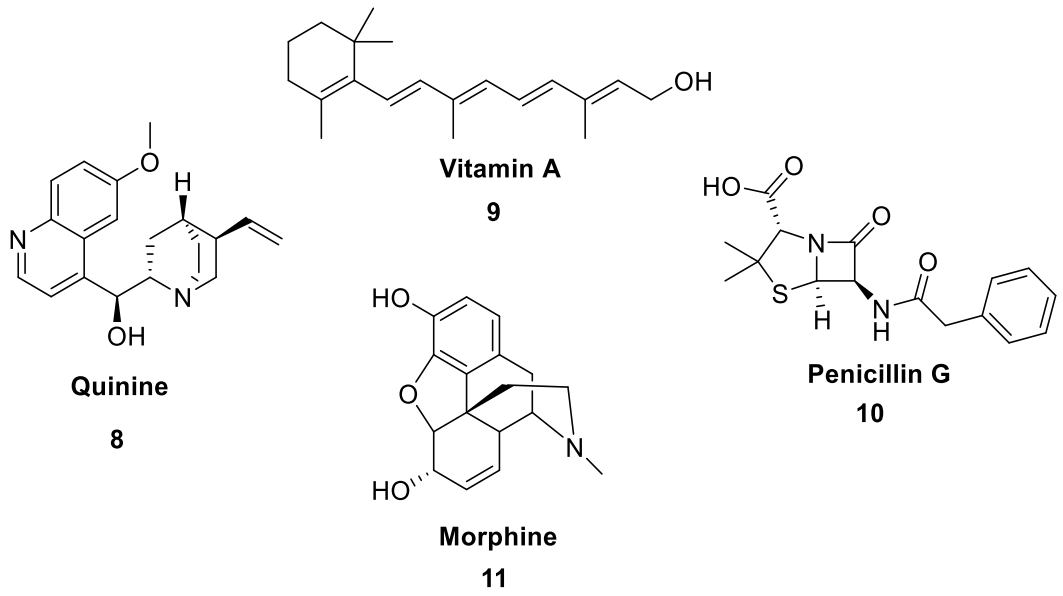

Figure 1.11. Some examples of natural product-derived drug molecules.

The inevitable rise of life-debilitating infectious diseases, arising from the continuous emergence of antibiotic resistance, requires new forms of treatment and chemotherapy to be found to curb this potential crisis. NPs have been shown to be excellent templates for the development of novel therapies. The extensive structural and chemical biodiversity of NPs evolved from the complex interactions between organisms and their environment to enhance survival and increase competitiveness, making them an ideal starting point for new drug design.[9]

1.4.2 Peptide natural products as a source of new drug entities

Peptides represent a unique class of pharmaceutical compounds. In terms of molecule structural complexity and size, they sit between small molecules and proteins. Yet, biochemically and therapeutically, they are distinct from both.[59] Proteins are naturally occurring oligomers assembled from alpha-amino acids, linked by an amide bond. In nature, peptides are typically assembled from 20 standard amino acids, which are distinguished by the different nature of the functionality located at the α-carbon. In proteins, a vast structural diversity is enabled by programming the specific sequence in

which the amino acids are assembled (primary sequence), and, to some extent, by modulating the length of the final oligomer. Arbitrarily, within the community, peptides are considered to be small proteins or protein fragments of less than 50 amino acids. Proteins play several key roles in all living organisms, in general controlling and regulating a broad variety of cellular functions. For most proteins, their functionality is intimately linked to their ability to adopt a discrete and specific three-dimensional structure that is encoded through its primary sequence.

Peptides have profoundly impacted the development of the modern pharmaceutical industry, and they have contributed significantly to the advancement of biological and chemical science.[60] Fundamental studies in the first half of the 20th century were aimed at understanding the structures and physiological role of peptide hormones. For instance, insulin, oxytocin, gonadotropin-releasing hormone, and vasopressin have influenced many major advances in pharmacology, biology, and chemistry, as well as other enabling technologies, essential for what we now know as modern drug discovery. There is no better illustration for this statement than the discovery and development of the 51 amino acid (aa) hormone insulin (**Figure 1.12**), which stands as one of the monumental scientific achievements of the era.[59]

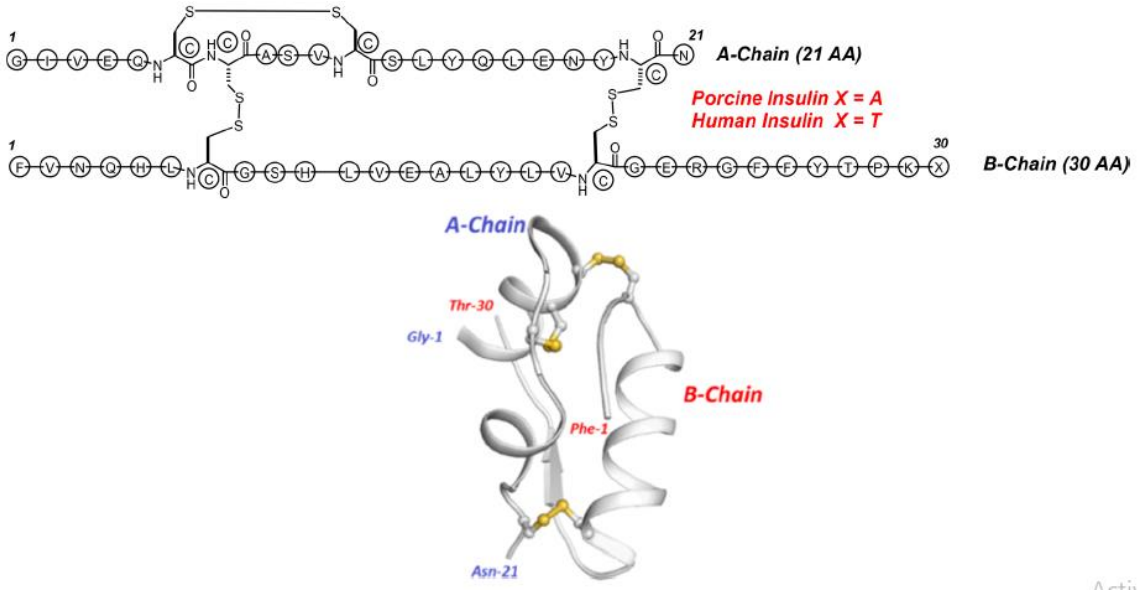

Figure 1.12. Two- and three-dimensional structures of Insulin. Adapted from Henninot *et al*.[61]

The utilisation of peptides as therapeutics has evolved over time, and continues to evolve, with changes in drug development and treatment paradigms. Peptides isolated from natural sources, such as Insulin and adrenocorticotropic hormone (ACTH), provided life-saving medicines in the first half of the 20th century. When sequence elucidation and chemical synthesis of peptides became feasible in the 1950s, peptides such as Oxytocin and Vasopressin were developed and entered clinical use. However, the enthusiasm for peptide therapeutics was subsequently tempered by certain limitations of native peptides, such as short plasma half-lives and negligible oral bioavailability.[59]

1.4.3. AMPs with antiparasitic activity

The control and elimination of parasitic diseases are nowadays further complicated by the emergence of drug resistance. Drug resistance is a serious threat as there are not many effective antiparasitic drugs available. The global burden of parasitic diseases, including those that are vector-borne and cause intestinal helminthiases, is a public health issue because of the associated high disability-adjusted life year values, with the lowest at 666,000 to as high as 72 million.[62] Additionally, the search for new therapeutics is urgently needed to treat infections caused by drug-resistant parasites, which are typically challenging to eliminate in endemic areas.[63,64] AMPs present the advantage of generality over specificity to their target. This condition makes it more difficult for the parasite to develop resistance in comparison to available drugs, for example, primaquine which targets the redox system of the malaria parasite.[65] Another important characteristic of AMP is that it has diverse biological effects.

There are numerous different sources of AMPs, including human body secretions. Human peptides are secreted physiologically by certain organs such as salivary glands, a good example are histatins. They are human oral anti-microbial peptides secreted by the salivary glands into the saliva and related to immunity.[66] They have been studied as well for NTDs.[67] There are other sources of AMPs with antiparasitic effects. Venoms, from

snakes and invertebrates to poisons, plants, bacteria and even synthetic ones. Their mechanism of action can be shown as a conceptual framework in **Figure 1. 13**.

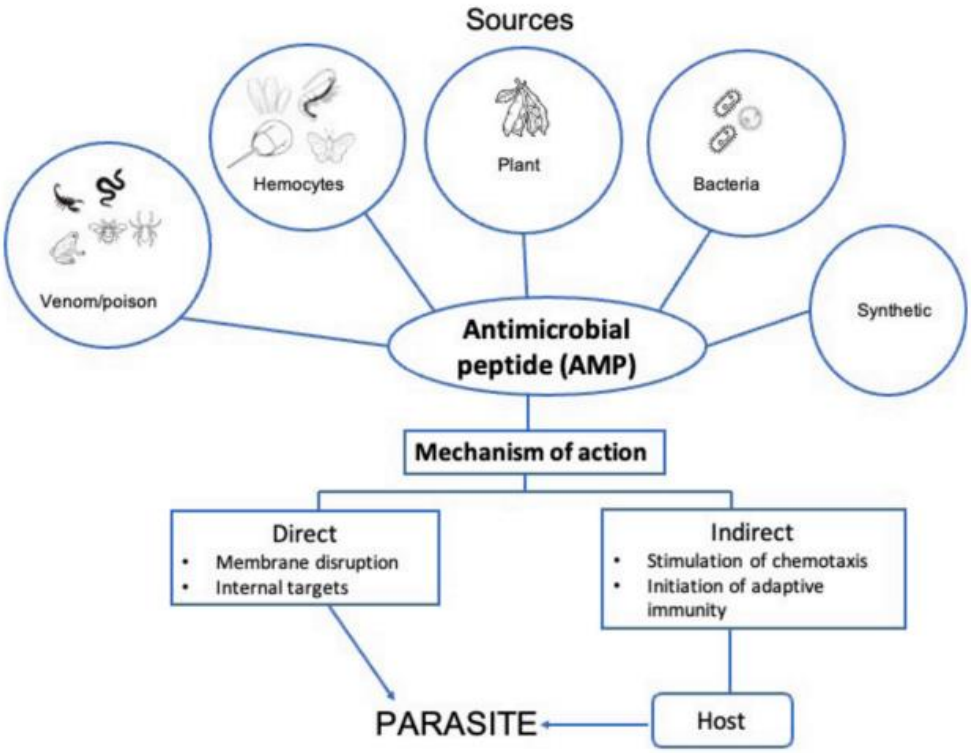

Figure 1.13. Different sources of AMPs and the mechanism of action to parasites, adapted from Nogrado *et al*.[62]

Many eukaryotes produce AMPs, such as vertebrate and invertebrate animals and even plants.[65,68] There is an abundance of AMPs among eukaryote, because AMPs play a major role in their innate immune response.[69,70] Particular parasitic diseases are vector-borne by arthropods, **Figure 1.13**. These organisms are unaffected by these parasites and have adapted to coexist. For this reason, it is surmised that these organisms have antiparasitic compounds.[71] Different examples of AMPs, from different sources, are detailed in **Table 1.2**.

Table 1.2. List of antimicrobial peptides (AMPs) with antiparasitic activities from different sources

Entry	AMP name	Source	Antiparasitic activity
		Venom	
1	batroxicidin	Lancehead (Bothrops atrox)	*T. cruzi* [72]
2	crotalicidin	South American pit viper (Crotalus durissus terrificus)	*T. cruzi*[73]
3	bombinin H2, H4	yellow-bellied toad (Bombina variegata)	*Leishmania*[74]
		Hemocytes of invertebrates	
4	Melittin	Bees (apis melifero)	*Leishmania Trypanosoma, toxoplasma*
5	tachyplesin	Japanese horseshoe crab (Tachypleus tridentatus)	*T. cruzi, T. braziliensis*[75]
6		**Plants**	
7	thionin	wheat (Triticum aestivum) and barley (Hordeum vulgare)	*L. donovani A. canicnum N. americanus*[76]
8	cO14	Viola odorata	*A. canicnum N. americanus*[77]

Venoms from insects of the order Hymenoptera, such as bees, ants and wasps, have been studied in detail.[78] The principal components of bee venom are amino acids, peptides, proteins, enzymes, sugars, biogenic amines, volatile compounds, phospholipids and pheromones. The most studied compound from bee venom and the most abundant component representing 50%–60% of the dry weight of this venom is melittin (**Entry 4, Table 1.2**). Melittin comprises 26 amino acids[79] and is cationic because of arginine and lysine residues. The antimicrobial activity of melittin is nonspecific cytolytic activity, which involves forming pores in biological membranes.[79,80] Several studies have provided evidence that melittin is active against Leishmania, Trypanosoma and Toxoplasma.[80] The antiprotozoal activity of melittin involves membrane disruption and reduction of the

membrane potential of mitochondria. More importantly, melittin may function in synergy in the presence of other AMPs and may also modulate immune responses, which may facilitate vaccine development.[80] AMPs, also called host defence peptides (HDP), are a growing class of peptide-based molecules, with a wide spectrum of biological activities. Several living organisms, such as bacteria, fungi, plants, invertebrates, non-mammalian vertebrates, and mammals, generate AMPs. They are involved in innate immunity and the induction of resistance against such anti-microbial peptides is uncommon.[81] AMPs exhibit broad-spectrum antimicrobial properties, acting by the direct elimination of infectious pathogens (bacteria, viruses, fungi, and parasites) or by modulating the immune response. They activate and recruit immune cells resulting in the enhancement of pathogen elimination and/or in the control of inflammation, wound healing, and angiogenesis.[82,83]

1.4.4 AMPS with antileishmanial activity

Over the last 20 years, antimicrobial peptides (AMPs) are a major class of peptide natural products that have gained considerable interest in both academia and industry.[84,85] Numerous AMPs, like melittin, cecropin, cathelicidin, defensin, magainin, dermaseptin, eumenitin, and histatin, have proven to be active on different *Leishmania* species, see **Table 1.3**.[67] The interest in AMPs is largely due to the fact that they have been proposed as one potential solution to the development of new topical agents to treat CL.[7–10]

Table 1.3 Antimicrobial peptide with activity against *Leishmania*.

Entry	AMP	Sequence	Leishmania species
1	**Melittin**	GIGAVLTTGLPALISWIKRKRQQ	*L. major*[86] *L. panamensis*[87] *L. donovani* promastigotes *L. infantum* promastigotes and amastigotes[88]
2	**Cecropin***		*L. aethiopic* *L.panamensis amastigotes*[87]
	Cecropin-A	KWKLFKKIEKVGQNIRDGIIKAGPAVAWVGQATQIAK	
	Cecropin-D	ENFFKEIERAGQRIRDAIISAAPAVETLAQAQKIIKGGD	*Leishmania (V) L. panamensis promastigotes*[89]
3	**Cathelicidin**		*L. donovani* promastigotes and amastigotes[90]
	LL-37	LLGDFFRKSKEKIGKEFKRIVQRIKDFLRNLVPRTES	
	RI-BMAP-28	GIRIIPVIIPGYKKWARLIKRGLSRLGG	*L. major* amastigotes[91] *L. major* promastigote[90]
	D-BMAP-28	GGLRSLGRKILRAWKKYGPIIVPIIRIG	*L. major* promastigote[91]
4	**Defensin**		
	MBD1	MKTHYFLLVMICFLFSQMEPGVGILTSLGRRTDQYKC LQ HGGFCLRSSCPSNTKLQGTCKPDKPNCCK	*L. major*
	MBD2	MRTLCSLLLICCLLFSYTTPAVGSLKSIGYEAELDHCH TN GGYCVRAICPPSARRPGSCFPEKNPCCKYMK	*L. major* *L. major*[92] *L. amazonensis*[93]
	MBD3	MRIHYLLFAFLLVLLSPPAAFSKKINPVSCLRKGGRCW	
	Vu-Def	NRCIGNTRQIGSCGVPFLKCCKRK MKTCENLADTYRGP	
5	**Magainin**		
	MG-H1	GIKKFLHIIWKFIKAFVGEIMNS	*L. donovani* promastigotes
	MG-H2	IIKKFLHSIWKFGKAFVGEIMNI	*L. donovani* promastigotes
	F5W-magainin	GIGKWLHSAKKFGKAFVGEIMNS	*L. donovani* promastigotes[94]

6	**Temporin***		*L. donovani promastigotes*
	Temporin A	FLPLIGRVLSGIL	*L. pifanoi* amastigotes[95]
	Temporin B	LLPIVGNLLKSLL	*L. braziliensis*, *L. major* *L. infantum*
	Temporin-She	FLPALAGIAGLLGKIF	*L. infantum*, *L. major*, *L. tropica*, *L. amazonensis*, and *L. braziliensis* promastigotes [96]
	SHd	FLPAALAGIGGILGKLF	*L. braziliensis* promastigotes *L. infantum* axenic amastigotes[95]
7	**Histatin**		
	Hst5	DSHAKRHHGYKRKFHEKHHSHRGY	*L. donovani* promastigotes , *L. pifanoi* axenic[97]
	D- Hst5	D- DSHAKRHHGYKRKFHEKHHSHRGY	
	Dhvar4	KRLFKKLLFSLRKY	

* Indicates C terminal domain is an amide

Cell membrane disruption is the primary mechanism of action adopted by all the AMPs highlighted in **Table 1.3**. However, some of the AMPs have additional mechanisms of action (apoptosis, mitochondrial dysfunction, immune response modulation, and DNA damage).[67] Current drugs used in clinical treatment for leishmaniasis exert similar mechanisms of action to AMPs. For example, Amphotericin B principally affects the cell membrane[98] and can also modulate the immune response.[99] Miltefosine generates a cell death mechanism (apoptosis)[100,101] and affects the mitochondrial function[102] and the immune response[103] Pentavalent antimonials cause DNA damage and can indirectly act by regulating the immune response.[104,105]

The Temporins are AMPs isolated from frog skin and they typically consist of 10 to 17 amino acids.[106] They are α-helical AMPs with highly cationic and amphipathic properties that allow them to target different pathogens. Both Temporin A and Temporin B (**Table 1.3**, **Entry 6**) were reported to display activity on *L. donovani* promastigotes and *L. pifanoi* amastigotes.[95] Their leishmanicidal action is favoured by their capacity to induce

membrane permeation causing severe damage to the parasite membrane.[95] Likewise, Temporin SHd (**Table 1.3**, **Entry 6**) showed effective activity against promastigote forms of numerous Leishmania (*L. infantum*, *L. major*, *L. tropica*, *L. amazonensis*, and *L. braziliensis*) with a similar mechanism of action. Temporin SHd was also active against *L. infatum* axenic amastigotes.[95] Recently, the anti-microbial activity of the peptide Temporin-She (**Table 1.3**, **Entry 6**), a temporin SH paralog from the Sahara frog (Pelophylax saharicus) was investigated.[96] Temporin-She was active against *L. braziliensis* and *L. major* promastigotes at 10.5 and 11.6 µM, respectively. It was highly potent against *L. infantum* as well, with an IC_{50} value of 4.6 µM.[67]

Additionally, Histatins are human oral AMPs that have been reported to have antileishmanial properties. The histatin family contains 12 small histidine-rich cationic AMPs with the most abundant ones being histatin 1, 3, and 5.[66] The other histatins are known to be proteolytic derivatives of histatins 1 and 3.[107] Histatins are effective against several different microbes. Regarding their anti-leishmanial activity, only histatin 5 (HST-5) (**Table 1.3**, **Entry 7**), its D-enantiomer (**Table 1.3**, **Entry 7**) and its synthetic analog Dhvar4 (**Table 1.3**, **Entry 7**) have been studied for activity, against *L. donovani* promastigotes and *L. pifanoi* axenic amastigotes. HST-5 displayed antileishmanial activity at micromolar concentrations, with lethal doses of 50~7.3 µM against *L. donovani* promastigotes and ~14.4 µM against *L. pifanoi* axenic amastigotes. D- Hst5 and Dhvar4 were found to be more active against both *L. donovani* promastigotes and *L. pifanoi* axenic amastigotes than HST-5.[97]

Given the limitations of the existing antiparasitic treatments, the reported features of AMPs make them promising candidates to replace currently available therapies. Specifically, in the case of cutaneous leishmaniasis (CL), it is possible that topical; AMP-based treatments could get approval for clinical use in an accelerated time frame compared to oral treatments.[67]

In additional, due to some of the advantages that AMPs offer, such as high potency, high selectivity, potentially low toxicity, and low accumulation in tissues, the pharmaceutical

industry is developing them as therapeutics for a range of diseases, and several clinical trials are being conducted.[38] Companies like Theravance and Vicuron Pharmaceuticals are two of the major American companies largely dedicated to the development of peptide antibiotics.[46] However, it should be noted that taking peptide derived molecules, into clinical trials is not without its challenges.[108] For example, MSI-78 (pexiganan acetate, a potent antimicrobial peptide designed from Magainin) entered phase III of clinical trials and showed efficacy against diabetic foot ulcer infections,[109] but the FDA disapproved the use of Magainin based on the inadequacy of the trial design.

1.5 Challenges in developing peptide-based drugs

The bioavailability and biodistribution of peptide drug candidates, which include absorption, transport, and the passage of biological membranes and cellular barriers, are determined by a combination of their physicochemical properties, such as aqueous solubility, lipophilicity, H-bond formation, chemical stability, and metabolic stability (proteolytic and/or enzymatic degradation). With a few exceptions, peptides composed of natural amino acids are inherently poor drug candidates, due to their intrinsic physicochemical properties and pharmacokinetic profiles. When compared to therapeutic proteins and antibodies, peptide drug candidates have notable drawbacks: they generally have low stability in plasma, they are sensitive to proteases, and they can be cleared from circulation in a few minutes.

Thus, the main limitations generally attributed to therapeutic peptides[110] are low oral bioavailability (injection is generally required); a short half-life because of their rapid degradation by proteolytic enzymes of the digestive system and blood plasma; rapid removal from the circulation by the liver (hepatic clearance) and kidneys (renal clearance); poor ability to cross physiological barriers because of their general hydrophilicity; and high conformational flexibility. This sometimes results in a lack of selectivity involving interactions with different receptors or targets (poor specific biodistribution), causing activation of several targets and leading to side effects; eventual risk of immunogenic

effects; and high synthetic and production costs (the production cost of a 5000 Da molecular mass peptide exceeds the production cost of a 500 Da molecular mass small molecule by more than 10-fold, but not 100-fold).[110,111]

To overcome the aforementioned barriers in peptide drug discovery, molecules resembling peptides are being developed by many groups within both academia and industries.[112] Such molecules are referred to as “peptidomimetics”, and, among these, there is a class of compounds known as peptoids (**Figure 1.14**).[113] Like peptides, peptoids are oligomeric in nature and they contain side chains (R), which may comprise a wide variety of different functional groups. However, a peptoid’s backbone is devolved entirely of tertiary amide bonds, and this, in turn, gives them a range of different physical and biological properties to those of peptides.[113] Most notably a peptoid’s tertiary amide backbone makes this class of molecule highly resistant to proteolytic degradation.[114]

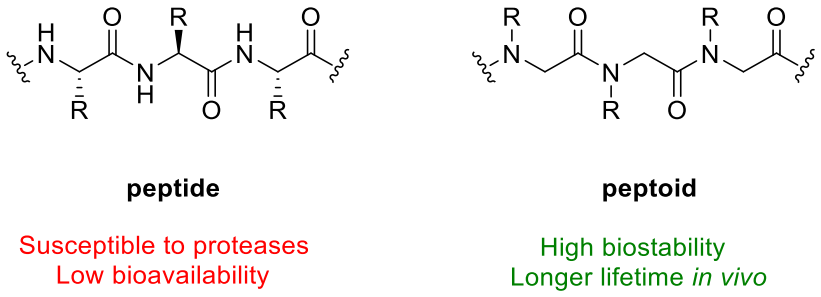

Figure 1.14. A structural comparison of α-peptides and α –peptoids. Adapted from Bolt *et al*.[113]

1.6 Peptoids with activity against NTDs

Peptoids share certain structural similarities with peptides, as illustrated in **Figure 1.15**. However, in a peptoid, the polymer backbone consists of amide bonds where the side chain functionality is bonded to the nitrogen, rather than the α-carbon, so the repeating monomer of a peptoid is an *N*-substituted glycine. This means that there are no stereogenic centres on the backbone of peptoids, compared to peptides, which instead have a chiral backbone.[38]

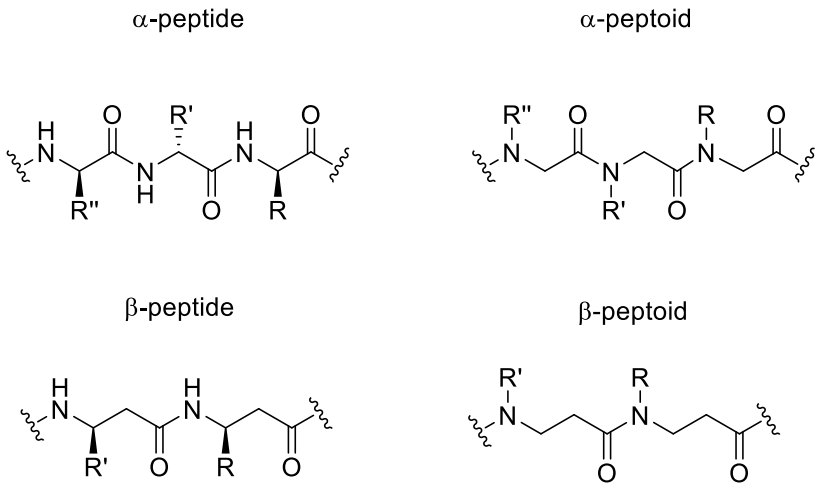

Figure 1.15. Structures of generic α-peptoids and peptides oligomers. B-peptoids and β-peptides with the extra methylene unit in the backbone are also shown.

The lack of amide hydrogens (due to the *N*-substitution) has several important effects on the structure of peptoids. In peptides and proteins, amide protons can undergo intrachain hydrogen bonding, which is key for the formation of secondary structural motifs, such as α-helices and β-sheets. In peptoids, the absence of this amide proton leads to greater chain flexibility compared to peptides and prevents intra- and inter-chain hydrogen bonding. In addition, the lack of a hydrogen bonding donor on the backbone prevents backbone-driven aggregation, which can help to increase bioavailability. Therefore, peptoids' secondary structures are formed almost exclusively through electrostatic and steric interactions. Peptoids are protease resistant, and they are not denatured by solvent changes or increased temperatures that usually disrupt hydrogen bonding patterns in peptides. To date, peptoids have been developed to meet a wide variety of biomedical applications, ranging from inhibitors of protein-protein interactions,[46,109] molecular scaffolds,[115] ,nucleic acid binders,[115–117] lung surfactant protein mimics,[117] biomimetic materials,[108,110] or molecular transporters for drug delivery.[21,118,119,]

There is also a growing number of reports in the literature that outline the antimicrobial activities of peptoids[108,117,120] including those in which peptoids display anti-parasitic properties against NTDs. For example, peptoids with activity against *L. mexicana*, the

causative agent of CL, have been reported (**Table 1.4**). It is interesting to note that some of the peptoids identified in these early studies not only have activity against promastigotes (insect-stage parasites) but also against the clinically more relevant axenic amastigotes (mammalian-stage parasites) (**Table 1.4**, **Entries 5** and **7**). These early investigations also demonstrated a clear difference in the sensitivity of the two different parasite forms of *L. mexicana* towards linear peptoids, with amastigotes being found to be significantly more resistant.

Table 1.4 Linear peptoids with antileishmanial activity against *L. mexicana*.[121]

Example structure

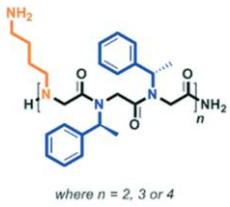

Entry	Peptoid sequence	ED_{50} (μM)	
		Promastigotes	Amastigotes (axenic)
1	$(NLysNpheNphe)_4$	15	>100
2	$(NahNspeNspe)_4$	11	>100
3	$(NLysNspeNspe)_4$	8	>100
4	$(NLysNspeNspe)_3$	5	>100
5	$(NaeNspeNspe)_4$	7	17
6	$(NaeNspeNspe)_3$	10	>100
7	$(NamyNspeNspe)_2(NLysNspeNspe)_2$	11	16

The linear peptoids in the early studies by Bolt *et al*.[121] against *L. mexicana* were designed around the subunit NxNyNy, which is repeated either two, three, or four times to give 6-, 9-, or 12-mers, respectively. For Ny either the chiral aromatic building block *N*spe or the achiral *N*phe was chosen. **Table 1.4**, **Entries 1-4** from the library prepared showed activity against the promastigote form of *L. mexicana* having ED_{50} values of <20 μM. Moreover, a

shorter peptoid with 3 subunits (**Table 1.4**, **Entry 5**) was found to be the most active, with an ED_{50} value of 7 μM. Only this linear peptoid was found to have an ED_{50} value of <20 μM (17 μM) against *L. mexicana* axenic amastigotes from the first library reported.[67] Finally, a linear peptoid with two different subunits (**Table 1.4**, **Entry 7**) represented the first peptoid published to have activity in the low μM range against *L. mexicana* promastigotes and axenic amastigotes, and also to retain activity against the clinically significant intramacrophage amastigotes.[121]

1.6 Project aims

As discussed, there is currently a pressing need to develop a range of new compounds that can be used to treat the parasitic infections that sit on the WHO's NTD list. Historically, the use of natural products has offered a good starting point with regards to drug development.

Previous work within the Cobb group has shown that naturally occurring cyclic peptides known as Chaiyaphumines[122] have antiparasitic activity against both American and African trypanosomiasis. The first aim of this project is to develop an improved route to resynthesise the naturally occurring Chaiyaphumines. Once the reaction conditions are developed, amide analogues of the natural peptides will also be prepared. The peptides prepared will be used to probe the structural and stability differences between the ester (natural product) and amide analogues, and also to help develop a better understanding of their anti-parasitic mode of action.

Several naturally occurring antimicrobial peptides (AMPs), such as those from the Temporin family, have previously been shown antileishmanial activity. The second aim of this project is to contribute to the existing knowledge regarding the potential application of AMPs as templates for the design of new agents to treat NTD parasitic infections. To do this a small library of AMPs will be prepared and tested against *L. mexicana*, *major* and *amazonensis*. Before any biological testing, dose-response assays, such as Alamar blue,

will be optimized to have a consistent protocol for all the biological assays discussed in this work.

The final aim of this project is to look to develop a novel library of short lipopeptoids for anti-parasitic screening. This will be achieved using a Ugi multi-component synthetic approach similar to that recently reported by Donate *et al*.[123] After having prepared a small library of functionalised peptoids, these will be tested for biological activity against *L. mexicana* parasites.

1.7 References

1. Feasey, N., Wansbrough-Jones, M., Mabey, D. C. W. & Solomon, A. W. Neglected tropical diseases. *Br Med Bull* **93**, 179–200 (2010).
2. WHO. Book Review: Working to Overcome the Global Impact of Neglected Tropical Diseases. *Perspect Public Health* **132**, 192–192 (2010).
3. Rodriguez-morales, A. J. *Current Topics in Neglected Tropical Diseases*. *Current Topics in Neglected Tropical Diseases* (IntechOpen, 2019).
4. Collier, P. *The Bottom Billion: Why the Poorest Countries are Falling and What Can Be Done About It*. *Social Work Education* (2007).
5. Hotez, P. J., Fenwick, A., Savioli, L. & Molyneux, D. H. Rescuing the bottom billion through control of neglected tropical diseases. *The Lancet* **373**, 1570–1575 (2009).
6. Huppatz, C. & Durrheim, D. N. Control of neglected tropical diseases [10]. *New England Journal of Medicine* **357**, 2407–2408 (2007).
7. WHO. *Neglected tropical diseases, hidden successes, emerging opportunities Successes*. (2006).
8. Hotez, P. J. *et al.* The Global Burden of Disease Study 2010: Interpretation and Implications for the Neglected Tropical Diseases. *PLoS Negl Trop Dis* **8**, e2865 (2014).
9. Dodd, R. & Cassels, A. Health, development and the Millennium Development Goals. *Ann Trop Med Parasitol* **100**, 379–387 (2006).
10. WHO. *Changing history*. *World Health Report 2004: Changing History* (2004).
11. Center for Disease Control and Prevention. Parasites. https://www.cdc.gov/parasites/about.html (2022).
12. CDC. Parasites. (2021).
13. Pretzel, J., Mohring, F., Rahlfs, S. & Becker, K. Antiparasitic peptides. *Adv Biochem Eng Biotechnol* **135**, 157–192 (2013).

14. Addisu, A. *et al.* Neglected tropical diseases and the sustainable development goals: an urgent call for action from the front line. *BMJ Glob Health* **4**, e001334 (2019).

15. Bern, C., Maguire, J. H. & Alvar, J. Complexities of Assessing the Disease Burden Attributable to Leishmaniasis. *PLoS Negl Trop Dis* **2**, e313 (2008).

16. Hotez, P. J. & Ferris, M. T. The antipoverty vaccines. *Vaccine* **24**, 5787–5799 (2006).

17. Cheuka, P., Mayoka, G., Mutai, P. & Chibale, K. The Role of Natural Products in Drug Discovery and Development against Neglected Tropical Diseases. *Molecules* **22**, 58 (2016).

18. Perera, M., Whitehead, M., Molyneux, D., Weerasooriya, M. & Gunatilleke, G. Neglected Patients with a Neglected Disease? A Qualitative Study of Lymphatic Filariasis. *PLoS Negl Trop Dis* **1**, e128 (2007).

19. Trachoma: Situation and Trends. https://www.who.int/gho/neglected_diseases/trachoma/en/ (2020).

20. Anand Bhopal , Thomas Callender, A. F. K. and S. R. Strength in numbers? Grouping, fund allocation and coordination amongst the neglected tropical diseases. *VIEWPOINTS* **3**, 1–6 (2013).

21. Fenwick, A. The global burden of neglected tropical diseases. *Public Health* **126**, 233–236 (2012).

22. Weiss, M. G. Stigma and the social burden of neglected tropical diseases. *PLoS Negl Trop Dis* **2**, (2008).

23. WHO. *Integrating neglected tropical diseases*. *World Health Organization* (2017).

24. Renslo, A. R. & McKerrow, J. H. Drug discovery and development for neglected parasitic diseases. *Nat Chem Biol* **2**, 701–710 (2006).

25. Cavalli, A. & Bolognesi, M. L. Neglected Tropical Diseases: Multi-Target-Directed Ligands in the Search for Novel Lead Candidates against Trypanosoma and Leishmania. *J Med Chem* **52**, 7339–7359 (2009).

26. World Health Organization. https://www.who.int/ (2019).

27. WHO. Chagas disease. https://www.who.int/news-room/fact-sheets/detail/chagas-disease-(american-trypanosomiasis) (2021).

28. de Oliveira, R. G., Cruz, L. R., Mollo, M. C., Dias, L. C. & Kratz, J. M. Chagas Disease Drug Discovery in Latin America—A Mini Review of Antiparasitic Agents Explored Between 2010 and 2021. *Frontiers in Chemistry* vol. 9 (2021).

29. Pérez-Molina, J. A. & Molina, I. Chagas disease. *The Lancet* **391**, 82–94 (2018).

30. WHO. Trypanosomiasis, human African (sleeping sickness). (2023).

31. PAHO/WHO. *Plan of action to strengthen the surveillance and control of leishmaniasis in the americas 2017-2022*. (2017).

32. Abadías-Granado, I., Diago, A., Cerro, P. A., Palma-Ruiz, A. M. & Gilaberte, Y. Cutaneous and Mucocutaneous Leishmaniasis. *Actas Dermo-Sifiliograficas* vol. 112 601–618 (2021).

33. van Griensven, J. & Diro, E. Visceral Leishmaniasis. *Infectious Disease Clinics of North America* vol. 26 309–322 (2012).

34. Van Griensven, J. & Diro Ermias. Visceral Leishmaniasis: Recent Advances in Diagnostics and Treatment Regimens. *Infect Dis Clin North Am* **33**, 79–99 (2019).

35. WHO. Leishmaniasis. (2022).

36. WHO. Leishmaniasis: Map Gallery. (2023).

37. Vedantu. Leishmania Life Cycle. (2022).

38. Altamura, F., Rajesh, R., Catta-Preta, C. M. C., Moretti, N. S. & Cestari, I. The current drug discovery landscape for trypanosomiasis and leishmaniasis: Challenges and strategies to identify drug targets. *Drug Dev Res* 1–28 (2020).

39. Docampo, R. & Moreno, S. N. Current chemotherapy of human African trypanosomiasis. *Parasitol Res* **90**, S10–S13 (2003).

40. Wenning, F. W. *Bayer Sustainable Development Report 2004*. *Bayer AG* (2004).

41. Brun, R., Blum, J., Chappuis, F. & Burri, C. Human African trypanosomiasis. *The Lancet* **375**, 148–159 (2010).

42. Bern, C. *et al.* Evaluation and Treatment of Chagas Disease in the United States. *J Am Med Assoc* **298**, 2171–2181 (2007).

43. Coura, J. R. & De Castro, S. L. A critical review on chagas disease chemotherapy. *Mem Inst Oswaldo Cruz* **97**, 3–24 (2002).

44. Müller Kratz, J., Garcia Bournissen, F., Forsyth, C. J. & Sosa-Estani, S. Clinical and pharmacological profile of benznidazole for treatment of Chagas disease. *Expert Rev Clin Pharmacol* **11**, 943–957 (2018).

45. Gaspar, L. *et al. Running title: 50 Years After Nifurtimox: Current and Future Chemotherapy For Chagas Disease Curr Med Chem* **22**, 4293-4312 (2015).

46. Viotti, R. *et al.* Long-Term Cardiac Outcomes of Treating Chronic Chagas Disease with Benznidazole versus No Treatment. *Ann Intern Med* **144**, 724 (2006).

47. Russomando, G. *et al.* Treatment of congenital chagas' disease diagnosed and followed up by the polymerase chain reaction. *American Journal of Tropical Medicine and Hygiene* **59**, 487–491 (1998).

48. Schijman, A. G. *et al.* Aetiological treatment of congenital Chagas' disease diagnosed and monitored by the polymerase chain reaction. *Journal of Antimicrobial Chemotherapy* **52**, 441–449 (2003).

49. Pérez-Ayala, A. *et al.* Chagas disease in Latin American migrants: a Spanish challenge. *Clinical Microbiology and Infection* **17**, 1108–1113 (2011).

50. Singh, R. K., Pandey, H. P. & Sundar, S. Visceral leishmaniasis (kala-azar): Challenges ahead. *Indian Journal of Medical Research* **123**, 331–344 (2006).

51. Maltezou, H. C. Drug resistance in visceral leishmaniasis. *J Biomed Biotechnol* **2010**, (2010).

52. de la Torre, B. G. & Albericio, F. The Pharmaceutical Industry in 2020. An Analysis of FDA Drug Approvals from the Perspective of Molecules. *Molecules* **26**, 627 (2021).

53. G. de la Torre, B. & Albericio, F. The Pharmaceutical Industry in 2018. An Analysis of FDA Drug Approvals from the Perspective of Molecules. *Molecules* **24**, 809 (2019).

54. Lachance, H., Wetzel, S., Kumar, K. & Waldmann, H. Charting, Navigating, and Populating Natural Product Chemical Space for Drug Discovery. *J Med Chem* **55**, 5989–6001 (2012).

55. Gerry, C. J. & Schreiber, S. L. Chemical probes and drug leads from advances in synthetic planning and methodology. *Nat Rev Drug Discov* **17**, 333–352 (2018).

56. Lee, M. L. & Schneider, G. Scaffold architecture and pharmacophoric properties of natural products and trade drugs: Application in the design of natural product-based combinatorial libraries. *J Comb Chem* **3**, 284–289 (2001).

57. Lovering, F., Bikker, J. & Humblet, C. Escape from flatland: Increasing saturation as an approach to improving clinical success. *J Med Chem* **52**, 6752–6756 (2009).

58. Davison, E. K. & Brimble, M. A. Natural product derived privileged scaffolds in drug discovery. *Curr Opin Chem Biol* **52**, 1–8 (2019).

59. Lau, J. L. & Dunn, M. K. Therapeutic peptides: Historical perspectives, current development trends, and future directions. *Bioorg Med Chem* **26**, 2700–2707 (2018).

60. *Handbook of Biologically Active Peptides*. (Academic Press, 2013).

61. Henninot, A., Collins, J. C. & Nuss, J. M. The Current State of Peptide Drug Discovery: Back to the Future? *J Med Chem* **61**, 1382–1414 (2017).

62. Nogrado, K., Adisakwattana, P. & Reamtong, O. Antimicrobial peptides: On future antiprotozoal and anthelminthic applications. *Acta Tropica* vol. 235 (2022).

63. Baker, C. H. & Welburn, S. C. The Long Wait for a New Drug for Human African Trypanosomiasis. *Trends in Parasitology* vol. 34 818–827 (2018).

64. Capela, R., Moreira, R. & Lopes, F. An overview of drug resistance in protozoal diseases. *International Journal of Molecular Sciences* vol. 20 (2019).

65. Vale, N., Aguiar, L. & Gomes, P. Antimicrobial peptides: A new class of antimalarial drugs? *Frontiers in Pharmacology* vol. 5 275 (2014).

66. Khurshid, Z. *et al.* Histatin peptides: Pharmacological functions and their applications in dentistry. *Saudi Pharmaceutical Journal* **25**, 25–31 (2017).

67. El-Dirany, R. *et al.* Activity of anti-microbial peptides (Amps) against leishmania and other parasites: An overview. *Biomolecules* **11**, (2021).

68. Zhang, Q. Y. *et al.* Antimicrobial peptides: mechanism of action, activity and clinical potential. *Military Medical Research* vol. 8 (2021).

69. Hancock, R. E. W. & Diamond, G. The role of cationic antimicrobial peptides in innate host defences. *Trends Microbiol* **8**, 402–410 (2000).

70. Pasupuleti, M., Schmidtchen, A. & Malmsten, M. Antimicrobial peptides: key components of the innate immune system *Crit Rev Biotechnol* **32** 143-171 (2012).

71. Lacerda, A. F., Pelegrini, P. B., De Oliveira, D. M., Vasconcelos, É. A. R. & Grossi-de-Sá, M. F. Anti-parasitic peptides from arthropods and their application in drug therapy. *Frontiers in Microbiology* vol. 7 (2016).

72. Mello, C. P. *et al.* Evaluation of the antichagasic activity of batroxicidin, a cathelicidin-related antimicrobial peptide found in Bothrops atrox venom gland. *Toxicon* **130**, 56–62 (2017).

73. Bandeira, I. C. J. *et al.* Antichagasic effect of crotalicidin, a cathelicidin-like vipericidin, found in Crotalus durissus terrificus rattlesnake's venom gland. *Parasitology* **145**, 1059–1064 (2018).

74. Mangoni, M. L. *et al.* Effect of natural L- to D-amino acid conversion on the organization, membrane binding, and biological function of the antimicrobial peptides bombinins H. *Biochemistry* **45**, 4266–4276 (2006).

75. Löfgren, S. E., Miletti, L. C., Steindel, M., Bachère, E. & Barracco, M. A. Trypanocidal and leishmanicidal activities of different antimicrobial peptides (AMPs) isolated from aquatic animals. *Exp Parasitol* **118**, 197–202 (2008).

76. Berrocal-Lobo, M., Molina, A., Rodríguez-Palenzuela, P., García-Olmedo, F. & Rivas, L. Leishmania donovani: Thionins, plant antimicrobial peptides with leishmanicidal activity. *Exp Parasitol* **122**, 247–249 (2009).

77. Colgrave, M. L. *et al.* Anthelmintic activity of cyclotides: In vitro studies with canine and human hookworms. *Acta Trop* **109**, 163–166 (2009).

78. Herzig, V. Arthropod assassins: Crawling biochemists with diverse toxin pharmacopeias. *Toxicon* vol. 158 33–37 (2019).

79. Carpena, M., Nuñez-Estevez, B., Soria-Lopez, A. & Simal-Gandara, J. Bee venom: An updating review of its bioactive molecules and its health applications. *Nutrients* vol. 12 1–27 (2020).

80. Memariani, H. & Memariani, M. Melittin as a promising anti-protozoan peptide: current knowledge and future prospects. *AMB Express* vol. 11 (2021).

81. Zasloff, M. *Antimicrobial peptides of multicellular organisms*. *NATURE* | vol. 415 www.nature.com (2002).

82. Hilchie, A. L., Wuerth, K. & Hancock, R. E. W. Immune modulation by multifaceted cationic host defense (antimicrobial) peptides. *Nature Chemical Biology* vol. 9 761–768 (2013).

83. Kumar, P., Kizhakkedathu, J. N. & Straus, S. K. Antimicrobial peptides: Diversity, mechanism of action and strategies to improve the activity and biocompatibility in vivo. *Biomolecules* vol. 8 (2018).

84. Lewies, A., Wentzel, J., Jacobs, G. & Du Plessis, L. The Potential Use of Natural and Structural Analogues of Antimicrobial Peptides in the Fight against Neglected Tropical Diseases. *Molecules* **20**, 15392–15433 (2015).

85. Boparai, J. K. & Sharma, P. K. Mini Review on Antimicrobial Peptides, Sources, Mechanism and Recent Applications. *Protein Pept Lett* **27**, 4–16 (2019).

86. Pereira, A. V. *et al.* Melittin induces in vitro death of Leishmania (Leishmania) infantum by triggering the cellular innate immune response. *Journal of Venomous Animals and Toxins Including Tropical Diseases* **22**, (2016).

87. Pérez-Cordero, J. J., Lozano, J. M., Cortés, J. & Delgado, G. Leishmanicidal activity of synthetic antimicrobial peptides in an infection model with human dendritic cells. *Peptides (N.Y.)* **32**, 683–690 (2011).

88. Pilar DIAZ-ACHIRICA, Josep UBACH, Almudena GUINEA, David ANDREU & Luis RIVAS. The plasma membrane of Leishmania donovani promastigotes is the main target for CA(1–8)M (1–18), a synthetic cecropin A–melittin hybrid peptide. *Biochemistry Journal* **330**, 453–460 (1998).

89. Patiño-Márquez, I. A., Patiño-González, E., Hernández-Villa, L., Ortíz-Reyes, B. & Manrique-Moreno, M. Identification and evaluation of Galleria mellonella peptides with antileishmanial activity. *Anal Biochem* **546**, 35–42 (2018).

90. Marr, A. K., Cen, S., Hancock, R. E. W. & McMaster, W. R. Identification of synthetic and natural host defense peptides with leishmanicidal activity. *Antimicrob Agents Chemother* **60**, 2484–2491 (2016).

91. Lynn, M. A. *et al.* Effect of BMAP-28 antimicrobial peptides on Leishmania major promastigote and amastigote growth: Role of leishmanolysin in parasite survival. *PLoS Negl Trop Dis* **5**, (2011).

92. Kareshk, A. T. *et al. Host-parasite Responses Outcome Regulate the Expression of Antimicrobial Peptide Genes in the Skin of BALB/c and C57BL/6 Murine Strains Following Hydatic cyst View project Risk factors for anthroponotic cutaneous leishmaniasis View project medical parasitology Host-parasite Responses Outcome Regulate the Expression*

of Antimicrobial Peptide Genes in the Skin of BALB/c and C57BL/6 Murine Strains Following Leishmania major MRHO/IR/75/ER Infection. vol. 13 http://ijpa.tums.ac.ir (2018).

93. dos Santos Cabrera, M. P. *et al.* Interactions of mast cell degranulating peptides with model membranes: A comparative biophysical study. *Arch Biochem Biophys* **486**, 1–11 (2009).

94. Guerrero, E., Saugar, J. M., Matsuzaki, K. & Rivas, L. Role of positional hydrophobicity in the leishmanicidal activity of magainin 2. *Antimicrob Agents Chemother* **48**, 2980–2986 (2004).

95. Mangoni, M. L. *et al.* Temporins, small antimicrobial peptides with leishmanicidal activity. *Journal of Biological Chemistry* **280**, 984–990 (2005).

96. André, S. *et al.* Functional characterization of temporin-she, a new broad-spectrum antibacterial and leishmanicidal temporin-sh paralog from the sahara frog (Pelophylax saharicus). *Int J Mol Sci* **21**, 1–19 (2020).

97. Luque-Ortega, J. R., Hof, W., Veerman, E. C. I., Saugar, J. M. & Rivas, L. Human antimicrobial peptide histatin 5 is a cell- penetrating peptide targeting mitochondrial ATP synthesis in Leishmania. *The FASEB Journal* **22**, 1817–1828 (2008).

98. Saha, A. K., Mukherjee, T. & Bhaduri, A. *Mechanism of action of amphotericin B on Leishmania donovani promastigotes*. *Molecular and Biochemical Parasitology* vol. 19 (1986).

99. Murray, H. W. & Delph-Etienne, S. *Roles of Endogenous Gamma Interferon and Macrophage Microbicidal Mechanisms in Host Response to Chemotherapy in Experimental Visceral Leishmaniasis*. *INFECTION AND IMMUNITY* vol. 68 http://iai.asm.org/ (2000).

100. Verma, N. K. & Dey, C. S. Possible mechanism of miltefosine-mediated death of Leishmania donovani. *Antimicrob Agents Chemother* **48**, 3010–3015 (2004).

101. Paris, C., Loiseau, P. M., Bories, C. & Bréard, J. Miltefosine Induces Apoptosis-Like Death in Leishmania donovani Promastigotes. *Antimicrob Agents Chemother* **48**, 852–859 (2004).

102. Zuo, X. *et al.* Miltefosine induces apoptosis-like cell death in yeast via Cox9p in cytochrome c oxidase. *Mol Pharmacol* **80**, 476–485 (2011).

103. Wadhone, P. *et al.* Miltefosine Promotes IFN-γ-Dominated Anti-Leishmanial Immune Response. *The Journal of Immunology* **182**, 7146–7154 (2009).

104. Murray, H. W., Montelibano, C., Peterson, R. & Sypek, J. P. *Interleukin-12 Regulates the Response to Chemotherapy in Experimental Visceral Leishmaniasis*. https://academic.oup.com/jid/article/182/5/1497/862559 (2000).

105. Basu, J. M. *et al.* Sodium antimony gluconate induces generation of reactive oxygen species and nitric oxide via phosphoinositide 3-kinase and mitogen-activated protein kinase activation in Leishmania donovani-

infected macrophages. *Antimicrob Agents Chemother* **50**, 1788–1797 (2006).

106. Ali Ladram & Pierre Nicolas. Antimicrobial peptides from frog skin: biodiversity and therapeutic promises. *Frontiers in Bioscience- Landmark* **21**, 1341–1371 (2016).

107. Hajishengallis, G. & Russell, M. W. Innate Humoral Defense Factors. in *Mucosal Immunology: Fourth Edition* vols 1–2 251–270 (Elsevier Inc., 2015).

108. Deslouches, B. & Di, Y. P. Antimicrobial peptides with selective antitumor mechanisms: prospect for anticancer applications. *Oncotarget* **8**, 46635–46651 (2017).

109. Spicer, S. K. *et al.* Toward a clinical antifungal peptoid: Investigations into the therapeutic potential of AEC5. *Biopolymers* **110**, (2019).

110. Pichereau, C. & Allary, C. Therapeutic peptides under the spotlight. *EBR - European Biopharmaceutical Review* 88–93 (2005).

111. Bray, B. L. Large-scale manufacture of peptide therapeutics by chemical synthesis. *Nat Rev Drug Discov* **2**, 587–593 (2003).

112. Vlieghe, P., Lisowski, V., Martinez, J. & Khrestchatisky, M. Synthetic therapeutic peptides: science and market. *Drug Discov Today* **15**, 40–56 (2010).

113. Bolt, H. L. *et al.* Exploring the links between peptoid antibacterial activity and toxicity. *Medchemcomm* **8**, 886–896 (2017).

114. Luo, Y. *et al.* Peptoid Efficacy against Polymicrobial Biofilms Determined by Using Propidium Monoazide-Modified Quantitative PCR. *ChemBioChem* **18**, 111–118 (2017).

115. Fox, J. L. Antimicrobial peptides stage a comeback. *Nat Biotechnol* **31**, 379–382 (2013).

116. Wagner, D. & Young, L. S. Nontuberculous mycobacterial infections: A clinical review. *Infection* **32**, 257–270 (2004).

117. Culf, A. S. Peptoids as tools and sensors. *Biopolymers* **110**, (2019).

118. Wender, P. A. & al., et. The design, synthesis, and evaluation of molecules that enable... *Proc Natl Acad Sci U S A* **97**, 13003–13008 (2000).

119. Huang, W., Seo, J., Lin, J. S. & Barron, A. E. Peptoid transporters: effects of cationic, amphipathic structure on their cellular uptake. *Mol Biosyst* **8**, 2626 (2012).

120. Eggimann, G. A., Bolt, H. L., Denny, P. W. & Cobb, S. L. Investigating the anti-leishmanial effects of linear peptoids. *ChemMedChem* **10**, 233–237 (2015).

121. Bolt, H. L., Eggimann, G. A., Denny, P. W. & Cobb, S. L. Enlarging the chemical space of anti-leishmanials: A structure-activity relationship study

of peptoids against: Leishmania mexicana, a causative agent of cutaneous leishmaniasis. *Medchemcomm* **7**, 799–805 (2016).

122. Grundmann, F. *et al.* Antiparasitic Chaiyaphumines from Entomopathogenic Xenorhabdus sp. PB61.4. *J Nat Prod* **77**, 779–783 (2014).

123. Previdi, D. *et al.* Synthesis and antileishmanial activity of some functionalized peptoids. *J Braz Chem Soc* **30**, 1334–1340 (2019).

2. Naturally occurring peptides

2.1 Peptide natural products

Natural products (NPs) are chemical entities produced by living organisms. They are biosynthesised by complex metabolic pathways and in many cases they perform a function that aids a host organisms' survival.[1,2] In this latter role NPs are known as 'secondary metabolites', i.e. metabolites not directly necessary for the survival of the host. NPs can often display multiple biological activities many of which are mediated via interactions with different proteins inside the cell.[3] Given this NPs have evolved to have optimum interactions with a range of biological macromolecules or targets, and, as such, they can display a very high selectivity for a given target.[4]

Given the aforementioned properties, NPs represent an excellent source of biologically validated scaffolds for the design and development of new drug entities.[5] Thus, medicinal chemists often look to target not only the synthesis of bioactive NPs themselves, but also libraries of structurally related compounds for biological evaluation.[6] The desire to modify the original NP structure is driven by the pursuit of improving key pharmacokinetic or pharmacodynamic properties (e.g. chemical stability or lipophilicity).[7,8]

2.1.1 Antiparasitic Chaiyaphumines

In 2014 Grundmann *et al*.[4] successfully isolated a novel family of natural products, called the Chaiyaphumines (**Figure 2.1**), from entomopathogenic *Xenorhabdus* bacteria (*PB61.4)*, which was isolated from nematodes of the genus *Steinernema websteri.*

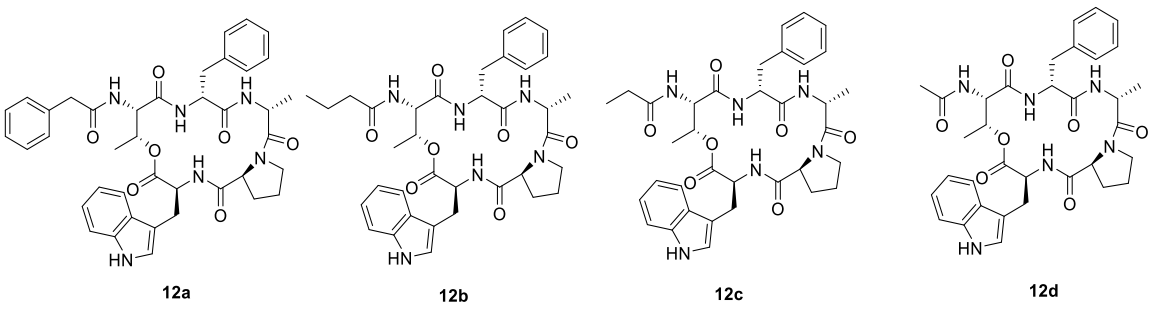

Figure 2.1. Isolated natural Chaiyaphumines **12a-12d**.

The isolated Chaiyaphumines were tested for activity against *Trypanosoma brucei rhodesiense, Trypanosoma cruzi*, and *Plasmodium falciparum*, and their toxicity against mammalian L6 cells was also determined. Chaiyaphumines **12a** and **12c** in particular were found to have promising biological activity in the assays carried out (**Table 2.1**).

Table 2.1 Bioactivity of **12a** and **12c** against different protozoa and cytotoxicity (IC_{50} in μM)[a]. Table adapted from Grundmann *et al*.[5]

Natural Chaiyaphumines	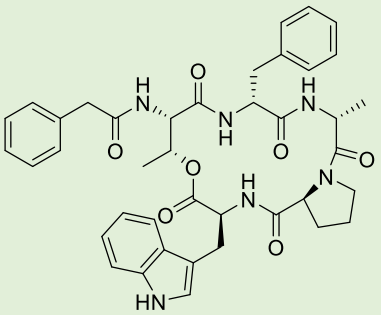 **12a**	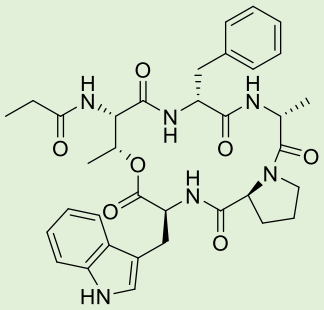 **12c**	**Ref**
T. brucei rhodesiense STIB900	5.11	77.58	0.01
T. cruci Tulahuen C4	56.4	98.94	1.73
P. falciparum NF 54	0.61	15.4	0.006
mammalian L6 cells	92.25	>151	0.02

[a]The positive reference (Ref) compounds used is different for each target organism. It is melarsoprol for *Trypanosoma brucei rhodesiense*, benznidazole for *Trypanosoma cruzi*, chloroquine for *Plasmodium falciparum* NF 54, and podophyllotoxin for mammalian L6 cells.

To confirm their chemical structure and to investigate the relationship between Chaiyaphumine structure and antiparasitic activity, a total synthesis of these compounds was undertaken previously by the Cobb group (Unpublished). A set of analogues in which the ester bond in the peptide macrocycle was replaced by an amide was also synthesised as part of this initial work (**Scheme 2.1**).

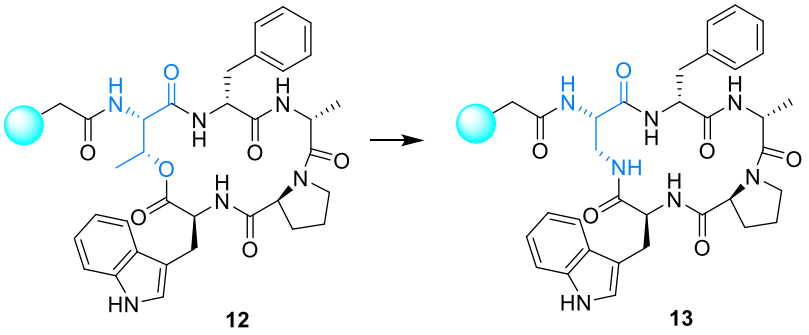

R= Ph (a), Et (b), c (Me), d (H)

Scheme 2.1. Lactone linkage replaced by a lactam highlighted in blue.

After the total synthesis of the four amide and natural Chaiyaphumines, the samples were assayed by Dr Marcel Kaiser at the Swiss Tropical and Public Health Institute, where the bioassays reported in the literature were repeated. This allowed direct comparison between the synthesised materials and the literature-reported natural Chaiyaphumines. The amide analogues that were prepared were also sent for bioactivity testing to evaluate whether the amide linkage modification had affected the biological behaviour of this class of compound. The results obtained from this work are shown in **Table 2.2**.

Table 2.2 Antiparasitic Activity and Cytotoxicity of Synthetic Chaiyaphumines and Lactam Analogues[a]

Compound		IC_{50} (μM)				
		T. b. rhodesiense	***T. cruzi***	***P. falciparum***	***L. donovani*[a]**	**Mammalian L6 cells**
Natural Chaiyaphumine	**12a**	7.96 (5.11)	9.01 (56.4)	2.96 (0.61)	>10	>10 (92.25)
	12c	60.9 (77.58)	90.0 (98.94)	21.6 (15.4)	>100	>100 (>151)
Amide Chaiyaphumine analogues	**13a**	61.4	76.7	2.87	>100	>100
	13b	7.00	8.67	4.7	>10	>10
	13c	5.93	8.18	>5	>10	>10
	13d	63.1	79.5	>50	>100	>100
Ref [b]		0.01 (0.01)	1.91 (1.73)	0.004 (0.006)	0.127	0.016 (0.02)

Literature values for the naturally isolated compounds published previously are shown in brackets.[2] [a]Axenic amastigotes. [b]Melarsoprol (*T. b. rhodesiense*), benznidazole (*T. cruzi*), chloroquine (*P. falciparum*), miltefosine (*L. donovani*) or podophyllotoxin (mammalian L6 cells).

Regarding the amide analogues (**13a**-**13d**), it is interesting to note that, while they showed similar potent antiparasitic activity, they exhibited an inverse biological profile (compared to the natural compounds) with respect to the nature of the N-terminal capping moiety. In fact, low micromolar activity (6-9 μM) was demonstrated for aliphatic amide analogues **13b** and **13c**, whereas phenylacetyl **13a** exhibited negligible activity against *T. b. rhodesiense* and *T. cruzi*. These results highlight the importance of the ester bond in modulating Chaiyaphumine antiparasitic activity, and they demonstrate the potential that the Chaiyaphumines offer as a peptide scaffold for the development of new antiparasitic agents (**Figure 2.2**).

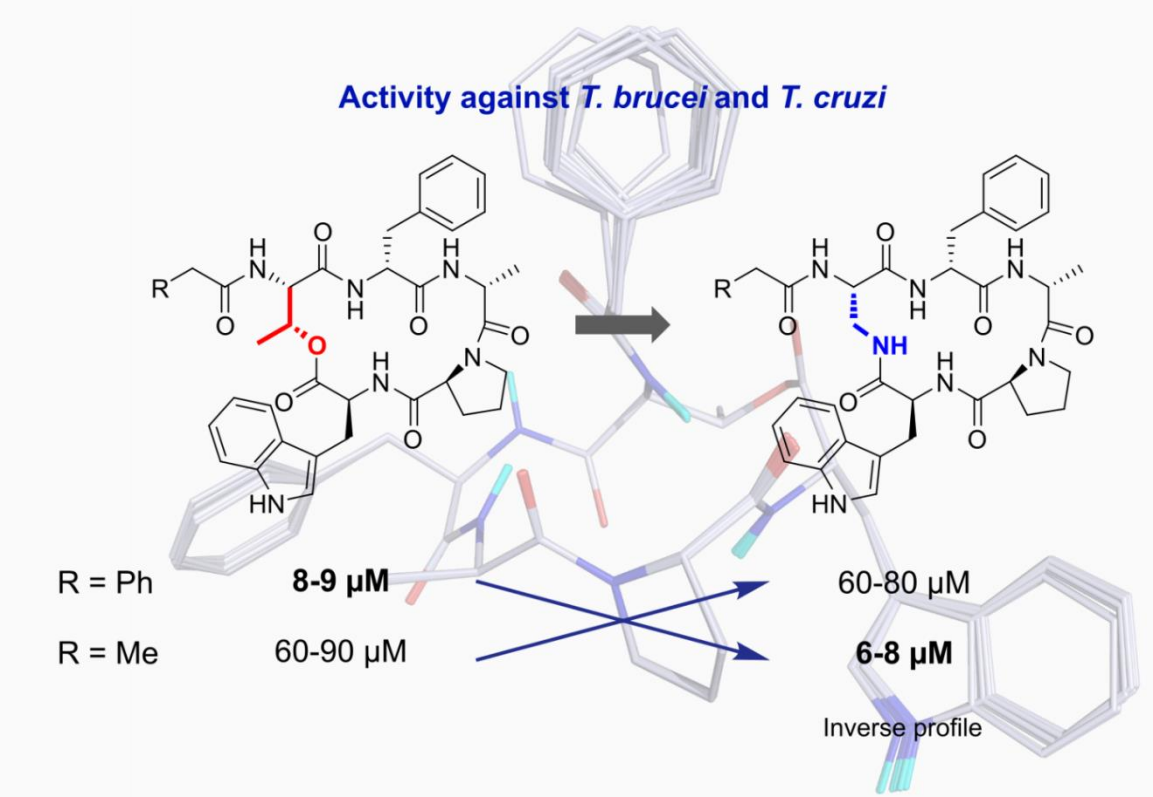

Figure 2.2. Antiparasitic activity of synthetic Chaiyaphumines analogues.

2.1.2 Chapter aims

The primary aim of this project is to resynthesise the Chaiyaphumines (natural and amides) while looking to improve the overall synthetic routes to them. With the targets obtained, crystallography studies will be carried out to have a better understanding of their mechanism of action, and also to probe the structural differences between the ester and amide rings.

After an optimised total synthesis is developed, an alanine scan will be carried out on one or more of the most active compounds to help determine the residues that are critical for biological activity.

2.2 Synthesis of Natural Chaiyaphumines

The first step in the synthesis of the target cyclic peptides is the preparation of the linear peptide precursors. To begin with, the linear precursor peptides were synthesised by Fmoc solid-phase peptide synthesis (SPPS) on 2-chlorotrityl chloride resin. They were

then subjected to different acetylation reactions before the linear peptides were cleaved from the resin, as detailed in **Section 6.3.1**. The substituent group (R) is phenyl in the case of Chaiyaphumine **12a**, and ethyl in the case of Chaiyaphumine **12b**. The general planned synthetic procedure for the synthesis **12a** and **12b** is shown in **Scheme 2.2**.

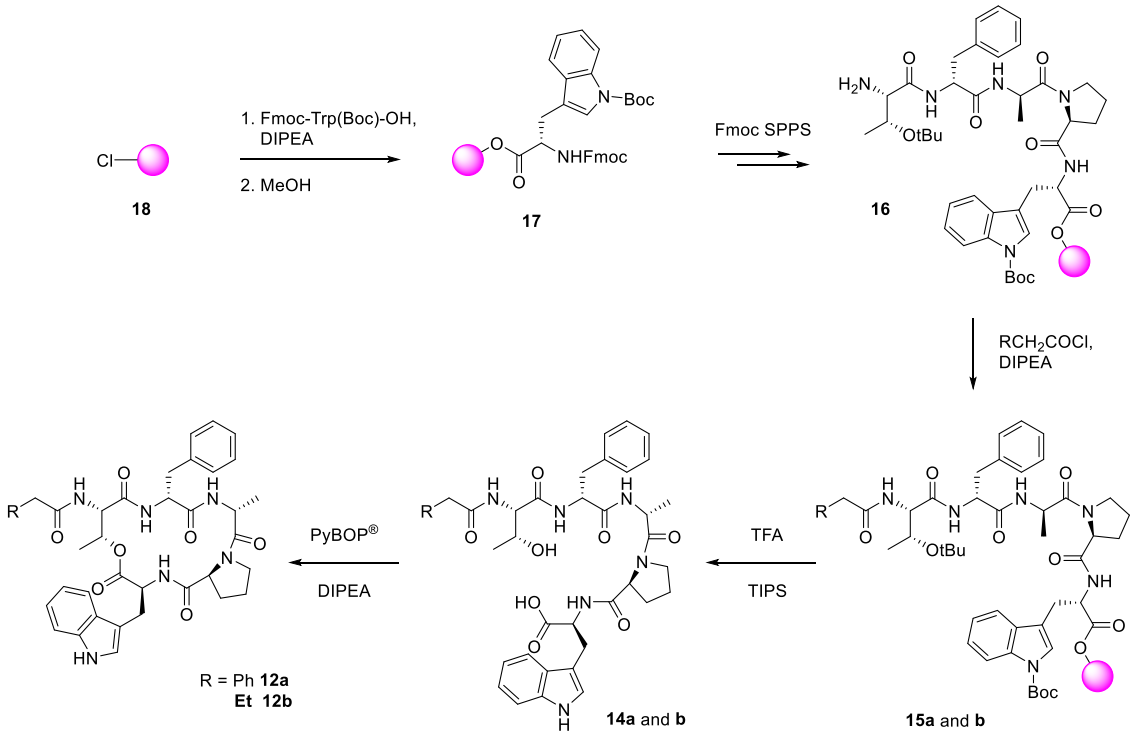

Scheme 2.2. An overview of the general synthetic plan to access the natural Chaiyaphumines **12a** and **12b**.

2.2.1 Synthesis of Linear Peptide Precursors

The synthesis of the linear peptide precursors for **12a** and **12b** was initially carried out on a 0.1 mmol scale. 2-Chlorotrityl chloride resin was pre-swollen for 1 h in DMF, followed by the addition of Fmoc-Trp(Boc)-OH (1 equiv) and DIPEA (5 equiv) in DMF (2 × 1 h). After washing with 5 portions of DMF, the resin was capped via treatment with MeOH (15 min). The swelling was repeated in DMF for at least 1 h before continuing with the synthesis. After loading of the resin, a small amount was separated and deprotected with 20 % piperidine in DMF and washed with the same solvent. It was washed twice with ether. Once dried, a Kaiser test was carried out.

A Kaiser test [1,9] was performed to determine if the resin was fully loaded or not. Since the resin was found not to be fully loaded (as indicated by the dark blue colour), another attempt to load the resin was carried out. This was achieved with DCM, which made the first step faster than the previously utilised protocol (**Scheme 2.3**). Thus, the esterification was higher than in DMF.[10,11] Firstly, the remaining resin was pre-swelled in DCM and the loading was carried out in the same solvent. Secondly, the resin was washed with five portions of DCM and the resin was capped with MeOH for at least 15 min. Finally, it was washed with five portions of DMF for it to be MeOH-free. It was pre-swelled in DMF for at least 30 minutes before the Fmoc SPPS. This optimised protocol is detailed in **Section 6.3.1**.

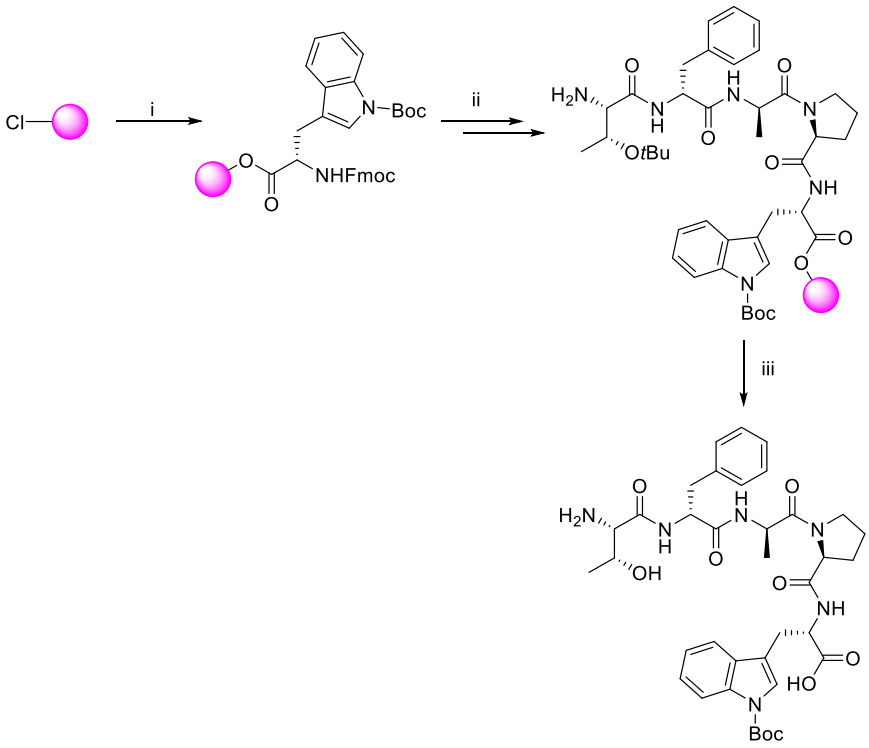

Scheme 2.3. Synthesis of the linear precursor pentapeptide. Reagents and conditions: (i) Fmoc-Trp(Boc)-OH, DIPEA, DCM, RT, 2 × 1 h; cap with MeOH, 15 min; swell in DMF, 1 h; (ii) SPPS (General Experimental Procedure **5.3.1**); (iii) TFA: water: TIPS (95:0.5:0.5), RT, 4h.

[1] A Kaiser test is a colour test to monitor completeness of amino acid coupling in Solid Phase Peptide Synthesis (SPPS) and Solid Phase Organic Synthesis (SPOS). An intensive blue colour is generated by reaction of ninhydrin with free primary amines. The test can be used to monitor the presence of free amine after deprotection (dark blue colour) and the completeness of the amino acid coupling step (yellow colour). The test is routinely applied qualitatively and quantitatively.

2.2.2 Natural Chaiyaphumines

To begin with, the linear peptide precursor (**14a**, **Scheme 2.2**) for **12a** was prepared using the general method (see **Section 6.3.1**), the N-terminal acylation was carried out with phenylacetyl chloride. The resin was washed twice with DCM, then it was shrunk in Et_2O to remove any excess DCM in preparation for the cleavage, using the general protocol outlined in **Section 6.3.2**. However, before carrying out the resin cleavage, a test cleavage was undertaken to confirm the presence of the desired precursor (see **Section 6.3.2**). Having prepared the test cleavage sample, the mass spec sample was submitted, and the spectra obtained is shown in **Figure 2.3**.

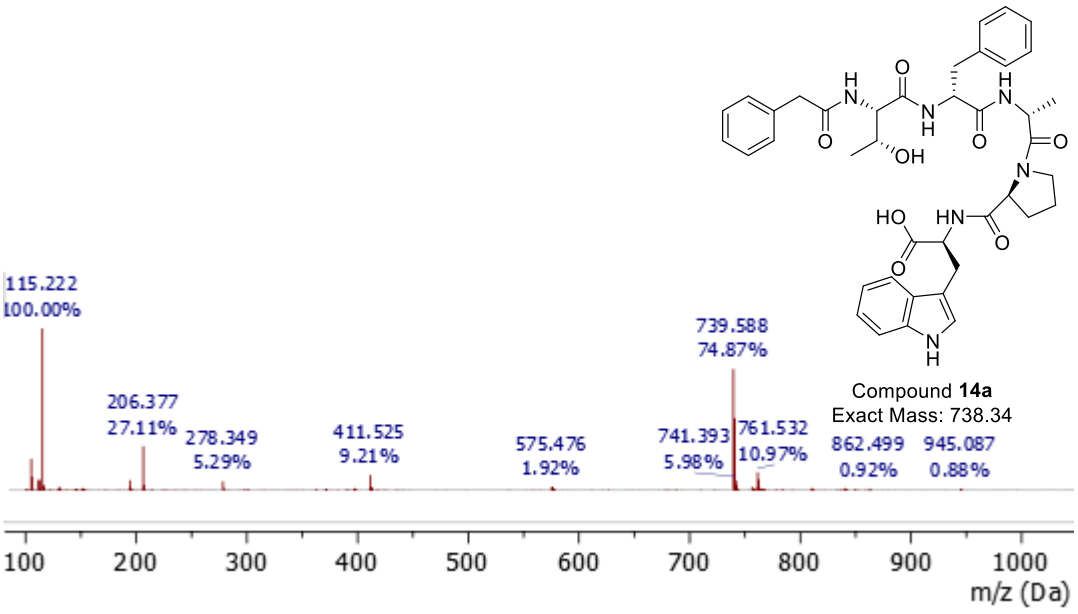

Figure 2.3. ESI LCMS viewed in positive mode, indicating the presence of compound **14a**.

Having confirmed the presence of the linear precursor (peak at *m/z* = 739.588), the loaded resin was stored overnight at -4 ˚C. The resin cleavage was carried out and the lyophilised product was an orange powder. The resulting product was characterised by LC-MS to confirm the presence of the desired linear precursor (**14a**) and it was stored at -16 ˚C prior to the cyclisation step (see **Section 6.3.1**).

The same synthetic procedure was then carried out with R= Et to give the linear precursor **14b** (**Scheme 2.2**). Full experimental details for the preparation of **14b** can be found in **Section 6.3.1**.

2.2.3 Synthesis of the Target Cyclic Peptides

Cyclisation of the linear peptide precursors

Initially, as previously reported by Dr Sam Lear, (PhD student in the Cobb Group),[12] the cyclisation of the linear precursor peptide **14a** was carried out in a solution at high dilution using a final peptide concentration of 1 mg/mL (**Table 2.3, Entry 1**).

The required total volume of MeCN was calculated for each peptide, and a minimum volume of DMF was taken to dissolve the crude linear precursor to avoid the removal of the solvent under vacuum. This solution was added dropwise over a period of 2 h to a stirred solution of PyBOP® (3.0 equiv) and DIPEA (6.0 equiv) in the remaining volume of MeCN, and the reaction mixture was stirred for a further 3 h (**Table 2.3**, **Entry 1**). The same procedure was carried out with different reagents (**Table 2.3**, **Entries 2-3**). Finally, the cyclisation reaction was carried out without any base (**Table 2.3**, **Entry 4**).

Cyclic peptide **12a** proved impossible to separate from the tripyrrolidinophosphine oxide by-product, that was produced during PyBOP® mediated ester bond formation in the cyclisation step (**Table 2.3, Entry 1**). They were found to co-elute during HPLC purification (procedure outlined in **Section 6.2.6**). This is shown in LC-MS spectra, **Figure 2.4**.

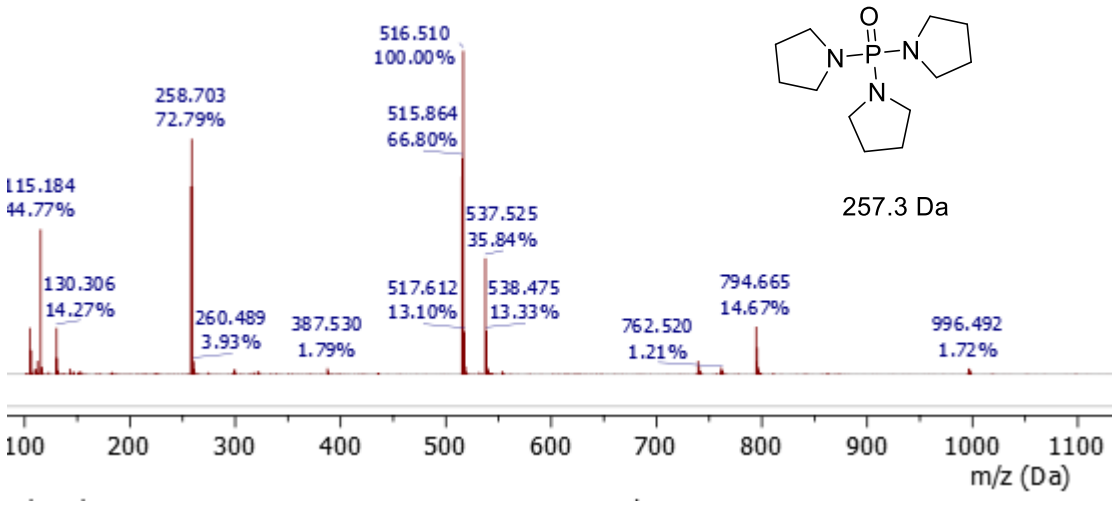

Figure 2.4. ESI LCMS viewed in positive mode, indicating the presence of the by-product PyBOP® at 258 *m/z*.

Due to the challenges in purification, the cyclisation step was therefore repeated using the coupling reagents HOBt and DIC, although this resulted in a second impurity (*m/z* = 863.60) that also proved impossible to remove from the final product (**Table 2.3**, **Entries 2-3**). Purification was carried out according to protocol **6.2.6**,it was non quantitative The by-product was hypothesised to result from the capping of the linear peptide by DIC (due to the initial large excess of the activator under the conditions used), thus preventing cyclisation.

While the synthesis of **12b** also initially produced a similarly impure product, the subsequent optimisation of the reaction and cleavage conditions, using syringe pump control with DIC/HOBt activation, significantly improved product quality (**Table 2.3, Entry 5**). In particular, syringe pump control allowed the formation of the desired product **12b** while avoiding intramolecular reactions due to high dilution conditions. Followed by purification step according to protocol **6.2.6**. A fully described protocol of compound **12b** can be found in **Section 6.3.3**.

Table 2.3 Cyclisation of Natural Chaiyaphumines

Entry	Starting material (SM)	SM scale (mmol)	Reaction conditions	*m/z* (Da)	Comment
1		0.007	PyBOP DIPEA MeCN: DMF 90:10	739.53	No product observed
2		0.007	PyBOP HOBt H_2O DIPEA MeCN: DMF 90:10	739.53	No product observed
3		0.007	DIC HOBt H_2O DIPEA MeCN: DMF 90:10	739.53	No product observed
4	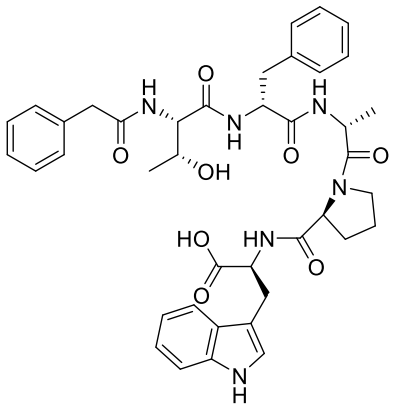 Compound **14a** Exact Mass: 738.34	0.001	DIC HOBt H_2O DCM anh.	721.48	Cyclised peptide **12a** formed
		0.013	DIC HOBt H_2O DCM anh.	721.48	Cyclised peptide **12a** formed
		0.015	DIC HOBt H_2O DCM anh.	721.48	Cyclised peptide **12a** formed*
5	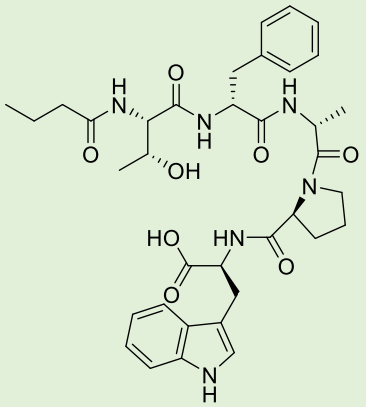 Compound **14b** Exact Mass: 690.34	0.0015	DIC HOBt H_2O DCM anh.	673.49	Cyclised peptide **12b** formed
		0.0015	DIC HOBt H_2O THF anh.	673.49	Cyclised peptide **12b** formed
		0.0015	DIC HOBt H_2O THF anh. 66 ˚C	673.49	Cyclised peptide **12b** formed
		0.007	DIC HBOt.H_2O THF anh. 70 ˚C	673.49	Cyclised peptide **12b** formed*

*RP- HPLC purification conditions flow rate = 2-2.2 mL min^{-1}; linear gradient elution 0–100% solvent B over 80 minutes, then 50–100% B over 15 minutes (solvent A = 0.1% TFA in 95% H_2O, 5% MeCN, solvent B = 0.1% TFA in 5% H_20, 95% MeCN). Relevant fractions were collected, lyophilized and analysed by LC-MS.

2.3 Synthesis of the Chaiyaphumines Amide Analogues

Having improved the cyclisation step and the purification process for the preparation of the natural products (**12a-12b**, see **Section 2.2.2**), it was decided to use these conditions to prepare the amide analogues. For the cyclisation step it was proposed to start without any base present and then, if necessary, to use DIPEA (**Scheme 2.4**), as they had worked well in the preparation of **12a** and **12b.**

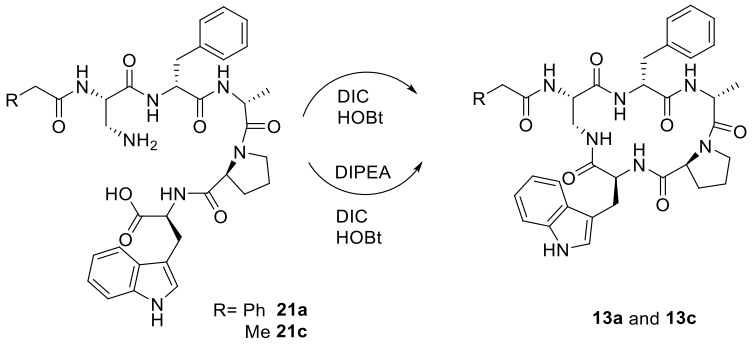

Scheme 2.4. Proposed general cyclisation step of a linear amide precursor to give **13a** and **13c**

2.3.1 Chaiyaphumine Amide 13a

The required linear peptide precursor **21a** was synthesised on a 0.1 mmol scale, as described in **Section 6.3.5**, and capped with phenylacetyl chloride, before undergoing resin cleavage and deprotection, as described in detail in **Section 6.3.2**. The linear precursor **21a** was obtained and characterised, as described in **Chapter 6**.

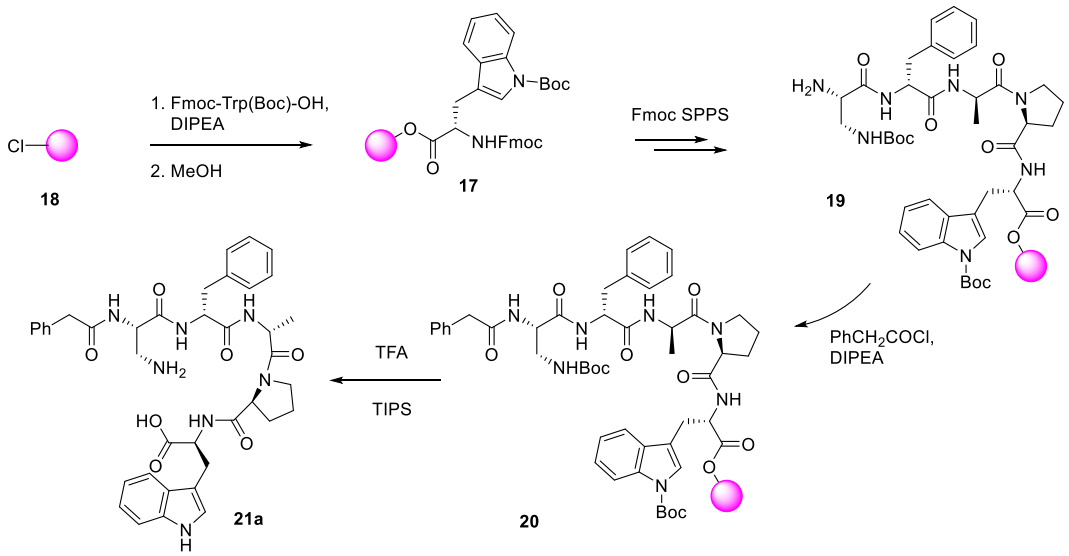

Scheme 2.5. Synthesis of the linear precursor amide analogue **21a**.

2.3.2 Cyclisation of amide linear precursor 21a

The solution phase cyclisation of 5 mg of the linear precursor **21a** was carried out according to the procedure outlined in **Section 6.3.3** and was attempted in two different solvents, MeCN and THF (**Scheme 2.6**). Different solvent conditions for the cyclisation (ester formation) had been reported before by Gholap *et al*.[13] during their preparation of Chaiyaphumine A.

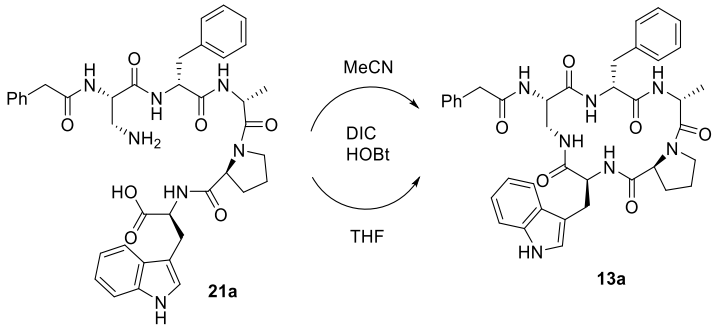

Scheme 2.6. Proposed cyclisation step of linear amide precursor **21a** to give amide analogue **13a**.

Cyclisation I

The linear precursor, compound **21a**, was dissolved in 5 mL of MeCN and stirred for 10 min at room temperature. However, its solubility in MeCN was not as good as with the other natural linear peptide precursor **14a**.

HOBt (3 equiv.) were added and the mixture was stirred until the total dissolution of this reagent, after 5 min 3 equiv. of DIC was added. The reaction was then stirred for 4 hours at room temperature until a 50 µL aliquot was separated for LC-MS and HPLC analysis, which showed that the starting material was still present. The reaction was therefore stirred at room temperature overnight. Another sample was prepared with 50 µL of the reaction mixture in a 50:50 H_2O/MeCN solution and the LC-MS and HPLC analysis was repeated. Several peaks were observed in the analytical HPLC spectra but importantly no starting material was present.

Sample preparation for purification was carried out via addition of 5 mL of water to the mixture. The sample was centrifuged, and the supernatant was purified. With a final peptide concentration of approximately 0.5 mg/mL of a 50:50 H_2O/MeCN solution, a reversed-phase HPLC purification of the crude material was carried out.

Three major peaks were shown in the analytical reverse phase HPLC trace. They were separated and analysed using LC-MS. The first and last peaks were found to contain a compound with the mass of the product (**13a**) (*m/z* =706.82). The second and major peak in the HPLC trace was shown to contain an unknown impurity with a *m/z* = 820.42.

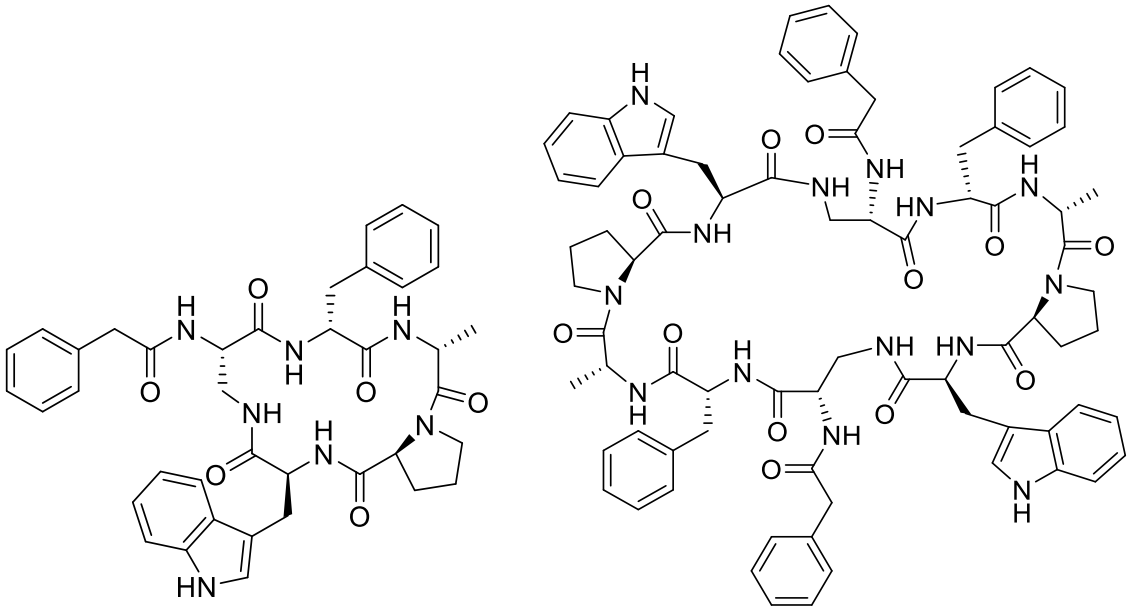

13a
Exact mass: 705.33 Da
m/z=706.82
$[M+H]^+$

22a
Exact mass: 1410.65 Da
m/z=706.33
$[M+2H]^{2+}$

Figure 2.5. Cyclic monomer **13a** and its dimer **22a**, which is formed as a by-product.

It was assumed that one of the HPLC fraction peaks with *m/z*= 706.82 was the desired product, and the other could potentially be a dimer of it with a $[M + 2H]^{2+}$ (**Figure 2.5**). An accurate mass of both samples was carried out and confirmed the first peak to be the desired product (**13a**), and the other peak to be the cyclic dimer (**22a**) as pictured in **Figure 2.6**.

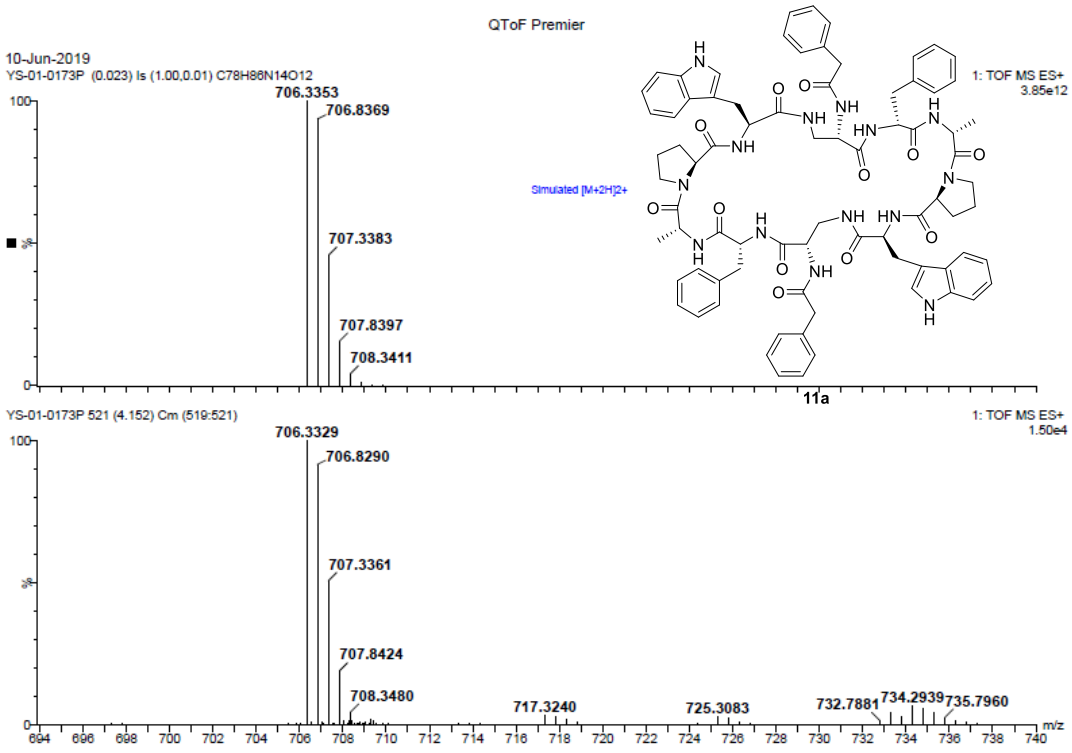

Figure 2.6. Accurate mass spectrum of the dimer (compound **22a**). The molecular ion is annotated, and peaks are attributed with a 0.5Da of the distance between them showing the difference between it and the monomer.

Cyclisation II

Another attempt at the amide cyclisation was carried out using THF as the solvent. Here 5 mg (1 equiv.) of compound **21a** was dissolved in 5 mL of dry THF at room temperature in a closed vial with N_2 to maintain the inert atmosphere. 3 equiv. of HOBt was added and the mixture was stirred until 3 equiv. of DIC was added. The reaction was then stirred for 4 hours, at which time a 50 µL aliquot was removed for an LC-MS and HPLC analysis. It was shown that in both the MS and analytical HPLC spectra the starting material was still present. The reaction was therefore left to stir overnight at room temperature. Another sample was prepared with 50 µL of the reaction mixture in a 50:50 H_2O/MeCN solution.

The crude reaction mixture was dissolved with 5 mL of a 50:50 H_2O/MeCN solution for the purification step. The sample was centrifuged several times and the supernatant with a concentration of approximately 0.5mg/mL was purified. However, an unknown impurity proved impossible to separate from the desired product even with longer HPLC run times

(e.g. 60 - 110 min). Given the challenges with HPLC purification it was decided to carry on with the protocol shown in the first reaction with MeCN as the selected solvent – (**Cyclisation I**).

Optimisation of the Cyclisation

A scaled-up reaction was carried out with 10 mg (0.01192 mmol) of **21a** in order to optimise the HPLC purification step of the cyclisation reaction. The reaction was carried out using the reaction conditions detailed in **Cyclisation I**. An analysis of the crude reaction mixture by LC-MS showed that the product had been obtained, along with some of the unwanted dimer (**22a**). The crude reaction mixture was purified using reverse phase HPLC and concentration of 0.5 mg/ mL of compound per injection. Unfortunately, the same impurity peak with a *m/z*=820.42 was found to be present in the fractions that contained the desired cyclic peptide. A range of different HPLC programmes were investigated and the product was isolated with a suitable purity using a longer HPLC run time (e.g. 80 min programme details are given in **Section 6.2.6**). The analytical HPLC analysis of the isolated pure product **13a**,according to procedure **6.2.5**, is shown in **Figure 2.7**.

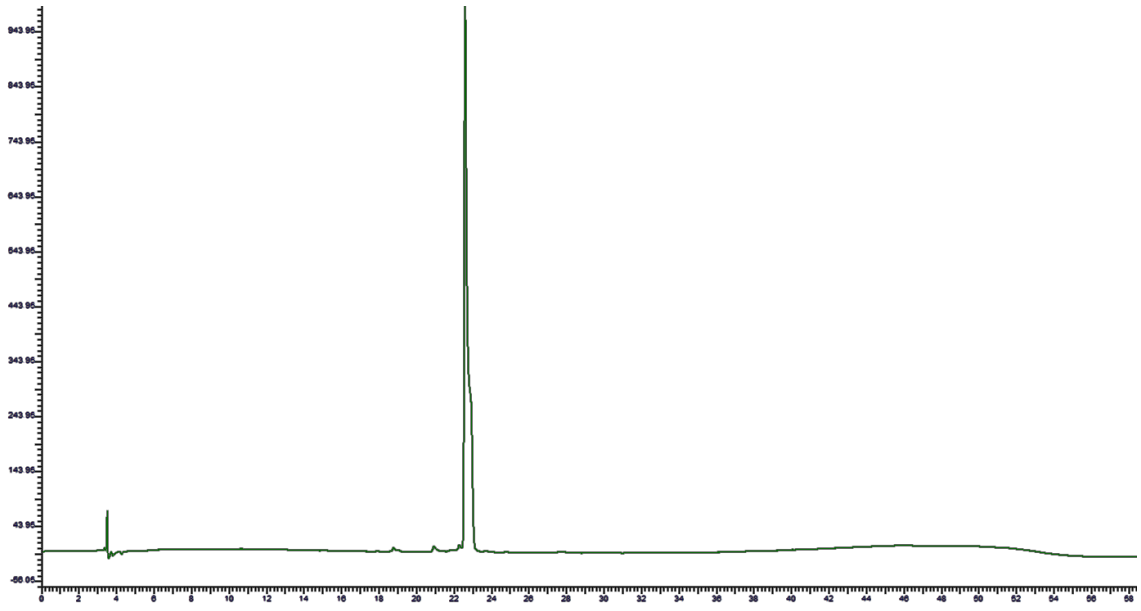

Figure 2.7 Analytical HPLC chromatogram (λ= 220 nm) of final compound **13a**.

A second large-scale reaction was carried out using 19.10 mg (0.02278 mmol) of compound **21a**. The scale-up showed that increasing the reaction scale seemed to lead to more dimer (**22**) formation. This could simply be an issue with the concentration of the linear precursor in the cyclisation reaction mixture. Furthermore, the unwanted by-product (*m/z*= 820.42) was also still present (**Figure 2.8**).

Having used up all of the linear peptide precursor **21a** in the initial investigations of the cyclisation and purification step, more starting material was prepared. Compound **21a** was re-synthesised on a 0.2 mmol scale according to the protocol detailed in **Section 6.3.6**.

Having access to more of the linear peptide precursor **21a** also allowed the cyclisation to be carried out again on a larger scale. To this end, the cyclisation (using **Cyclisation I** conditions), with 20 mg of compound **21a**, was carried out on a 0.02 mmol scale**.** However, an analytical HPLC analysis of the crude product showed that an impurity next to each of the major peaks was present (**Figure 2.8**). An LC-MS analysis showed that the desired product was the peak at 22.8min (*m/z*= 706.51), and two unknown impurities present at 22.4 min (*m/z*= 684.43) and at 25.0 min (m/z=820.42). The different purification conditions used to separate these peaks can be found in **Table 2.4**.

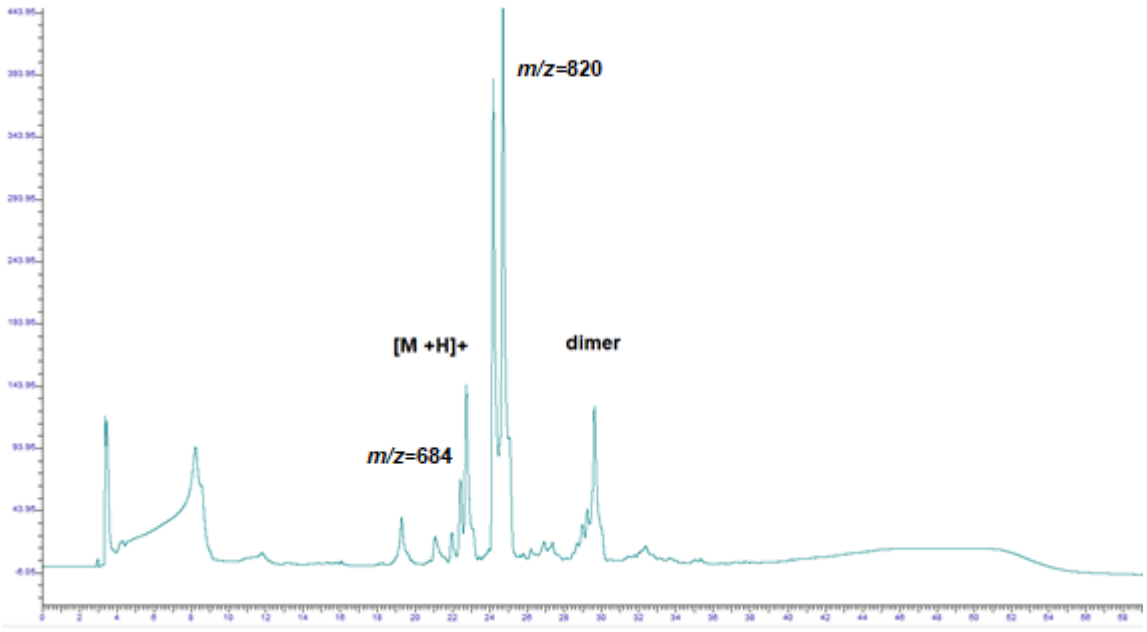

Figure 2.8. Analytical HPLC chromatogram (λ= 220 nm) of crude cyclisation reaction.

After the first purification of the entire crude reaction obtained from the with 20 mg (0.02 mmol) of starting material **21a** (**Table 2.4, Entry 1**) the resulting peptide **13a** was deemed not to be pure enough. Another attempt was made not only for purification optimisation but also to see if this impurity could be separated or not since the retention time is less than a minute with the desired product. Secondly, a smaller scale (0.007 mmol) attempt was made to see if this impurity could be separated or not. Thus, 7 mg of linear precursor **21a** were cyclised under the same reaction conditions, but under really diluted purifications conditions. In this way, several injections could be done during the purification step while analysing them simultaneously (**Table 2.4, Entry 2**). Once the conditions were optimised, another reaction was set up again in a 0.02 mmol scale (**Table 2.4, Entry 3**).

Table 2.4 Purification optimisation step of amide analogue **13a**.

Entry	Reagents	Purification conditions	Isolated Compound 13a Purity based on analytical HPLC*
1	Compound **21a** (1 equiv.) HOBt.H_2O (3 equiv.), DIC (3 equiv.)	10 mg/mL cc Linear gradient elution 0- 100 % B Flow: 2 mL min^{-1} 80 minutes	70% pure
2	Compound **21a** (1 equiv.) HOBt.H_2O (3 equiv.), DIC (3 equiv.)	1 mg/mL cc Linear gradient elution 20- 100 % B Flow: 2-2.2 mL min^{-1} 80-120 minutes	70-90% pure
3	Compound **21a** (1 equiv.) HOBt.H_2O (3 equiv.), DIC (3 equiv.)	5 mg/mL cc Linear gradient elution 20- 100 % B Flow: 2.2 mL min^{-1} 80 minutes	90% pure

*Analytical HPLC chromatogram after purification according to protocol **6.2.5**. Relevant fractions were collected, lyophilized and analysed by LC-MS.

Even though product **13a** was pure enough, the reaction conditions were still not ideal since the major peak is still an impurity, with *m/z* = 820.42 (**Figure 2.8**). As the starting material (compound **21a**) has a free amine instead of a hydroxyl group (compound **14a**),

it was hypothesised that the linear peptide **21a** could have been protonated. In fact, the major peak could be an adduct that belongs to the starting material that is not being cyclised. Furthermore, as the resin cleavage is carried out with TFA, this could mean that the free amine is forming an adduct as an acid salt. The free amine from the amide bond (**Figure 2.9A**, highlighted in red) is meant to be reacting with the COOH group from the C-terminal Trp (**Figure 2.9A**, highlighted in green). If the amine is protonated it is no longer available to do this (**Figure 2.9B**). If this were the case, then the addition of more base to the reaction mixture should solve this problem.

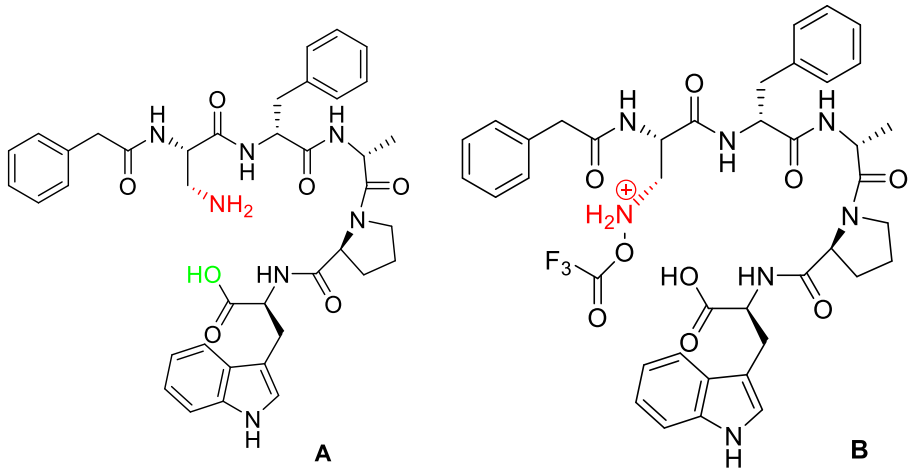

Figure 2.9. Starting material – Linear peptide (**21a**) under acidic cleavage conditions.

To begin with, reactions were set up with only three equivalents of DIPEA as a base. After monitoring the reaction, it was left overnight since it is a slow reaction (**Table 2.5, Entry 1**). Secondly, another reaction was carried out under the same conditions. Moreover, an HPLC sample was prepared of the reaction crude and its trace showed the same result as before. Thus, more base was added (**Table 2.5, Entry 2**). Finally, a scale-up reaction was carried out with 0.034 mmol of linear peptide **21a**. Subsequently, the peptide was dissolved in MeCN with a final concentration of 1 mg/mL, DIPEA was added, and, at least 30 minutes later, the coupling reagents were added too. The chosen conditions are shown in **Table 2.5, Entry 3**.

Table 2.5 Cyclisation conditions for linear peptide **21a**.

Entry	Reagents	Conditions	Isolated Compound 13a
1	Compound **21a** (1 equiv.) HOBt.H_2O (3 equiv.), DIC (3 equiv.) DIPEA (3 equiv.)	Overnight Room temperature	No material isolated
2	Compound **21a** (1 equiv.) HOBt.H_2O (3 equiv.), DIC (3 equiv.) DIPEA (3 equiv.) x2	Overnight Room temperature Starting material is still present DIPEA addition 42 ˚C Overnight	70-90% pure*
3	Compound **21a** (1 equiv.) DIPEA (20 equiv.) HOBt.H_2O (3 equiv.), DIC (3 equiv.)	1. DIPEA addition x30 minutes 2. reagents	95% pure*

*Analytical HPLC chromatogram after purification according to protocol **6.2.5**. Relevant fractions were collected, lyophilized and analysed by LC-MS.

Finally, amide analogue **13a** was obtained with the conditions displayed in **Table 2.5**, **Entry 3**. The analytical HLPC trace of peptide **13a** shows that its purity is now 95% (**Figure 2.10**) and its full characterisation can be found in **Section 6.3.6**.

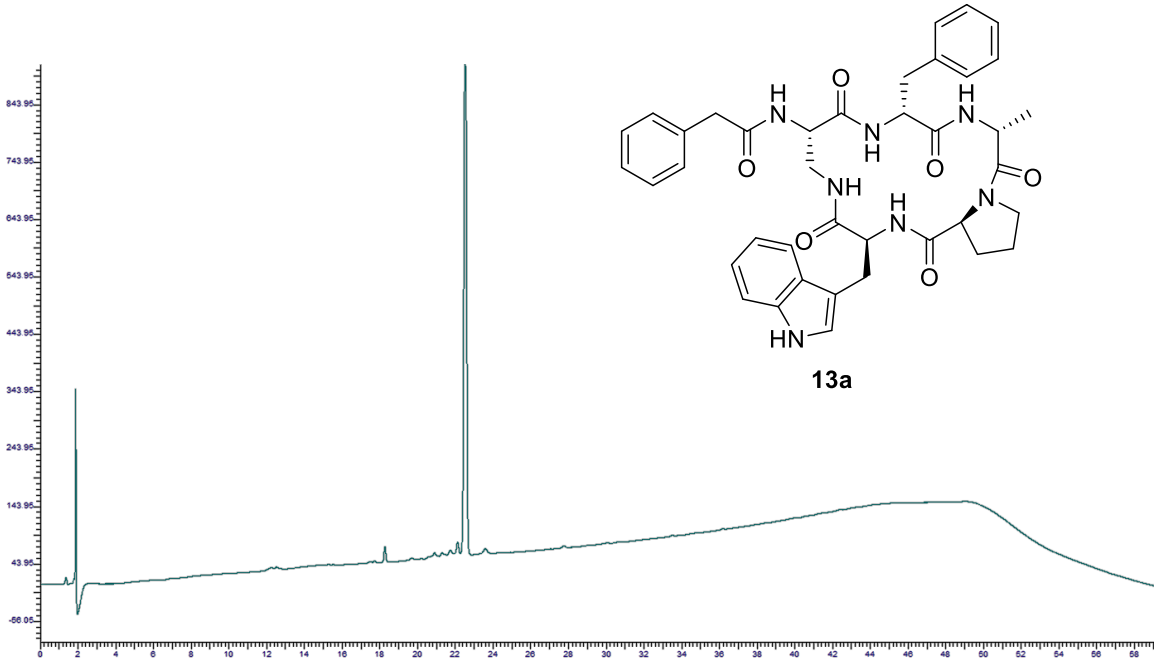

Figure 2.10. Analytical HPLC chromatogram (λ= 220 nm) of cyclic amide peptide **13a**.

Chaiyaphumines Amide 13c

The linear peptide sequence **21c** was synthesised on a 0.1 mmol scale, as described in **Section 6.3.5**, and capped with propionyl chloride, before undergoing resin cleavage and deprotection, as described in **Section 6.3.2**.

Initially, it was decided to try both cyclisation protocols outlined in **Scheme 2.4**. To begin with, the cyclisation of compound **21c** was carried out without base, and only HOBt and DIC, in a ratio of 1:3:3 equiv., were used. Following the initial protocol, the cyclisation reaction was carried out with 10 mg (0.1287 mmol) of starting material **21c**. After 1.5 h, a 20 µL aliquot was separated for a 200 µL 50:50 H_2O/MeCN mass spec sample. LC-MSanalysis of the crude sample showed that no starting material present was present and that full conversion to a product with *m/z* = 644.19 (assigned to $[M+H]^+$) had occurred. Purification was carried out according to the protocol detailed in **Section 6.2.6** Unfortunately, after characterisation, an accurate mass determined that it was not the desired product but actually a dimer with $[M + 2H]^{2+}$.

Finally, the optimised protocol for compound **13a** was used for the synthesis of **13c**. The cyclisation step was carried out as before with linear peptide **21c** as the starting material (**Table 2.5**, **Entry 3**). The final characterisation of product peptide **13c** can be found in **Section 6.3.5**.

2.4 Alanine Scan of Chaiyaphumines

The cyclic peptide **13a** was selected for an initial alanine scan since it had been the easiest to purify using reverse-phase HPLC. The alanine scan peptides of **13a** that were successfully prepared are shown below in **Table 2.6**. The full experimental procedures used for the synthesis of cyclic peptides **23** to **25** are outlined in **Section 6.3.7**.

It is interesting to note that compound **25** (**Table 2.6, Entry 3**) has no proline residue in its sequence. Given this, it was thought that the cyclisation of this linear peptide might prove to be problematic, but actually, the cyclization reaction worked very well.

Finally, all compounds were purified by reverse phase HPLC using slightly different conditions in each case. The successful isolation of these analogues can be seen in **Table 2.6**. The full details regarding the synthesis and characterisation of these peptides are given in **Section 6.3.7**.

Table 2.6 Alanine scan characterisation.

Entry	Isolated Compound	*m/z*	Analytical HPLC trace*
1	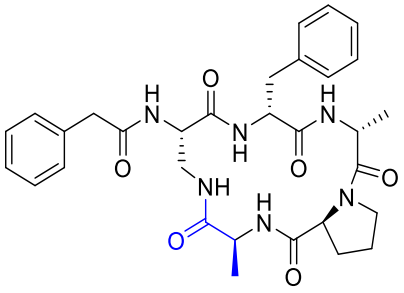 **23** 590. 2 Da	591.27	
2	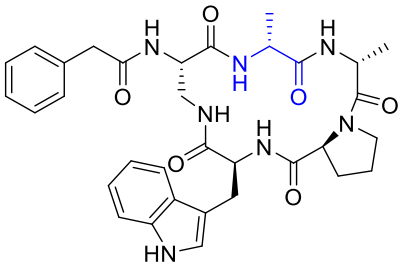 **24** 629.3 Da	630.33	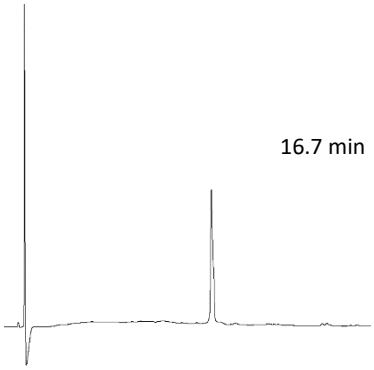
3	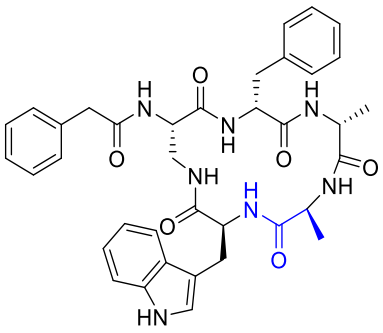 **25** 679.3 Da	680.30	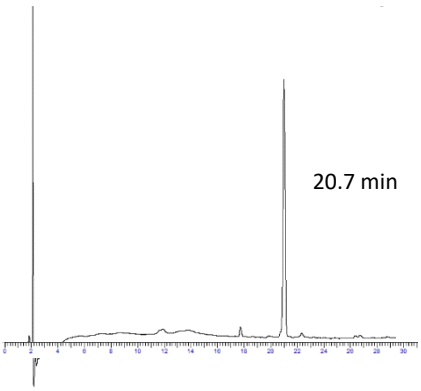

*Analytical HPLC chromatogram after purification according to protocol **6.2.6**. HPLC trace: absorbance recorded at 220 nm, gradient 0-100% B over 40 min, as indicated (A = 5:95:0.05 *v/v%* MeCN/H_2O/TFA; B = 95:5:0.03 *v/v%* MeCN/H_2O/TFA).

2.5 Chapter Summary

A series of natural products known as Chaiyaphumines were studied with the primary aim of successfully synthesising these biologically active cyclic peptides more efficiently. In

addition to this, a set of analogues, in which the ester bond in the peptide macrocycle was replaced by an amide, were also synthesised (**Scheme 2.1**).

While this work was ongoing a paper was published by Batel *et al*.[14] In this work they compared the macrolactonization and macrolactamization approaches for the total synthesis of the natural Chaiyaphumines (**Figure 2.11**). Within their findings, they describe the challenges of the macrolactonization step and suggest another linear precursor approach in order to obtain the desired lactone containing natural peptide.

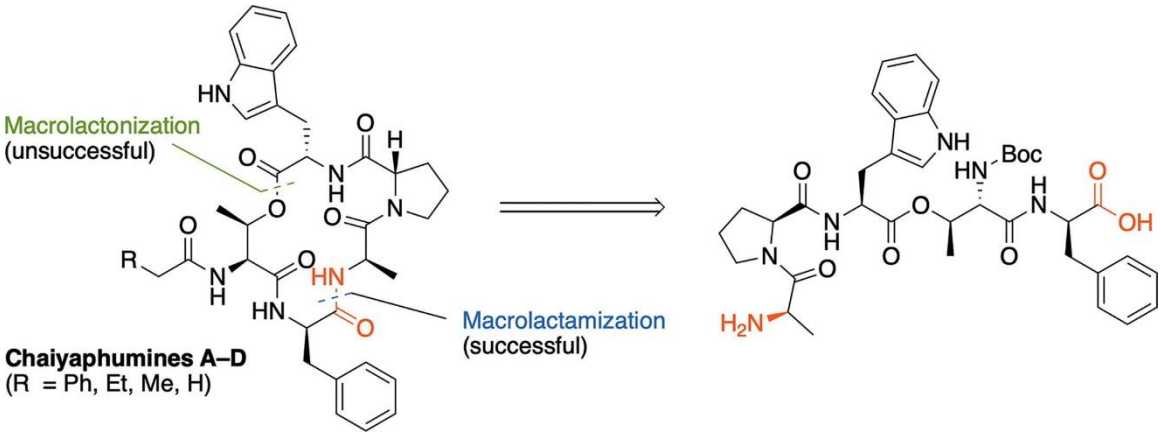

Figure 2.11. Macrolactonization and macrolactamization approaches of the total synthesis of the natural Chaiyaphumines adapted from Batey *et al*. [14]

Firstly, in the Batey work different macrolactonization conditions compared to what we had pursued were investigated, including the use of MNBA (2-methyl-6-nitrobenzoic anhydride) as an esterification precursor. [15] The use of lanthanide additives was found to improve macrolactonization for pentadepsipeptide ring formation in their previous work on cyclic acyldepsipeptide, also known as ADEPs.[15] The attempted macrolactonization conditions failed and as such a macrolactamization was carried out with the linear *N*-Boc protected peptide precursors as shown in **Figure 2.11**. Chaiyaphumines **12a-12d** were purified by column chromatography and HPLC. They were fully characterised by NMR analysis and an X-ray structure of Chaiyaphumine **12d** was obtained. X-ray analysis was

something that had been attempted on the compounds prepared in this chapter, but we had been unable to obtain suitable crystals for structural characterisation.

Secondly, comparing both works, Batey *et al*.[14] proposed a total synthesis approach and structural analysis of natural Chaiyaphumines as antimalarial compounds. Based on previous work done in the Cobb group, natural Chaiyaphumines **12a** and **12c** showed antiparasitic activity with the parasites responsible of sleeping sickness and chagas disease (NTDs). On this work, we proposed an optimization of the natural unstable cyclic peptides and successfully prepared Chaiyaphumine amide analogues which proved to maintain their biological activity (**Figure 2.2**).

Due to time restraints during the COVID-19 pandemic it was not possible to do a detailed NMR analysis on the Chaiyaphumine lactam analogues that were obtained, and this is an area for future investigation (**Chapter 5**). Ideally, we would like to compare the NMR analysis of our Chaiyaphumine lactam analogues to the natural occurring ester peptides reported by Batey *et al*.[14] in order to get a better understanding of our previously obtained biological results.

Overall, a series of natural Chaiyaphumines (esters) and Chaiyaphumine analogues (amide) were prepared on a small scale, optimized and then scaled up. Some of the compounds prepared have previously shown antiparasitic activity against a range of different protozoa (See **Section 2.1.1**). We are now looking to test all of the cyclic peptides prepared against *Leishmania mexicana, Leishmania amazonensis and Leishmania major* as this has not yet been attempted. Moreover, we will also look to test the alanine scan peptides for activity against other NTDs. Peptides will be tested against the parasites responsible for both Chagas disease (via collaborations in the GCRF NTD network – Silber lab USP) and African sleeping sickness (Marcel Kaiser). Having these alanine scan peptides tested against *T. cruzi* and *T. brucei rhodesiense* will help to established if any of the amino acids within the sequence are crucial for antiparasitic activity. Understanding this will allow further libraries of this class of peptide to be prepared.

2.6 References

1. Lovering, F., Bikker, J. & Humblet, C. Escape from flatland: Increasing saturation as an approach to improving clinical success. *J Med Chem* **52**, 6752–6756 (2009).

2. Firn, R. D. & Jones, C. G. Natural products ? a simple model to explain chemical diversity. *Nat Prod Rep* **20**, 382 (2003).

3. Maplestone, R. A., Stone, M. J. & Williams, D. H. The evolutionary role of secondary metabolites — a review. *Gene* **115**, 151–157 (1992).

4. Grundmann, F. *et al.* Antiparasitic Chaiyaphumines from Entomopathogenic Xenorhabdus sp . PB61.4. *J Nat Prod* **77**, 779–783 (2014).

5. Lachance, H., Wetzel, S., Kumar, K. & Waldmann, H. Charting, Navigating, and Populating Natural Product Chemical Space for Drug Discovery. *J Med Chem* **55**, 5989–6001 (2012).

6. Jayaseelan, K. V., Moreno, P., Truszkowski, A., Ertl, P. & Steinbeck, C. Natural product-likeness score revisited: an open-source, open-data implementation. *BMC Bioinformatics* **13**, 106 (2012).

7. Athar, M., Sona, A. N., Bekono, B. D. & Ntie-Kang, F. Fundamental physical and chemical concepts behind ‘drug-likeness’ and ‘natural product-likeness’. *Physical Sciences Reviews* **4**, 1–18 (2019).

8. Ertl, P., Roggo, S. & Schuffenhauer, A. Natural Product-likeness Score and Its Application for Prioritization of Compound Libraries. *J Chem Inf Model* **48**, 68–74 (2008).

9. E. Kaiser, R. L. C., C. D. B. and P. L. C. Color Test for Detection of Free Terminal Amino Groups in the Solid-Phase Synthesis of Peptides. *Short communications* 595 (1970).

10. Chazti, K. B. O., Gatos, D. & Stavropoulos, G. 2-Chlorotrityl chloride resin: Studies on anchoring of Fmoc-amino acids and peptide cleavage. *Int J Pept Protein Res* **37**, 513–520 (1991).

11. Hoekstra, W. The 2-Chlorotrityl Resin a Worthy Addition to the Medicinal Chemists Toolbox. *Curr Med Chem* **8**, 715–719 (2001).

12. Lear, S. Total Synthesis of Bioactive Peptides and Whole Proteins. (Durham University, 2016).

13. Gholap, S. S. & Ugale, S. R. A Total Synthesis of the Cyclic Depsipeptide Chaiyaphumine-A. *ChemistrySelect* **2**, 7445–7449 (2017).

14. Lu, H. & Batey, R. A. Total synthesis of chaiyaphumines A-D: A case study comparing macrolactonization and macrolactamization approaches. *Tetrahedron Lett* **108**, (2022).

15. Shiina, I. An adventurous synthetic journey with MNBA from its reaction chemistry to the total synthesis of natural products. *Bull Chem Soc Jpn* **87**, 196–233 (2014).

3. Antimicrobial peptides

3.1 Temporins

The Temporin peptides were selected as a class of AMPs for further study as activity had previously been reported for members of this family, e.g. Temporins A, 1Sa, and L, against *Leishmania mexicana*, *Leishmania donovani*, and *Leishmania pifanoi* species.[1] An extensive family of Temporins had also previously been tested at concentrations of 50 μM and 100 μM against both *L*. *mexicana* parasite forms, amastigotes and promastigotes (Dr F. Chadbourne, Cobb Group **Figure 3.1**). *L*. *mexicana*, is a causative agent of cutaneous leishmaniasis (CL) and is the main parasite species of interest in the Cobb group.[2]

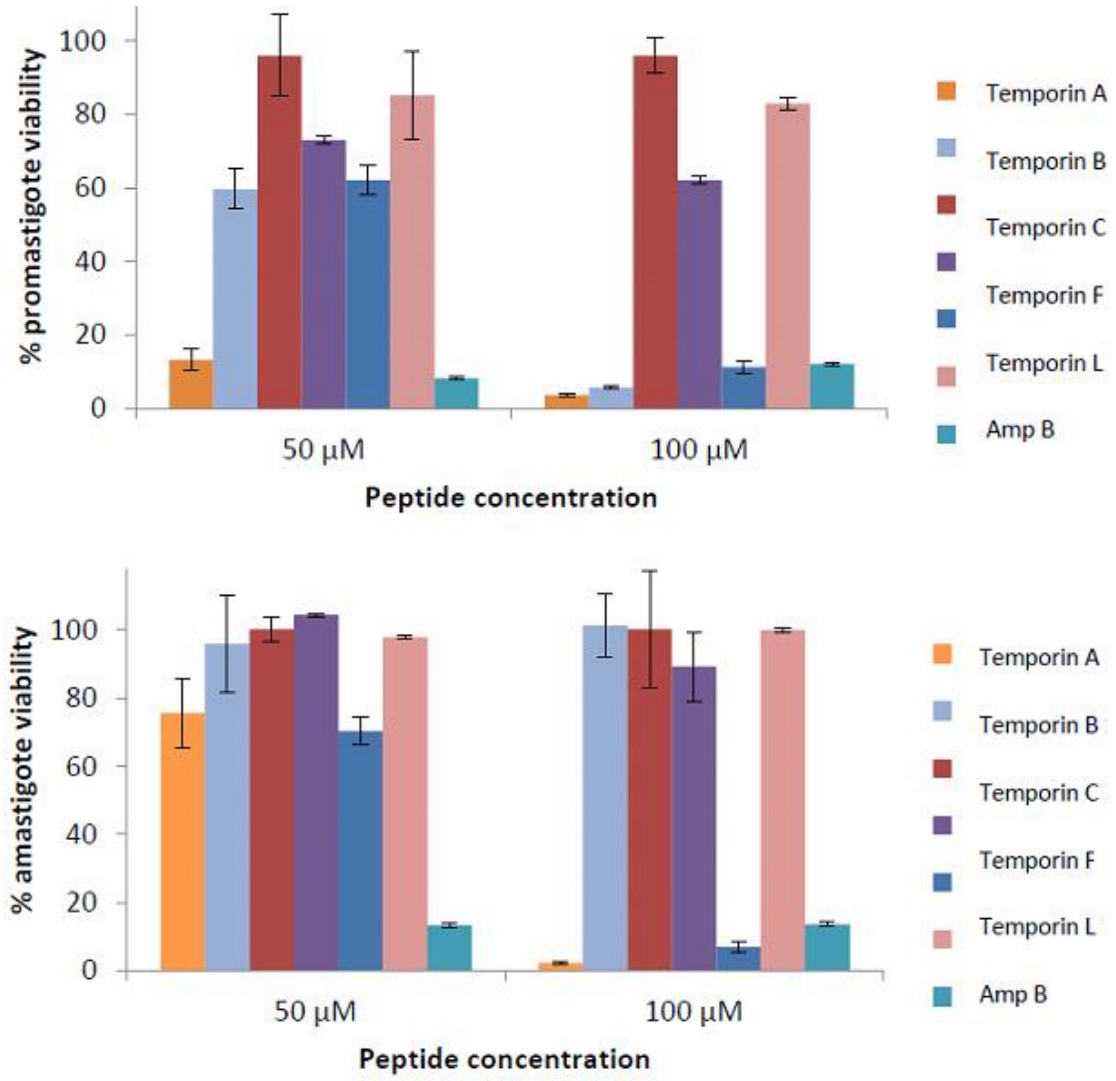

Figure 3.1. Graphs showing % promastigote and amastigote viability, respectively, following a 24-hour incubation period with peptides at 50 µM and 100 µM.[2]

While some AMPs present additional mechanisms of action against parasites, the Temporin peptides appeared to act via cell membrane permeation, see **Section 1.4.4**.[3] Given the complexity associated with altering cell membrane structure the chance of parasite resistance emerging rapidly to this class of peptides is relatively low. Direct and indirect AMPs mechanisms of action have been described in **Section 1.4.3**.

The investigation's initial aims were to synthesise a focused library of selected Temporin peptides and then screen these peptides for activity against *L. mexicana* parasites. The

target peptides selected were based on the previous results obtained by Dr F. Chadbourne (Cobb Group, PhD), see **Table 3.1**. Alanine scan results indicate that there are no residues within the natural Temporin A (**Table 3.1**, **Entry 1**) sequence that are suitable for further modification to enhance the antileishmanial activity. The only one which showed a slightly antiparasitic activity is shown in **Table 3.1**, **Entry 2**. Lysine and alanine scans of Temporin L indicate that the nature of positively charged residues in the sequence of Temporin L affects the antileishmanial activity of the peptide. Removal of a charged residue from Temporin L (a peptide with reported antibacterial and antileishmanial activity) does appear to reduce antileishmanial activity. However, in this study, there was not sufficient time to determine if this also affects the haemolytic activity as a relatively high haemolytic activity of natural Temporin L currently prevents this peptide from being developed as a therapeutic agent.

Table 3.1. Antiparasitic activity of Temporins and their analogues

Entry	Peptide sequence	Known biological activity	*L. mexicana* activity (%cell viability)		Rationale for selection
			Promastigotes	Amastigotes	
1	Temporin A* FLPLIGRVLSGIL-NH_2	Gram+, Virus, Chemotactic	57% at 100 µM 63% at 12.5	23% at 12.5 µM 98% at 100	Temporin A cytotoxic to murine macrophages (RAW 264,7 line) at 500 µM[1,4]
2	Temporin A analogue TA3 FLALIGRVLSGIL-NH_2		71% at 200 µM		
3	Temporin B* LLPIVGNLLKSLL-NH_2	Gram +	38% at 50 µM		
4	Temporin 1Sa* FLSGIVGML GKLF-NH_2	Gram +			
5	Temporin C LLPILGNLLNGLL-NH_2	Gram +	Inactive against both lifecycle stages.		
6	Temporin F FLPLIGKVLSGIL-NH_2	Gram+	Inactive against both lifecycle stages.		
7	Temporin L FVQWFSKFLGRIL-NH_2	Gram+ & Gram-, Fungi, Mammalian cells, Cancer cells		60% cell viability at 50 µM and 10% at 100 µM respectively	Temporin L to be cytotoxic to RAW 264.7 cells at 250 µM Better results in amastigotes than in promastigotes. Temporin L possesses high toxicity against erythrocytes.[5]
8	Temporin analogue TL10 FVQWFSKFLARIL-NH_2		22%	20%	
9	Temporin analogue TL11 FVQWFSKFLGAIL-NH_2		20%	20%	

3.1.1 Aims

The AMPs shown in **Table 3.1** will be prepared and screened for activity against *L. mexicana*. Firstly, it would be interesting to prepare Temporin A and B since they are the most common ones to optimize, if necessary, the experimental conditions with the other

peptides. Once obtained, purification conditions will be optimized in order to have a consistent protocol for each peptide. Secondly, we will prepare the remaining Temporin peptides from **Table 3.1** using Automated SPPS. Some of these peptides have previously been prepared using manual Fmoc SPPS (e.g. Temporin L and Temporin 1Sa).[1] Given COVID, we sought to optimize an automated SPPS approach that could then be used to rapidly access second generation analogues.

3.1.2 Peptide synthesis

The peptides shown in **Table 3.1** were prepared via Fmoc SPPS using a CEM microwave automated peptide synthesizer (**Chapter 6**, **Section 6.4.2**). They were prepared on a 0.1 mmol scale (130 mg of Rink Amide AM resin). Fmoc amino acids (5.0 equiv. with respect to the resin) were coupled using HOBt (5.0 equiv. with respect to the resin), DIC (10.0 equiv. with respect to the resin), and the CEM Microwave (10 min, 20 W, 75 ◦C). Fmoc deprotection was carried out using piperidine 20%, DMF, and the CEM microwave (3 min, 20W, 75 ◦C). Final peptide cleavage was achieved as detailed in **Section 6.4.1**. Temporin A, primary structure FLPLIGRVLSGIL-NH_2 was synthesized using the general Fmoc-SPPS procedure outlined in **Scheme 3.1**. The synthesis was carried out on a 0.1 mmol scale and microwave-assisted peptide couplings were used (See **Experimental Section 6.4.1**).

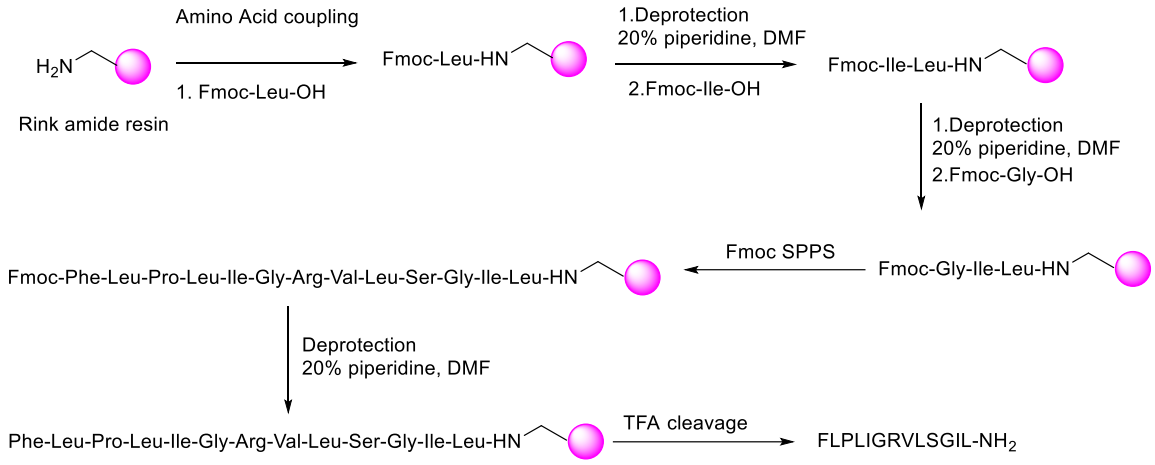

Scheme 3.1. General Fmoc-SPPS synthesis approach applied for the formation of Temporin peptides. The sequence shown in the reaction scheme is for Temporin A. The following protected AA were used Fmoc-Ser(tBu)-OH and Fmoc-Arg(Pbf)-OH.

Initially, the synthesis of Temporin A was carried out to test the reaction conditions, with a well-known peptide, that had also previously been prepared within the group (Dr Frances Chadbourne, Cobb Group).[2] Following the SPPS protocol, a test cleavage was carried out and a 20 µL aliquot was separated for a 200 µL 50:50 H_2O/MeCN mass spec sample. LC-MS analysis of the sample, viewed in positive mode, showed a peak with *m/z*= 699.788 which can be assigned to Temporin A $[M+2H]^{2+}$ providing conformation that the peptide had been made (**Figure 3.2)**. The analytical HPLC trace of the crude Temporin A peptide crude is shown in **Figure 3.3**, proving the impurity of the resulting crude in multiple peaks to separate, apart from a shoulder next to the desired peak, in the crude mixture by RP-HPLC. The crude peptide was lyophilised and then stored at -16 °C before purification.

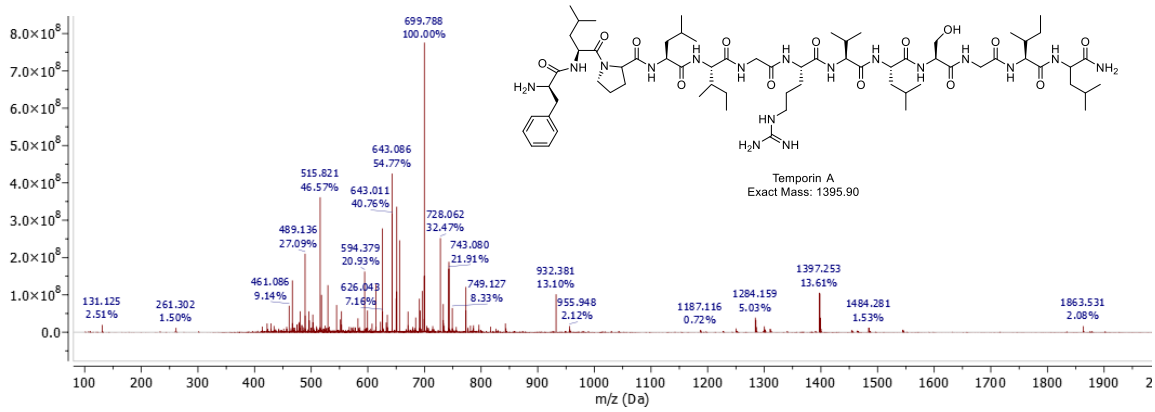

Figure 3.2. ESI LCMS viewed in positive mode, with analysis of the test cleavage of Temporin A

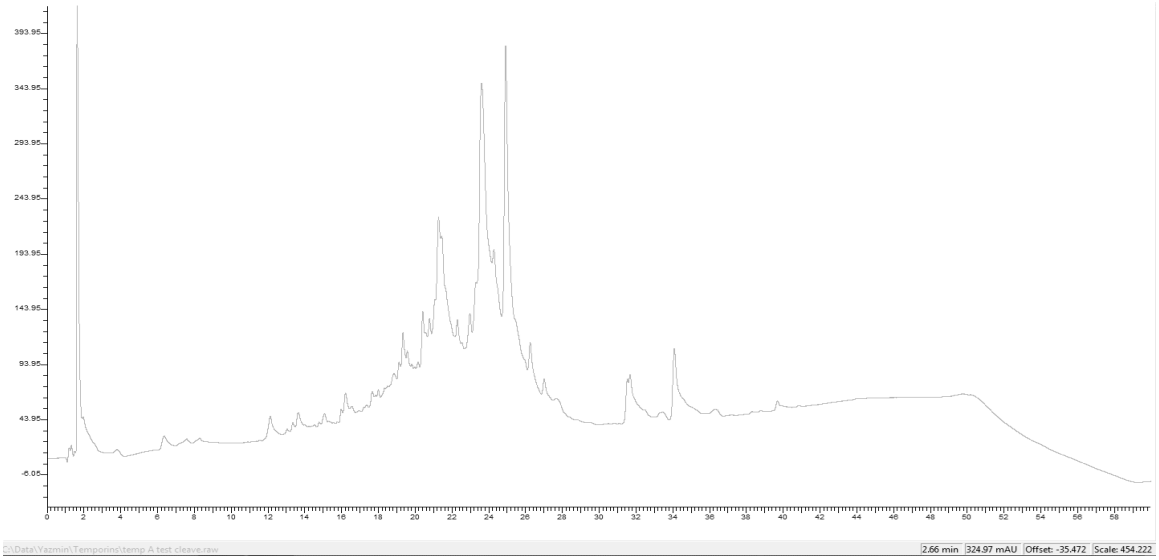

Figure 3.3. Analytical HPLC chromatogram (λ= 220 nm) of the test cleavage of Temporin A.

Temporin B showed a cleaner crude analytical HPLC trace, so it was decided to purify this analogue, to begin with (**Figure 3.4**). The purification of Temporin B would also be used to set up a general purification method for all of the Temporin peptides synthesized.

Temporin B purification was carried out by RP-HPLC according to general procedure **Section 6.2.6**. Fractions were isolated and identified to isolate the desired product. As expected from the HPLC analytical trace, shown in **Figure 3.4**, the majority peak was indeed Temporin B with an elution time of around 26 min. The LC-MS sample showed a peak with *m/z*= 697.580 assigned to $[M+2H]^{2+}$ as shown in **Figure 3.5**. Moreover, the analytical HPLC trace showed the purity of this natural peptide (**Figure 3.6**).

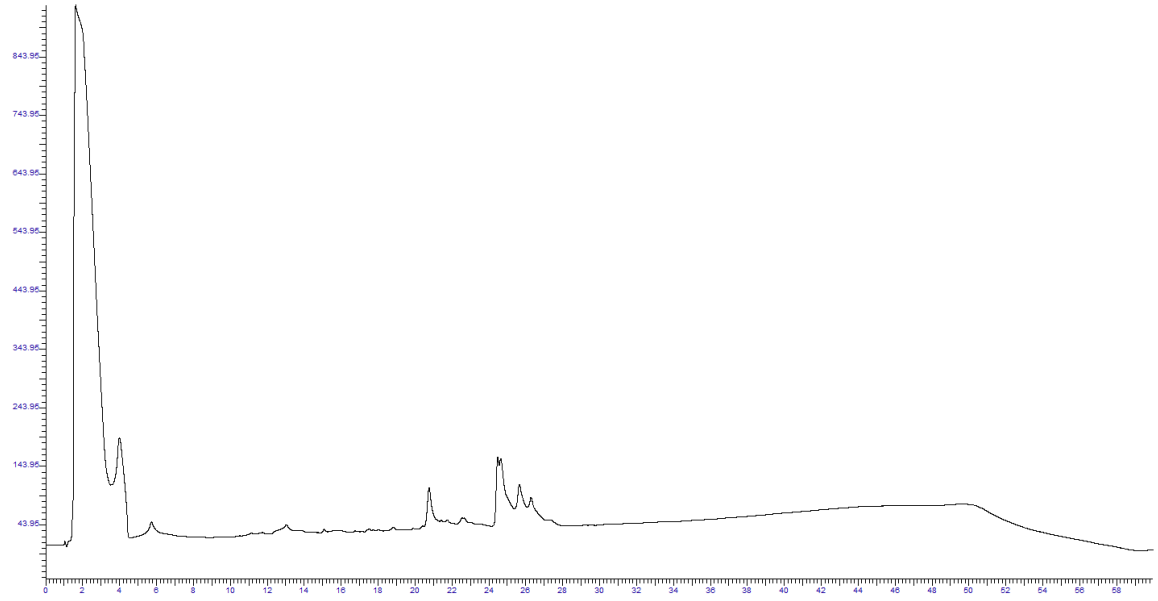

Figure 3.4. Analytical HPLC trace of the test cleavage of Temporin B.

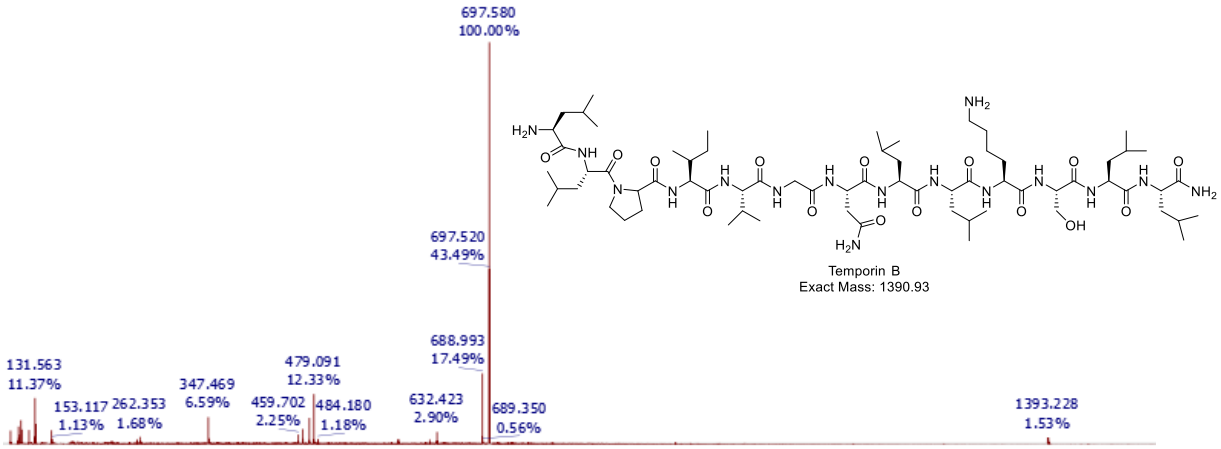

Figure 3.5. ESI LCMS was viewed in positive mode, indicating the presence of Temporin B.

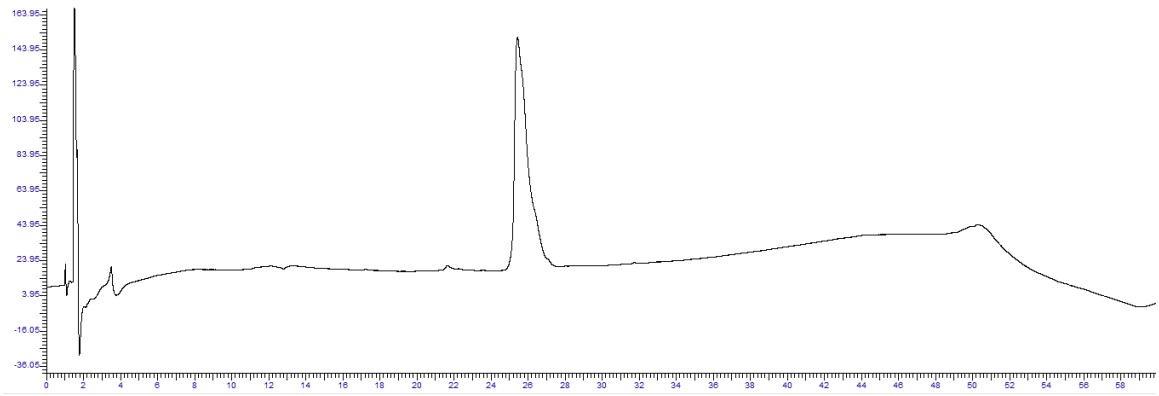

Figure 3.6. Analytical HPLC chromatogram (λ= 220 nm) of purified Temporin B.

3.1.2 Temporin peptide purification

The Temporin peptides (shown in **Table 3.1**) and their analogues were successfully prepared using automated Fmoc SPPS which represents an important step forward in the synthesis of these peptides. The introduction of an automated peptide synthesis route has several benefits in terms of both time and peptide recovery compared to the corresponding manual SPPS approaches. It should be noted that some optimization of the MW coupling steps was needed depending on the peptide.

Prior to purification crude peptides were analysed by LC-MS and analytical RP-HPLC. Unfortunately, due to time restraints (COVID lab reduced hours) only Temporin C and TL11 could be purified fully by semi-prep HPLC. The analytical HPLC trace of the crude Temporin C peptide is shown in **Figure 3.7**.

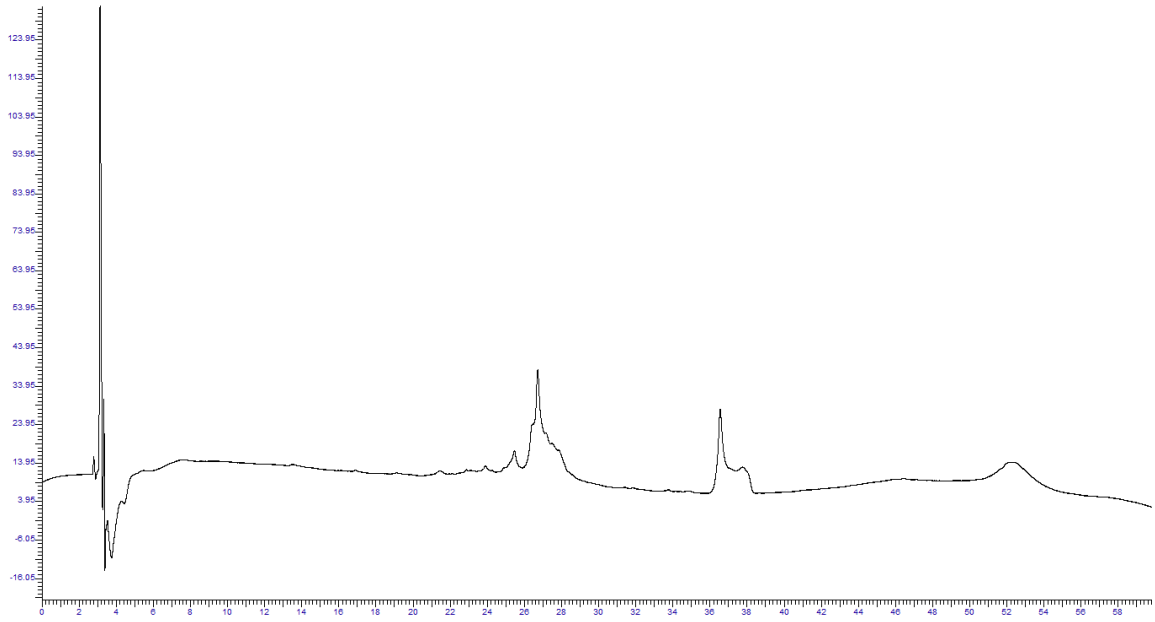

Figure 3. 7. Analytical HPLC chromatogram (λ= 220 nm) of the crude Temporin C.

Purifying according to the protocol outlined in **Section 6.2.6** had showed good results (Temporin B – **Figure 3.6**) but it is a rather slow process overall. Due to the fact that the loading capacity of the reverse phase system is low with a C_{18} column allowing a loading maximum of 1 mg/mL, without losing resolution or damaging the RP column. It was decided to try an Interchim Puriflash system which has a bigger C_{18} column allowing a

loading maximum of 40 mg/mL, provided by the analytical service at Durham University. However, when trying to inject more than 5 mg/mL the system pressure will increase significantly. Thus, formic acid was added to the injection sample. A loading capacity of 3.9 mg/mL was chosen. After purification fractions were collected, analysed, and freeze-dried. Temporin C was successfully purified, its full characterization is provided in **Section 6.4.2**.

An attempt to purify the Temporin analogue TL11 was carried out using the Interchim Puriflash purification system. Unfortunately, even after optimisation on this system the separation that could be achieved was not great and this made obtaining pure fractions of the target peptide challenging (**Figure 3.8**).

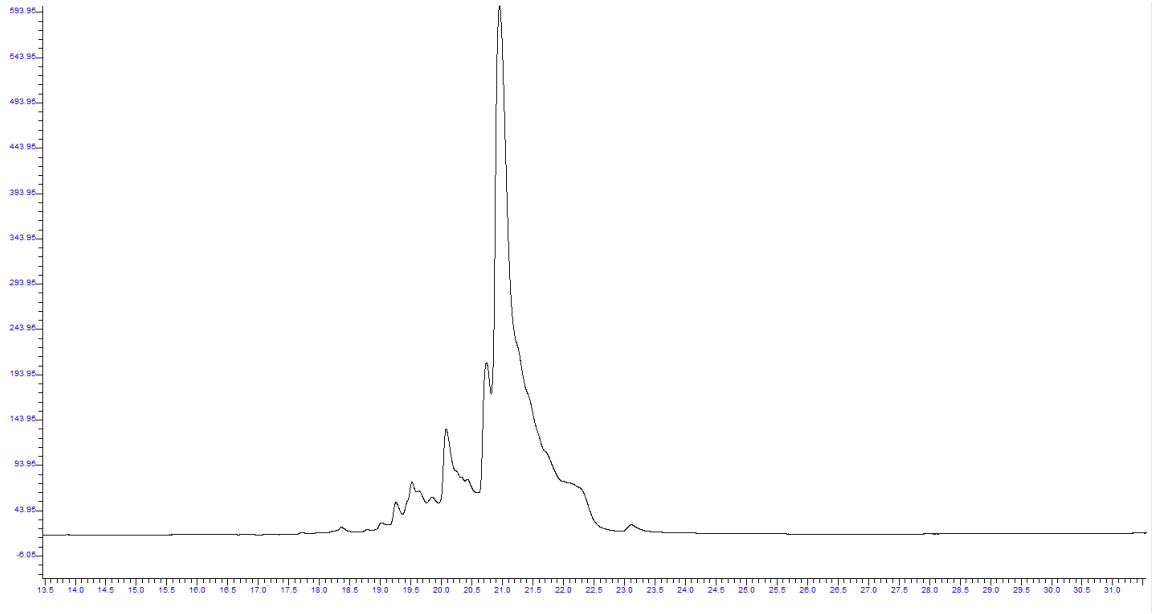

Figure 3.8. Analytical HPLC chromatogram (λ= 220 nm) of purified **TL11** by Puriflash system.

The AMPs prepared needed to be obtained in >90% purity in order to carry out dose-response biological assays. Given the purity requirements the temporin analogue TL11 that had been collected (**Figure 3.8**) was repurified by RP HPLC according to the usual protocol outlined in **Section 6.2.6**. After this process the target TL 11 was obtained in a much higher purity (**Figure 3.9**) and full characterization details are provided in **Section 6.4.2**.

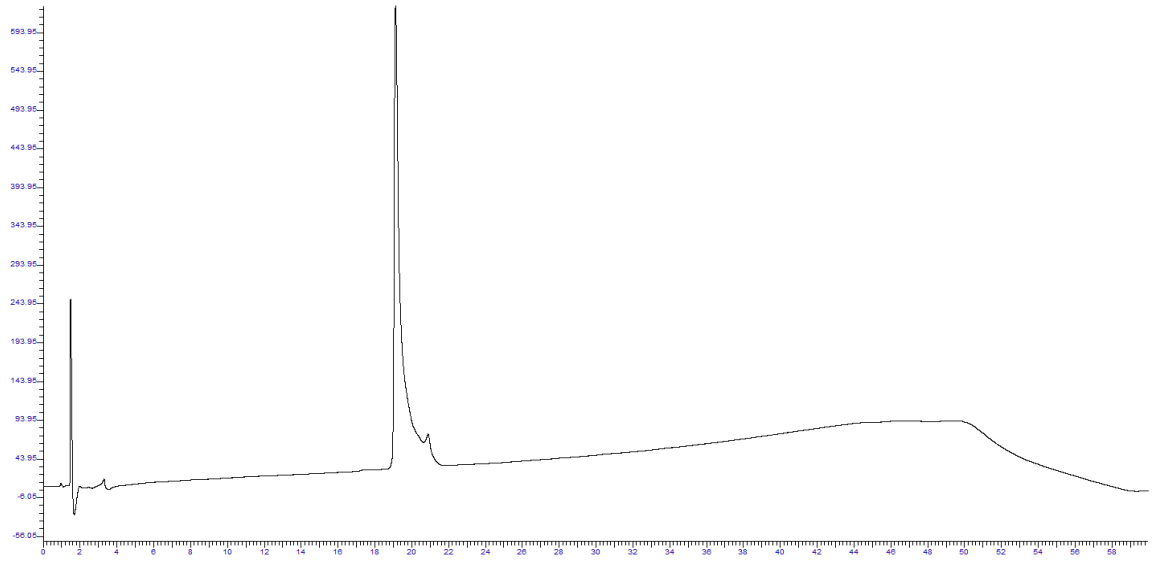

Figure 3.9. Analytical HPLC chromatogram (λ= 220 nm) of purified **TL11**.

Given time constraints the decision was made to procure Temporins A and Temporin L form a commercial supplier (Cambridge Research Biochemicals, UK).

3.3 Histatins

Some AMPs, including members of the histatin (HST) family, are known to have metal binding properties, the extent and function of which remains largely unclear. As part of an ongoing collaboration with the Karerra group (Durham Biosciences Dept) to investigate the metal bind properties of AMPs, a 4th year Master's project was set up to prepare a series of HSTs. Further details about this project are provided in **Appendix A1**.

The weakly amphipathic nature of HSTs makes them particularly interesting as therapeutics since they act on pathogens using an alternative mechanism to other AMPs, that typically induce cell membrane lysis.[6] Given this and the fact that very little data about HSTs against parasitic NTDs has been published we decided to include them in our study alongside the Temporins.

3.3.1 Synthesis of the histatin variants

The synthesis of HST-5 (**Table 3.2, Entry 1**) and six variants (**Table 3.2, Entries 2-7**) which lack certain metal-binding residues, was carried out using automated microwave assisted Fmoc SPPS.

Table 3.2. Sequences of target histatin variants and natural HST-5; residues which vary from the original HST-5 sequence are in red. The characterised Zn binding site (Zn_1) and the Cu binding sites (in bold) are indicated. A second putative Zn binding site is also present (Zn_2).

Entry	Histatin variant	Amino acid sequence	Molecular weight (g mol^{-1})
1	HST-5 (3)	**DSH**AKR**HH**GY KRKFHEKHHS HRGY	3036.30
2	H3,7A;H15-19A (4)	**DS**AAKR**AH**GY KRKFAEKAAS HRGY	2706.03
3	H15-19A (5)	**DSH**AKR**HH**GY KRKFAEKAAS HRGY	2838.11
4	H3,7A (6)	DSAAKR**AH**GY KRKFHEKHHS HRGY	2904.17
5	D1A;H7,8A (7)	ASAAKRAAGY KRKFHEKHHS HRGY	2794.15
6	D1A (8)	ASAAKR**HH**GY KRKFHEKHHS HRGY	2926.22
7	H7,8A (9)	**DSH**AKRAAGYKRKFHEKHHS HRGY	2904.17

Starting with histatin variant **D1A; H7,8A (7)**, (**Table 3.2**, **Entry 5**) Fmoc SPPS was carried out on a CEM synthesiser (Liberty Blue, Automated Microwave Peptide Synthesiser; Durham, UK) on a 0.1 mmol scale, Fmoc-Tyr(tBu)-Wang resin (0.161 g/mol) as a preloaded resin, using the reagents specified for general SPPS automated protocol in **Section 6.4.3**. Unlike loading the first amino acid onto an amide-based resin, the first coupling reaction onto an ester-based resin can be more challenging and often lower yielding. This can be overcome by using a commercially available preloaded Wang resin.[7]

Upon completion of the synthesis the tyrosine preloaded Wang resin with the desired peptide sequence was then transferred to a reaction vessel for resin cleavage under acidic conditions (**Section 6.4.1**). The crude reaction mixture was analysed by LC-MS (**Figure 3.10**).

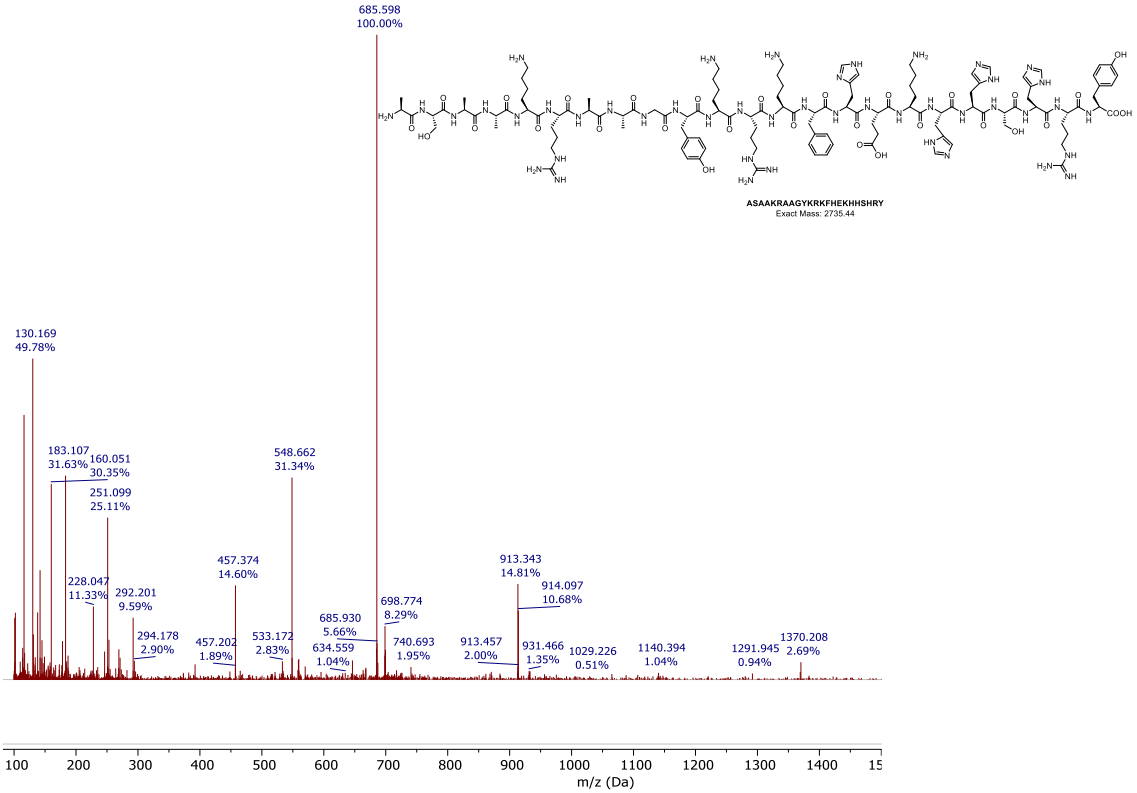

Figure 3.10. ESI LCMS viewed in positive mode, indicating the presence of peptide with a Gly deletion [**ASAAKRAAGYKRKFHEKHHSHRY**].

From the LC-MS trace (**Figure 3.10**) it can be seen that the desired HST variant was not obtained, but rather a peptide sequence with a deletion was identified. **Figure 3.10** shows the peptide ionization with peak with a *m/z*= 685.598 assigned to $[M+4H]^{4+}$ as the molecular ion. A clear ionization and fragmentation pattern is shown from $[M+5H]^{5+}$ up to $[M+2H]^{2+}$. This data indicates the possible deletion of a Gly residue. After analysis of the peptide synthesis history, which explains every step of the peptide sequence run on the CEM synthesiser, an error was identified. The software showed that with a preloaded resin, the first amino acid in the sequence is not considered for the subsequent SPPS. Thus, the software program on the peptide synthesiser deletes the first amino acid in the sequence giving a 23 amino acid peptide with a Gly deletion (which matches the LC-MS data seen in **Figure 3.10**).

Another attempt to prepare peptide **D1A; H7,8A** (**Table 3.2**, **Entry 5**) was undertaken but with a modification on the CEM software programme. This time the entire 24 amino acid

peptide sequence was added, including the preloaded Tyr amino acid in the sequence at the C terminus. After resin cleavage, target peptide synthesis in the crude was confirmed with $[M+H]^+$ *m/z* = 2795.3 in MALDI (**Figure 3.11**). The first HST mutant **D1A; H7,8A** (**Table 3.2**, **Entry 5**) was obtained with a clean crude. Peptide was purified according to the protocol detailed in Section **6.2.6**, full characterization of peptide **D1A; H7,8A** can be found in **Section 6.4.3**.

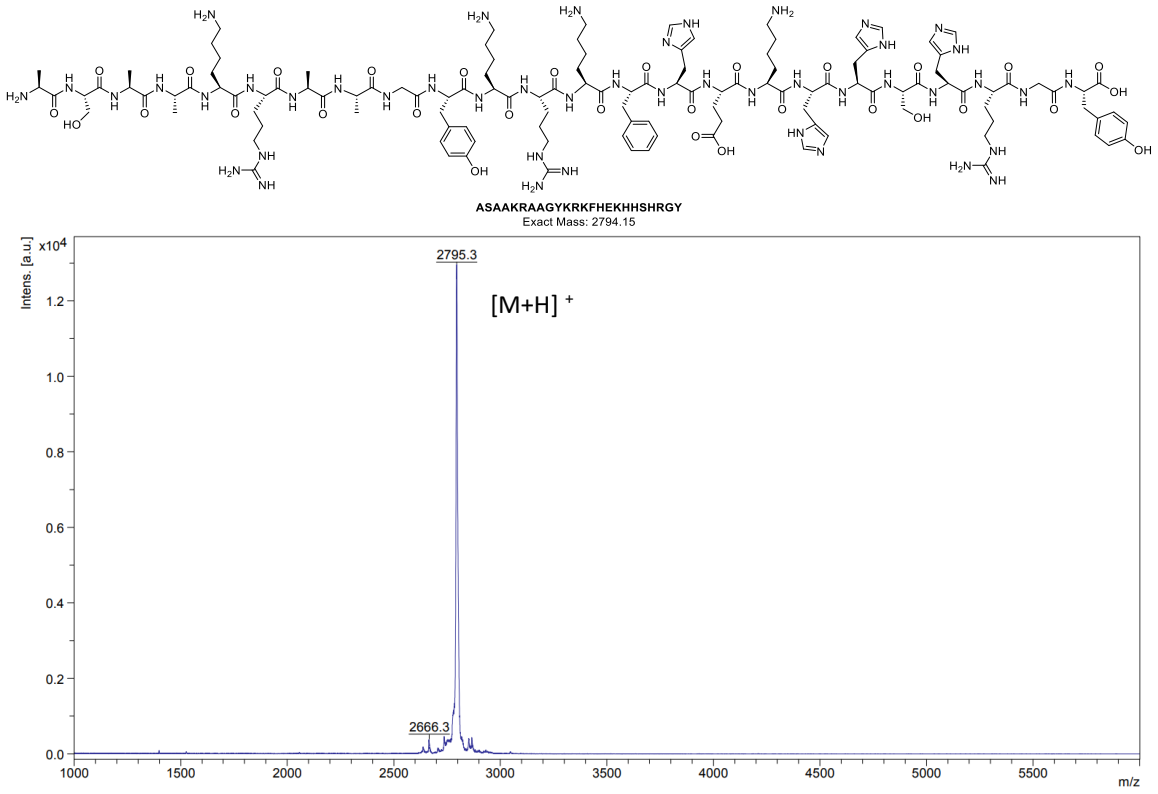

Figure 3.11. MALDI indicating the presence of peptide **D1A; H7,8A (7)**.

The CEM automated Fmoc SPPS of the remaining HST targets (**Table 3.2**) were optimized individually due to the length and complexity of their sequences. The peptides prepared were purified by preparative RP-HPLC according to experimental **Section 6.2.6**. An example of the typical RP-HPLC trace obtained is shown for HST-5 in **Figure 3.12**.

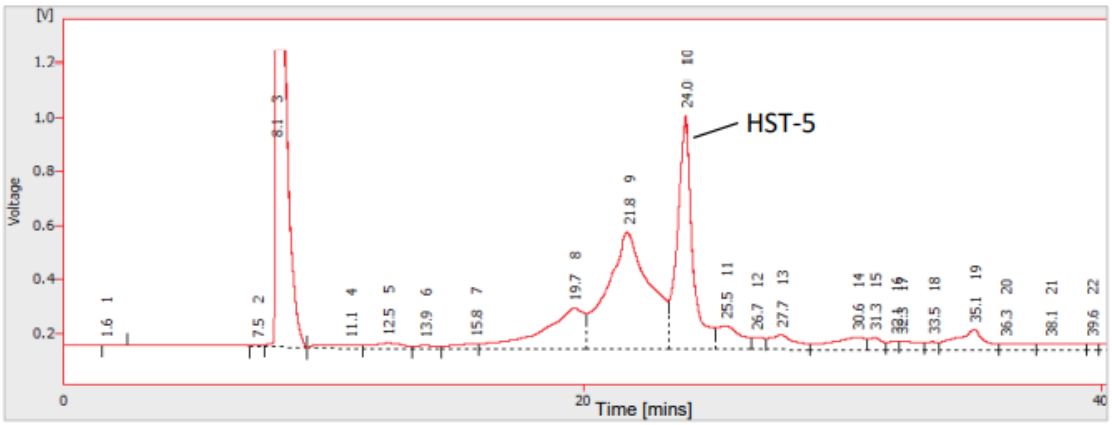

Figure 3.12. Preparative RP-HPLC chromatogram (λ= 220 nm) of HST-5 (3), with elution peak of HST-5 at 24.0 mins.

Preparative RP-HPLC methodology separates the sample based on hydrophobicity, the first peak (8.1 mins) is the solvent peak (sample injection with TFA addition). The peak at 23.47 - 24.30 mins eluted at approximately 75.1% solvent A and 24.9% solvent B (**Section 6.2.6**); it was collected and analysed by LC-MS and analytical HPLC.

HST-5 was successfully purified, as a singular clean peak at 9.3 mins the analytical HPLC trace (**Figure 3.14**), which was shown to contain the desired peptide from the LC-MS fragmentation patterns. Likewise, the peak due to impurities (21.8 mins, **Figure 3.12**) was collected and analysed by ESI-MS and analytical HPLC, these were mainly due to deletions as detailed in **Figure 3.13**.

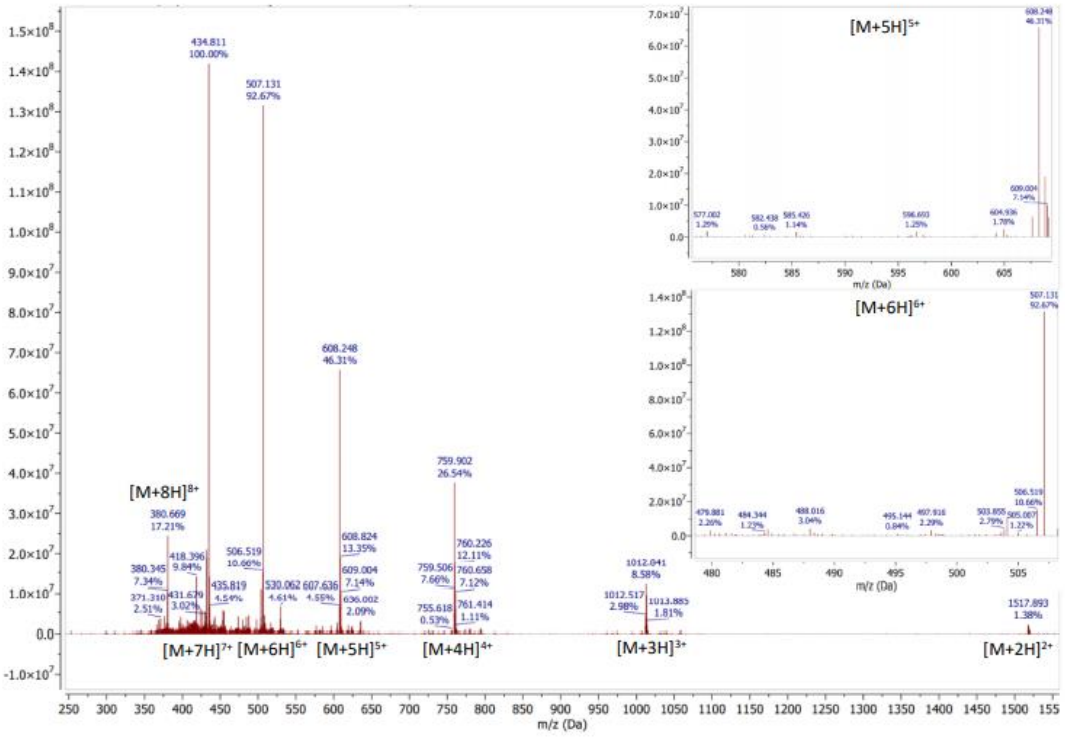

Figure 3.13. ESI LCMS of HST-5, viewed in positive mode, show $[M+2H]^{2+}$ - $[M+8H]^{8+}$ peaks, with the Molecular ion as $[M+ 3H]^{3+,}$ and also sub panels showing the peaks due to single amino acid deletions present as impurities.

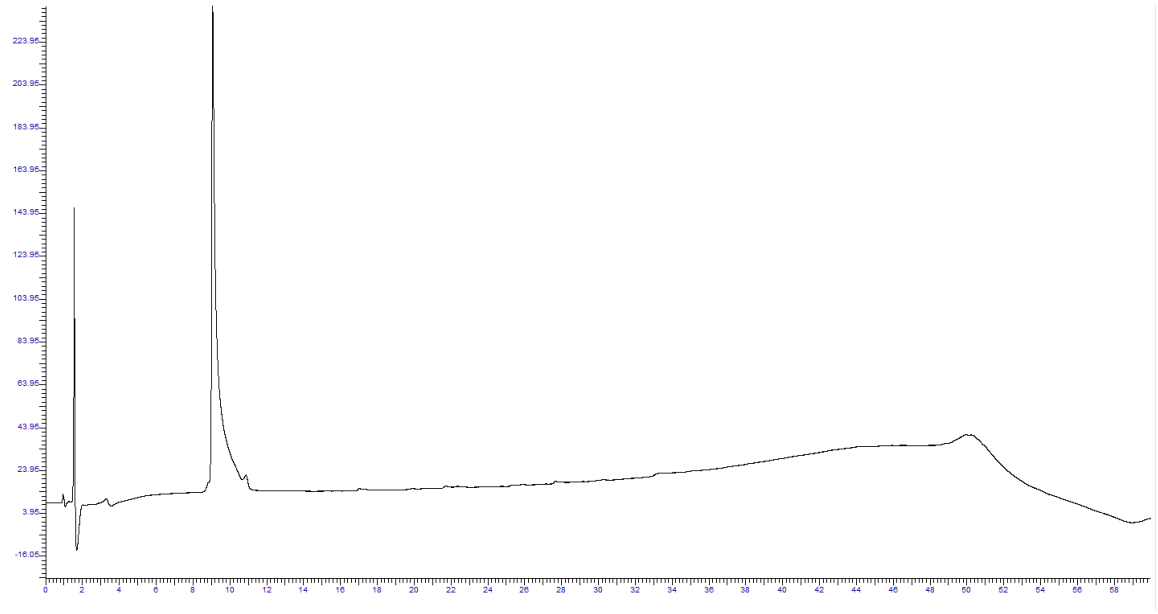

Figure 3.14. Analytical HPLC chromatogram (λ= 220 nm) of desired product HST-5.

3.5 Leishmaniasis assay validation

The Temporin and HST derived peptides were screened against both promastigote and axenic amastigote *L. mexicana* using an optimised Alamar Blue assay.[8] To determine the most effective protocol for Alamar Blue® assay of *Leishmania mexicana* procyclic promastigotes and axenic amastigotes two 96 well plates were set up for each parasite stage using serial dilution to achieve a triplicate series of cell culture concentrations between 8.0 x10^6 cells/ml and 1.56 x 10^4 cells/ml.

Both sets of plates also contained a triplicate control for each parasite stage medium to indicate the minimum fluorescence that would be observed for cells incapable of metabolising Alamar Blue®, detailed protocol in **Section 6.7**. Following the recommended reagent protocol, 10% *v/v* Alamar Blue® was added to each well.[8] One pair of plates was then incubated at 26°C and the other at 32°C, one for promastigotes and the latter for axenic amastigotes with fluorescence measurements taken in different conditions to determine which are the optimal ones. The aim is to determinate the cell concentration and incubation times where there is a linear correlation between the plating density of parasites and the fluorescent readout for the assays. Temperatures were chosen

according to the parasite stages, temperature used to culture axenic amastigotes (32°C) and the corresponding one for promastigotes (26°C).

The *Leishmania* life cycle is summarised in **Section 1.2.1**. Each parasite stage has a different functioning period in where they are considered healthy and differentiate from each other clearly.

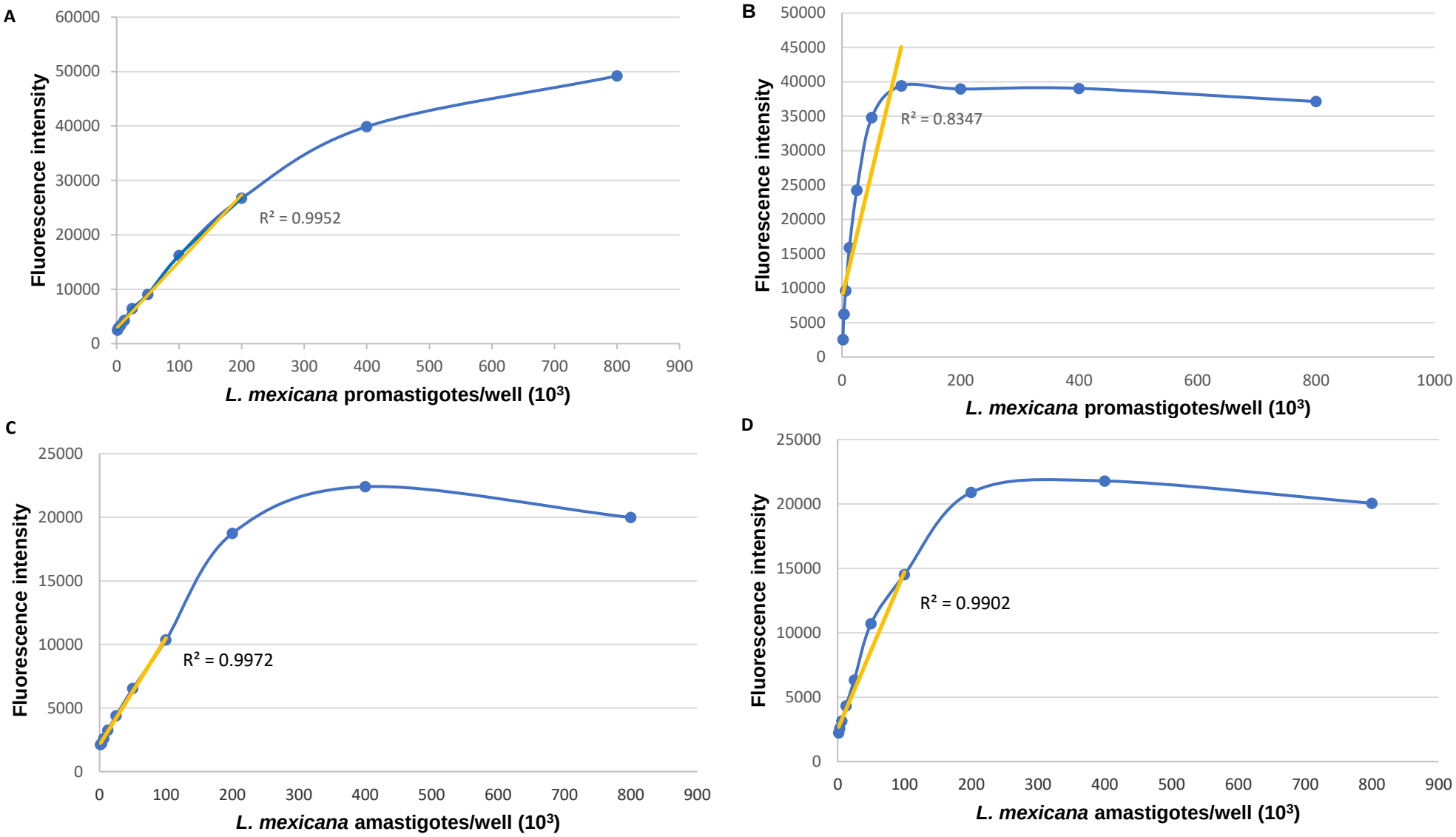

Figure 3.15. Alamar Blue® fluorescence assay validation for L. mexicana assay conditions; (A) *L. mexicana* promastigotes, 24 h incubation, 26°C; (B) *L. mexicana* promastigotes, 48 h incubation, 26°C; (C) *L. mexicana* amastigotes, 24 h incubation, 32°C; (D) *L. mexicana* amastigotes, 48 h incubation, 32°C.

Alamar Blue® was reduced by *L. mexicana* promastigotes and axenic amastigotes in a time dependant manner, as seen in **Figure 3.15**. It was determined that a 4-hour incubation is an inadequate time interval, as cell viability cannot be assessed effectively due to the small variance between the observed fluorescence for high concentrations of healthy parasites and those of the control (or low concentrations of healthy cells).[8]

L. mexicana promastigotes assays are charted in Graphs **A** and **B** on **Figure 3.15**. Overall, a linear correlation between fluorescence and cell concentration is shown when the promastigotes are healthy. Particularly, Graph **A** showed that an Alamar Blue® addition, with a 4-hour incubation, after 20-hour of incubation at 26°C has a linear correlation between the fluorescence and cell concentration. A 24-hour incubation provided the widest range of observed fluorescence between high concentrations of healthy promastigotes and those of the control wells or low concentrations of healthy promastigotes. It is a fact that the cell concentration cannot be more than 2.0 $x10^6$ cells/ml for this assay. In effect, 1.0 $x10^6$ cells/ml was the chosen one. Details of this Alamar Blue® assay can be found in **Section 6.7**.

Whereas for *L. mexicana* axenic amastigotes a smaller range of fluorescence was discerned at 32 °C in both assays, **Figure 3.15 C** and **D**. Also, this can be accounted for by the level of fluorescence detected from the control wells. As detailed in **Section 6.7.2** axenic amastigote form of *L. mexicana,* cultured in media at pH 5.5, grows more slowly than promastigotes.

Finally, two other promastigote form *Leishmania* species were tested for optimal assay conditions as above, *L. major* and *L. amazonensis* (**Figure 3.16**). Both species showed a linear correlation of the cell density and the fluorescent readout.

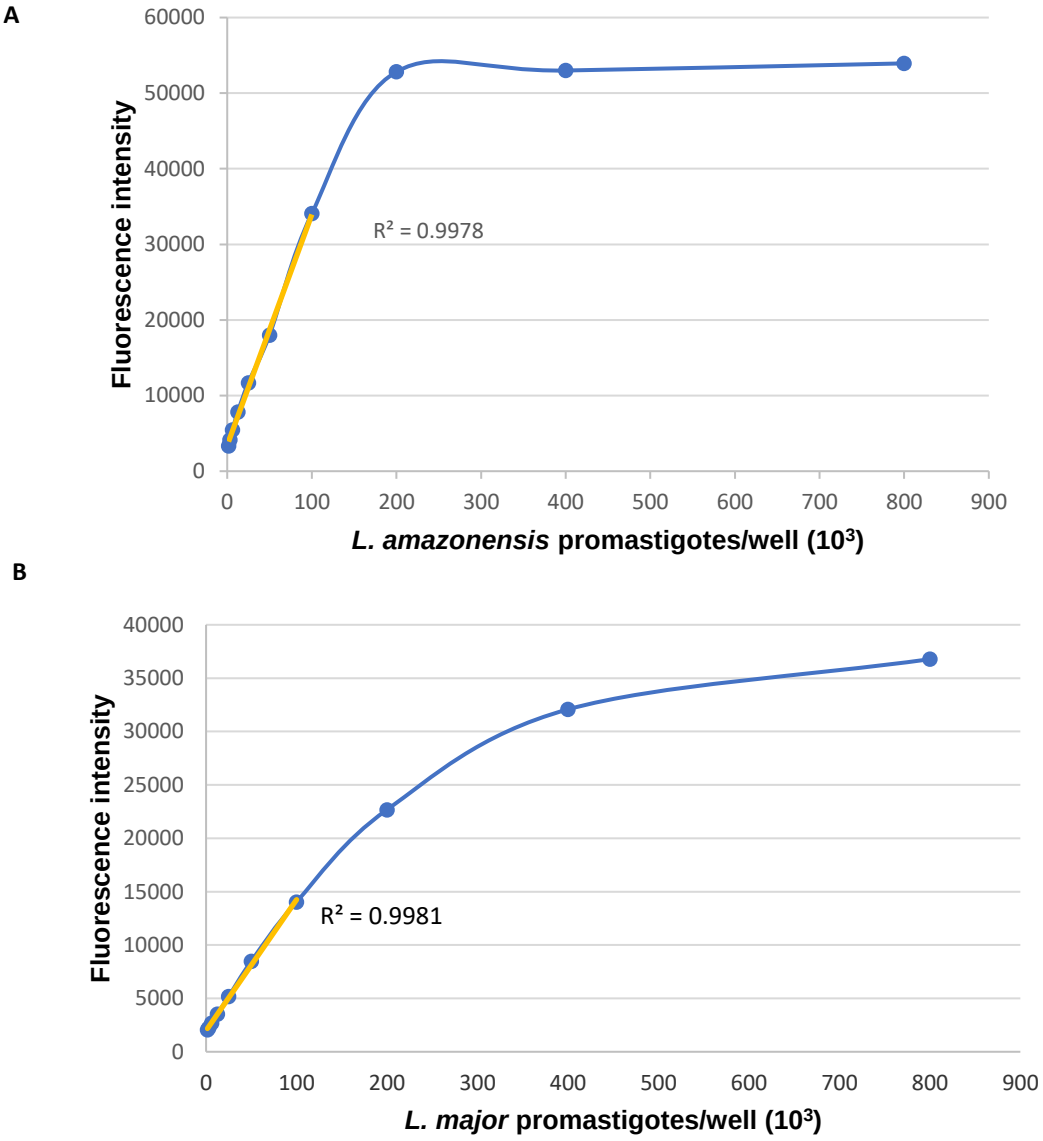

Figure 3.16. Alamar Blue® fluorescence assay validation conditions for; (A) *L. amazonensis* promastigotes, 24 h incubation, 26°C; (B) *L. major* promastigotes, 24 h incubation, 26°C.

For the above-mentioned reasons, the most effective assay for promastigote form of *Leishmania* parasites used in this work, is with a temperature set at 26°C with a 4 h Alamar Blue® addition in total of 24 hours assay incubation. The assay is run at the native culture temperature for *L. mexicana* promastigotes. Thus, administering the Alamar Blue® assay at 26°C not only provides the widest range of fluorescence results, allowing for the most accurate determination of cell viability; but it also allows the promastigotes to proliferate and differentiate naturally. All three parasites' species, *L. mexicana, L. amazonensis* and

L. major, showed a linear correlation between their fluorescence and a cell concentration of 1.0 x10^6 cells/ml. Assays details can be found specifically for each one in **Section 6.7**.

3.6 Biological results

A small 5-peptide library was tested against *L. mexicana, L. amazonensis* and *L.* major. All of these parasite species can cause cutaneous leishmaniasis (CL) (for details see **Section 1.6**). Temporins were chosen to be tested against other parasites since they have only previously been tested within the Cobb group against *L. mexicana*.[1] Temporins were tested at a single concentration of 200 μM according to the protocol detailed in **Section 6.7**. If the peptides displayed any activity of greater than 50% of cell inhibition in the first screen at 200 μM, then EC_{50} values could be obtained. Results are shown in **Table 3.3**.

Table 3.3. Biological activity of Temporins screened at 200 μM.

Entry	Peptide sequence	Known biological activity	Activity (%cell viability)			
			L. major	*L. amazonensis*	*L. mexicana*	
			Promastigotes	Promastigotes	Promastigotes	Amastigotes
1	Temporin A* FLPLIGRVLSGIL-NH_2	Gram+, Virus, Chemotactic	0 %	0 %	0 %	53 %
2	Temporin B* LLPIVGNLLKSLL-NH_2	Gram +	47 %	83 %	95 %	64 %
3	Temporin C LLPILGNLLNGLL-NH_2	Gram +	55 %	86 %	94 %	66 %
4	Temporin L FVQWFSKFLGRIL-NH_2	Gram+ & Gram-, Fungi, Mammalian cells, Cancer cells	0 %	1 %	0 %	81 %
5	Temporin analoque TL11 FVQWFSKFLGAIL-NH_2		1 %	16 %	23 %	60 %

Temporin A and Temporin L showed strong activity against the promastigotes forms of *L.major*, *L. amazonensis* and *L. mexicana* (**Table 3.3**, **Entries 1** and **4**). Unfortunately, their antiparasitic activity drops significantly against the axenic amastigotes form of *L. mexicana*. Temporin analogue (TL 11) has a similar tendency with 60 % axenic amastigotes growth seen at a single concentration of 200 μM, (**Table 3.3**, **Entry 5**). Thus, the specific nature of positively charged residues in the sequence of Temporin L appears to slightly affect antileishmanial activity.

Temporin C has more than 50 % cell viability against promastigote form of *L. major*, showing no significant activity against the other species, (**Table 3.3**, **Entry 3**). Similarly, Temporin B does not seem to have any activity against *L. mexicana* in this single-concentration study, although, reported studies show activity with lower concentrations. For example, 38 % cell viability at 50 μM against the promastigote form of *L. mexicana* was previously reported by the Cobb group.[2] The reasons for the differences in activity seen are unclear. Further studies should be carried out to determine its peptide EC_{50}, such as a dose-response assay.

The HST library was found to be highly soluble in water so there was no need to use DMSO. Testing was carried out at 50 μM, against the promastigote forms of *L. major*, *L. amazonensis* and *L. mexicana* but no anti-parasitic activity was observed. Interestingly a low level of antiparasitic activity was seen against the axenic amastigote form of *L. mexicana* for some of the HST peptides at 50 μM. For this reason, the histatins analogues were tested also at 100 μM against the axenic amastigote form of *L. mexicana* (**Table 3.4**). However, neither HST-5 nor any of its variants showed less than 50 % cell availability against the axenic *L. mexicana* at 100 μM.

Table 3.4. Biological activity of Histatins and Histatin analogues.

Entry	Histatin variant	Activity (%cell viability)			
		L. major	*L. amazonensis*	*L. mexicana*	
		Promastigotes	Promastigotes	Promastigotes	Amastigotes
1	HST-5 **DSH**AKR**HH**GY KRKF**HEKHH**S HRGY	100 %	100 %	100 % at 50 μM	100 % at 50 μM and 100 μM respectively
2	H3,7A; H15-19A **DSA**AKR**AH**GY KRKFAEKAAS HRGY	100 %	100 %	100 % at 50 μM	100 % at 50 μM 79 % at 100 μM respectively
3	H15-19A **DSH**AKR**HH**GY KRKFAEKAAS HRGY	100 %	100 %	100 % at 50 μM	82 % at 50 μM 88 % at 100 μM respectively
4	H3,7A DSAAKR**AH**GY KRKF**HEKHH**S HRGY	100 %	100 %	100 % at 50 μM	100 % at 50 μM and 82 % at 100 μM respectively
5	D1A; H7,8A ASAAKRAAGY KRKF**HEKHH**S HRGY	100 %	100 %	100 % at 50 μM	100 % at 50 μM and 73% at 100 μM respectively
6	D1A (8) ASAAKR**HH**GY KRKF**HEKHH**S HRGY	100 %	100 %	100 % at 50 μM	78 % at 50 μM and 87% at 100 μM respectively
7	H7,8A (9) **DSH**AKRAAGYKRKF**HEKHH**S HRGY	100 %	100 %	100 % at 50 μM	74% at 50 μM and 100% at 100 μM respectively

3.7 Chapter Summary

A selection of AMPs derived from the Temporin (**Table 3.1**) and Histatin (**Table 3.2**) families were prepared using automated Fmoc Solid-Phase Peptide Synthesis (SPPS). According to their peptide sequences modifications were carried out in order to obtain the best synthesis conditions for their preparation. Temporin purification proved challenging as detailed in **Section 3.1.2**. As a result, a small Temporin library was prepared and tested against different species of *Leishmania* parasites as detailed in **Table 3.3**. HST-5 was prepared, along with some variants, with more than 95% purity.

All the AMPs prepared were tested against three different types of leishmania parasites: *L. major*, *L. amazonensis* and *L. mexicana*. Temporin library showed to have significant antiparasitic activity against the promastigote form of *L. major* (**Table 3.3**). To the best of our knowledge is the first time that peptides from the Histatin family have been tested against these specific *Leishmania* parasite species. According to the literature, HST-5 has only been tested against *L. pifanoi* (causative agent of cutaneous leishmaniasis, CL) and *L. donovani,* (causative agent of visceral leishmaniasis, VL). HST-5 has been shown to be active at micromolar concentrations against *L. donovani* promastigotes (with a lethal dose of LC_{50}=7.3 µM) and *L. pifanoi* axenic amastigotes (LC_{50}=14.4 µM). [9] In this study, HST-5 does not show any antiparasitic activity against the promastigote nor the axenic amastigote form of *L. mexicana* (**Table 3.4**).

3.8 References

1. CHADBOURNE, FRANCES, L. The design and Synthesis of peptide-inspired antileishmanial agents. (2014).
2. Chadbourne, F. L., Raleigh, C., Ali, H. Z., Denny, P. W. & Cobb, S. L. Studies on the antileishmanial properties of the antimicrobial peptides temporin A, B and 1Sa. *Journal of Peptide Science* **17**, 751–755 (2011).
3. Nogrado, K., Adisakwattana, P. & Reamtong, O. Antimicrobial peptides: On future antiprotozoal and anthelminthic applications. *Acta Tropica* vol. 235 (2022).

4. Mangoni, M. L. *et al.* Temporins, small antimicrobial peptides with leishmanicidal activity. *Journal of Biological Chemistry* **280**, 984–990 (2005).

5. Rinaldi, A. C. *et al. Temporin L : antimicrobial, haemolytic and cytotoxic activities, and effects on membrane permeabilization in lipid vesicles*. *Biochem. J* vol. 368 (2002).

6. Melino, S., Santone, C., Di Nardo, P. & Sarkar, B. Histatins: Salivaryx peptides with copper(II)- and zinc(II)-binding motifs Perspectives for biomedical applications. *FEBS Journal* **281**, 657–672 (2014).

7. Lüttenberg, S., Sondermann, F. & Scherkenbeck, J. Anthelmintic PF1022A: Stepwise solid-phase synthesis of a cyclodepsipeptide containing N-methyl amino acids. *Tetrahedron* **68**, 2068–2073 (2012).

8. Mikus, J. & Steverding, D. *A simple colorimetric method to screen drug cytotoxicity against Leishmania using the dye Alamar Blue*. *Parasitology International* vol. 48 (2000).

9. Luque-Ortega, J. R., Hof, W., Veerman, E. C. I., Saugar, J. M. & Rivas, L. Human antimicrobial peptide histatin 5 is a cell- penetrating peptide targeting mitochondrial ATP synthesis in Leishmania. *The FASEB Journal* **22**, 1817–1828 (2008).

4. Peptoids

4.1 Anti-leshmanial effects of peptoids

As previously discussed, antimicrobial peptides (AMPs) offer one potential solution to the development of new topical agents for the treat of cutaneous leishmaniasis (CL).[1] However, like all peptide-based therapeutics AMPs face the challenge of being inherently susceptible to enzymatic degradation. In light of this peptidomimetics like peptoids (**Figure 4.1**), potentially offer a better opportunity for the development of new treatments for a range of diseases[2] including CL.[3–5]

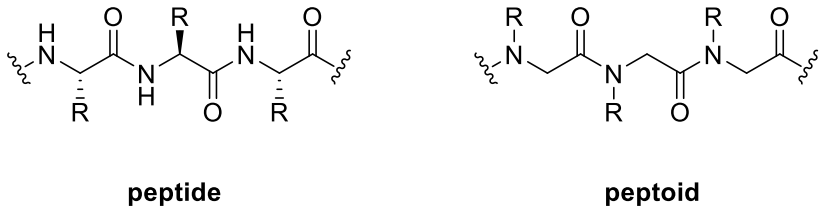

Figure. 4.1. Comparison of α-peptide and α-peptoid chemical structures.

Peptoids (or poly-*N*-substituted glycines) have considerable potential for development as new anti-infective agents because they are cheaper to manufacture and are substantially more stable under physiological conditions than peptides.[6,7] Their antibacterial activity against a range of Gram-positive and Gram-negative bacteria, selectivity for bacterial cells, and low haemolytic activity are all similar to the values reported for leading AMPs.[4] The Cobb group has recently reported that peptoids have activity against the parasite species *L. mexicana*, demonstrating for the first time that this class of peptidomimetic also have anti-leishmanial activity.[4,5]

4.1.1 Ugi reactions for peptoid synthesis

Multicomponent reactions have been utilised in almost all synthetic organic chemistry fields and they are often employed to rapidly access novel scaffolds for the development of bioactive small molecules. In particular, isocyanide-based multicomponent reactions

have gained significant interest within the scientific community as an efficient, convenient, timesaving, and atom-economical approach to the rapid generation of chemical diversity.[8] In 1958, isocyanides became generally available via the dehydration of formylamines.[9] One year later, the four-component reaction of isocyanides (U-4CR) was introduced into the field.[10] The one-pot Ugi four-component reaction (U-4CR) reaction has a very broad substrate tolerance and it can convert almost all combinations of substrates into the target Ugi products.[8,11] The Ugi reaction is a 4CR reaction involving a ketone or aldehyde, an amine, an isocyanide, and a carboxylic acid that react to form a bis-amide (**Scheme 4.1**).

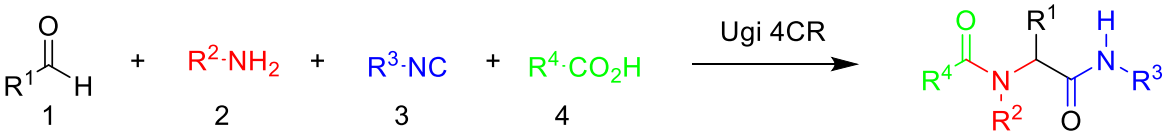

R^1,R^2,R^3,R^4= alkyl or aryl

Scheme 4.1. General reaction scheme for the Ugi four-component reaction (Ugi 4CR). Adapted from Previdi *et al*.[8]

The mechanism is believed to involve an initial formation of an imine via condensation of the amine and aldehyde. The imine is then protonated by the carboxylic acid component and this species is attacked by the nucleophilic isonitrile and subsequently the carboxylic acid. In the final step a Mumm rearrangement leads to the formation of the α-amino amide product (**Scheme 4.2**).[9]

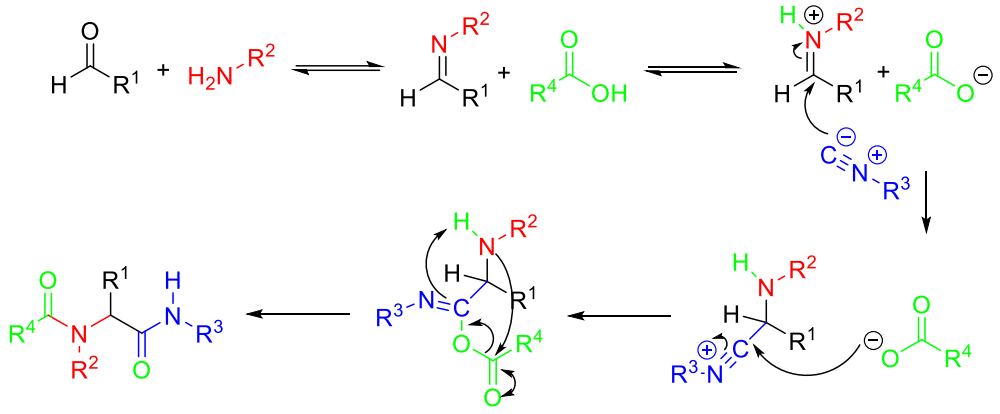

Scheme 4.2. Reaction mechanism of the Ugi 4CR.

Recently, the Ugi reaction has seen a renewed interest in its applications because it is easily performed in almost any solvent, and it is environmentally friendly. This one-pot reaction is accomplished just by gathering together the four components.[8] Aside from the advantages of atom economy, high efficiency, and benign conditions, the Ugi reaction also enables the construction of peptoid backbones.[9]

4.1.2 Ugi- derived peptoid library with antiparasitic activity

Recently Donate *et al*.[7] employed the Ugi reaction to prepare a small library of linear peptoids. They used a microwave assisted approach which enable efficient synthesis of the lipopeptoid library. The peptoid library prepared was tested against the promastigote stage of *L. amazonensis*. A selection of compounds from this peptoid library and their antiparasitic activities are shown in **Table 4.1**. The active peptoids have a similar backbone but when a modification to the carbon chain in compound **30** is made, a significant decrease in the biological activity is observed (peptoid **32**). In addition, if an aromatic ring is present, this activity is recovered, as shown in compound **34**.

Table 4.1 Functionalised active peptoids tested *in vitro* in the promastigote stage of *L. amazonensis*. Adapted from Donate *et al*.[7]

Entry	Aldehyde	Amine	Isocyanide	Acid	Product	IC_{50} (μM)
1	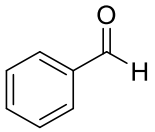	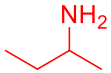	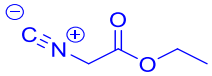	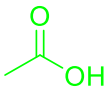	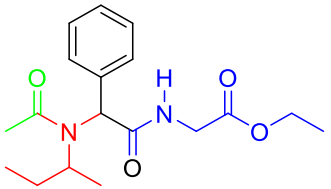	2.8
	26	**27**	**28**	**29**	**30**	
2	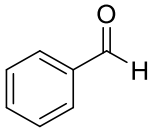		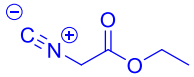	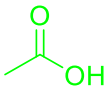	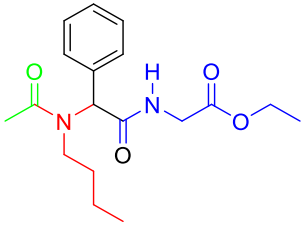	60.6
	26	**31**	**28**	**29**	**32**	
3	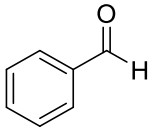	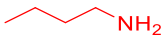	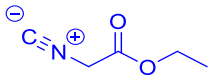	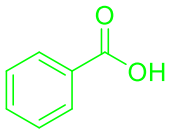	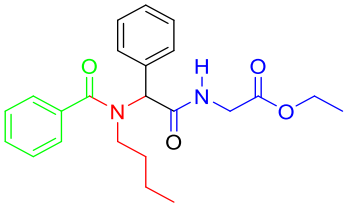	2.6
	26	**31**	**28**	**33**	**34**	

4.1.3 Chapter aims

The synthesis of a library of lipopeptoids using a Ugi reaction will be carried out. The library design will take inspiration from the data shown in **Table 4.1**.[7] After purification, the library of lipopeptoids prepared will be tested against both stages of the *L. mexicana* parasite: promastigotes and axenic amastigotes. Based on the anti-leishmanial activity observed a second-generation library will be designed, prepared and tested for anti-leishmanial activity.

4.2 Ugi 4CR peptoid synthesis

Note *– Some aspects of this work were carried out by Mr Ian Roberts (UG Durham), who was a Laidlaw summer student in the Cobb group working directly under my supervision.*

Initially, we attempted to carry out the Ugi 4CR reaction using the reaction set up and conditions reported by Donate *et al*[7], without microwave (MW) assistance (**Scheme 4.3**).

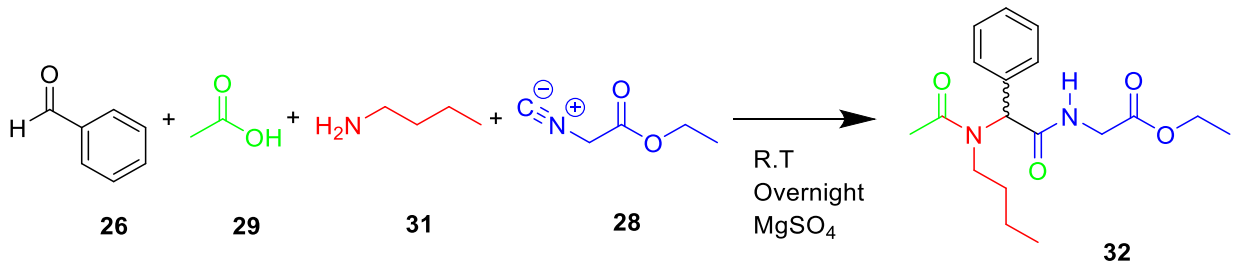

Scheme 4.3. Solvent-free Ugi 4CR reaction reported by Donate *et al*.[7]

As such a reaction was carried out without any solvent and it was run in the presence of anhydrous $MgSO_4$ under a nitrogen atmosphere, where benzaldehyde (**26**) (2 equiv.), butylamine (**31**) (2 equiv.), and glacial acetic acid (**29**) (2 equiv.) were all mixed in the flask. Finally, ethyl isocyanoacetate (**28**) was added (1 equiv.) using a syringe, and the reaction mixture was left to stir overnight at room temperature (R.T.). The reaction was monitored by TLC where consumption of the limiting reagent, ethyl isocyanoacetate (**28**), was followed.

Upon completion of the reaction, the crude mixture was filtered and washed with MeOH (x3). The crude reaction mixture was then purified by column chromatography using DCM/MeOH (95:5 *v/v*) as the eluent. From the analysis of the products obtained after purification, it appeared that a Passerini product had been formed instead of the desired four-component Ugi product (**Figure 4.2**). A singlet is present in the ^{1}H NMR with a shift of 6.10 ppm. This was believed to be the C-H proton from the 3-component reaction (3CR) product (**35**) which is next to an ester and not an amide bond. The LC-MS data with an *m/z* = 280.12 (assigned to $[M+H]^{+}$) also supported the production of the Passerini product, compound **35**.

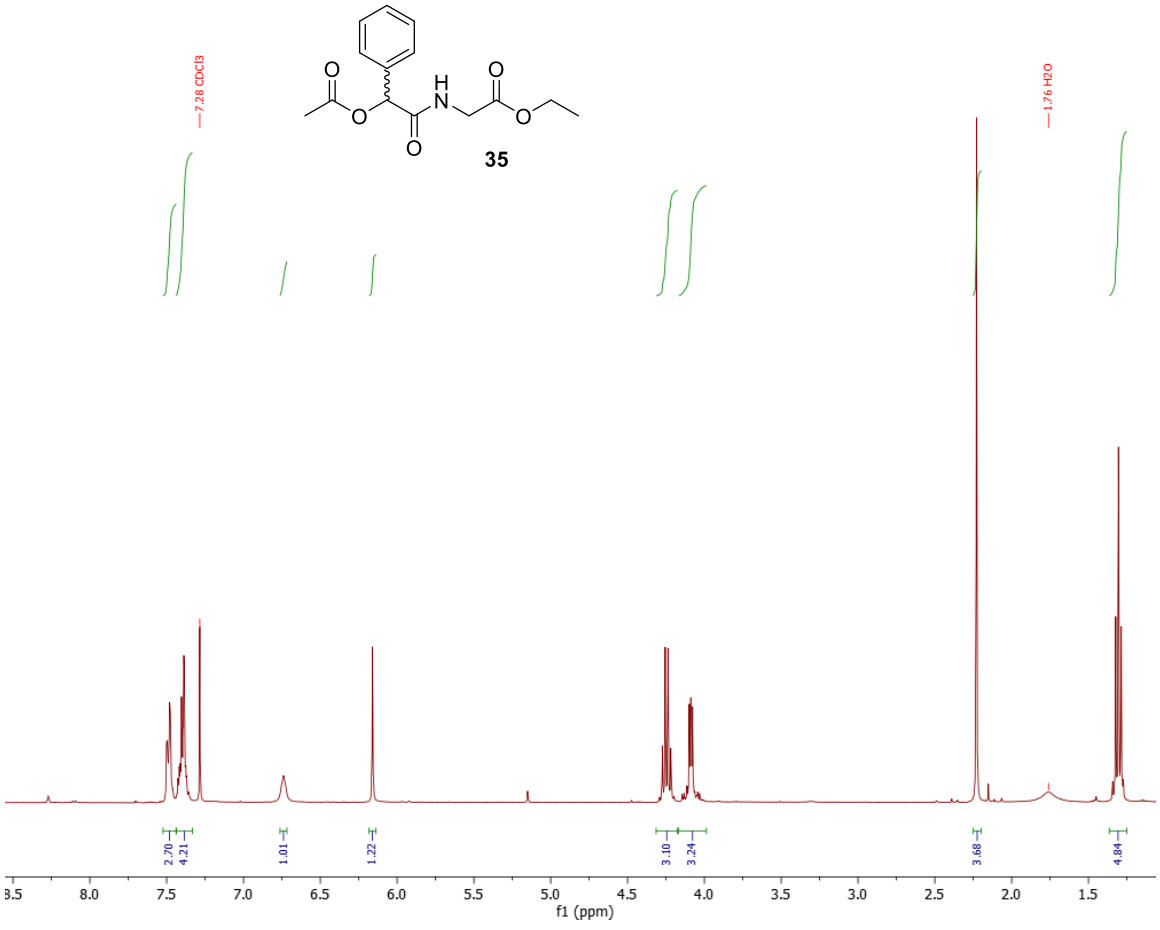

Figure 4.2. ^{1}H NMR ($CDCl_3$) spectra of compound **35**.

The Passerini reaction, also known as a 'three-component reaction', will be discussed in more detail in **Section 4.6**. A second attempt at the Ugi reaction was made, and this time the reaction was left to stir for a longer period of time. The total consumption of the starting

material was confirmed by TLC after 5 days. Unfortunately, the crude reaction again showed a mixture of both the 3CR-Passerini product (**35**) and what could potentially be the 4CR-Ugi product (**32**) by NMR analysis. LC-MS analysis of the crude reaction mixture also showed the presence of both compounds.

In order to investigate the formation of **35** in more detail another reaction was conducted under the same experimental conditions, but without the amine as a building block. The R_f of the major product from this reaction was found to be identical to the suspected Passerini compound (**35**) which had been formed in the Ugi reaction. The purified Passerini 3CR product (**35**) was fully characterised, and the data is given in the experimental **Section 6.6**. This confirmed **35** as the by-product in the previously attempted Ugi reaction.

Several further reactions were run with the same set of starting materials (e.g., **Scheme 4.3**) but in all cases a mixture of both the 3CR-Passerini product (**35**) and the 4CR-Ugi product (**34**) were isolated. It was therefore decided to try to optimise this reaction by adding a solvent, varying the temperature, and changing the acid component used to benzoic acid (**33**) (**Scheme 4.4**).

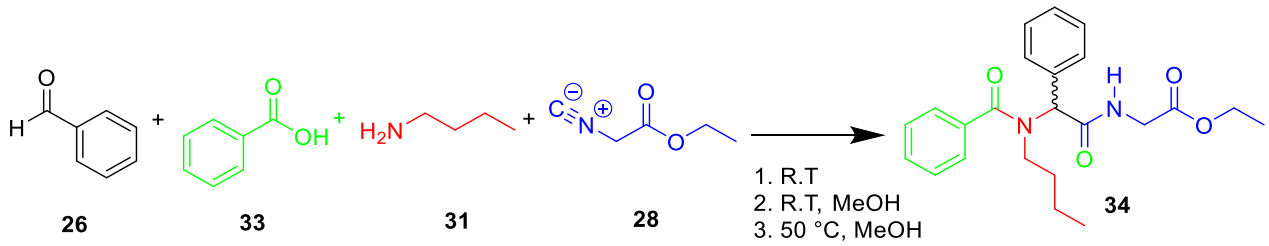

26 33 31 28 34

Scheme 4.4. Ugi reaction optimisation. The three different reaction conditions to be trialled are given (1-3).

We were keen to investigate if the 3CR product (**35**) that was being obtained was a consequence of the pKa of the initially chosen acid component (acetic acid (pKa = 4.20). Benzoic acid, with a pKa= 4.76, was thought to be less likely to potentially protonate the amine component in the reaction, thus potentially avoiding the formation of the 3CR product.

Reactions 1-3 (**Scheme 4.4**) were set up and run. All reactions were monitored by TLC for 7 days. **Reaction 1** (**Scheme 4.4**) did not show any progression regarding isocyanate (**28**) consumption after 7 days. It was also noted that some of what was believed to be the isocyanate failed to dissolve completely. Similarly, the heated test reaction did not show any progress, i.e., more isocyanate consumption, after 2 days (**Reaction 3, Scheme 4.4**). However, Reaction 2 was found to have consumed all of the isocyanate starting material after 7 days of reaction (**Scheme 4.4**).

Therefore, the most suitable reaction conditions appeared to be minimal solvent, room temperature, and using a 7-day reaction time (**Reaction 2, Scheme 4.4**) - detailed in **Section 6.5.1**. Using the conditions in **Reaction 2** the desired Ugi product (**34**) was obtained in a 55% yield. The ^{1}H NMR for **34** is given in **Figure 4.3** and full characterisation data is provide in **Chapter 6**, **Section 6.5.5**.

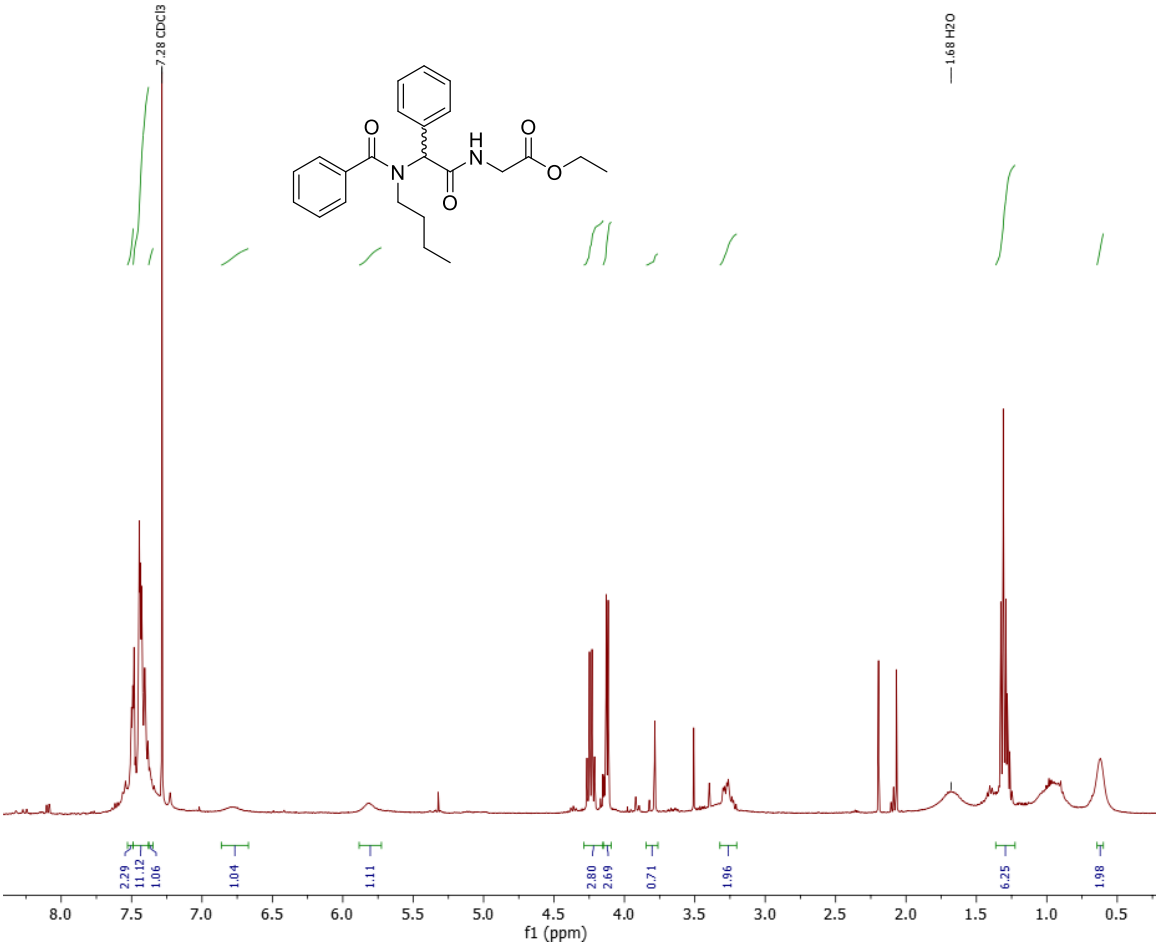

Figure 4.3. ^{1}H NMR ($CDCl_3$) for Ugi product **34**.

The optimised conditions were then used to prepare a small library of Ugi derived lipopeptoids (**Figure 4.4**). To access a diverse chemical space, a functionalised peptoid library was designed with different isocyanates, amines and carboxylic acids. In addition, some Boc analogues were also prepared to probe the differences between molecules with and without a positive charge. The synthesis of the peptoid library was attempted (experimental details given in **Section 6.5.1**). Challenges with the purification of the final products in some cases meant that not all of the target peptoids were isolated in a pure (>90%) form. **Figure 4.4** summaries the outcomes of the library synthesis.

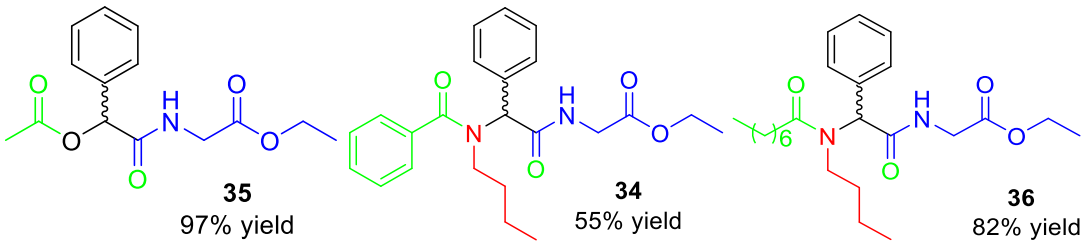

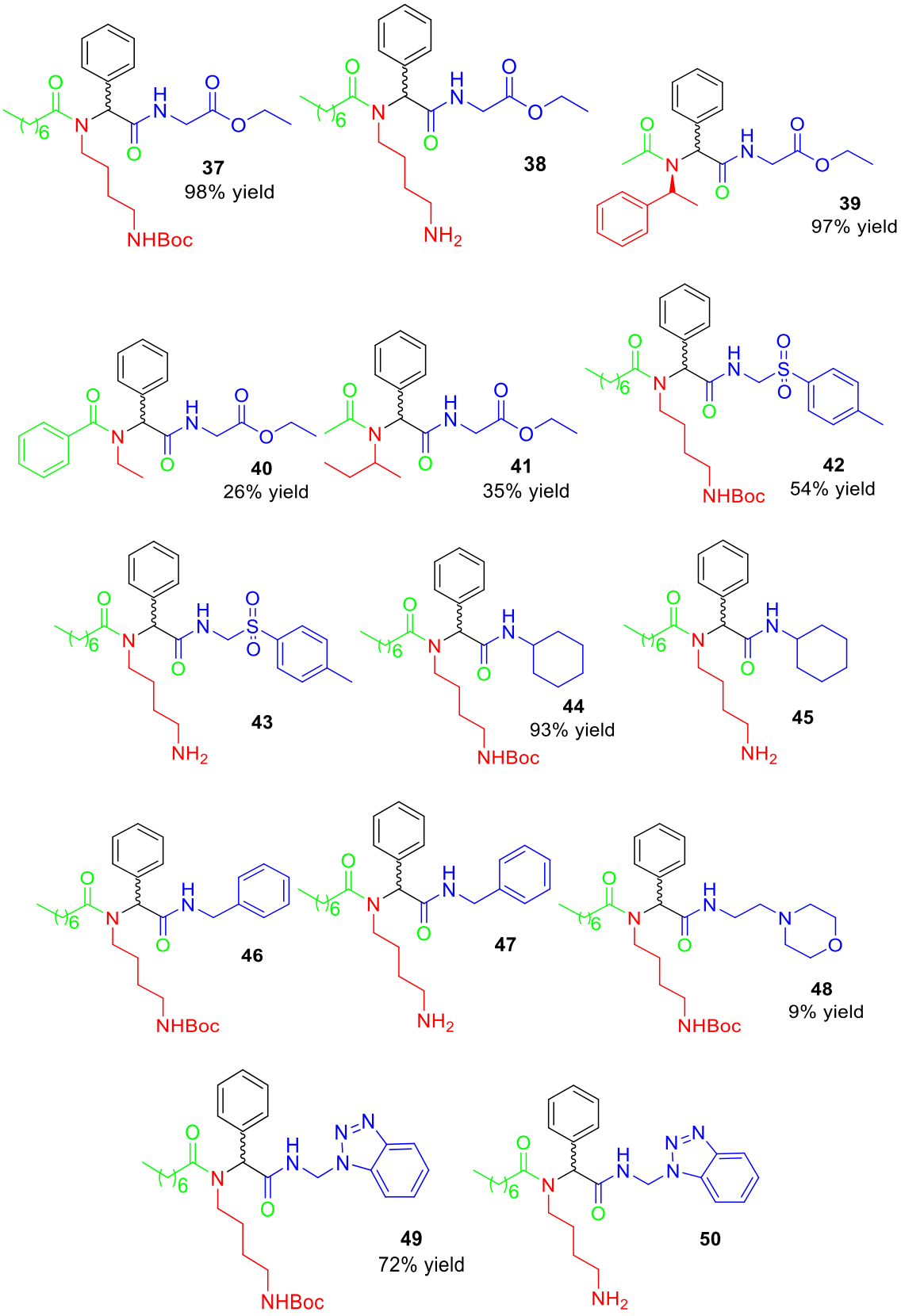

Figure 4.4. Functionalised peptoid library prepared using Ugi 4CR. (Please note that yields are not given for **38**,**43**,**46**,**47** and **50** because their purity is below 95% based on ^{1}H NMR)

It is worth noting that for some of the lipopeptoids that contain a Boc group, acidic deprotection was carried out as shown in **Scheme 4.5** to generate the free amine series of compounds.

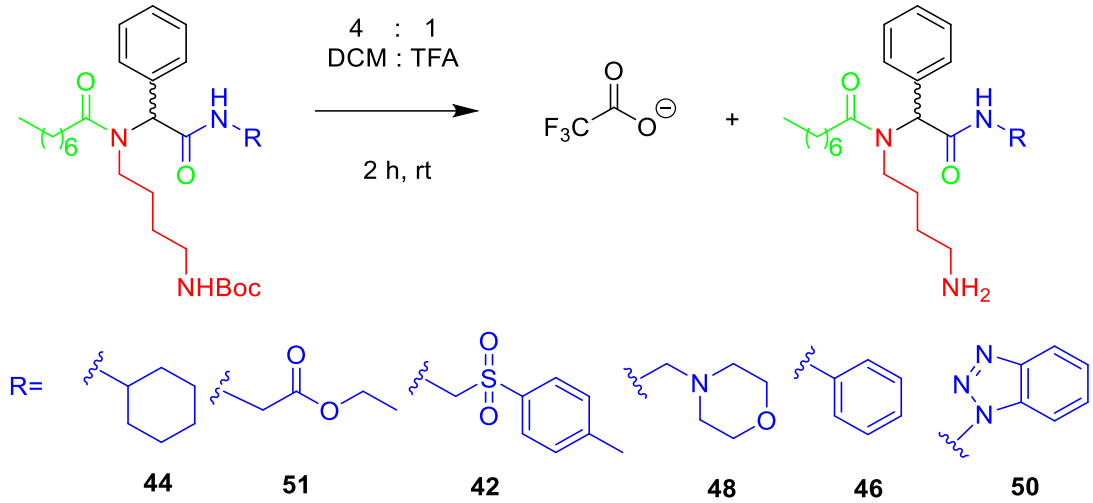

Scheme 4.5. Boc deprotection of general peptoid.

4.3 Analysis of anti-leishmanial activity of 1st generation library

Initially, all the compounds prepared (**Figure 4.4 –** both pure and "crude" materials) were tested against *L. mexicana* promastigotes and axenic amastigotes at a single fixed concentration of 50 μM. It should be noted that the while compounds were obtained with a purity range between 70-90% the decision was made to test all materials prepared. If the compounds displayed an activity of greater than 50% in the first screen at 50 μM, then EC_{50} values were obtained. The results obtained from this initial biological screen are given in **Table 4.2**.

Table 4.2 Peptoids tested against *L. mexicana.*

Entry	Compound	*L. mexicana* axenic amastigotes survival (%) at 50μM-	EC_{50} (μM) axenic amastigotes	*L. mexicana* promastigotes survival (%) at 50μM-	EC_{50} (μM) promastigotes
1	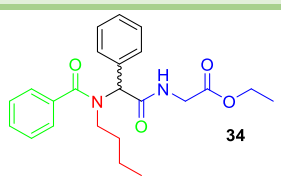 34	31.30	8.61	37.48	53.42
2	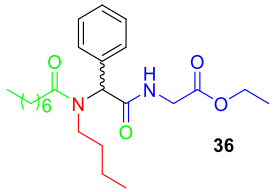 36	4.13	6.21	34.74	44.50
3	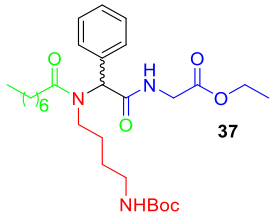 37	Not tested	-	6.87	28.54
4	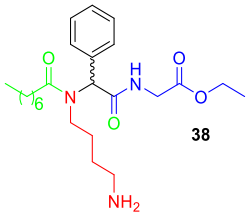 38	>100	-	89.87	-
5	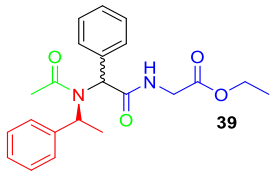 39	38.69	6.69	72.30	-
6	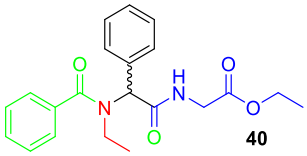 40	31.52	3.83	5.62	27.92
7	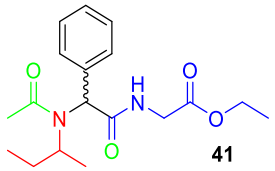 41	79.22	>50	>100	-
8	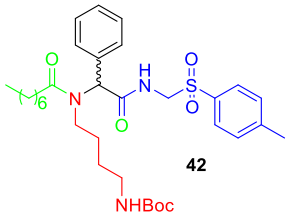 42	9.99	26.39	6.88	34.95

9	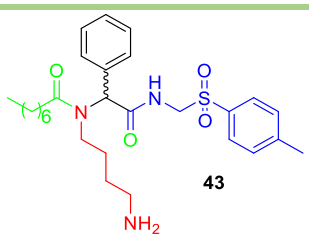 **43**	9.99	>50	>100	-
10	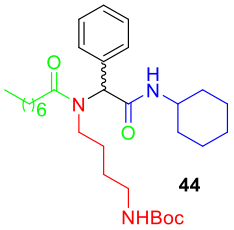 **44**	50.87	5.04	93.19	-
11	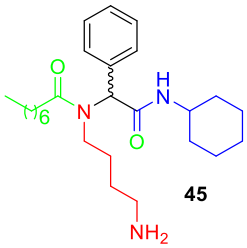 **45**	>100	>50	>100	-
12	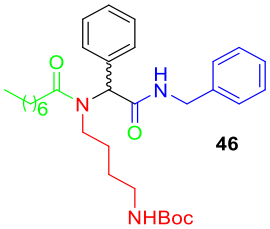 **46**	40.25	24.41	8.27	19.47
13	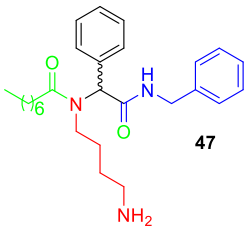 **47**	>100	>50	>100	-
14	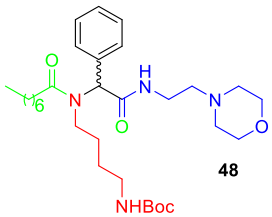 **48**	77.56	>50	73.99	-
15	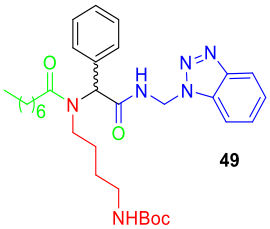 **49**	46.22	31.58	4.84	28.74

16	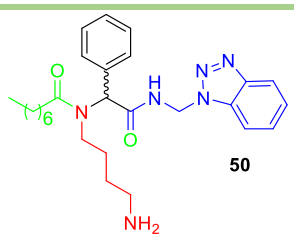 **50**	97.17	>50	81.20	-

Compounds **38**,**43**,**46**,**47** and **50** have a purity below 95% (determined by ^{1}H NMR) but were screened to have a preliminary study and therefore to determine whether the biological activity was present or not.

Compound **40** (**Table 4.2, Entry 7**) was found to have activity against both the promastigote and axenic amastigote stages of the *L. mexicana* parasite. It has an EC_{50} = 27.92 µM against the promastigote stage of the parasite, and, interestingly, a lower EC_{50} (3.83 µM) against the axenic amastigote stage.

Compounds **42** and **43** (**Table 4.2, Entries 9** and **10**) also have similar activity against axenic amastigotes, with EC_{50}'s of 26.39 µM and > 50 µM respectively. In contrast, against promastigotes, these positively charged analogues lack antiparasitic activity. This lack of activity against the promastigote form of the parasite is seen with analogues in the library that have a free amine/positive charge, such as compounds **37**, **45**, **47**, and **50** (highlighted in red in **Table 4.2**, **Entries 4**, **12**, **14**, and **17**).

It is worth noting that for most peptoids in this library, the amastigotes are more susceptible than the promastigotes. In general AMPs exhibit the opposite effect with the promastigote form of the parasite typically being more susceptible.[12] Large differences in the cell surface coat of each parasite stage will clearly play a role in the selectivity seen for both the peptoid library screened here and AMPs. Three peptoids **42**, **46** and **49**, all showed very similar activity not only against the promastigote but also against the amastigotes. EC_{50} values were between 20-30 µM (**Table 4.2**, **Entries 9**, **13** and **16**). These peptoids have different building blocks only in one component (highlighted in blue) (**Table 4.2**).

The biological data obtained for our library was compared to that reported by Donate *et al*.[7] While the spp of *leishmania* tested in both cases was different (e.g. *L. mexicana* versus *L. amazonensis*), it was thought that such a comparison would be useful to identify

compounds that may have broader spectrum activity. It was also only possible to compare data for promastigotes, as no axenic amastigote data was reported in the Donate *et al*.[7] study. The comparison data is presented in **Table 4.3**.

Table 4.3 Peptoids with anti-leishmanial activity

Entry	Product	EC_{50} (μM) promastigotes *L. mexicana*	IC_{50} (μM) promastigotes *L. amazonensis* [7]
1	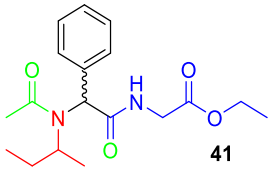 **41**	>100	2.80
2	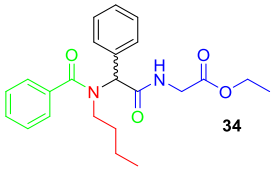 **34**	53.42	2.61
3	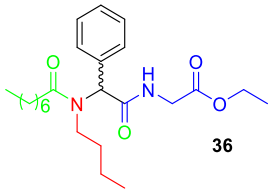 **36**	44.50	>10

The comparison of this limited data shows that peptoids can display promising levels of antiparasitic activity but activity against one species does not imply activity against another species of Leishmania (e.g. see compound **41**, **Entry 1**, **Table 4.3**). This result is similar to what is commonly observed and reported in the literature for AMPs.

To summarise the data, in the initial screening, at a fixed concentration of 50 μM, a range of the lipopeptoids were found to have activity against both the promastigote and axenic amastigote forms of *L. mexicana*. The compounds which killed more than 50% of the cell population were selected to calculate accurate EC_{50}. In particular, it is worth noting compound **40** which was found to have activity in the low μM range against *L. mexicana* axenic amastigotes with a EC_{50}= 3.83 μM (**Entry 6**, **Table 4.2**).

4.4 Design of a second-generation peptoid library

Based on the analysis of the initial biological data it was felt that it would be worth investigating variants of compound **40** (e.g. **Figure 4.6**). This would enable us to see how this structural modification affects not only the peptoids' physical properties but also their biological activity.

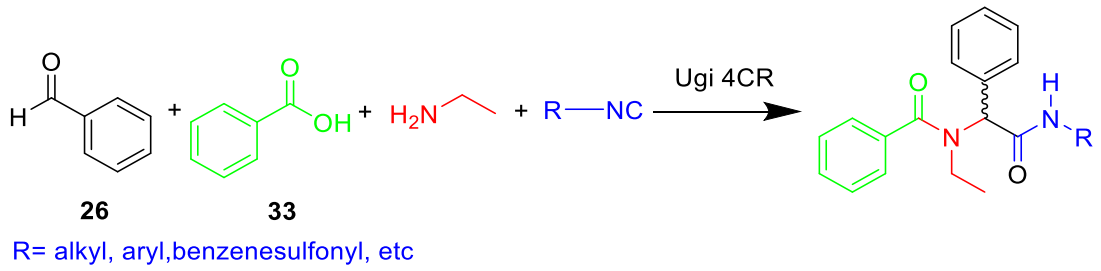

26 **33**

Scheme 4.6. Potential initial modifications in the peptoid scaffold of compound **40**

In addition to probing the structural features that impact biological activity, further investigation into the Ugi mediated peptoid synthesis was also warranted. From the initial library several peptoids, with a purity between 70-90%, were found to exhibit biological activity. Some of these compounds even had anti-leishmanial activity against the axenic amastigote form of the parasite (EC_{50} values below 5 µM, **Table 3.2**). Thus, there was desire to try and improve their overall synthesis and purity. The second-generation library which was based on compound **40** was designed by Mr Michael A. Bronswyk, an MChem project student in Cobb Group who worked under my supervision. Due to COVID-19 laboratory restrictions, the library was prepared by the author of this thesis and not Mr Michael A. Bronswyk. This work aimed to perform a structure-activity relationship (SAR) study on the lead compound (**40**) (**Figure 4.5**).

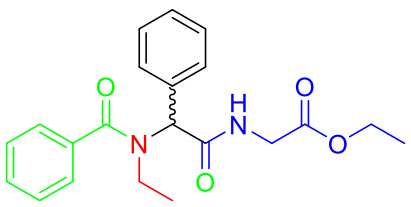

Figure 4.5 Lead compound (**40**) for production of the second-generation library.

Structural modification will be achieved by altering the amine (red), and isocyanide (blue) building blocks and the aromaticity of the benzene groups, see **Scheme 4.6**, as part of the future work discussed in **Section 4.4**. Some examples of these structural modifications are proposed in **Figure 4.6**.

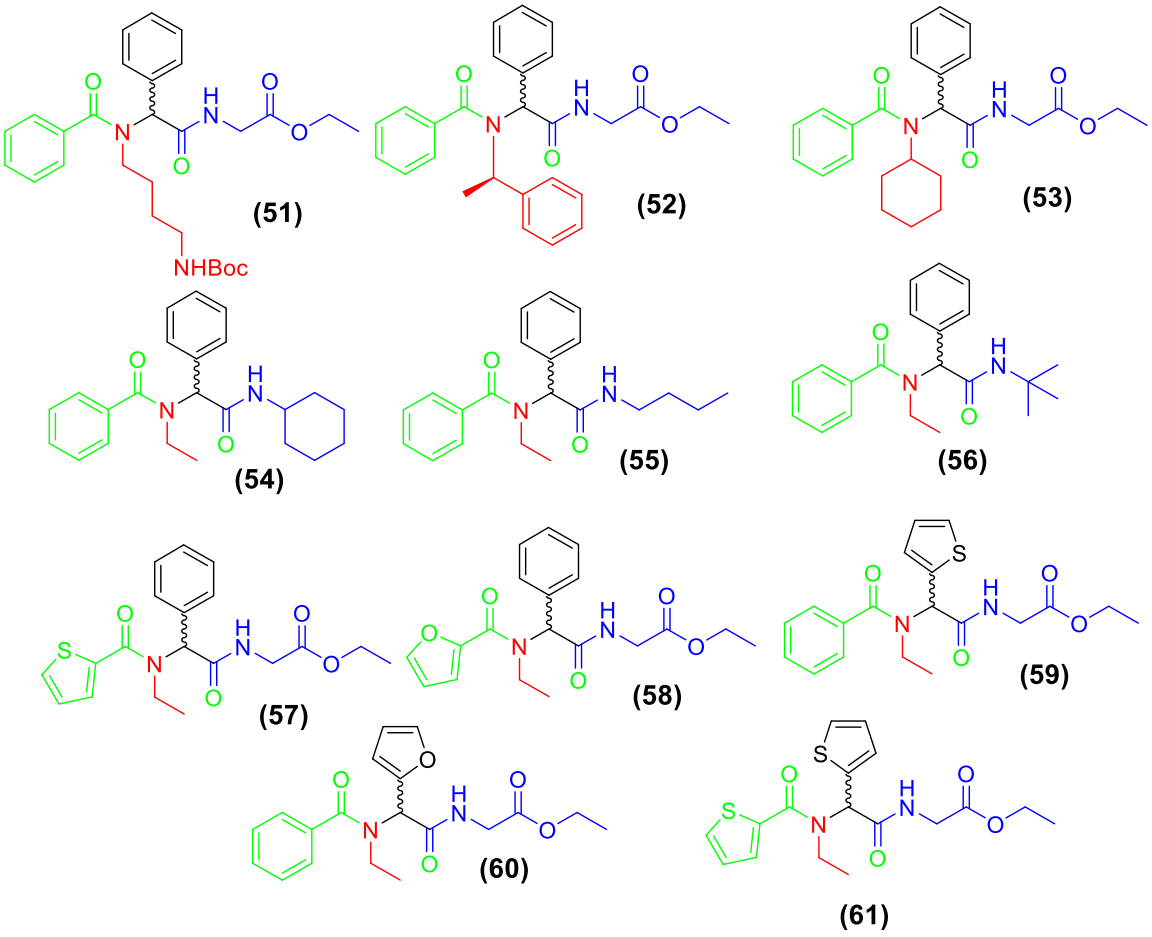

Figure 4.6. Target peptoids prepared as part of a second-generation lipopeptoid library.

Compound **52** was prepared, and an optimisation of the purification conditions was carried out to obtain a Ugi-4CR, after a basic work-up and a slow gradient solvent mixture during purification (as detailed in **Section 6.5.2**). Compound **52** incorporatesthe chiral aromatic amine (*N*spe monomer), which helped increase the efficacy against *L. mexicana* in a previous peptoid study reported by the Cobb group.[7] The acetic acid analogue of **52**,

synthesised by Donate *et al*, showed moderate activity against *L. amazonensis* promastigotes (45.80 ± 0.66 % inhibition at 100 µM). [8] For completeness, compound **52** was synthesised to establish the impact of the aromatic benzoic acid on the biological activity. The *sec*-butyl amino analogue (**41**), which contains a chiral centre at the same carbon, had significantly improved efficacy against *L. amazonensis* promastigotes compared to the *N*spe analogue, with an IC_{50} = 2.80 ± 0.38 µM, which could be a result of reduced hydrophobicity and sterics (**Table 4.3**). The optimisation of the purification step used in the preparation of the peptoids shown in **Figure 4.6** will be discussed in detail in **Section 4.5**.

In the initial screen *N*-Boc-1,4-butanediamine peptoids **42** and **46** (**Figure 4.4**) showed promising anti-leishmanial activity against both the axenic amastigote and promastigote forms of *L. mexicana*. This inspired the synthesis of **51**, the *N*-Boc-1,4-butanediamine analogue of the lead compound (**40**). The Boc protecting group was not removed in this study, as the free amine group which tends to enhance antibacterial activity, was actually found in the initial biological screen to significantly decrease anti-leishmanial activity (**Table 4.2**). In both peptoid libraries, the 1st generation library prepared (**Figure 4.4**) and the one reported by Donate *et al*[7], amines which contained alkyl groups of varying chain length were used. Neither study, utilised alicyclic amines although cyclohexane had incorporated into some compounds via the use of cyclohexyl isocyanide (e.g. compound **44**, **Figure 4.4**). Therefore, cyclohexylamine was used to synthesise peptoid **53** (**Figure 4.6**) to probe the effect that increased steric bulk at this position might have on both the Ugi synthesis and biological activity. The presence of an aromatic group at the isocyanide position, in general, increased the biological activity against the axenic amastigote form of the parasite (**Table 4.2**). Peptoids **55** and **56** were designed to test the isocyanide group with an alkyl group, **Figure 4.6**. *Tert*-butyl isocyanide was incorporated in **56** as this significantly increased the steric bulk at this position, with a Tolman cone angle of 182° for $P(^tBu)_3$ compared to 170° for PCy_3 and 145° for PPh_3, indicative of **45** and **47** respectively.

With a cone angle greater than 180°, this would also effectively shield the adjacent NH group. If compound **56** shows significantly reduced biological activity this could indicate that there are favourable interactions between the NH group and the biological target, such as hydrogen bonding.

The nature of the aromatic substituents was also expanded to included heteroaromatic derivatives, with thiophene and furan, being incorporated into the peptoid library (compounds **57- 61**, **Figure 4.6**). The purpose of including heteroaromatics was to explore potential interactions with the biological target. In addition, heteroaromatics can often enhance solubility in the aqueous phase as they reduce the overall hydrophobicity of a given molecule.

4.5 Attempted optimization of peptoid purification methods

In the initial 1st generation peptoid library preparation, methanol (MeOH) was used to wash the crude reaction mixture to remove impurities. In the synthesis of the 2nd generation library however, saturated sodium bicarbonate ($NaHCO_3$) was investigated as an alternative. With pKa 6.34 dependent on reaction, $NaHCO_3$ could more easily remove slightly acidic impurities in the reaction, such as benzoic acid 4.20 pKa, as illustrated in the ^{1}H NMR spectrum of (**51**) (**Figure 4.7** and **Figure 4.8**). $MgSO_4$ was then added to the crude reaction mixture to remove any water that had been formed during the extraction.

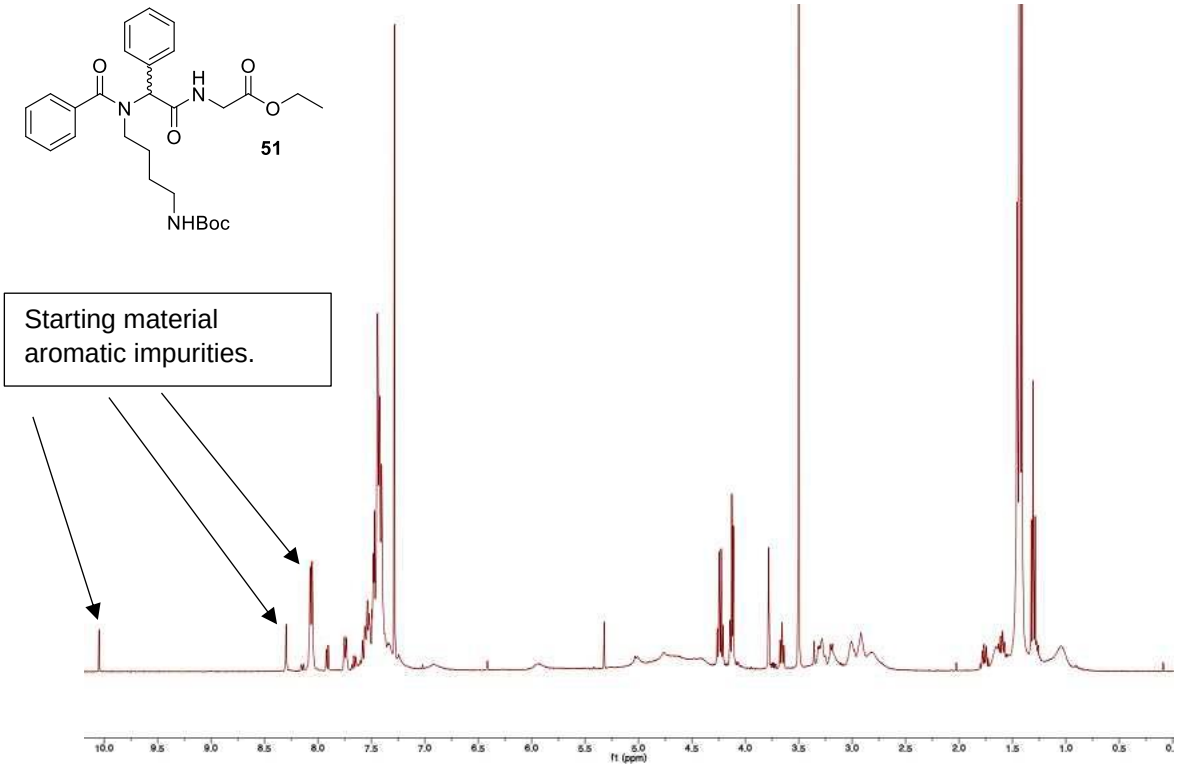

Figure 4.7. ^{1}H NMR ($CDCl_3$) spectrum for the crude mixture of compound **51**.

The singlet peak at 10.12 ppm (**Figure 4.7**) is indicative of the CH proton in benzaldehyde, one of the building blocks of peptoid **51**. After **51** was washed with sodium bicarbonate, the singlet at 10.12 ppm was no longer presented in the ^{1}H NMR spectrum (**Figure 4.8**), suggesting that the excess benzaldehyde has been removed. This is further evidenced by the reduction in peaks in the aromatic region of the spectra (7.5 – 8.5 ppm). The impurity peaks retained in the NMR spectrum between 1.0 ppm to 4.5 ppm (**Figure 4.8**), are indicative of residual isocyanide and amine building blocks, which are to be removed via column chromatography.

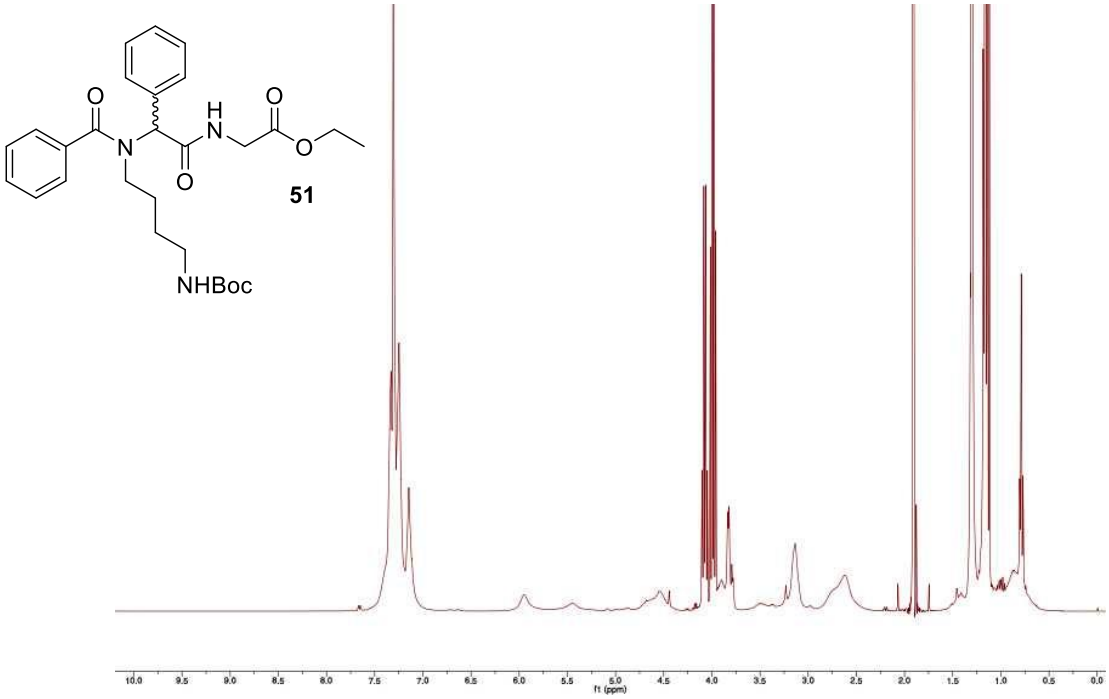

Figure 4.8: ^{1}H NMR ($CDCl_3$) spectrum of compound **51** post wash with sodium bicarbonate.

In addition to this, it was also evident that there needed to be greater separation between the product and residual starting materials within the crude mixture during purification by column chromatography. As an example, **52** was flushed through the column as an impure mixture with DCM/MeOH (98:2, *v/v*) as the eluent. Traces of benzaldehyde were still present, in addition to a small amount of the P-3CR product, which due to similarities in structure, has a similar polarity. Thin layer chromatography (TLC) plates of crude **52** (**Figure 4.9**), show how the less polar hexane/ EtOAc (50:50 *v/v*) solvent system provides greater separation between reagents and products, indicated by a number of spots and separation over the TLC plate compared to the DCM/MeOH (98:2 *v/v*).

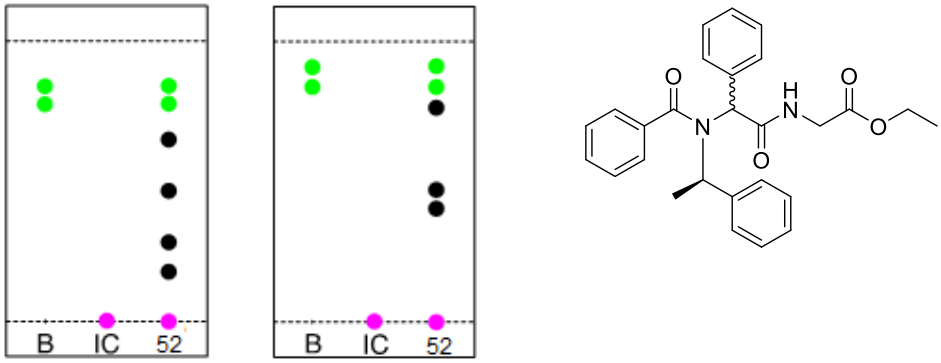

Figure 4.9: TLC plate of crude mixture (**52**), ***B*** = Benzaldehyde, ***IC*** = ethyl isocyanoacetate in Hexane/ EtOAc (50:50 *v/v*) (left) and DCM/MeOH (90:10, *v/v*) (right).

Given the TLC separation, a prep plate was carried out using hexane/ EtOAc (50:50 *v/v*) as a solvent system. Unfortunately, the recovered target product was found to still not have a purity of >90% (LC-MS shown in **Figure 4.10)**. Further NMR characterization also confirmed its low purity.

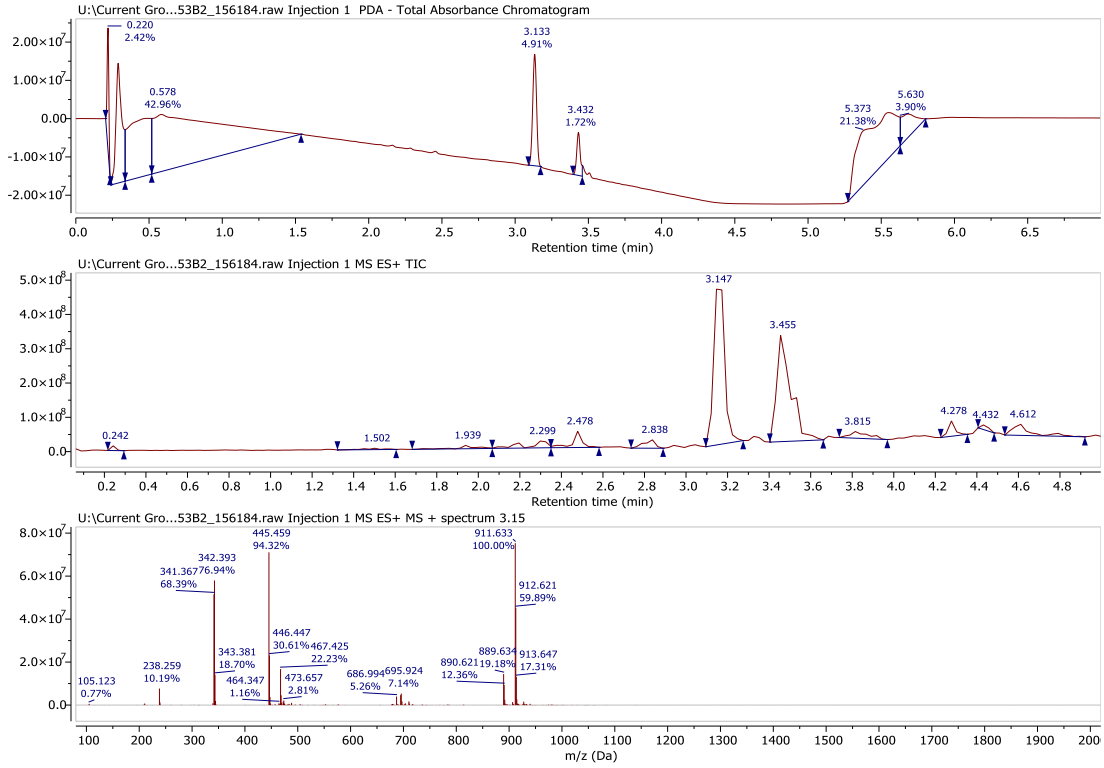

Figure 4.10. ESI LCMS viewed in positive mode, indicating the presence of compound **52**.

Peptoids **51** and **52** have different molecular structures and yet both were found to be difficult to purify. Despite adding a basic workup step and changing the solvent system in the purification step, peptoids were still not pure enough (e.g. did not have a purity >90%

by NMR analysis). A similar situation occurs with **53** (**Figure 4.6**). Cyclohexylamine was used to probe the effect that increased steric bulk at this position might have on both the Ugi synthesis and biological activity. The increased steric bulk of the amine used in the preparation of **53** had a detrimental effect on the Ugi reaction, resulting in a reduced yield of 25% being obtained (compound **53**, **Figure 4.6**). However, the purity of **53** was not greater than 90% (as determined by NMR) and as such an optimised purification method was therefore still needed.

After the synthesis of **54**, the crude reaction mixture was washed with saturated sodium bicarbonate. A sample was then submitted for liquid chromatography-mass spectrometry (LC-MS) and ^{1}H NMR spectroscopy. This provided evidence of the P3CR product (**62**), with a *m/z* = 338.18 assigned to $[M+H]^+$ being formed as the major component in the mixture. The formation of the 3CR reaction product was thought to be the result of an insufficient amount of amine being present in the reaction relative to the isocyanate (1:9 ratio was used). A similar result, e.g. formation of the P3CR product/ mixture of products, was obtained in the case of the reactions that were set to prepare peptoids **56**, **57**, **59** and **60**. The reaction and purification of peptoids **54**, **55**, **56** and **58** (**Figure 4.6**) will be discussed in detailed in **Section 4.6**.

4.5.1 Boc analogues

The previously reported Donate *et al*.[7] purification conditions which utilised DCM/MeOH did not work well for our compounds (e.g. see TLC example - **Figure 4.9**). Several of the compounds prepared in the 1st generation peptoid library proved to be challenging to purify to >90% and pure, their structures are shown in **Figure 4.11**.

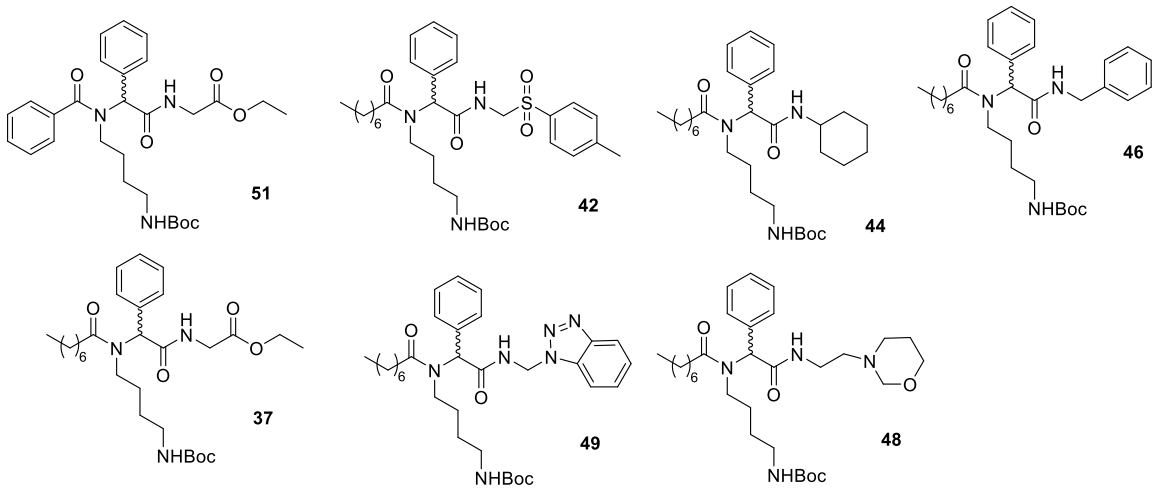

Figure 4.11. Boc protected peptoids from the 1st generation library that proved challenging to obtain in >90% purity.

It was decided to remake the compounds shown in **Figure 4.11** and attempt to optimise the purification conditions. A summary of the work that was carried out is provided in **Table 4.4**.

Table 4.4. Purification conditions used for Boc analogues.

Entry	Compound	Purification conditions	Purity >90 % *	Isolated yield
1	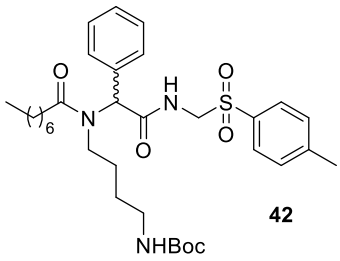 **42**	Column chromatography DCM/MeOH 90:10	No	Non quantitative
2		Prep plate Hexane/ EtOAc 50:50	No	Non quantitative
3		Combiflash 24g RediSep Gold column 20-40 microns Hexane/ EtOAc	Yes	18%
4	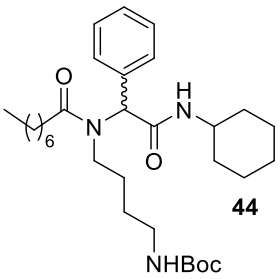 **44**	Column chromatography DCM/MeOH 90:10	No	Non quantitative
5		Prep plate Hexane/ EtOAc 50:50	No	Non quantitative
6		Combiflash 24g RediSep Gold column 20-40 microns Hexane/ EtOAc	Yes	49%
7	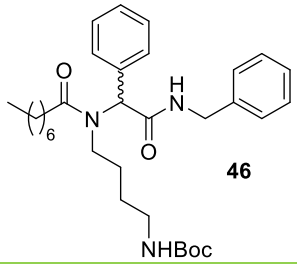 **46**	Column chromatography DCM/MeOH 95:5	Yes	30%
8	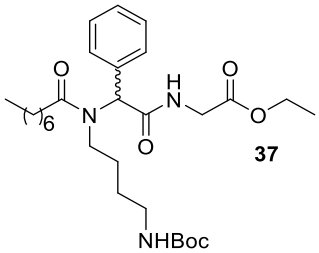 **37**	Column chromatography Hexane/ EtOAc 40:60	Yes	9%

9		Column chromatography Hexane/ EtOAc	No	
10	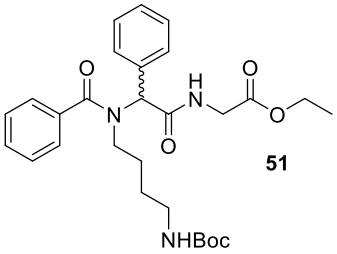 **51**	Combiflash RediSep column 40-60 microns	Yes	21%
11		Combiflash RediSep column 40-60 microns	Yes	35%
12		Combiflash RediSep Gold column 20-40 microns	Yes	38%
13	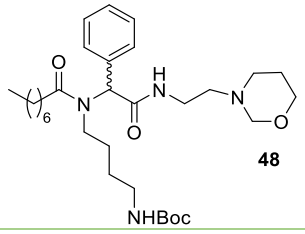 **48**	Column chromatography DCM/MeOH 96:4	No	
14		Combiflash RediSep Gold column 20-40 microns	No	
15	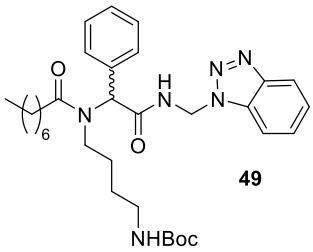 **49**	Column chromatography DCM/MeOH 90:10	No	
16		Prep plate DCM/ MeOH 90:10	No	Non quantitative
17		Combiflash RediSep Gold column 20-40 microns Hexane/ EtOAc	Yes	Only 5mg

*Purity based on ^{1}H NMR analysis

Compound **46** was prepared again on a 0.457 mmol scale according to the protocol detailed in **Section 6.5.1** and obtained in a low yield (30%). It was the only Boc analogue prepared and obtained with a purity of greater than 90% by column chromatography with DCM/MeOH as a solvent mixture-**Table 4.4**, -**Entry 7**.

After an initial standard column purification both compounds **42** and **44** were repurified using a preparative TLC plate with Hexane/ EtOAc (50:50 *v/v*) as a solvent system **Table 4.4**, **Entries 2** and **5** respectively. Given the poor yields, the reactions were carried out on a large scale to try and ensure that enough material could be obtained for biological testing.

For compound **51** and **37** preparation was scaled up 5 times (from an 0.457 mmol scale to a 2.285 mmol scale). Moreover, a protocol for the peptoids that are Boc protected was needed. Thus, a workup was added as previously detailed, for compound **51**, in **Section 4.6**.

A slower gradient was attempted with Hexane/EtOAc as a solvent mixture for the purification of compound **37,** the product was obtained with an isocratic gradient of 40:60 v/*v* Hexane/EtOAc and less than 10% yield- (**Table 4.4**, **Entry 8**). Another purification was carried out with compound **51**, monitoring the column carefully by TLC and comparing the R_f with the starting materials- **Table 4.4**, **Entry 9**. Unfortunately, the desired product was not pure enough by NMR analysis and was collected for further repurification.

Given the complexity of the reactions mixtures and the continued lack of results with manual column chromatography (and preparative TLC) it was decided to try using a an automated Combiflash Nextgen 100 equipped with redisep columns.

Compound **51** was repurified in a standard 10 min program on the Combiflash using Hexane/EtOAc as a solvent system with an automated peak collection by UV detection. This led to **51** being obtained in >90% purity in a 21% yield (**Table 4.4**, **Entry 10**).

Given the improved purification conditions, **51** was re-synthesised on a 2.285 mmol scale and different purification Combiflash conditions were tested. Firstly, the same type of redsip silica gel disposable flash column with 40-60 microns was used with a UV detection of 254 and 280 nm (**Table 4.4**, **Entry 11**). Secondly, a smaller particle size column was chosen, the redsip Gold silica gel disposable flash column with 20-40 microns. The latter column provided the best purification results, and **51** was obtained in a 38% yield (**Table 4.4**, **Entry 12**).

Compounds **42** and **44** were re-synthesized on a 0.457 mmol scale and purified successfully under optimized conditions shown in **Table 4.4 Entries 3** and **6**, respectively.

Compound **48** was scaled up 3 times (1.37 mmol scale) and purification was attempted using manual column chromatography, but the target peptoid was not isolated (**Table 4.4**,

Entry 13). Another attempt was carried out with the automated purification conditions, shown in - **Table 4.4**, **Entry 13**. In this case **48** was identified by LC-MS but NMR characterization showed that the material recovered had a purity of less than 90%. It was therefore decided not to move forward with this particular peptoid. Similarly, it was not possible to obtain **49** in a purity of greater than 90% **Table 4.4**, **Entries 15** and **16**. An attempt was even made to collectall the fractions obtained for **49** from the initial purification attempts and repurified by Combiflash, **Table 4.4**, **Entry 17**. Even this approach did not yield any of **49** in which the purity was greater than 90%. Given the lack of purity no attempt to prepare the free amine of **49** via acidic deprotection was attempted**.**

Given that pure forms of peptoids **37**, **44**, **46** and **51**, from **Table 4.4** could be obtained these compounds were deprotected (removal of Boc) under acidic conditions. This yielded peptoids **38**, **45**, **47** and **67** all of which were full characterised (details can be found in **Section 6.5.5**).

4.5.2 Synthesis of peptoids using MW assistance

The 1st generation peptoid library was prepared as detailed in **Section 4.2** (see **Chapter 6, Section 6.5.1**). This entire library was deemed pure enough for the initial biological testing against *L mexicana* parasites with all compounds having a 70-90% purity. As mentioned, further investigation of the peptoid synthesis was warranted. Using this approach, detailed in **Section 6.5.1**, it was not possible to obtain all of the peptoids in a purity of greater than 90%. Peptoids which were analogues of compound **40** (the lead compound from the initial screening) that had proven difficult to prepare using the original conditions (see **Section 4.5**) were also selected. It was decided that a selection of peptoids should be remade in order to try and obtain purity levels of > 90% (**Figure 4.12**).

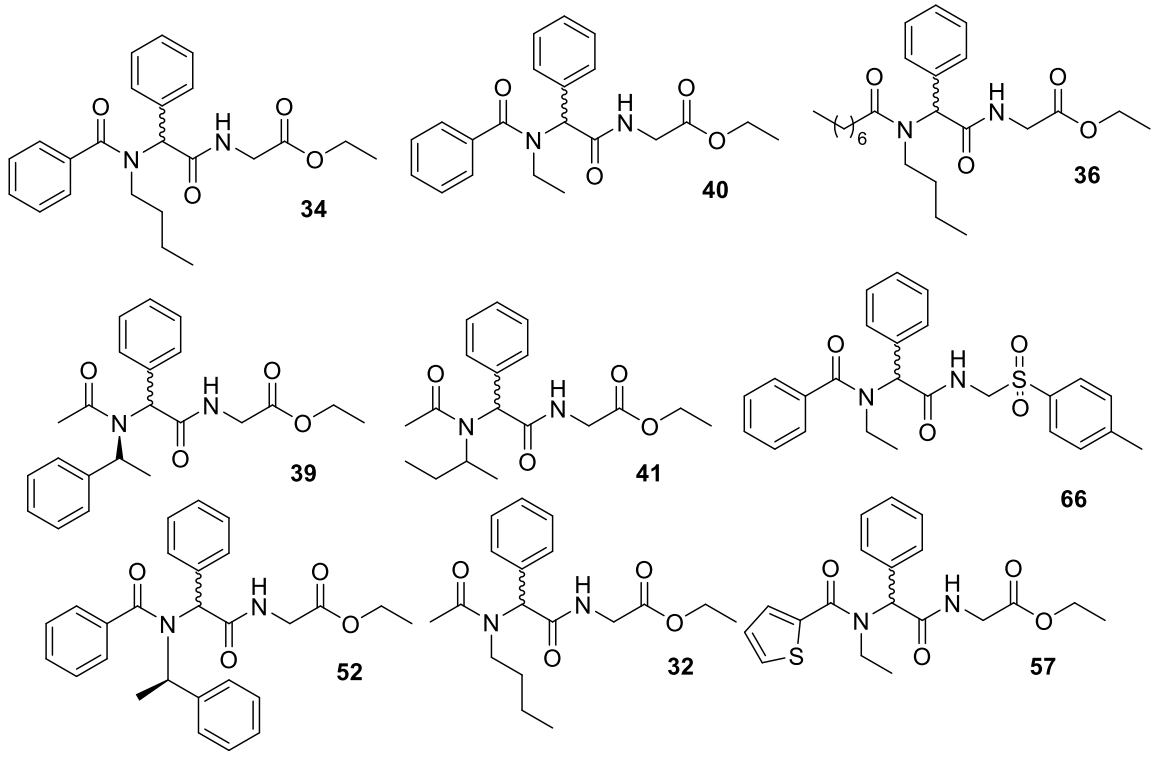

Figure 4.12. Peptoids that proved challenging to obtain in >90% purity selected for repurification. (**32**, **52**,**57** and **66** are peptoids that were not prepared in the 1st generation library).

The purification protocols used for each of the peptoids synthesised can be found in **Table 4.5**.

Table 4.5 Peptoids purification optimization

Entry	Compound	Purification conditions	Purity >90 %*	Isolated yield
1	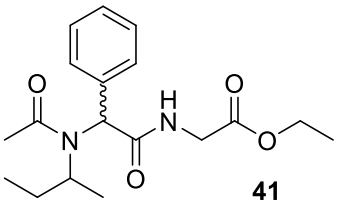 **41**	Column chromatography DCM/MeOH 90:10	No	-
2		Column chromatography Hexane/ EtOAc	No	-
3	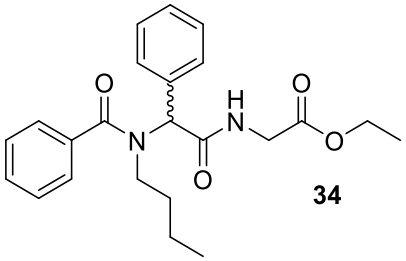 **34**	Column chromatography DCM/MeOH 90:10	No	-
4		Prep plate DCM/MeOH	70%	36%
5		Combiflash 12g RediSep Gold column 20-40 microns	80%	29%
6		Combiflash 12g RediSep Gold column 20-40 microns	90%	2%
7	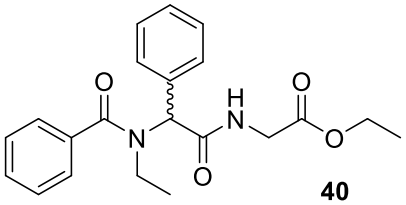 **40**	Prep plate DCM/MeOH 90:10	No	-
8		Combiflash 12g RediSep Gold column 20-40 microns Hexane/ EtOAc	No	-
9		Combiflash 12g RediSep Gold column 20-40 microns Isocratic hold Hexane/ EtOAc	80%	66%
10		PuriFlash reverse phase system Column: PFB-15C18XS-F0012	Yes	11%
11	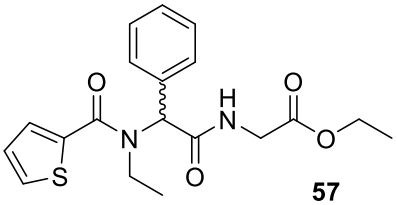 **57**	Combiflash 12g RediSep Gold column 20-40 microns Hexane/ EtOAc	Yes	78%

12	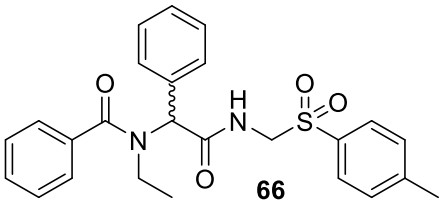 **66**	Combiflash 12g RediSep Gold column 20-40 microns Hexane/ EtOAc	Yes	48%
13	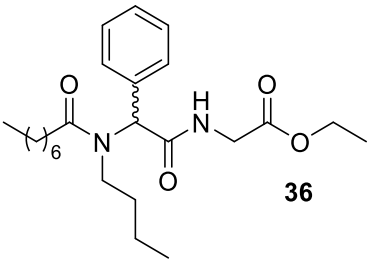 **36**	Prep plate DCM/MeOH 90:10	No	-
14		Combiflash 12g RediSep Gold column 20-40 microns Hexane/ EtOAc	80%	30%
15	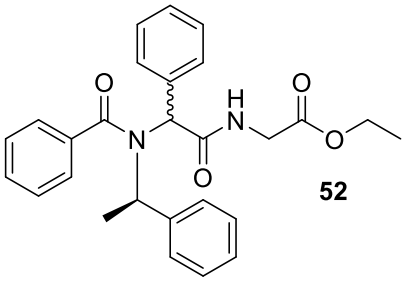 **52**	Column chromatography DCM/MeOH 95:5	70%	53%
16		Prep plate Hexane/ EtOAc 50:50	80%	48%

*Purity based on ^{1}H NMR analysis.

Compound **41** was scaled up to a 0.914 mmol scale according to the protocol detailed in **Section 6.5.1** and obtained with the same purity as before - **Table 4.5**, **Entry 1**. An unsuccessful repurification was carried out with another solvent system (Hexane/EtOAc) in a bigger column than before - **Table 4.5**, **Entry 2**. Compound **34** was also prepared according to the protocol detailed in **Section 6.5.1** and purified as reported by Donate *et al*.[7] as a part of the first-generation library-**Table 4.5**, **Entry 3**. A prep plate was carried out, giving the best purification conditions at that time without significant results (**Table 4.5**, **Entry 4**).

After using automated purification conditions along with another solvent system for the Boc analogues discussed in the previous section (**Section 4.5.1**), a similar approach was carried out with Compound **34**. It was prepared again according to the protocol in **Section 6.5.2** with a basic workup as detailed in **Section 4.6**. Purification was carried out with an automatic UV peak detection at 254 nm -**Table 4.5**, **Entry 5**. It was decided to repurify

these fractions with an isocratic gradient along with a supervised peak collection using both same column type and solvent mixture (**Table 4.5**, **Entry 6**). The ^{1}H NMR (**Figure 4.13**) shows the product was not a pure as required and the repurification did increased purity to >90% but a very low yield of the product was obtained - **Table 4.5**, **Entry 6**.

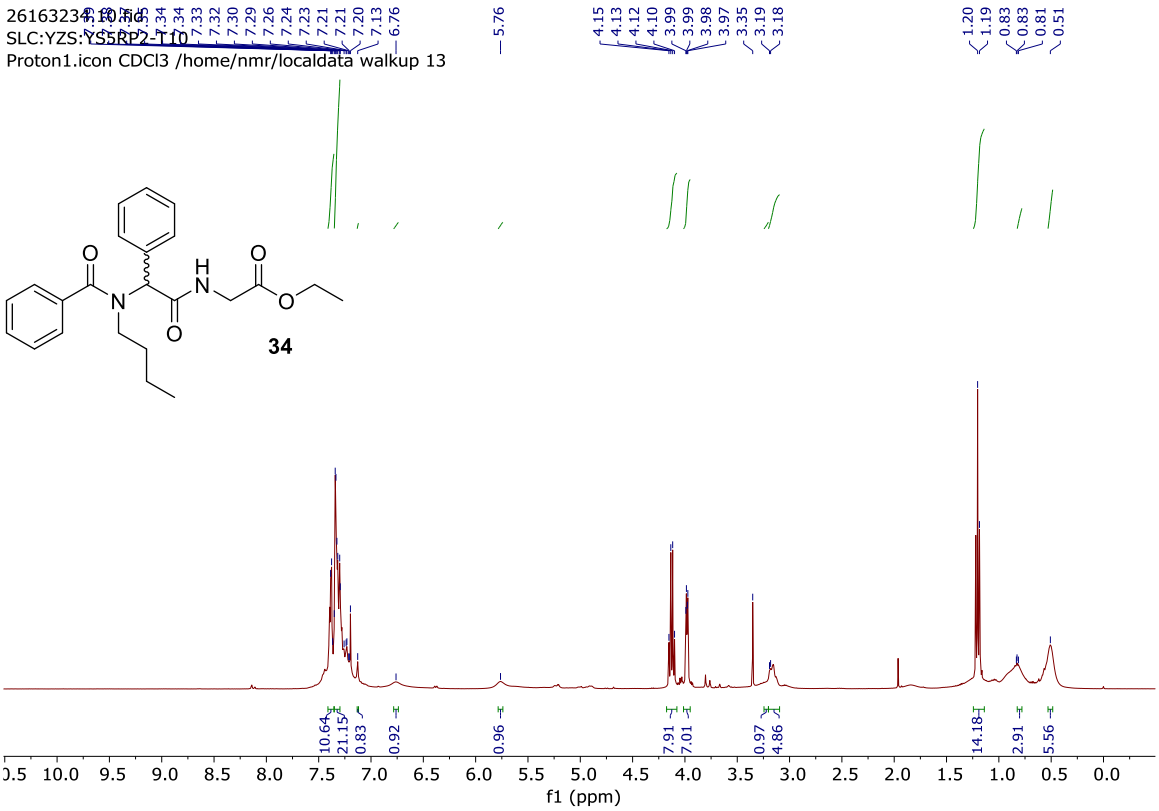

Figure 4.13. ^{1}H NMR ($CDCl_3$) of compound **34**.

Compounds **36** and **52** were initially prepared as detailed in **Section 4.2**. They were repurified by prep plates with no significant improvement in their purities due to the complex mixtures present - **Table 4.5**, **Entries 13** and **15**. Compound **36** was remade according to the protocol detailed in **Section 6.5.2**. Purification involved a basic workup and a purification by Combi flash. This gave the product in an approx. 30%, yield (**Table 4.5**, **Entry 14**) but a purity of <90%.

Peptoid **40** was prepared as part of the 1st generation library (protocol given in **Section 6.5.1**) was repurified using a prep plate but this did not give a product purity of >90%

(**Table 4.5**, **Entry 7**). Compound **40** was prepared again, now according to the procedure in **Section 6.5.2** in a 0.457 mmol scale. It was purified with the same automated conditions as **34**, and it yielded an impure mixture - **Table 4.5**, **Entry 8**. A repurification was carried out with the same automated purification conditions. An isocratic gradient was used when the desired peak was eluting with Hexane/EtOAc solvent mixture, **Table 4.5**, **Entry 9**. The NMR again showed that the compound was not as pure as required. An analytical HPLC sample was prepared and run according to the protocol detailed in **Section 6.2.5**. This revealed (**Figure 4.14**) that there was more than 2 min retention time of difference between the desired product (shown as $[M+H]^+$ peak) and its impurity. Given these results, it was decided to try and purify **40** by reverse phase HPLC.

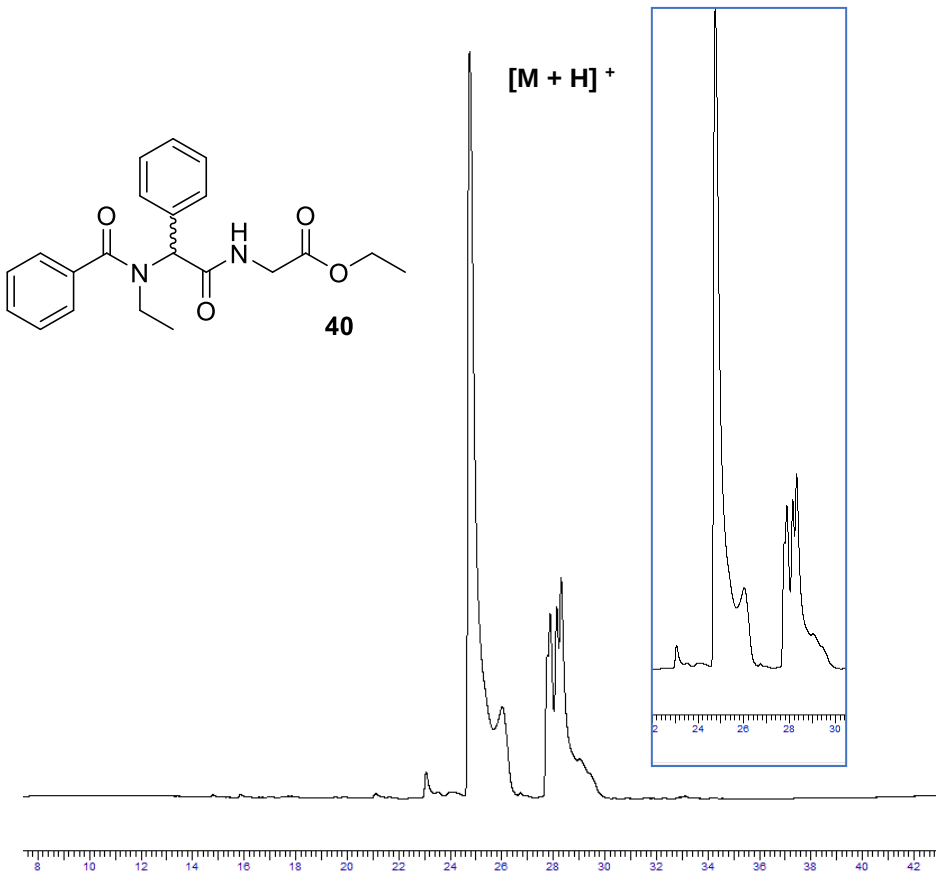

Figure 4.14.Analytical HPLC chromatogram (λ= 220 nm) of purification fraction of Compound **40**.

Purification of **40** was carried out using a PF XS 520 C_{18} Aq column with H_20: MeCN as a solvent mixture and a 60 min program (**Table 4.5**, **Entry 10**). Fractions were collected and analysed accordingly. Using this approach peptoid **40** was sucessfuly isolated with a purity of >90% as shown in **Figure 4.15**.

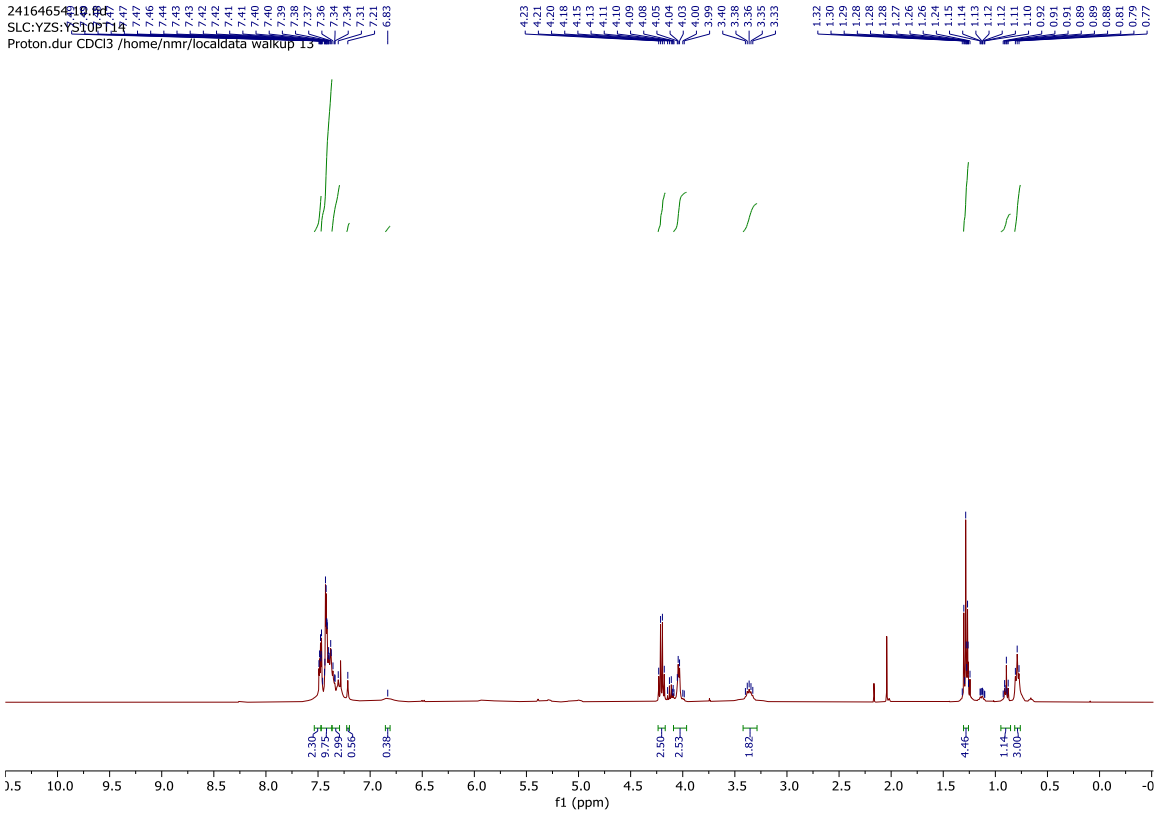

Figure 4.15. ^{1}H NMR ($CDCl_3$) of compound **40**.

Due to time restrains, optimized purification conditions using a reverse phase column (C_{18}) for the remaining compounds were chosen, see detailed procedure given in **Section 6.5.4**. A reverse phase system was set up in the Combi flash. It is the same instrument as the one detailed in **Table 4.5**. The solvent system was purged and replaced with the chosen aqueous solvent system with H_20 and MeCN. Instead of injecting directly the sample, like it was done with compound **40,** in the HPLC Pure Flash instrument, a dry loading was chosen to avoid any solubility issues.

Compounds **57** and **66** were prepared on a 0.457 mmol scale, crudes were prepared with Celite for dry loading in their adequate cartridges and purified directly with C_{18} reverse

phase system. Using this approach, the desired products were obtained in purities of >90% (**Table 4.5**, **Entries 11** and **12**).

Table 4.6. Purification conditions used for MW synthesised peptoids.

Entry	Compound	Purification conditions	Purity >90 %*	Isolated yield
1	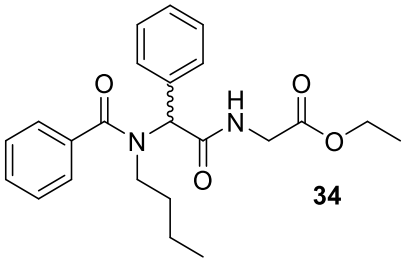 **34**	Combiflash 15.5 g Reusable RediSep Rf Gold® C_{18} Reversed Phase column, 20–40 microns 20-65%MeCN	Yes	87%
2	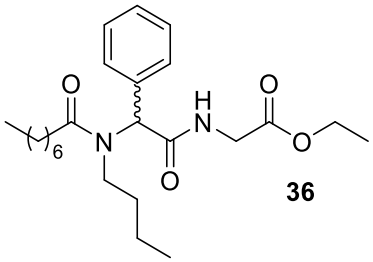 **36**	Combiflash 15.5 g Reusable RediSep Rf Gold® C_{18} Reversed Phase column, 20–40 microns 20-80%MeCN	No	-
3		Combiflash 15.5 g Reusable RediSep Rf Gold® C_{18} Reversed Phase column, 20–40 microns 30-65%MeCN	Yes	19%
4		Combiflash 15.5 g Reusable RediSep Rf Gold® C_{18} Reversed Phase column, 20–40 microns 10-80%MeCN	No	-
5	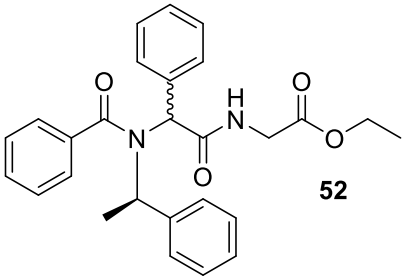 **52**	Combiflash 15.5 g Reusable RediSep Rf Gold® C_{18} Reversed Phase column, 20–40 microns 20-65%MeCN	Yes	77%*
6		Combiflash 15.5 g Reusable RediSep Rf Gold® C_{18} Reversed Phase column, 20–40 microns 43.9-67.5%MeCN	Yes	52%*

7	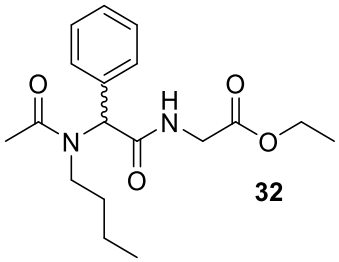 **32**	Combiflash 15.5 g Reusable RediSep Rf Gold® C_{18} Reversed Phase column, 20–40 microns	Yes	28%

* Reaction was split into 3 (**Table Entries 4-6**). Therefore, yields are based on crude input of **52** and an initial scale of 0.305 mmol. Purity based on ^{1}H NMR analysis.

Once lab access was again granted using microwave assistance was investigated to tackle some of the more challenge peptoids. It was decided to start with compound **34** to see which microwave conditions might work the best for the Ugi reactions that were being attempted. Different reaction timings with the same temperature of 60°C were investigated and the optimised conditions are described in **Section 6.5.3**.

Compound **36** (**Table 4.6**, **Entry 2**) was prepared according to the optimised procedure (**Section 6.5.3**). Combi flash reverse phase purification conditions, (**Section 6.5.4**), with a general linear gradient of 20% -80% B over 20 minutes (where A = H_2O; B = MeCN). Compound **36** was not isolated.

Similarly, compound **52** was prepared (**Section 6.5.3**) on a 0.914 mmol scale. Different purification gradients were attempted with the crude compound on the Combi flash reverse phase purification system. Firstly, a general linear gradient of 10% -80% B over 40 minutes (where A = H_2O; B = MeCN) - **Table 4.6**, **Entry 4**. Secondly, considering the product elution time another linear gradient was set up of 20% -65% B over 27 minutes (**Table 4.6**, **Entry 5**). Finally, an isocratic attempt was carried out at 43,9% B with no product elution ending in a gradient of 43.9% to 67.5%B over 20 minutes (**Table 4.6**, **Entry 6**). Chromatograms of all the Rf purification conditions were analysed along with the isolation of the desired product. The optimised conditions (**Table 4.6**, **Entry 5**) are detailed in **Section 6.5.4**. Compounds **34** and **36** (**Table 4.6**, **Entries 1** and **3**) were also purified under these conditions and yielded the target compounds in purities of >90%.

Peptoid **32** had proven to be challenging to prepare and isolate. A final attempt to obtain this peptoid using same microwave reaction conditions (as detailed in **Section 6.5.3**) was carried out. Compound **32** was purified according to (procedure given in **Section 6.5.4**) and this afforded the product in a purity of greater than 90% (**Table 4.6**, **Entry 7**).

4.5.3 Analysis of the biological and biophysical properties of peptoid library

After having successfully obtained a small peptoid library with a purity of greater than 90%, using a Ugi 4CR approach we sought to carry out biological testing. Initially, all the compounds prepared (**Section 4.5**) were tested against *L. mexicana* promastigotes and axenic amastigotes at a single concentration of 50 µM. Compounds that displayed an activity of greater than 25% in the first screen at 50 µM, were then progressed for further evaluation and their EC_{50} values were obtained. The results obtained from are given in **Table 4.7**.

Table 4.7. Pure peptoids tested against *L.mexicana**.

Entry	Compound	*L. mexicana* promastigotes survival (%) at 50μM-	*L. mexicana* axenic amastigotes survival (%) at 50μM-	EC_{50} (nM) axenic amastigotes
1	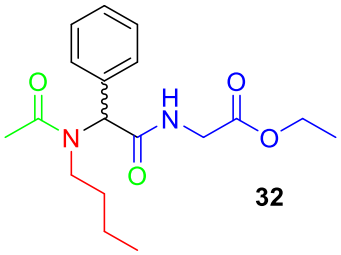 **32**	95	42	-
2	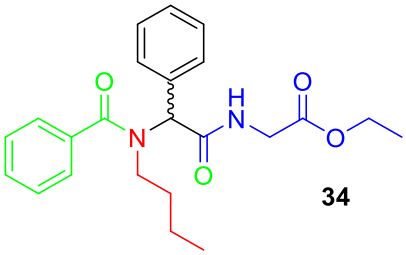 **34**	45	8	3
3	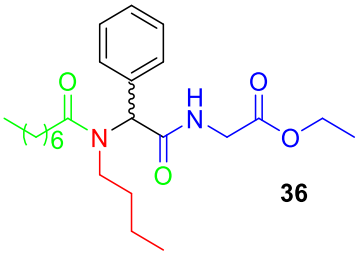 **36**	60	28	12
4	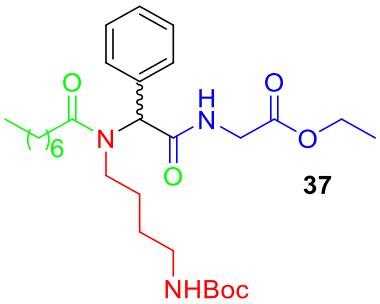 **37**	10	0	Solubility issues
5	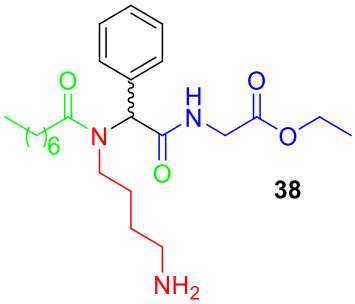 **38**	96	50	-

		59	1	9
6	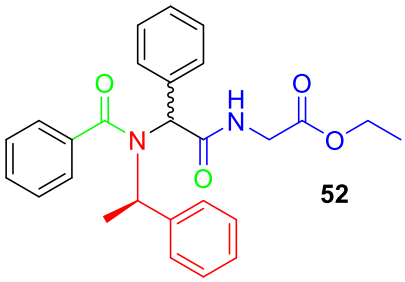 **52**			
7	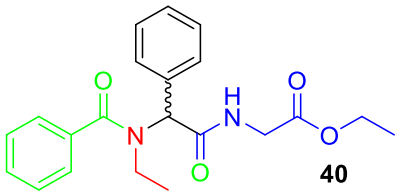 **40**	99	24	10
8	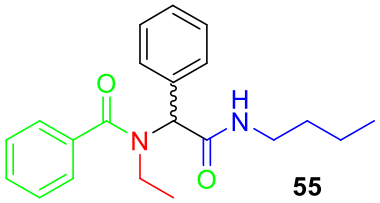 **55**	94	55	-
9	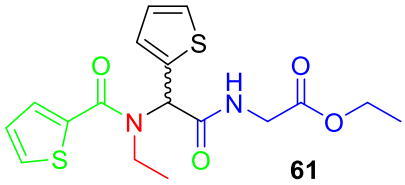 **61**	97	36	-
10	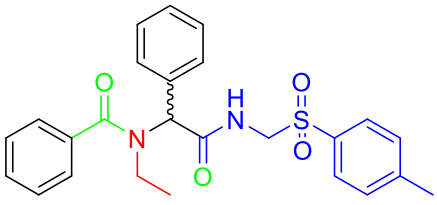 **66**	98	20	11
11	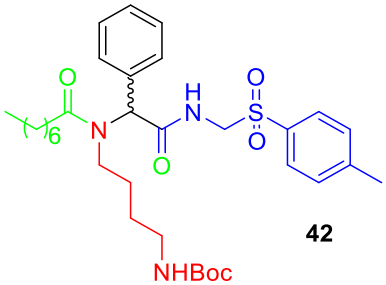 **42**	13	5	9
12	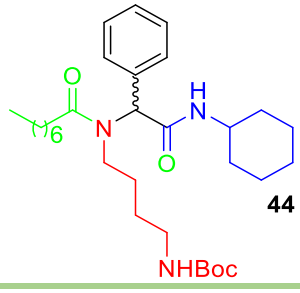 **44**	53	70	-

13	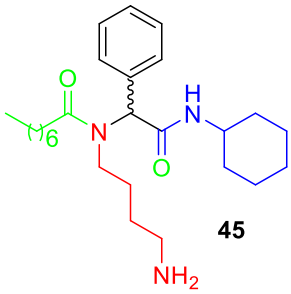 **45**	94	41	-
14	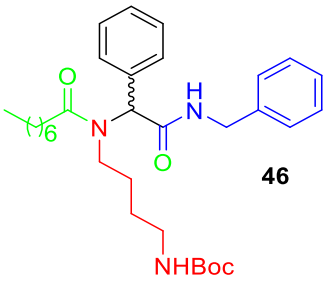 **46**	14	4	25
15	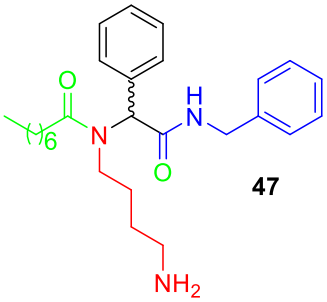 **47**	94	51	-
16	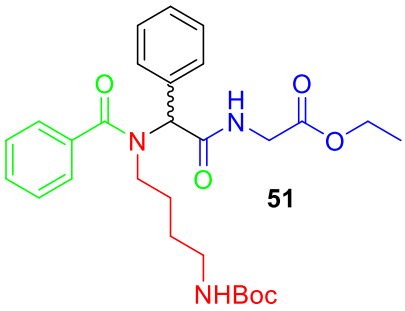 **51**	94	7	6
17	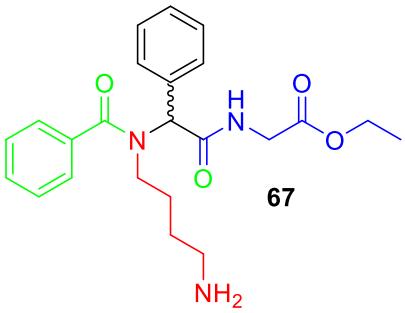 **67**	-	31	-

*All products had a purity greater than 90% as determined by NMR analysis.

In an attempt to rationalise the differences in biological activity seen in **Table 4.7**, some physicochemical properties for the compounds in the library were calculated using ChemAxon (**Table 4.8**).

Table 4.8 Analysis of the peptoid library's physical properties.

Entry	Compound	Lipinski's rule of five	Log P	H bond donor count	H bond acceptor count
1	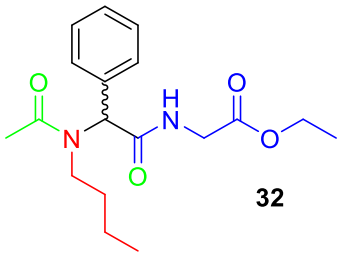 **32**	Yes	1.55	1	3
2	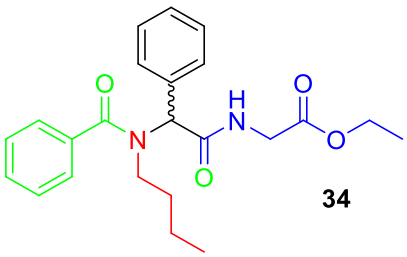 **34**	Yes	3.41	1	3
3	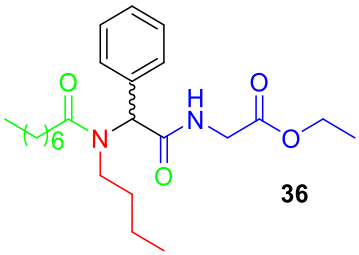 **36**	Yes	4.48	1	3
4	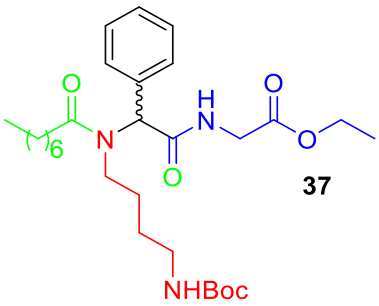 **37**	No	4.43	2	4
5	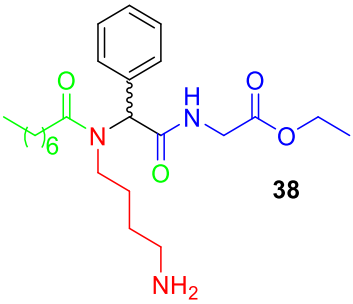 **38**	Yes	2.93	2	4

6	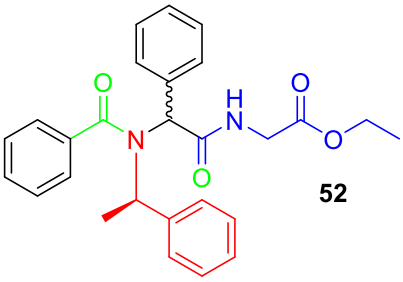 **52**	Yes	4.42	1	3
7	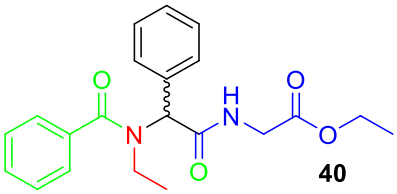 **40**	Yes	2.44	1	3
8	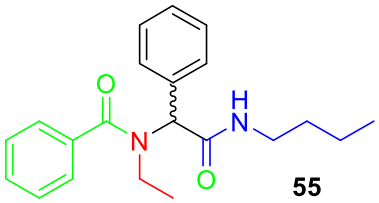 **55**	Yes	3.78	1	2
9	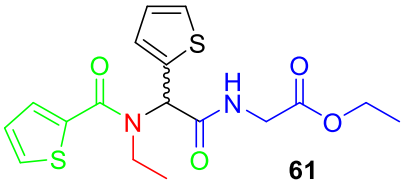 **61**	Yes	2.27	1	3
10	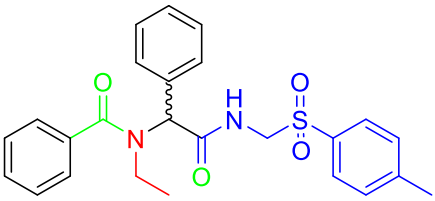 **66**	Yes	3.72	1	4
11	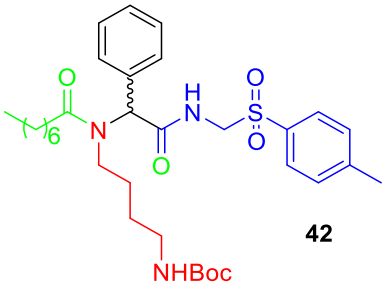 **42**	No	5.71	2	5
12	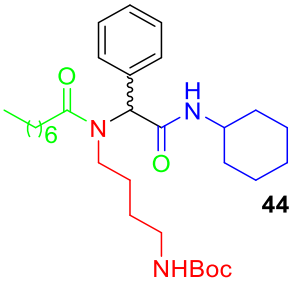 **44**	No	6.24	2	3

13	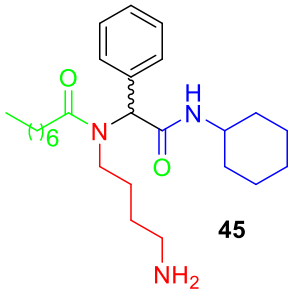 **45**	Yes	4.75	2	3
14	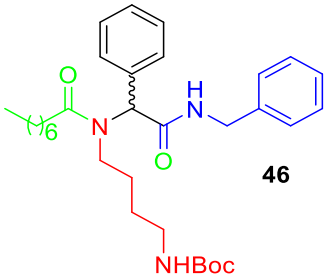 **46**	No	6.17	2	3
15	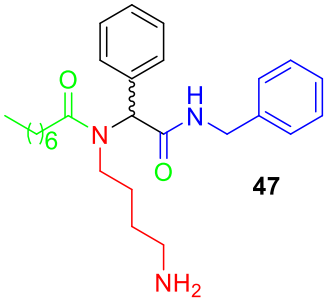 **47**	Yes	4.68	2	3
16	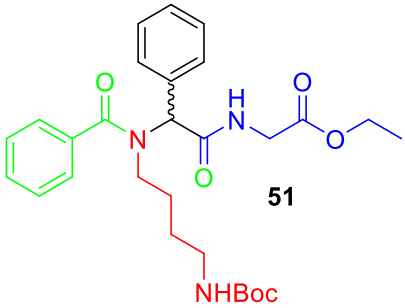 **51**	Yes	2.84	2	4
17	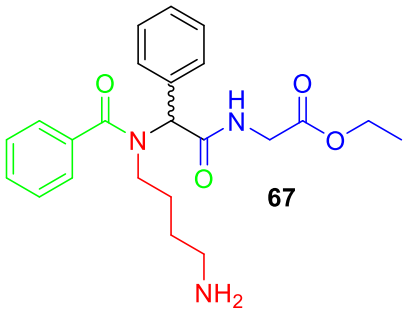 **67**	Yes	1.35	2	4

From **Table 4.8** it can be seen that 13 out of 17 peptoids adhere to Lipinski's rule of five. Most of the compounds also have a hydrophobicity that lies between 2.27 to 4.75. The peptoids that have a lipid tail, a 7-carbon side chain highlighted in green in the peptoid

backbone, have a LogP value between 2.93-6.24 (**Table 4.8**, **Entries 4**, **11**, **12**, **14** and **16**). Whereas those that do not, have lower LogP values. As expected, the lipopeptoids with a free amine have lower LogP values compared to those that do not (**Table 4.8**, **Entries 5**, **13**, **15** and **17**). The hydrogen bond donor capacity varies from 1 to 2, whilst their accepting capacity varies from 2 to 5.

A previous study, published by the Cobb group,[5] showed that the hydrophobicity of side chains in a peptoid sequence can influenced the anti-parasitic activity of the compound. An amine containing peptoid monomer (residue) with a shorter CH_2 chain was found to be more biological active against the axenic amastigote form of the parasite compared to a similar monomer that had a longer CH_2 side chain.[5] This could be the case for compound **52** (**Table 4.8**, **Entry 6**) since they also corresponded to Lipinski's rule of five and with a LogP<5. Thus, the results are promising. Peptoid **40** which was found to have a good level of antiparasitic activity with an EC_{50} = 10 nM (axenic amastigotes) but not better than its analogue, which contained an amine monomer with a longer CH_2 side with an EC_{50}= 3 nM (**Table 4.7**, **Entries 7** and **2** respectively)

Finally, having a part of the library with a lipid tail, a 7-carbon side chain, as part of the peptoid scaffold was useful to see how this would affect the antiparasitic activity (**Table 4.7**, **Entries 4**,**11**, **12**, **14** and **16**). In addition, some lipopeptoids are neutral and others can carry a positively charge. Differences in hydrophobicity/ charge and its effects on activity can be seen by comparing compound **46** (neutral) and its free amine analogue **47** (**Table 4.8**, **Entries 14** and **15**), which have a comparable antiparasitic activity against the axenic amastigote form of the parasite. Compound **46** does not follow Lipinski's rule of 5 but displayed a 4% growth of axenic amastigote form of the parasite being one of the best compounds among the Boc analogues. The neutral compound has a LogP>5, meaning that it will potentially have low aqueous solubility, compromising bioavailability as shown in **Figure 4.16**. On the other hand, some analogues with the same lipid tail possess the same solubility issue (LogP>5) when they are neutral, but they do not when they contain

a free amine (e.g., **44** and **46**). A clear example is **37** which experienced solubility issues (**Table 4.7**, **Entry 4**) which led to inconclusive results whereas its deprotected analogue **38** (with a free amine) has a 50% growth of the axenic amastigote form of *L. mexicana* (**Table 4.7**, **Entry 5**). The same goes for Lipinski's rule which the latest (**Table 4.8**, **Entry 5**) adheres to whereas **37** does not (**Table 4.8**, **Entry 5**).

In general, it is the case that removal of the Boc group to give the free amine peptoid resulted in a decrease in antiparasitic activity. Only one pairing, peptoids **44** and **55**, showed a reverse trend and removal of the Boc group enhanced antiparasitic activity (**Table 4.7**, **Entries 12** and **13**).

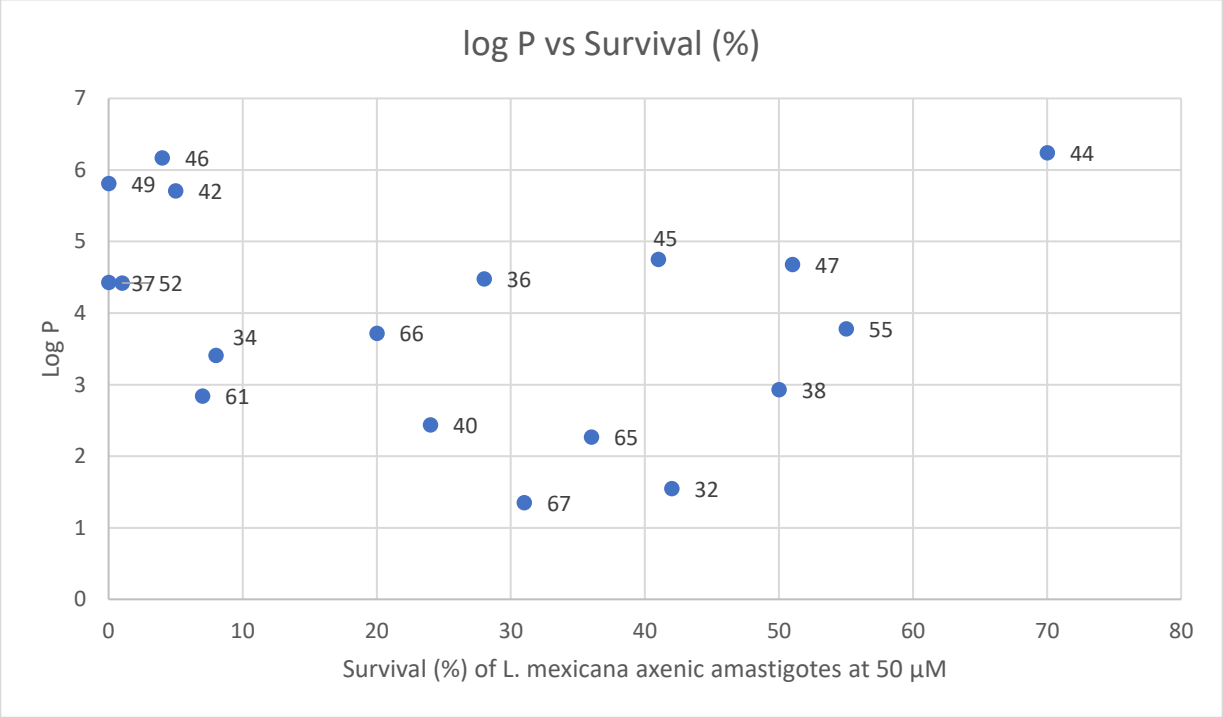

Figure 4.16. Log P vs percentage of survival of *L. mexicana* axenic amastigotes at a fixed concentration of 50 µM.

As **Figure 4.16** shows there does not seem to be a simple correlation between hydrophobicity and antiparasitic activity for the library of compounds screened. Except for compound **37,** which experiences solubility issues within an acidic pH in the axenic

amastigotes of *L. mexicana* assay (pH = 5.5), the other Boc analogues shown antiparasitic activity with a Log P>5, compounds **42** and **46** in **Figure 4.16**.

4.6 Anti-leishmanial activity of the Passerini-derived compounds

The isolation of the Passerini by-products (α-hydroxy carboxamides – **Scheme 4.7**) in this investigation led to the formation of a small library of compounds.

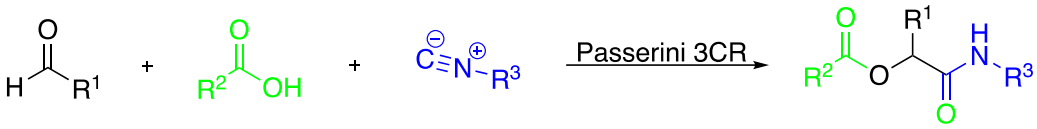

Scheme 4.7. General three-component Passerini reaction.

For example, compound **35** was isolated as a by-product isolated from an attempted Ugi reaction (**Scheme 4.8**). In this particular case it was hypothesised that the amine used (**31**) might have been protonated by the acetic acid (**29**) in the reaction mixture, and thus it was not available to react in the Ugi 4CR.[13,14]

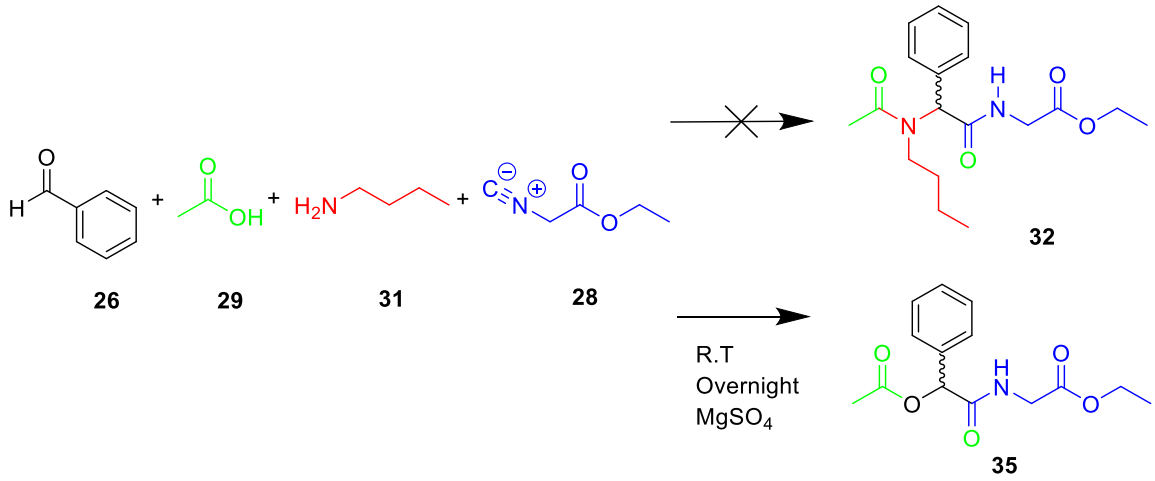

Scheme 4.8. Isolation of a Passerini by-product (**35**) from the attempted Ugi reaction to access peptoid **32**.

During the preparation of the second-generation library, it was shown that the ratio of amine to isocyanate has to be significant in order to obtain Ugi 4CR product (see **Section 4.5**). As a result, compounds **63**, **64** and **65** were also isolated as by-products the same way as compound **35** (**Figure. 4.17**).

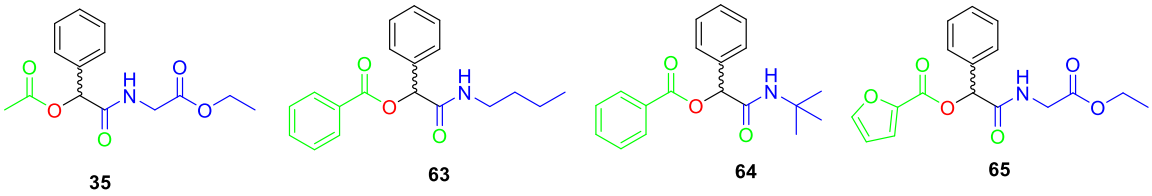

Figure 4.17. Passerini compounds isolated from Ugi reaction as by-products.

Reaction mixtures obtained in **Section 4.5** were analysed and purified. The crude reaction mixture of peptoid **56** (**Figure 4.6**) contained an even greater concentration of the Passerini compound (**64**, **Figure 4.17**). The by-product was successfully isolated and purified via column chromatography using DCM/MeOH (95:5 *v/v*) as the eluent, to give **64** in a yield of 92%. Alternatively, for the synthesis of **55** and **58**, both the Ugi and Passerini products were present in appreciable yields; **63** and **65** respectively. Utilising Hexane/ EtOAc (50:50 *v/v*) as the eluent, both the Ugi and Passerini products were isolated via column chromatography, with the Passerini product eluting first. The products were distinguished via ^{1}H NMR spectroscopy as detailed in **Section 4.2**.

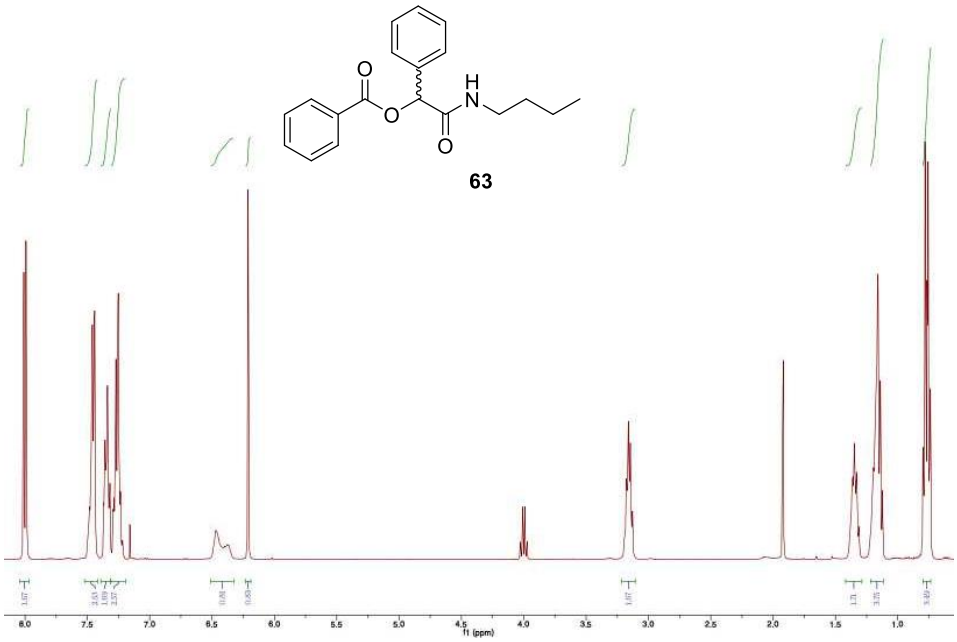

Figure 4.18: ^{1}H NMR ($CDCl_3$) spectrum for the three-component Passerini product **63**.

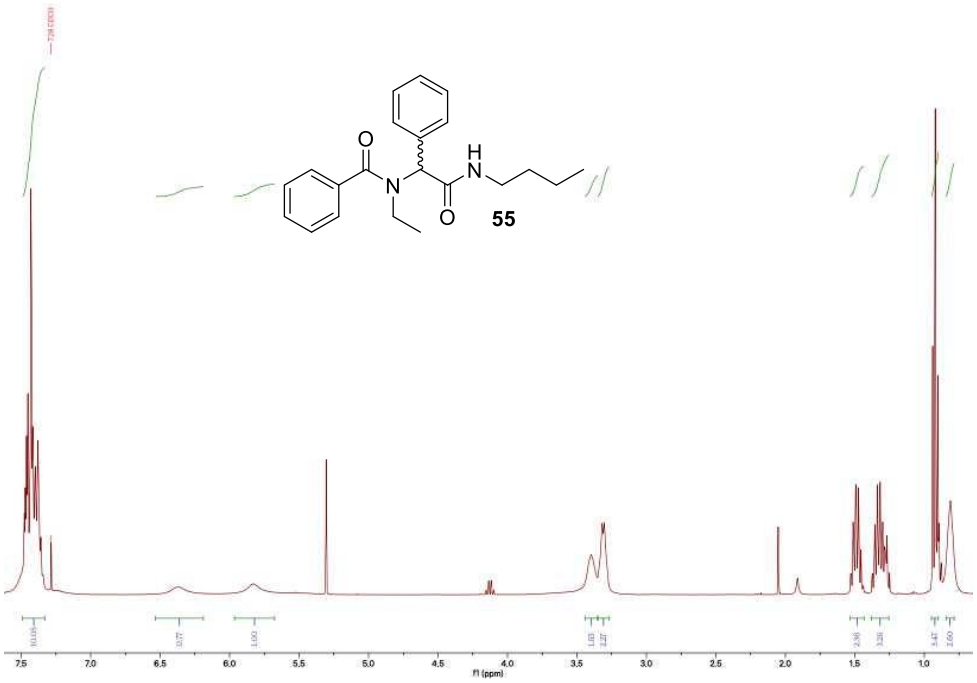

Figure 4.19. ^{1}H NMR ($CDCl_3$) spectrum for the four-component Ugi product **55**.

As an example, the singlet at 6.22 ppm (**Figure 4.18**) was believed to be the C-H proton for the three-component product (**63**), by comparison with singlet from the second fraction (**Figure 4.19**) at 5.83 ppm. The downfield shift of the C-H peak in the second fraction is

consistent with being adjacent to a nitrogen atom in the amide bond (**55**), as opposed to the more shielding oxygen atom in the ester bond of the three-component product (**63**). In addition, the increased number of peaks in the NMR spectrum in **Figure 4.18**, from 0.5 – 3.5 ppm, are characteristic of the amine substituent protons. The ^{13}C NMR spectroscopy of both fractions corroborates these findings as the spectrum of the predicted Passerini product (**63**) contained a peak at 76.0 ppm, indicative of a carbon next to an oxygen atom which was not present in the NMR spectrum of the Ugi product (**55**). Finally, both products were characterized in detail and the data is given in **Section 6.6** and **6.5.5**, respectively.

In order to have a better understanding of the factors that led to the formation of the α-hydroxy carboxamides, two experiments were set up (**Scheme 4.9**), The stoichiometric quantities of the reagents were altered. The ^{1}H NMR spectrum of both reaction mixtures was analysed, resulting in Experiment 1 (**Scheme 4.9**) yielding a product with a greater purity. Passerini compound **62** was isolated, and its full characterization can be found in **Section 6.6**.

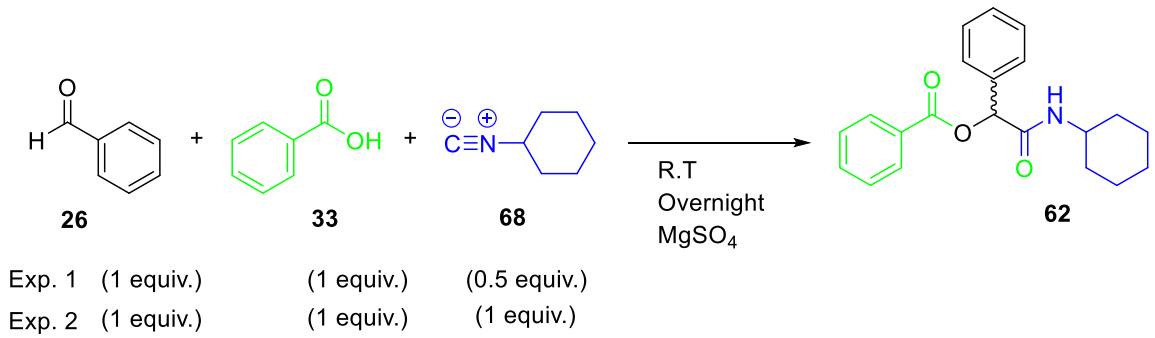

Scheme 4.9. Reaction scheme for alternative stoichiometries of reactants for the synthesis of **62**. (**26**) Benzaldehyde, (**33**) Benzoic acid, (**68**) cyclohexyl isocyanide and (**62**) N-cyclohexylcarbamoyl-[1-(phenyl)-1-benzoate].

An interesting point to note is the α- hydroxy carboxamide (compound **35**, **Figure 4.17**) was tested with the first library and showed 50% inhibition against axenic amastigotes of *L. mexicana* at a single concentration of 50 μM. A benefit of this library is that compounds **62 – 65** can be used to evaluate the effectiveness of the varying isocyanide groups, see

Figure 4.20. In addition, the biological activity of compounds **63** and **65** can be directly compared with their peptoid analogues, this will be the first time a direct comparison has been possible.

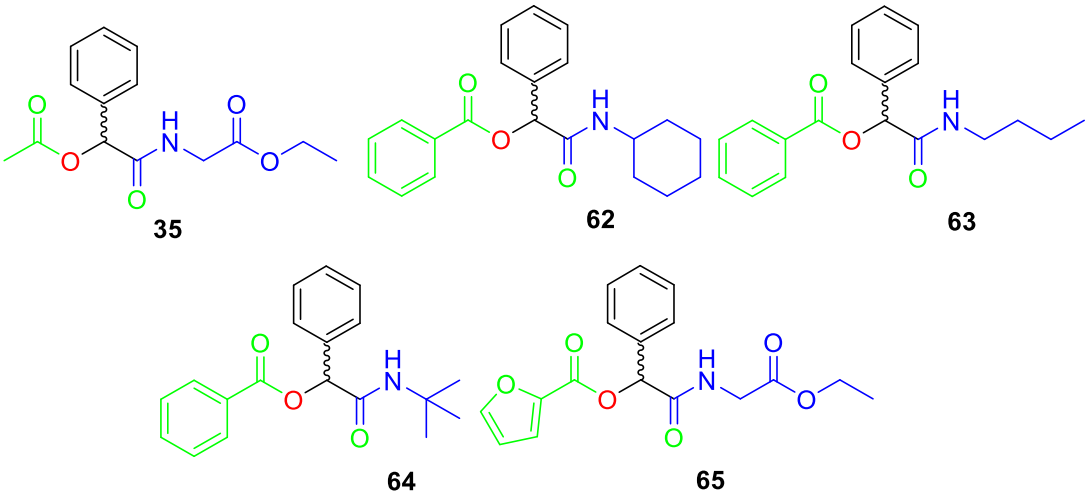

Figure 4.20. α-hydroxy carboxamide library formed via a three-component Passerini reaction.

4.6.1 Passerini library biological and biophysical properties

The Passerini (α-hydroxy carboxamide) compounds that were isolated (**Figure 4.20**) were tested for antiparasitic activity against both the promastigotes and axenic amastigotes forms of *L. mexicana* parasite (**Table 4.9**).

Table 4.9. Final products tested against *L. mexicana.*

Entry	Compound	*L. mexicana* promastigotes survival (%) at 50μM-	*L. mexicana* axenic amastigotes survival (%) at 50μM-
1	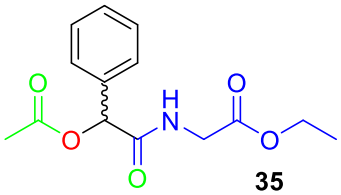 **35**	97	50
2	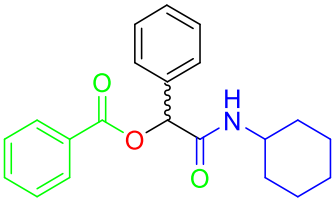 **62**	79	37
3	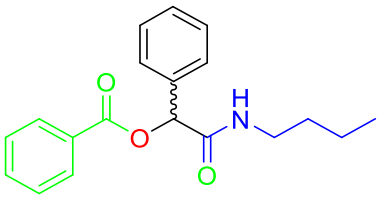 **63**	93	39
4	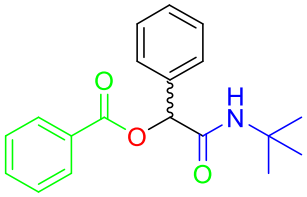 **64**	100	33
5	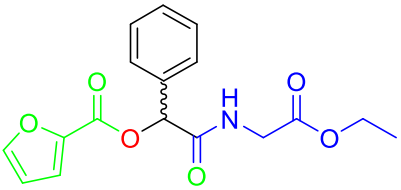 **65**	100	49

Although none of the compounds tested have particular potent antiparasitic activity against *L. mexicana*, the data obtained allowed a direct comparison between the Ugi and Passerini derived scaffolds to be made. For example, carbomide **63** (**Table 4.9**, **Entry 3**) was found to be more active against the axenic amastigote form of *L. mexicana*, with a 39% growth compared to a 55% for peptoid **55** (**Table 4.7**, **Entry 8**). Furthermore, although

only a small number of compounds were screen here to the best of our knowledge, this is the first example of Passerini compounds being evaluated for antileishmanial activity.

Just as for the peptoid library in an attempt to understand more about the factors underpinning the biological activity seen in **Table 4.9** some physicochemical properties for the compounds in the Passerini library were calculated using ChemAxon (**Table 4.10**). All of the Passerini compounds adhere to Lipinski's rule of five. The compounds that have two aromatic rings have a higher Log P between 3.86-4.60 whereas those that do not as expected have lower Log P values. Overall, as expected, the hydrogen bond donor capacity variability is one, whilst their accepting capacity varies from 2 to 3.

Table 4.10 Analysis of the Passerini library's physical properties.

Entry	Compound	Lipinski's rule of five	Log P	H bond donor count	H bond acceptor count
1	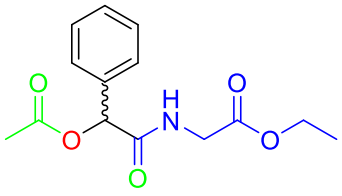 **35**	Yes	0.734	1	3
2	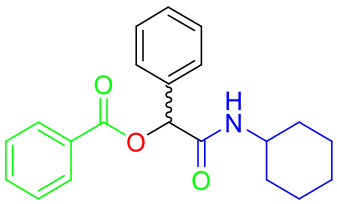 **62**	Yes	4.607	1	2
3	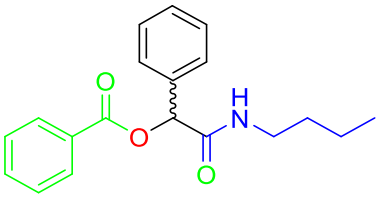 **63**	Yes	4.132	1	2
4	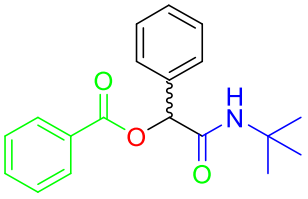 **64**	Yes	3.862	1	2
5	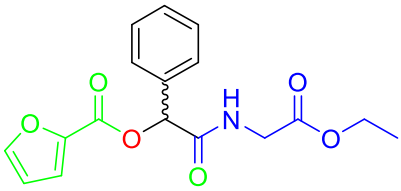 **65**	Yes	1.849	1	3

Hydrophobicity of this small library can be clearly seen in **Figure 4.21**. α-hydroxy carboxamides which have a higher Log P have a less percentage of survival than those which are hydrophilic which have half percentage of axenic amastigotes growth. Compounds with a Log P less than 2 seem to be less active as charted for **65** and **35**, **Figure 4.21**.

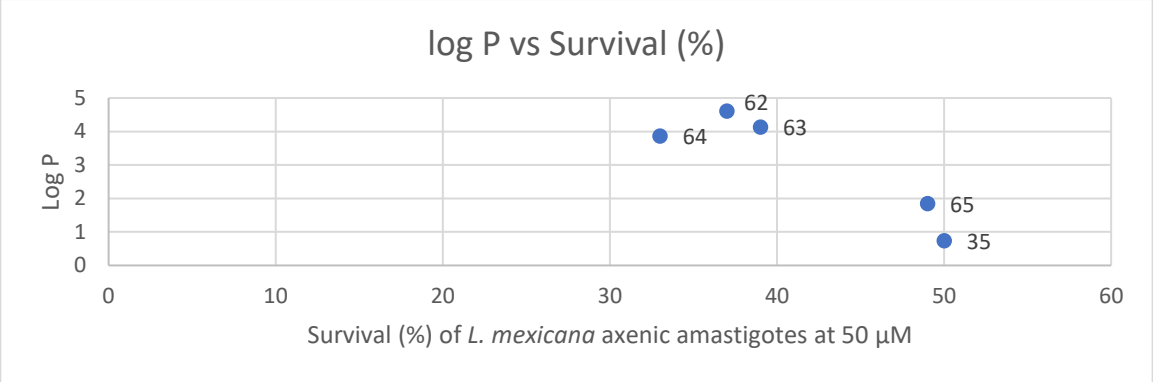

Figure 4.21. Log P vs percentage of survival of *L. mexicana* axenic amastigotes at a single concentration of 50 µM.

4.7 Chapter summary

Inspired by the earlier work of Donate *et al*.[7] that investigated the application of Ugi-derived peptoids (Ugi-4CR) as anti-leishmanials (**Table 4.1**), a first-generation library of lipopeptoids was prepared using a Ugi multicomponent reaction (**Figure 4.4**). We conducted the synthesis with inexpensive reagents and obtained the desired products with a purity between 70-90%. Preparing a lipopeptoid library that contain compounds with a Boc group allowed to analyse the potential antiparasitic effect of its analogues with their free amine while maintaining the same backbone structure. Linear peptoids with antileishmanial activity have been reported by the Cobb group.[4]

Having successfully obtained the target compounds (**Section 4.4.1**), an initial biological screening against *L. mexicana* (promastigote and axenic amastigote stages) at a fixed 50 µM concentration was carried out (**Table 4.2**). As a preliminary screening, peptoids which killed more than 50% of the cell population were selected to calculate accurate EC_{50}. Compound **40** was found to have activity in the low µM range against *L. mexicana* axenic amastigotes and it was selected as the lead compound (**Figure 4.5**) for a 2nd generation library. Design of a 2nd generation library is detailed in **Section 4.4**. Target peptoids chosen to be prepared are pictured in **Figure 4.6**.

Overall, we attempt to prepare 40 peptoids using a Ugi-4CR in a one-pot reaction obtaining a limited number of them in high purity. Different purifications methods were carried out with different peptoids. The purification of the peptoids proved to be challenging due to solubility and high polarity issues. For most cases the issues could be resolved, e.g. using a reverse phase purification system as described in **Section 4.5**.

Finally, both α-hydroxy carboxamide and peptoids' libraries were screened against both the promastigote and axenic amastigote stages of the *L mexicana* parasite. Several peptoids showed antiparasitic activity against both the promastigote and amastigote forms of the parasite. In particular, 7 peptoids were shown to have activity against *L. mexicana* axenic amastigotes in the low μM range. In particular peptoid **34** is worth highlight as it had an EC_{50} = 0.003 μM (**Table 4.7**, **Entry 2**).

As future work, preparing the enantiomeric pure analogue of peptoid **34**, with the stereochemistry fixed, would potentially provide more information about its specific antiparasitic activity (**Chapter 5**). While the biological results obtained to date are encouraging, it would be interesting to see if the most active compounds against the axenic form of the parasite retain activity against the intramacrophage form of the *L. mexicana*.

4.8 References

1. Chadbourne, F. L., Raleigh, C., Ali, H. Z., Denny, P. W. & Cobb, S. L. Studies on the antileishmanial properties of the antimicrobial peptides temporin A, B and 1Sa. *Journal of Peptide Science* **17**, 751–755 (2011).
2. Culf, A. S. Peptoids as tools and sensors. *Biopolymers* **110**, (2019).
3. Bicker, K. L. & Cobb, S. L. Recent advances in the development of anti-infective peptoids. *Chemical Communications* **56**, 11158–11168 (2020).
4. Eggimann, G. A., Bolt, H. L., Denny, P. W. & Cobb, S. L. Investigating the anti-leishmanial effects of linear peptoids. *ChemMedChem* **10**, 233–237 (2015).
5. Bolt, H. L., Eggimann, G. A., Denny, P. W. & Cobb, S. L. Enlarging the chemical space of anti-leishmanials: A structure-activity relationship study of peptoids

against: Leishmania mexicana, a causative agent of cutaneous leishmaniasis. *Medchemcomm* **7**, 799–805 (2016).

6. Hotez, P. J. & Ferris, M. T. The antipoverty vaccines. *Vaccine* **24**, 5787–5799 (2006).

7. Mercer, D. K. & O'Neil, D. A. Peptides as the next generation of anti-infectives. *Future Med Chem* **5**, 315–337 (2013).

8. Previdi, D. *et al.* Synthesis and antileishmanial activity of some functionalized peptoids. *J Braz Chem Soc* **30**, 1334–1340 (2019).

9. Ugi, I., Werner, B. & Dömling, A. The Chemistry of Isocyanides, their MultiComponent Reactions and their Libraries. *Molecules* **8**, 53–66 (2003).

10. Ugi I, Meyr R, Fetzer U & Steinbrückner C. Versuche mit Isonitrilen. *Angew Chem* **71**, 386 (1959).

11. Rabêlo, W. F. & Echemendía, R. Synthesis of novel 1,4 naphthoquinone-based molecules by an Ugi-type four-component reaction. *Synth Commun* **49**, 515–521 (2019).

12. El-Dirany, R. *et al.* Activity of anti-microbial peptides (Amps) against leishmania and other parasites: An overview. *Biomolecules* **11**, (2021).

13. Tao, Y., Wang, Z. & Tao, Y. Polypeptoids synthesis based on Ugi reaction: Advances and perspectives. *Biopolymers* **110**, (2019).

14. Reza Kazemizadeh, A. & Ramazani, A. Synthetic Applications of Passerini Reaction. *Curr Org Chem* **16**, 418–450 (2012).

5. Conclusions

The overarching aim of this thesis was to try and identify molecules which could be used as a starting point to develop lead compounds for the treatment of NTDs. This was driven by the fact that current therapies for the treatment of NTDs, like leishmaniasis have several limitations and drug resistance is an emerging concern. Three distinct classes of molecules were investigated and the key findings for each of these are highlighted below.

5.1. Peptide natural products as antiparasitics

In Chapter 2, natural products known as Chaiyaphumines were studied with the primary aim of successfully synthesising these biologically active cyclic peptides more efficiently. In addition to this, a set of analogues, in which the ester bond in the peptide macrocycle was replaced by an amide, were also synthesised (**Scheme 5.1**).

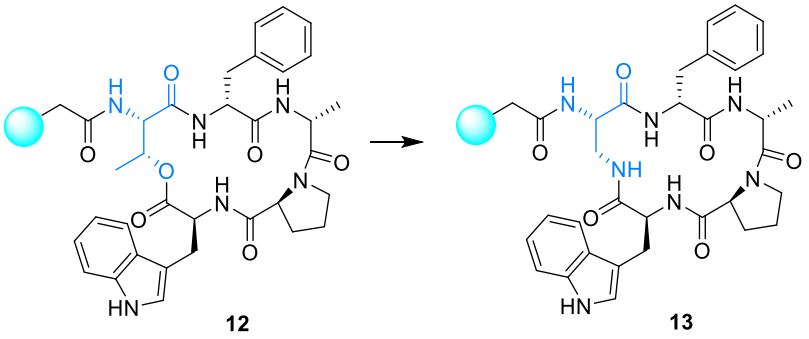

R= Ph (a), Et (b), c (Me), d (H)

Scheme 5.1. Lactone linkage replaced by a lactam highlighted in blue.

Fmoc Solid Phase Peptide Synthesis (SPPS) was applied for the synthesis of the required linear peptide precursors, and the cyclisation step was carried out in solution. The synthesis of the linear peptides was achieved without any issues, but the cyclisation step proved to be more challenging. In the case of the esters, a slow rate of cyclisation was observed in the presence of a base, and difficulties in the purification step were also encountered. During the cyclisation step, the cyclic peptide that was prepared proved to

be highly challenging to separate from the tripyrrolidinophosphine oxide by-product that arose from using PyBOP® in the ester formation. In an attempt to solve this issue, alternative coupling reagents were utilised in the cyclisation step, but similar issues were encountered. Carrying out the cyclisation step in the absence of a base gave more promising results, as highlighted in **Section 2.2.3**.

Having established a suitable synthetic route to the ester-containing natural products, we then looked to prepare amide analogues in which the lactone linkage was replaced by a lactam. Again, the linear precursors were easily prepared using Fmoc SPPS. The cyclisation (amide bond formation) of the linear peptide was carried out off resin and it was found that the lactam formation was aided by an excess of base. In particular, the addition of 20 equiv. of DIPEA to the linear peptides, for a period of time before the addition of coupling reagents, was crucial for the total conversion of the linear peptide as the starting material (**Scheme 5.2**). It was possible to repeat and scale up the synthesis of the lactam peptides without any issues.

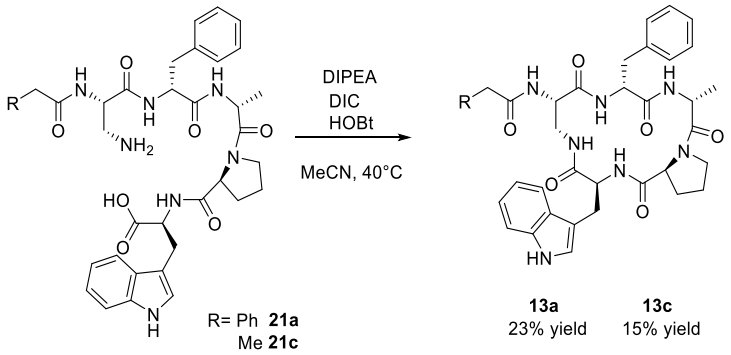

Scheme 5.2. Optimisation of the cyclisation step of amide analogues.

Having optimised both synthesis and purification protocols, we sought to carry out an alanine scan of one of the Chaiyaphumine amide analogues (**Compound 13a**, **Scheme 5.2**). Again, the linear precursors were easily prepared using Fmoc SPPS, as detailed in **Section 6.3.7**. The cyclisation (amide bond formation) of the linear peptides was carried out off resin with an excess of DIPEA, as a base. The alanine scan peptide synthesis

reactions were scaled up in a 0.2 mmol so that enough material could be purified for biological evaluation against selected protozoa.

Overall, a series of natural Chaiyaphumines and Chaiyaphumine amide analogues were prepared on a small scale. Once the protocols were optimized, it was possible to scale up the synthesis. Moving forward we will screen all the peptides prepared against *Leishmania mexicana, Leishmania amazonensis and Leishmania major* in house at Durham University. We will also carry out assays to determine the activity of all the peptide against the parasites responsible for both Chagas disease (via the Professor Ariel Silber's lab at the University of São Paulo- USP, Brazil) and African sleeping sickness (Dr. Marcel Kaiser, *Swiss Tropical* and Public Health Institute -*Swiss* TPH).

Based on the data obtained from the biological screening, and in particular the information gathered from the alanine scan we will seek to expand our library of cyclic peptides. This will be undertaken by incorporating non-natural amino acids at positions identified in the alanine scan as potentially being tolerant to substitutions (**Scheme 5.3**).

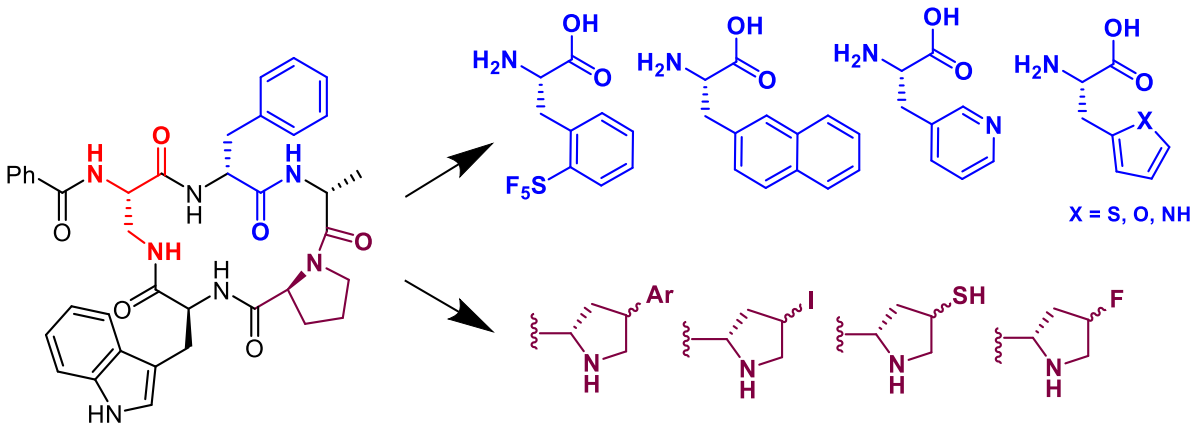

Scheme 5.3. 2nd Generation cyclic peptide library.

5.2 AMPs with antileishmanial activity

Chapter 3 summarises the work that was carried out to assess the anti-leishmanial properties of natural peptides, specifically antimicrobial peptides (AMPs) from two different families (histatins and temporins). The AMPs were prepared using automated Fmoc SPPS

and depending on their specific peptide sequences modifications to the standard software programmes were made to optimise yields and purity (General Procedure given in **Section 6.5.1**).

Firstly, a Temporin library was designed (**Table 3.1**) and prepared on a 0.1 mmol scale but due to time restraints (COVID-19), it was only possible to prepare 5-peptide library for biological assays.

Secondly, peptides from the histatin family (**Table 3.3**), which were originally prepared for metal binding studies (See **Appendix 1** for details), were prepared and purified. All 7 peptides were obtained with more than 95% purity. The histatin peptides were included in this study as their anti-parasitic activity has not been studied in any detail previously. For example, HST- 5 has only ever been tested against *L. pifanoi* and *L. donovani*.[1]

The AMPs that were prepared were screened against both promastigote and axenic amastigote forms of *L. mexicana* using an optimised Alamar Blue® assay. Once this assay was optimized, the same experimental conditions were used to screen the peptides against the promastigote forms of *L. major* and *L. amazonensis.*

According to the literature. both HST-5 and temporins have shown some antileishmanial activity (**Section 1.4.4**). In this study, none of the peptides prepared in this work had any relevant biological activity. Nonetheless, these results contribute to the comprehension of the potential that AMPs could have in new treatments for the global challenge that leishmania represents as an NTD.

5.3 Evaluating the anti-leishmanial activity of a Ugi-derived peptoid library

In Chapter 4, a library of peptoids was prepared using a Ugi multicomponent reaction. Ugi reactions offer an easy and efficient method to obtain peptidomimetic scaffolds from simple, cheap starting materials in a one-pot reaction. The Ugi approach also allows chemical diversity to be built flexibly and rapidly into a library of molecules. Using the Ugi

approach we were able to obtain a library of peptoids with a purity of between 70-90%. The library of compounds prepared was screen in an initial biological assay against *L. mexicana*, promastigote and axenic amastigote stages, at a fixed 50 µM concentration. Then EC_{50} values were obtained (**Section 4.4.1**). Peptoid **40** was found to have activity in the low µM range against *L. mexicana* axenic amastigotes (**Figure 5.1**).

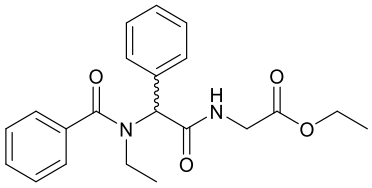

40

EC_{50} = 3.83 µM

Figure 5.1. Example of biological active peptoid prepared with activity against *L. mexicana* axenic amastigotes.

Using peptoid **40** as the "lead" from the initial work a second-generation library was designed incorporating different isocyanates and amines. Challenges in purification meant that obtaining purities of greater that 90% for some peptoids proved to be difficult. The purification step was challenging due to solubility and high polarity issues of the Ugi derived peptoids. After several attempts, the issue was solved using a reverse-phase purification system (**Section 4.5**). A library of 23 peptoids was prepared using a Ugi-4CR reaction with a purity of greater than 90% (by NMR analysis). Five 3 component products also known as Passerini were obtained.

The 23 compound peptoid library along with Passerini compounds were tested against the promastigote and axenic forms of *L. mexicana*. The compounds which were found to have killed more than 25% of the cell population, at the initial fixed 50 µM concentration, were selected for further investigation and accurate EC_{50} were determined for them. Peptoids with the most potent antiparasitic activity (axenic amastigotes) are shown in **Figure 5.2**.

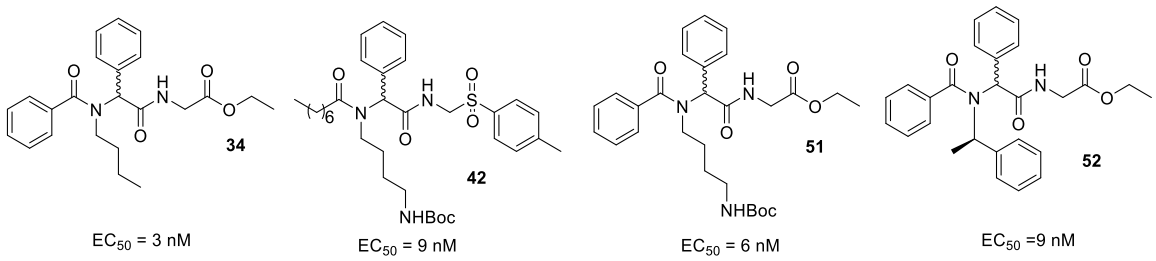

Figure 5.2. Peptoids prepared with activity against *L. mexicana* axenic amastigotes.

Within this study, we have enlarged the peptoid activity data available for the development of potential anti-leishmanial through a simple peptoid preparation with the multicomponent reaction. Not only did we prepare functionalised peptoids initially proposed in **Chapter 4**, but also other analogues with different chemical structures (**Table 4.7**). We were able to analyse the difference in activities between neutral compounds and those that could carry a positive charge. This allowed a better understanding of the relationship between hydrophobicity/ charge and bioactivity to be established.

Finally, preparing the enantiomeric pure analogue of peptoid **34**, with the stereochemistry fixed, would potentially provide more information about its specific antiparasitic activity (**Scheme 5.4**). Depending on the biological results of both enantiomers, if there is at least one of them with significant anti-leishmanial activity an enantiomerically pure library could be designed with the other active peptoids (**Table 4.7**).

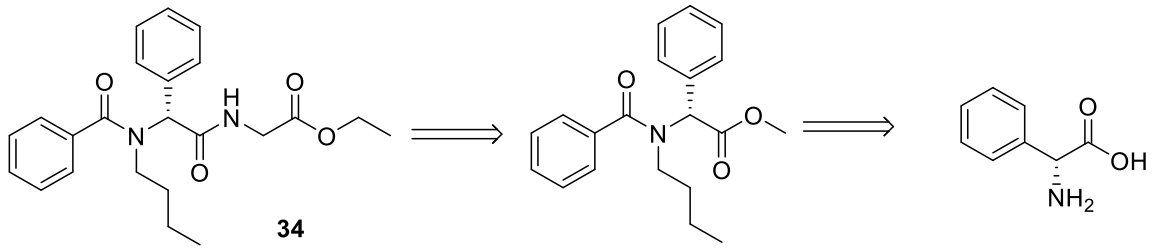

Scheme 5.4. Suggested synthetic route to enantiomerically pure **34**.

5.4 Refences

1. Luque-Ortega, J. R., Hof, W., Veerman, E. C. I., Saugar, J. M. & Rivas, L. Human antimicrobial peptide histatin 5 is a cell- penetrating peptide targeting mitochondrial ATP synthesis in Leishmania. *The FASEB Journal* **22**, 1817–1828 (2008).

6. Experimental

6.1 Materials and reagents

All reagents used in this project were purchased from Novabiochem and used without further purification unless otherwise specified. Peptide synthesis grade (HPLC) DMF was obtained from AGTC Bioproducts (Hessle, UK), PyBOP from Apollo Scientific (Stockport, UK) and NMR solvents which were purchased from Cambridge Isotopes Inc., supplied by Goss Scientific (Crewe, UK). All resins were purchased from Novabiochem (Darmstadt, Germany). These chemicals were used without further purification and stored under appropriate conditions, as detailed in the manufacturer's instructions. Bond Elut solid phase extraction cartridges (20 mL, polypropylene with two polypropylene frits) were purchased from Agilent Technologies and used as reaction vessels for peptide synthesis. Solvents were removed under nitrogen atmosphere. The following centrifuge was used: An Eppendorf centrifuge 5415D (for 1.5 mL tubes). A Radleys Discovery Technology shaker was also used to mix solutions where indicated and aqueous solutions were lyophilised using a Christ Alpha 1-2 LD Plus freeze-drier.

6.2 General methods

6.2.1 Liquid chromatography electrospray ionisation mass spectrometry

Liquid chromatography (LC)-mass spectrometry (ESI-MS) analyses were performed on a Acquity UPLC BEH C18 1.7μm (2.1 mm x 50 mm) column using a Waters Acquity UPLC system equipped with a photodiode array detector, providing absorbance data from 210 nm to 400 nm. A gradient with eluent A (0.1% formic acid in water) and eluent B (0.1% formic acid in acetonitrile) rising linearly from 5 to 95% of B in 3.8 min was applied at a flow rate of 0.6 mL min^{-1}. The continuous exit flow is then directed into the electrospray source of the mass spectrometer and analysed.

6.2.2 Quadrupole time-of-flight mass spectrometry

QToF-LC/MS analyses were performed on a Acquity UPLC BEH C18 1.7µm (2.1mm x 50mm) column using a Waters Acquity UPLC system coupled to Micromass QToF Premier mass spectrometer, also equipped with a photodiode array detector providing absorbance data from 210nm to 400 nm. A gradient with eluent A (0.1% formic acid in water) and eluent B (0.1% formic acid in acetonitrile) rising linearly from 0 to 99% of II during t= 0.0–5.0 min was applied at a flow rate of 0.6 mL min−1. The solvent flow from the UPLC was injected into a flow of acetonitrile which was introduced into the electrospray ion source. QToF MS/MS (ES+ ToF-ToF) was performed using the same equipment, enabling the detection of the fragmentation product ions that result from high energy sample ionization.

6.2.3 Matrix-assisted laser desorption/ionisation mass spectrometry

MALDI-ToF analysis was obtained using an Autoflex II ToF/ToF mass spectrometer (Bruker Daltonik GmBH) equipped with a 337 nm nitrogen laser. The sample solution (~1 mg mL^{-1}) was mixed with the matrix solution, typically α-cyano-4-hydroxycinnamic acid (~ 50 mg mL^{-1}) and 1 µL of the matrix/sample mixture was spotted to the MALDI target. The samples were analysed in positive detection mode with reflectron enhanced mass resolution for m/z between 500 and 5000 Da.

6.2.4 Nuclear magnetic resonance spectroscopy

NMR spectra were recorded on a Varian VNMRS-700 NMR spectrometer at 298 K. Depending on the sample, ^{1}H-NMR spectroscopic data was obtained at 600 or 700 MHz using 2-8 scans with a relaxation delay of 10 s between them. ^{13}C-NMR spectroscopic data was obtained at 151 or 176 MHz (1000-1208 repetitions, 2.5-3.0 s of relax. delay) and bi-dimensional ^{1}H-^{1}H NOESY experiments were run with a minimum mixing time of 150 ms, a spectral width between 6,000-8,000 Hz in both dimensions and a minimum of 2 transients with 2 x 256 increments. Final minimum FT size = 4096 x 2048 points.

Advance III spectrometer. Data was processed using Mestrenova 12® software, and chemical shifts are reported in ppm., relative to residual solvent peaks as internal standards ($CDCl_3$: δ^1H = 7.26 ppm, $\delta^{13}C$ = 77.1 ppm; CD_3OD: δ1H = 3.34 ppm, $\delta^{13}C$ = 49.00 ppm.). J couplings are given in Hertz (Hz). Multiplicities are given following the general accepted notation: s = singlet, d =doublet, dd = doublet of doublets, ddd = doublet of doublet of doublets, dt, doublet of triplets, m = multiplet, t = triplet, q = quartet, quint = quintet, bs = broad singlet.

6.2.5 Analytical chromatography (HPLC)

Samples from the different fractions collected from preparative HPLC were dissolved in H_2O: MeCN 50: 50 *v/v*% to approx. 1 mg mL^{-1} and their purities assessed by analytical HPLC. This analysis was performed on a X-Bridge C_{18} column (5.3µm, 4.6 x 100 mm, 40 °C) using a Perking-Elmer 200 series lc system supplied with auto-sampler, UV/Vis detector and a Peltier column oven. A linear gradient rising from solvent A (95: 5: 0.05 *v/v*% H_2O: MeCN: TFA) to 100% of solvent B (5: 95: 0.03 *v/v*% H_2O: MeCN: TFA) over 40 min was applied at a flow rate of 1 mL min^{-1}. Detection was performed in all cases at λ= 220 nm.

6.2.6 Preparative high-performance liquid chromatography

Crude peptides were dissolved into ~10 mL (50: 50 *v/v*% H_2O: MeCN) and purified by preparative RP-HPLC on a Discovery Bio wide pore C_{18}-5 column from Supelco (5 µm, 25 cm × 10 mm), using a Perking-Elmer 200 lc pump coupled to a Waters 486 tuneable absorbance detector recording at λ = 220 nm. An initial typical linear gradient was commonly employed where eluent A rose linearly from 0-100% of solvent B at a flow rate of 2 mL min^{-1} over a period of 60 minutes. Then the flow was maintained isocratically for 5 minutes at 100% of solvent B before returning to initial conditions (solvent A = 95: 5: 0.1 *v/v*% H_2O: MeCN: TFA; solvent B = 5: 95: 0.1 *v/v*% H_2O: MeCN: TFA). When needed and depending on the sequence, further optimization of the purification conditions was performed by either applying longer gradient times (0-100 *v/v*% solvent B over 110

minutes) or ideally by adjusting the gradient window to the product elution conditions (i.e. 0-50 *v/v*% solvent B in 60 minutes). Fractions corresponding to a single chromatographic peak were collected together, lyophilised and their identity and purity analysed by QToF-LC/MS and analytical HPLC.

6.3 General methods for solid phase peptide synthesis (SPPS)

6.3.1 Solid phase peptide synthesis of linear peptide precursors (ester cyclised natural peptides)

Loading of the 2-chlorotrityl chloride resin

2-Chlorotrityl chloride resin was pre-swollen (normally 70–400 mg, 0.1–0.4 mmol, typical loading between 1.10–1.32 mmol g^{-1}) for 10 min in DCM at room temperature. The resin was washed with two portions of DCM. The swelling was repeated for another 30 mins in DCM followed by addition of Fmoc-Trp(Boc)-OH (1 equiv.) and DIPEA (5 equiv.) in DCM (2 × 1 h). After washing with four portions of DCM, any unreacted resin was capped via treatment with MeOH (15 min). The resin was then washed with 5 portions of DMF and then left to swell in DMF for at least 1 h before continuation of the synthesis.

Fmoc SPPS Peptide synthesis

Manual Fmoc SPPS was carried out in a fritted polypropylene reaction vessel on a 0.2 mmol scale. All reactions were carried out at room temperature in DMF using 2 × 1 h couplings. Fmoc-protected amino acids were used with PyBOP® as the activator in the presence of DIPEA (2:2:4 equiv., apart from Fmoc-Pro-OH which used 5:5:10). Amino acid side chain functionality was protected as follows: Fmoc-Pro-OH, Fmoc-D-Ala-OH, Fmoc-D-Phe-OH and Fmoc-Thr(*t*Bu)-OH. The Fmoc group was removed by two successive treatments with 20% (*v/v*) piperidine solution in DMF (5 + 10 min). The resin was washed thoroughly with DMF between synthesis steps. Preswelling of loaded resin was carried out in DMF for a minimum of 1 h before use.

N-terminal acylation

After the Fmoc SPPS was completed, the N-terminal Fmoc group was removed. The resin was washed with four portions DCM in order to change the solvent for the final step. 10

equivalents of DIPEA were added in 2 mL of DCM while shaking at room temperature. After 5 minutes, the required acid chloride (5 equiv.) was added. The reaction was stirred for at least 1 hour at room temperature. The resin was then shrunk in Et_2O to remove DCM in preparation for peptide cleavage from the resin (using protocol **6.3.2**). If required, the peptide on resin was stored at -4 ˚C.

6.3.2 Cleavage protocol for acid-labile resin

The peptide-resin was shrunk using Et_2O and treated with 2.85 mL TFA, 0.15 mL deionized water and 0.15 mL TIPS for 3–4 h at room temperature. The resin was then removed by filtration and the crude product precipitated in Et_2O (20-30 mL). The mixture was left to precipitate overnight at -16 °C. The crude precipitated peptides were obtained by decanting the ether layer and then additionally washed using chilled Et_2O (2 x 7.5 ml). The ether phase was decanted; the cleavage cocktail was evaporated using a stream of N_2. Finally, the crude product was dissolved in a mixture of deionized H_2O/ MeCN and lyophilised.

When needed, test cleavage was performed by reacting a small number of peptide-resin beads in a small glass vial with 200 µL of the cleavage cocktail. After 15 minutes the beads were allowed to settle on the bottom of the vial and 20-50 µL of the supernatant was transferred to an Eppendorf tube with 1 mL of H_2O: MeCN 90:10% *v/v*. The samples were centrifuged, and an aliquot of the supernatant analysed by LC/MS spectrometry.

Linear peptide precursor 14a

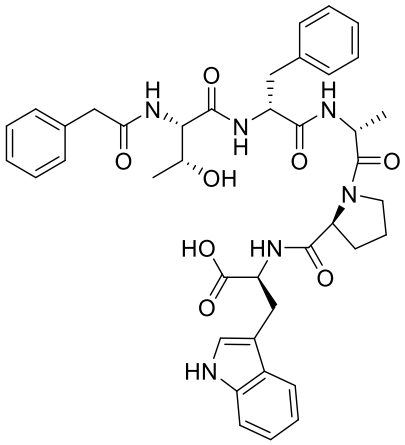

The linear peptide precursor **14a** (R=Phe) was prepared using the general methods described in **Section 6.3.1.** The peptide resin was washed with four portions of DCM in order to change the solvent for the final step. 174 µL (129.24 mg, 1mmol) of DIPEA was added in 2 mL of DCM with shaking at room temperature. After 5 minutes, phenylacetyl chloride (67.5 µL, 0.5 mmol) was added. The reaction was then stirred for at least 1 hour at room temperature. The resin was then washed twice with DCM and shrunk in Et_2O in preparation for peptide cleavage.

The peptide containing resin was stored at -4 ˚C overnight. The resin cleavage was carried out according to the procedure in **Section 6.3.2**. The resulting crude peptide was lyophilised to yield an orange powder. The presence of the target linear peptide was confirmed by LC-MS analysis ($C_{40}H_{47}N_6O_8$ [M + H]+ *m/z* =739.588). The resulting crude peptide was stored at -16 ˚C prior to it undergoing the cyclization step.

Linear peptide precursor 14b

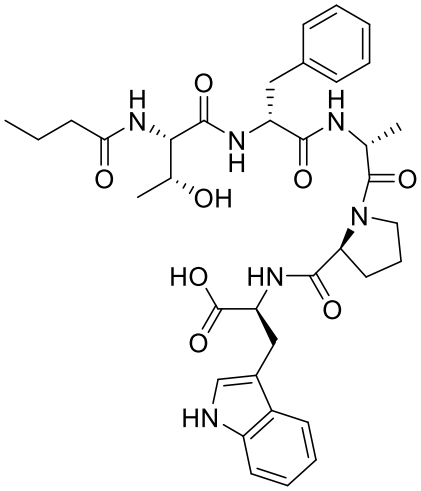

The linear peptide precursor **14b** (R=Et) was prepared using the general methods described in **Section 6.3.1**. The peptide resin was washed with four portions of DCM in order to change the solvent for the final step. 174 µL (129.24 mg, 1mmol) of DIPEA was added in 1.5 mL of DCM with shaking at room temperature. After 5 minutes, the butyryl chloride (52 µL, 0.5 mmol) was added. The reaction was then stirred for at least 1 hour at room temperature. The resin was then washed twice with DCM and shrunk in Et_2O in preparation for peptide cleavage.

The peptide containing resin was stored at -4 ˚C overnight. The resin cleavage was carried out according to the procedure in **Section 6.3.2.** The resulting crude peptide was lyophilised to yield an orange powder. The presence of the target linear peptide was confirmed by LC-MS analysis ($C_{36}H_{47}N_6O_8$ [M + H] + *m/z* =691.578). The resulting product was characterised showing the desired linear precursor and stored at -16 ˚C.

6.3.3 Cyclisation off Resin

Linear precursor, compound **14b**, was partially dissolved in 1 mL of H_2O and 200 µL of DIPEA was added. After this addition, **14b** was totally dissolved. The mixture was lyophilized affording a yellow oil ready for cyclisation step.

Compound **14b**, was dissolved in 5 mL of dry THF and stirred for 10 min at room temperature. Thus, precursor HOBt (3 equiv.) was added and the mixture was stirred until total dissolution of this reagent. After 5 min, 3 equiv. of DIC were added. The reaction was stirred ON at 70 ˚C. Reaction mixture was evaporated using a stream of N_2. Then, it was dissolved in a 5 mL mixture of deionized H_2O/ MeCN. The sample was centrifuged and the supernatant was removed for purification. With a final peptide concentration of approximately 0.5mg/ mL of a 50:50 H_2O/MeCN solution a reversed phase HPLC purification of the crude residue was done. The pure product **12b** was isolated as a white solid after lyophilisation in a non-quantitative amount.

6.3.4 Synthesis of the linear amide precursor

The loading of the 2-chlorotrityl chloride resin is described in **Section 6.3.1**.

Fmoc Sold Phase Peptide synthesis

Manual Fmoc SPPS was carried out in fritted polypropylene reaction vessels at 0.2 mmol-0.4 mmol scale. All reactions were carried out at room temperature in DMF using 2 × 1 h couplings. Fmoc-protected amino acids were used with PyBOP® as the activator in the presence of DIPEA (2:2:4 equiv, apart from Fmoc-Pro-OH which used 5:5:10). Amino acid side chain functionality was protected as follows: Fmoc-Pro-OH, Fmoc-D-Ala-OH, Fmoc-D-Phe-OH and Fmoc-Dpr(Boc)-OH. The Fmoc group was removed by two successive treatments with 20% (*v/v*) piperidine solution in DMF (5 + 10 min). The resin was washed thoroughly with DMF between synthesis steps. Preswelling of loaded resin was carried out in DMF for a minimum of 1 h before use. Finally, N-terminal acylation and resin cleavage are described in **Section 6.3.1** and **6.3.2**, respectively.

6.3.5 Cyclisation off Resin

The linear precursor was dissolved in MeCN with a final concentration of starting material 1mg/ mL. It was stirred for 10 min at room temperature until total dissolution. Thus, 20 equiv. of DIPEA, as a base, were added and this mixture was stirred for at least 30 minutes at room temperature. HOBt (6 equiv.) was added and the mixture was stirred until total dissolution of this reagent. Finally, 6 equiv. of DIC were added.

The reaction was stirred for 4 hours at room temperature until a 50 µL aliquot was separated for LC-MS and HPLC sample analysis. Analysis of the reaction mixture showed that the starting material was still present. The temperature was increased gradually to 42˚C. Once conversion started to improve, the reaction was stirred at 42˚C at this final temperature. Furthermore, final analysis probed to be starting material free.

6.3.6 Linear peptide precursor 21c

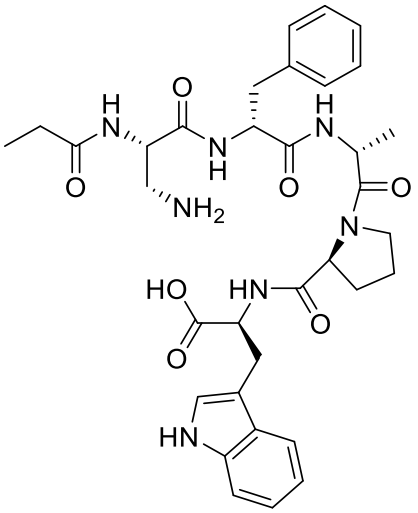

2-Chlorotrityl chloride resin was pre-swollen (76 mg, 0.1 mmol, loading 1,32 mmol g^{-1}) for 10 min in DCM at room temperature. Swelling was repeated for others 30 min in DCM followed by addition of Fmoc-Trp(Boc)-OH (54 mg, 0.1 mmol) and DIPEA (84 µL, 0.5 mmol) in 2 mL of DCM (2 × 1 h). After washing with four portions of DCM, unloaded resin was capped via treatment with 5 mL of MeOH (15 min). The resin was dried and washed with 3 portions of DMF and resin swelling was repeated in DMF for 1 h before continuation of the synthesis.

Manual Fmoc SPPS was carried out in fritted polypropylene reaction vessel and all reactions were carried out at room temperature in DMF using 2 × 1 h couplings. Fmoc-protected amino acids were used with PyBOP® as the activator in the presence of DIPEA (0.2:0.2:0.4 mmol, apart from Fmoc-Pro-OH which used 0.5:0.5:1). Amino acid side chain functionality was protected as follows: Fmoc-Pro-OH (170.38 mg, 0.5 mmol), Fmoc-D-Ala-OH (63.64 mg, 0.2 mmol), Fmoc-D-Phe-OH (79.06 mg, 0.2mmol) and Fmoc-Dpr(Boc)-OH (85.29, 0.2 mmol). The Fmoc group was removed by two successive treatments with 5 mL of 20% (*v/v*) piperidine solution in DMF (5 + 10 min). The resin was washed twice with DMF between synthesis steps. Preswelling of the loaded resin was carried out in DMF for 30 min before use.

Finally, the peptide resin was washed with four portions DCM in order to change the solvent for the final step. 174 µL (129.24 mg, 1mmol) of DIPEA was added in 2 mL of DCM while shaking at room temperature. After 5 minutes, propionyl chloride (43.70 µL, 0.5 mmol) was added. The reaction was stirred for 1 hour. The resin was washed 3 times with DCM, dried and stored at -4 ˚C. A test cleavage was done (see **Section 1.2.2**) on confirmation of the presence of the compound by LC-MS analysis ($C_{34}H_{44}N_7O_7$ [M + H] + m/z =662.736). Peptide cleavage from the resin was carried out as described in **Section 6.3.2**. The presence of the target peptide in the crude material obtained was confirmed and the peptide was stored at -16 ˚C.

Chaiyaphumines Amide Target 13c

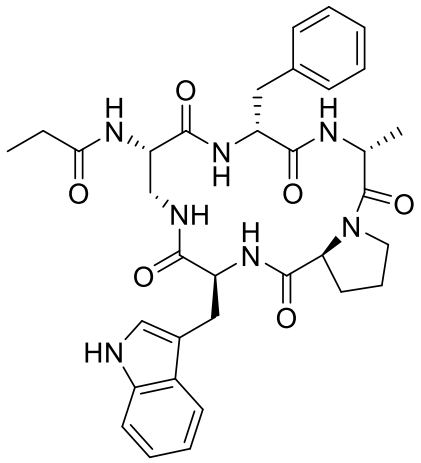

The linear peptide precursor **21c** (27 mg) was dissolved in 28 mL of MeCN. 20 equiv. of DIPEA were added and the mixture was stirred at room temperature for at least 30 min. HOBt (6 equiv.) was added and the mixture was stirred until total dissolution of this reagent. Finally, 6 equiv. of DIC were added and the temperature was raised gradually up to 42 ˚C. The reaction was stirred ON at 42 ˚C.

HPLC purification (110 min program, **Section 6.2.6**) gave peptide **13c** as a white solid (1.89 mg, 7%), HPLC R_t = 18.8 min (procedure **6.2.5**), HRMS *m*/*z* (ESI) 644.3176, consistent with empirical formula $C_{34}H_{42}N_7O_6$ with an accuracy of 3.3 ppm (accepted as $[M + H]^+$).

6.3.7 Chaiyaphumines Amide Target 13a

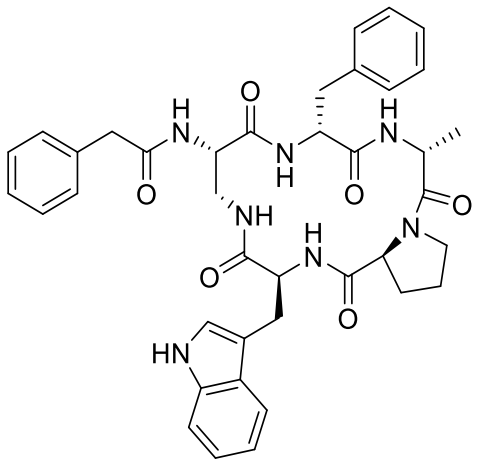

2-Chlorotrityl chloride resin was pre-swollen (75 mg, 0.1 mmol, loading 1,32 mmol g^{-1}) for 10 min in DCM at room temperature. Swelling was repeated for others 30 min in DCM followed by addition of Fmoc-Trp(Boc)-OH (54 mg, 0.1 mmol) and DIPEA (84 µL, 0.5 mmol) in 2 mL of DCM (2 × 1 h).

After washing with four portions of DCM, any unloaded resin was capped via treatment with 5 mL of MeOH (15 min). The resin was dry and washed with 3 portions of DMF and it swelling was repeated in DMF for 1 h before continuation of the synthesis.

Manual Fmoc SPPS was carried out in fritted polypropylene reaction vessel and all reactions at room temperature in DMF using 2 × 1 h couplings. Fmoc-protected amino acids were used with PyBOP® as the activator in the presence of DIPEA (0.2:0.2:0.4 mmol, apart from Fmoc-Pro-OH which used 0.5:0.5:1). Amino acid side chain functionality was protected as follows: Fmoc-Pro-OH (170.38 mg, 0.5 mmol), Fmoc-D-Ala-OH (63.64 mg, 0.2 mmol), Fmoc-D-Phe-OH (79.06 mg, 0.2 mmol) and Fmoc-Dpr(Boc)-OH (85.29, 0.2 mmol). The Fmoc group was removed by two successive treatments with 5 mL of 20% (*v/v*) piperidine solution in DMF (5 + 10 min). The resin was washed twice with DMF between synthesis steps. Preswelling of loaded resin was carried out in DMF for 30 min before use.

Finally, the peptide resin was washed with four portions DCM in order to change the solvent for the final step. 174 µL (129.24 mg, 1mmol) of DIPEA was added in 2 mL of DCM while shaking at room temperature. After 5 minutes, phenylacetyl chloride (77.30 mg, 0.5 mmol) was added. The reaction was stirred for 1 hour at room temperature. The resin was washed twice with DCM and dried. The resin cleavage was completed (see **Section 6.3.1**) and the lyophilised product was an orange powder. On confirmation of the presence of the target peptide (**21a**) by LC-MS analysis ($C_{39}H_{46}N_7O_7$ [M + H] + *m/z* =724.598.

Solution-phase cyclization of 18 mg of the linear precursor **21a** (**Section 6.3.5**), followed by HPLC purification yielded (0-80 *v/v*% solvent B in 100 minutes, **Section 6.2.6**) gave peptide **13a** as a white solid (4 mg, 23%), HPLC R_t = 22.8 min (procedure **6.2.5**), HRMS *m/z* (ESI) 706.3355, consistent with empirical formula $C_{39}H_{44}N_7O_6$ with an accuracy of 0.3 ppm (accepted as $[M + H]^+$).

6.3.8 Synthesis of the linear precursor for alanine scan

Synthesis of compound 23: Fmoc-Trp(Boc)-OH for L-Ala-OH

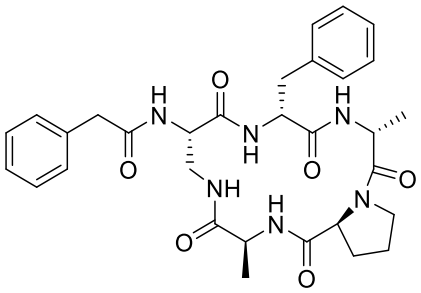

The experimental procedure is the same as described in **Section 6.3.3** except for the loaded of the resin since the first amino acid was replaced by an alanine with the same configuration of the first amino acid.

2-Chlorotrityl chloride resin was pre-swollen (151.20 mg, 0.2 mmol, resin loading: 1.22 mmol g^{-1}) for 10 min in DCM at room temperature. Swelling was repeated for 30 min in DCM followed by addition of Fmoc--Ala-OH (62.36mg, 0.2 mmol) and 174 µL of DIPEA (129.24 mg,1 mmol) in DCM (2 × 1 h). After washing with four portions of DCM, the unloaded resin was capped via treatment with 5 mL of MeOH (15 min). The loaded resin was washed with 5 portions of DMF and it swelling was repeated in DMF overnight at -4 ˚C, before continuation of the synthesis.

Manual Fmoc SPPS was carried out at room temperature in DMF using 2 × 1 h couplings. Fmoc-protected amino acids (0.4 mmol) were used with PyBOP® (208.15 mg, 0.4mmol) as the activator in the presence of 139 µL of DIPEA (103.6 mg, 0.8 mmol). Amino acid side chain functionality was protected as follows: Fmoc-Pro-OH (337.37 mg, 1 mmol), Fmoc-D-Ala-OH (124.73 mg, 0.4 mmol), Fmoc-D-Phe-OH (387.43 mg, 0.4 mmol) and Fmoc-Dpr(Boc)-OH (170.58 mg, 0.4 mmol). The Fmoc group was removed by two successive treatments with 5 mL of 20% (*v/v*) piperidine solution in DMF (5 + 10 min). The resin was washed thoroughly with DMF between synthesis steps.

Finally, the peptide resin was washed with four portions DCM in order to change the solvent for the final step. 174 µL (129.24 mg, 1mmol) of DIPEA was added in 2 mL of DCM

while shaking at room temperature. After 5 minutes, phenylacetyl chloride (154.59 mg, 1 mmol) was added. The reaction was stirred for 1 hour. The resin was washed twice with DCM, dried and stored at -4 ˚C prior to characterisation. Peptide total cleavage was carried out as described in **Section 6.3.2**. The presence of the linear peptide in the crude was confirmed by LC-MS analysis ($C_{31}H_{41}N_6O_7$ [M + H] + m/z =610.449.

Finally, the cyclization step was carried out with 16.8 mg of the linear peptide precursor (0.028 mmol) as detailed in **Section 6.3.5**. Followed by HPLC purification yielded (0-80 *v/v*% solvent B in 60 minutes, **Section 6.2.6**) peptide **23** as a white solid (4.5 mg, 28%), HPLC R_t = 18.6 min (procedure **6.2.5**), HRMS *m/z* (ESI) calculated for $[M+H]^+ C_{31}H_{38}N_6O_6$ $^+$= 591.2947. Found = 591.2941.

Synthesis of compound 24: Fmoc-D-Phe(Boc)-OH for D-Ala-OH

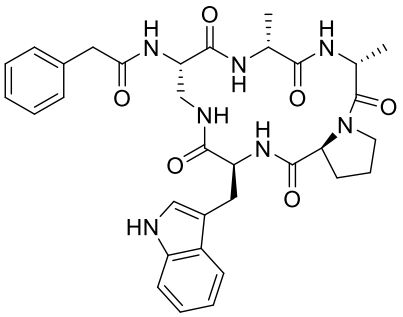

The loading of the 2-chlorotrityl chloride resin (151.50 mg, 0.2 mmol, resin loading: 1.22 mmol g^{-1}) with Fmoc-Trp (Boc)-OH was carried out as described in **Section 6.3.1**.

Manual Fmoc SPPS was carried out at room temperature in DMF using 2 × 1 h couplings. Fmoc-protected amino acids (0.4 mmol) were used with PyBOP® (208.15 mg, 0.4mmol) as the activator in the presence of 139 µL of DIPEA (103.6 mg, 0.8 mmol). Amino acid side chain functionality was protected as follows: Fmoc-Pro-OH (337.37 mg, 1 mmol,), Fmoc-D-Ala-OH (124.73 mg, 0.4 mmol), Fmoc-D-Ala-OH (124.73 mg, 0.4 mmol) and Fmoc-Dpr(Boc)-OH (170.58 mg, 0.4 mmol). The Fmoc group was removed by two successive treatments with 5 mL of 20% (*v/v*) piperidine solution in DMF (5 + 10 min). The resin was washed thoroughly with DMF between synthesis steps.

Upon completion of the sequence, the peptide resin was washed with four portions DCM in order to change the solvent for the final step. 174 µL of DIPEA (129.24 mg,1 mmol) of DIPEA was added in 2 mL of DCM while shaking at room temperature. After 5 minutes, phenylacetyl chloride (154.59 mg, 1 mmol) was added. The reaction was stirred for 1 hour. The resin was washed twice with DCM, dried and stored at -4 ˚C prior to a test cleavage.

The N-terminal acetylation was not complete; the resin was shrunk in DCM for 1 hour. another attempt was carried out at room temperature in DCM using 2 x 30 min coupling. Thus, 396 µL (517.0 mg,4 mmol) of DIPEA and 319.18 mg (2 mmol) of phenylacetyl chloride were used. The resin was washed twice and stored dried at -4 ˚C prior to a test cleavage. Peptide cleavage was carried out as described in **Section 6.3.2**. The presence

of the target linear peptide was confirmed by LC-MS analysis ($C_{33}H_{42}N_7O_7$ [M + H] + *m/z* =648.307. Finally, the cyclization step was carried out with 50 mg of linear precursor (0.077 mmol) as detailed in **Section 6.3.5**. Followed by HPLC purification yielded (0-80 *v/v*% solvent B in 60 minutes, **Section 6.2.6**) peptide **24** as a white solid (3.9 mg, 8%), HPLC R_t = 16.7 min (procedure **6.2.5**), HRMS *m/z* (ESI) calculated for $[M+H]^+$ $C_{41}H_{40}N_7O_6^+$= 630.3040. Found = 630.3021.

Synthesis of compound 25: Fmoc-Pro(Boc)-OH for L-Ala-OH

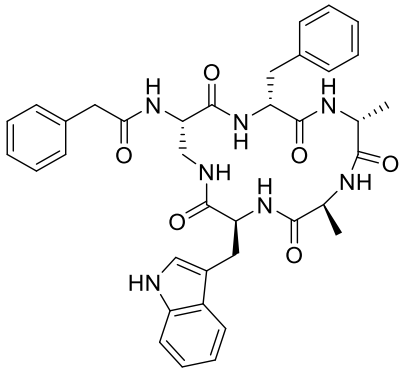

The loading of the 2-chlorotrityl chloride resin (151.50 mg, 0.2 mmol, resin loading: 1.22 mmol g^{-1}) was carried out as described in **Section 6.3.1**. Manual Fmoc SPPS was carried out at room temperature in DMF using 2 × 1 h couplings. Fmoc-protected amino acids (0.4 mmol) were used with PyBOP® (208.15 mg, 0.4mmol) as the activator in the presence of 139 of µL DIPEA (103.6 mg, 0.8 mmol). Amino acid side chain functionality was protected as follows: Fmoc-Pro-OH (337.37 mg, 1 mmol,), Fmoc-D-Ala-OH (124.73 mg, 0.4 mmol), Fmoc-D-Phe-OH (387.43 mg, 0.4 mmol) and Fmoc-Dpr(Boc)-OH (170.58 mg, 0.4 mmol). The Fmoc group was removed by two successive treatments with 5 mL of 20% (*v/v*) piperidine solution in DMF (5 + 10 min). The resin was washed thoroughly with DMF between synthesis steps.

The peptide resin was washed with four portions DCM in order to change the solvent for the final step. 174 µL of DIPEA (129.24 mg,1 mmol) of DIPEA was added in 2 mL of DCM

while shaking at room temperature. After 5 minutes, phenylacetyl chloride (154.59 mg, 1 mmol) was added. The reaction was stirred for 1 hour. The resin was washed twice with DCM, dried and stored at -4 ˚C prior to characterisation.

The N-terminal acetylation was found not to be complete. Thus, the resin was shrunk in DCM for 1 hour for another attempt. It was carried out at room temperature in DCM using 2 x 30 min coupling. The resin was shrunk in DCM for 1 hour. 20 equiv (517 mg, 4 mmol) of DIPEA were added in 2 mL of DCM while shaking at room temperature. After 5 minutes, 10 equiv. (319.18 mg, 2 mmol) of phenylacetyl chloride (77.30 mg, 0.5 mmol) were added. The resin was washed twice with DCM, dried and stored at -4 ˚C. Peptide cleavage was carried out as described in **Section 6.3.2**. The presence of the target linear peptide was confirmed by LC-MS analysis ($C_{37}H_{44}N_7O_7$ [M + H] + *m/z* =698.348.

Finally, the cyclization step was carried out with 6.5 mg of the linear precursor (0.009 mmol) as detailed in **Section 6.3.5**. HPLC purification yielded (0-80 *v/v*% solvent B in 60 minutes, **Section 6.2.6**) peptide **25** as a white solid (2.4 mg, 38%), HPLC R_t = 20.7 min (procedure **6.2.5**), HRMS *m/z* (ESI) calculated for $[M+H]^+ C_{37}H_{42}N_7O_6^+$= 680.3197. Found = 680.3220.

6.4 Automated Solid Phase Peptide Synthesis

6.4.1 General Procedures

All peptides were synthesised using of microwave assisted couplings performed on a CEM Discovery microwave system (Liberty Blue, Automated Microwave Peptide Synthesiser; Durham, UK). In each of the reaction conditions listed, pressure is not included as peptide couplings take place in open vessels and therefore pressure cannot be altered from room pressure, 14.50 psi.

General Procedure 1 - Swelling of resin

All peptides were synthesised on Rink Amide AM resin with 0.77 mmol/g loading unless otherwise stated. The resin was swollen in DMF (15 ml) for 15 minutes and washed prior to use in subsequent steps.

General Procedure 2 - Fmoc deprotection conditions

Fmoc deprotection of peptides was achieved by addition of 4.5 ml of a 20 % piperidine in DMF solution to the resin in a SPPS microwave vessel, then reacted using following conditions: Temperature 75 °C, Power 20 W, Time 5 minutes. Following Fmoc deprotection, the resin was washed with DMF (5 x 4 ml) using a vacuum manifold.

General Procedure 3 - Peptide Coupling conditions (amide bond formation)

Coupling of peptides was achieved by addition of four equivalents of the amino acid, dissolved in DMF (2 ml) to which was added four equivalents of HOBt™ in DMF (2 ml). The two solutions were mixed, and DIC (four equivalents) added. The solution was shaken and left four ten minutes before being added to deprotected resin in a SPPS microwave vessel, then reacted using the conditions outlined below: Temperature 75 °C, Power 20 W, Time 10 minutes. Following coupling, the resin was washed with DMF (2 x 5 ml) using a vacuum manifold.

General Procedure 4 - Resin cleavage

The resin was then transferred to a reaction vessel. During resin cleavage, the peptide-resin was shrunk in diethyl ether (Et_2O) and treated with a cleavage cocktail of TFA (3.8

mL), deionized water (0.2 mL) and TIPS (0.2 mL) for 3–4 hours at RT. The resin was then removed by filtration and the crude product precipitated in Et_2O (20- 30 mL). The mixture was left to precipitate overnight at -16 °C. The crude precipitated peptides were obtained by decanting the ether layer and then additionally washed using chilled Et_2O (2 x 7.5 mL). The Et_2O phase was decanted; the cleavage cocktail was evaporated using a stream of N_2. Finally, the crude product was dissolved in a mixture of deionized H_2O/ MeCN and lyophilised. Once the crude was obtained, peptide identity was confirmed with LC-MS.

6.4.2 Synthesis of Temporins

Temporin crude peptides were analysed after their long storage by LC-MS. Those same mass spectrometry samples were used for the analytical RP-HPLC to see their purity along with their mass spectra as detailed in **Section 3.1.2**. For a better clarity a temporin peptides are shown in **Table 6.1**.

Table 6.1. Temporins Summary table

Entry	Peptide sequence	Crude peptide	Pure peptide	Comercial peptide
1	Temporin A* FLPLIGRVLSGIL-NH_2			✓
2	Temporin TA3 FLALIGRVLSGIL-NH_2	✓		
3	Temporin B* LLPIVGNLLKSLL-NH_2		✓	
4	Temporin 1Sa* FLSGIVGML GKLF-NH_2	✓		
5	Temporin C LLPILGNLLNGLL-NH_2		✓	
6	Temporin F FLPLIGKVLSGIL-NH_2	✓		
7	Temporin L FVQWFSKFLGRIL-NH_2			✓
8	Temporin TL10 FVQWFSKFLARIL-NH_2	✓		
9	Temporin **TL11** FVQWFSKFLGAIL-NH_2		✓	

Temporin A: FLPLIGRVLSGIL-NH_2

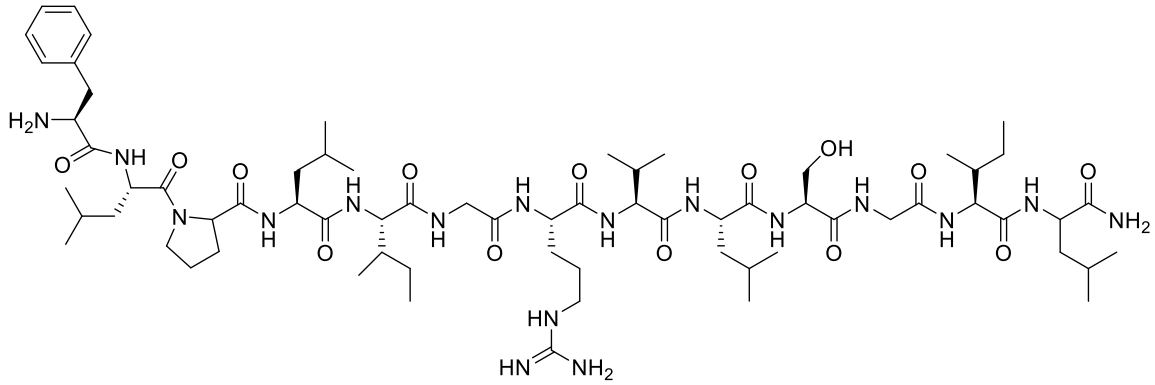

The synthesis of Temporin A [FLPLIGRVLSGIL-NH_2] was achieved following **General Procedures 1- 4** (**Section 6.4.1**) using 130 mg of Rink Amide resin (0.1 mmol). When all amino acids were coupled, a final Fmoc deprotection step was carried out by use of 20% piperidine/DMF, and the peptide cleaved from resin by use of TFA (90%), TIPS (5%) and H_2O (5%) for 3 hours at room temperature and dried by lyophilisation. On confirmation of the presence of the target peptide by LC-MS analysis ($C_{68}H_{118}N_{17}O_{14}$ $[M + H]^+$ *m/z* =1398.208), Temporin A was stored at -16 ˚C prior to the purification step RP-HPLC and dried by lyophilisation.

Temporin TA3: FLALIGRVLSGIL-NH_2

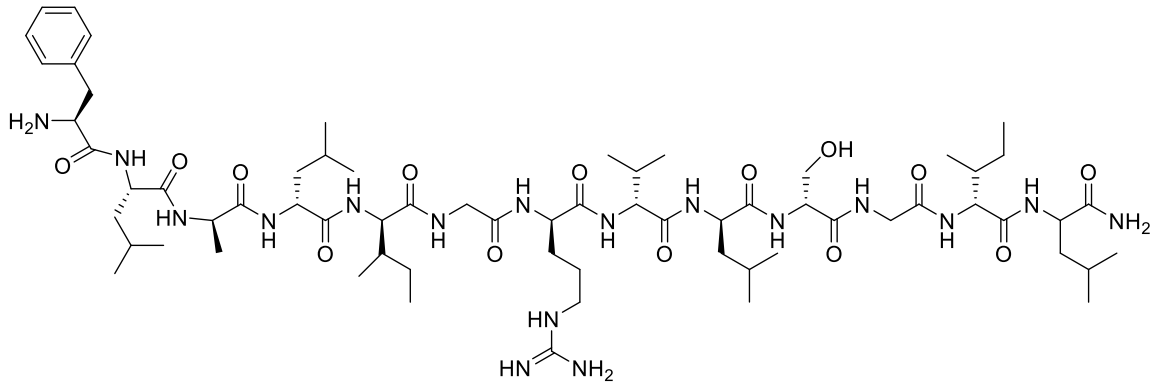

The synthesis of Temporin A3 [FLALIGRVLSGIL-NH_2] was achieved following **General Procedures 1- 4** (**Section 6.4.1**) using 130 mg of Rink Amide resin (0.1 mmol). When all amino acids were coupled, a final Fmoc deprotection step was carried out by use of 20% piperidine/DMF, and the peptide cleaved from resin by use of TFA (90%), TIPS (5%) and

H_2O (5%) for 3 hours at room temperature and dried by lyophilisation. On confirmation of the presence of the target peptide by LC-MS analysis ($C_{66}H_{116}N_{17}O_{14}$ $[M + H]^+$ *m/z* =1372.032), Temporin A3 was stored at -16 ˚C prior to purification step RP-HPLC and dried by lyophilisation

Temporin B: LLPIVGNLLKSLL-NH_2

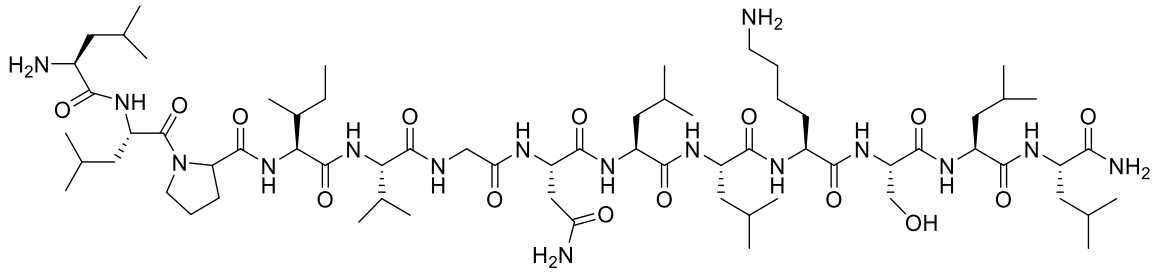

The synthesis of **Temporin B** [LLPIVGNLLKSLL-NH_2] was achieved following **General Procedures 1- 4** (**Section 6.4.1**) using 130 mg of Rink Amide resin (0.1 mmol). When all amino acids were coupled, a final Fmoc deprotection step was carried out by use of 20% piperidine/DMF, and the peptide cleaved from resin by use of TFA (90%), TIPS (5%) and H_2O (5%) for 3 hours at room temperature and dried by lyophilisation. HPLC purification of the crude (80 min program, **Section 6.2.6**) let to **Temporin B** as a white solid (6.5 mg, 20%), HPLC R_t =25.2 min (procedure **6.2.5**), HRMS *m/z* (ESI) calculated for $[M + H]^+$ $C_{67}H_{123}N_{16}O_{15}^+$ = 1391.9354. Found = 1392.9175.

Temporin C: LLPILGNLLNGLL-NH_2

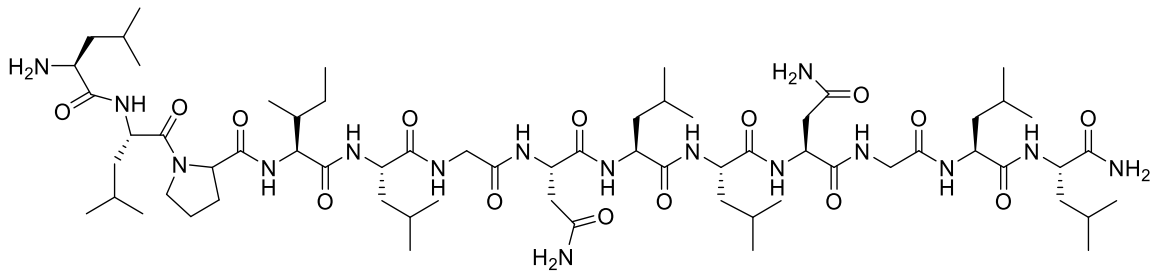

The synthesis of Temporin C [LLPILGNLLNGLL-NH_2] was achieved following **General Procedures 1- 4** (**Section 6.4.1**) using 130 mg of Rink Amide resin (0.1 mmol). When all amino acids were coupled, a final Fmoc deprotection step was carried out by use of 20%

piperidine/DMF, and the peptide cleaved from resin by use of TFA (90%), TIPS (5%) and H_2O (5%) for 3 hours at room temperature and dried by lyophilisation.

Crude peptide was dissolved in 1:1 MeCN: H_2O, filtered and injected in ~4 mg amounts (4 mL) per run onto an XBridge C18 column (19 x 100 mm) attached to an Interchim Puriflash system. A linear gradient of 30-45% B (where A = H_2O, 0.1% formic acid; B = MeCN) over 22 minutes, followed by 45-95% B for 5 minutes then a 95% B isocratic hold for 5 mins at a flow rate of 17 mL/min was used for separations unless otherwise stated. Absorbance data were collected at 220 nm. Selected fractions were analysed by MS and analytical HPLC and peak fractions of interest were pooled and lyophilised. HPLC purification of the crude let to **Temporin C** as a white solid (2.80 mg, 28%), HPLC R_t =26.6 min (procedure **6.2.5**), HRMS *m/z* (ESI) calculated for $[M + 2H]^{2+}$ $C_{65}H_{118}N_{16}O_{15}^{+}$ = 681.4481. Found = 681.4471.

Temporin F: FLPLIGKVLSGIL-NH_2

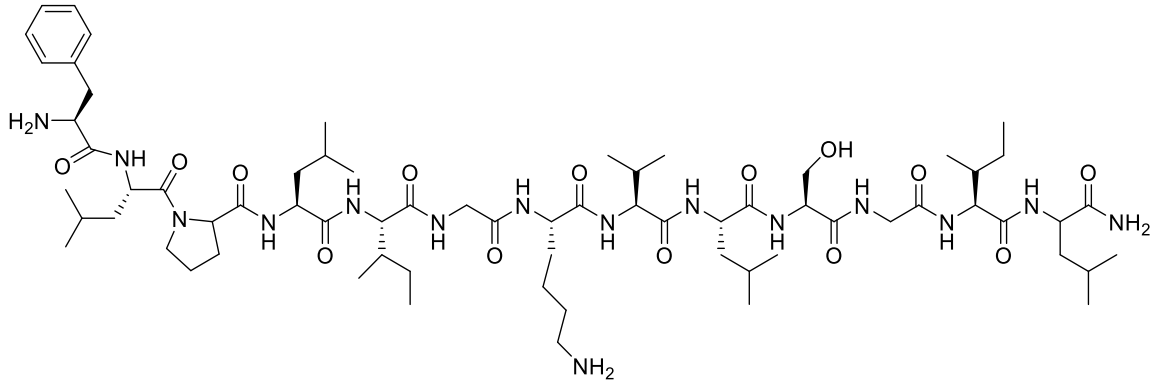

The synthesis of Temporin F [FLPLIGKVLSGIL-NH_2] was achieved following **General Procedures 1- 4** (**Section 6.4.1**) using 130 mg of Rink Amide resin (0.1 mmol). When all amino acids were coupled, a final Fmoc deprotection step was carried out by use of 20% piperidine/DMF, and the peptide cleaved from resin by use of TFA (90%), TIPS (5%) and H_2O (5%) for 3 hours at room temperature and dried by lyophilisation. On confirmation of the presence of the target peptide by LC-MS analysis ($C_{68}H_{118}N_{15}O_{14}$ $[M + H]^{+}$ *m/z* =1369.144), Temporin F was stored at -16 ˚C prior to purification step RP-HPLC and dried by lyophilisation.

Temporin L: FVQWFSKFLGRIL-NH_2

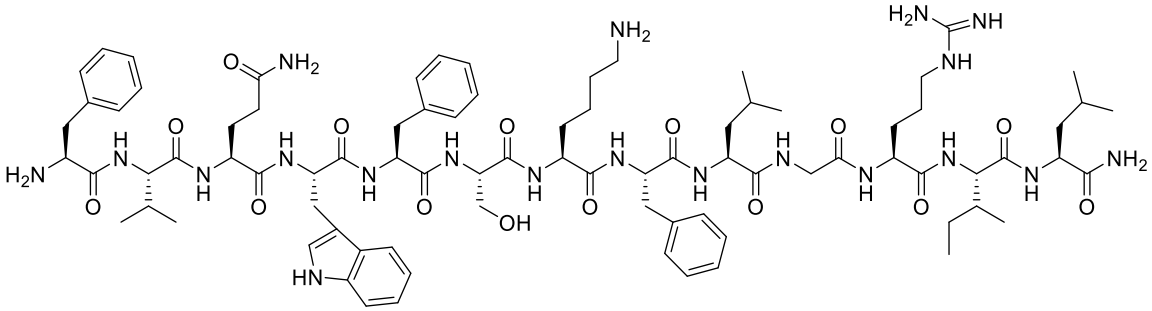

The synthesis of Temporin L [FVQWFSKFLGRIL-NH_2] was achieved following **General Procedures 1- 4** (**Section 6.4.1**) using 130 mg of Rink Amide resin (0.1 mmol). When all amino acids were coupled, a final Fmoc deprotection step was carried out by use of 20% piperidine/DMF, and the peptide cleaved from resin by use of TFA (90%), TIPS (5%) and H_2O (5%) for 3 hours at room temperature and dried by lyophilisation. On confirmation of the presence of the target peptide by LC-MS analysis ($C_{83}H_{123}N_{20}O_{15}$ $[M + H]^+$ *m/z* =1641.442), Temporin L was stored at -16 ˚C prior to purification step RP-HPLC and dried by lyophilisation.

Temporin TL10: FVQWFSKFLARIL-NH_2

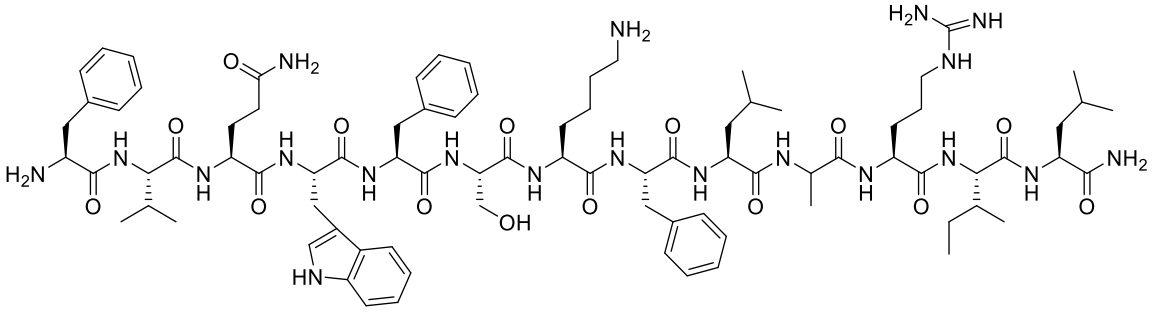

The synthesis of Temporin TL10 [FVQWFSKFLGRIL-NH_2] was achieved following **General Procedures 1- 4** (**Section 6.4.1**) using 130 mg of Rink Amide resin (0.1 mmol). When all amino acids were coupled, a final Fmoc deprotection step was carried out by use of 20% piperidine/DMF, and the peptide cleaved from resin by use of TFA (90%), TIPS (5%) and H_2O (5%) for 3 hours at room temperature and dried by lyophilisation. On confirmation of the presence of the target peptide by LC-MS analysis ($C_{84}H_{125}N_{20}O_{15}$ [M +

H]$^+$ *m/z* =1655.652), Temporin TL10 was stored at -16 ˚C prior to purification step RP-HPLC and dried by lyophilisation.

Temporin TL11: FVQWFSKFLGAIL-NH_2

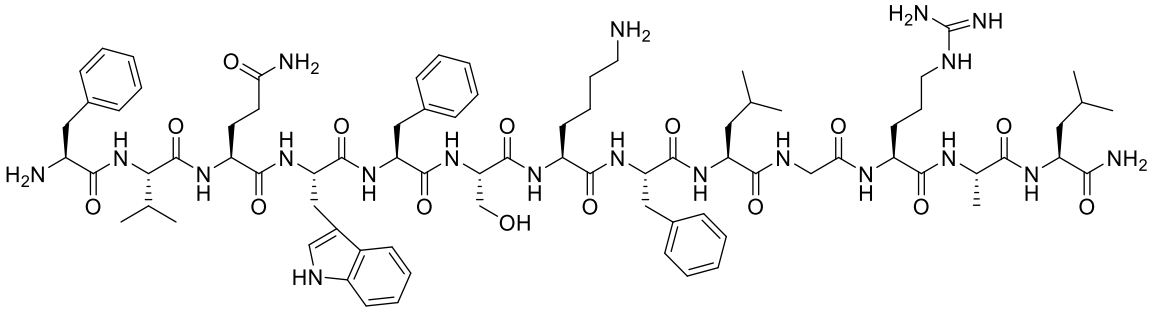

The synthesis of **Temporin TL11** [FVQWFSKFLGAIL-NH_2] was achieved following **General Procedures 1- 4** (**Section 6.4.1**) using 130 mg of Rink Amide resin (0.1 mmol). When all amino acids were coupled, a final Fmoc deprotection step was carried out by use of 20% piperidine/DMF, and the peptide cleaved from resin by use of TFA (90%), TIPS (5%) and H_2O (5%) for 3 hours at room temperature and dried by lyophilisation. HPLC purification of the crude (80 min program, **Section 6.2.6**) let to **Temporin TL11** as a white solid (7 mg, 31%), HPLC R_t =19.6 min (procedure **6.2.5**), HRMS *m/z* (ESI) calculated for $[M + 2H]^{2+}$ $C_{80}H_{118}N_{20}O_{15}^+$ = 799.4543. Found = 799.9521.

Temporin 1Sa: FLSGIVGML GKLF-NH_2

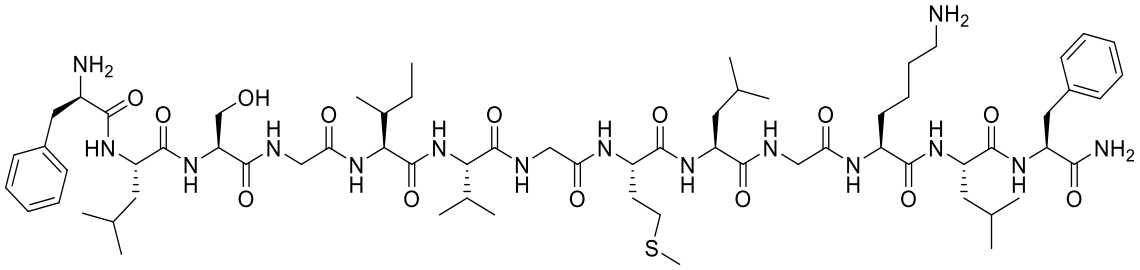

The synthesis of Temporin 1Sa [FLSGIVGML GKLF-NH_2] was achieved following **General Procedures 1- 4** (**Section 6.4.1**) using 130 mg of Rink Amide resin (0.1 mmol). When all amino acids were coupled, a final Fmoc deprotection step was carried out by use of 20% piperidine/DMF, and the peptide cleaved from resin by use of TFA (90%), TIPS (5%) and H_2O (5%) for 3 hours at room temperature and dried by lyophilisation. On confirmation of the presence of the target peptide by LC-MS analysis ($C_{67}H_{110}N_{15}O_{14}S$ $[M + H]^+$ *m/z*

=1382.214), Temporin 1Sa was stored at -16 ˚C prior to purification step RP-HPLC and dried by lyophilisation.

6.4.3 Synthesis of histatins

SPPS was carried out in CEM synthesiser with 161 mg of a preloaded Fmoc-Tyr(tBu)-Wang resin (with 0.62 mmol/g loading on a 0.1 mmol scale,), using the **general procedure 6.4.1**.

Histatin 5: DSHAKRHHGY KRKFHEKHHS HRGY

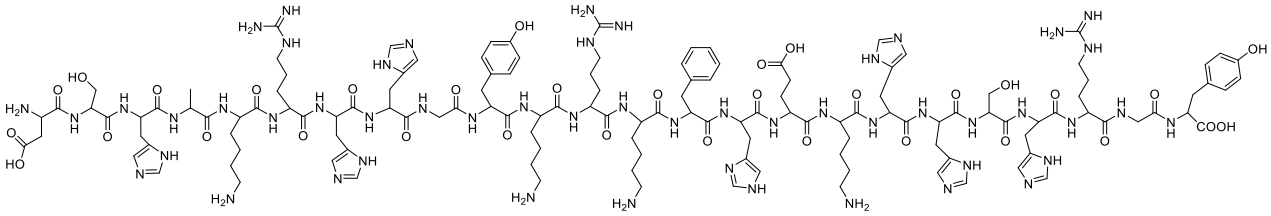

HPLC purification of the crude (80 min program, **Section 6.2.6**) let to peptide **HST 5** as a white solid (4.20 mg, 20%), HPLC R_t =9.9 min (procedure **6.2.5**), HRMS *m*/*z* (ESI) calculated for $[M + 7H]^{7+}$ $C_{133}H_{195}N_{51}O_{33}^{+}$ = 434.6532. Found = 434.6425.

Histatin H3,7A, H15-19A: DSAAKRAHGY KRKFAEKAAS HRGY

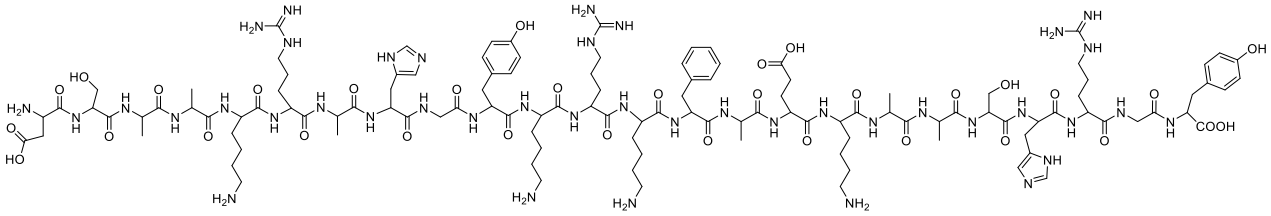

HPLC purification of the crude (80 min program, **Section 6.2.6**) let to peptide **H3,7A, H15-19A** as a white solid (2.90 mg, 21%), HPLC R_t =10.3 min (procedure **6.2.5**), HRMS *m*/*z* (ESI) calculated for $[M + 6H]^{6+}$ $C_{118}H_{185}N_{41}O_{33}^{+}$ = 451.9093. Found 451.9003.

Histatin H15-H19A: DSHAKRHHGY KRKFAEKAAS HRGY

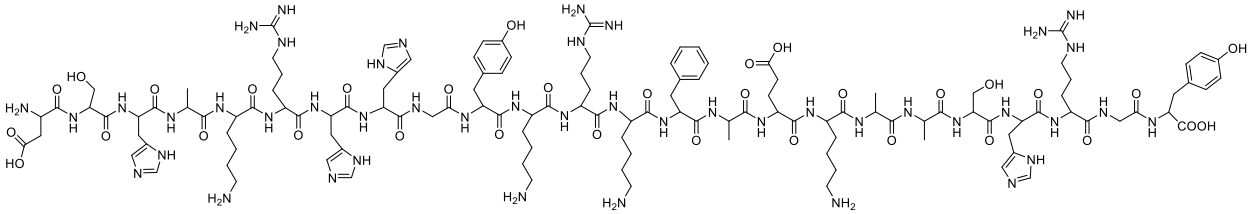

HPLC purification of the crude (80 min program, **Section 6.2.6**) let to peptide **H15-H19A** as a white solid (11.60 mg, 30%), HPLC R_t =9.3 min (procedure **6.2.5**), HRMS *m*/*z* (ESI) calculated for $[M + 7H]^{7+}$ $C_{124}H_{189}N_{45}O_{33}^{+}$ = 406.3582. Found = 406.3484.

Histatin H3,7A: DSAAKRAHGY KRKFHEKHHS HRGY

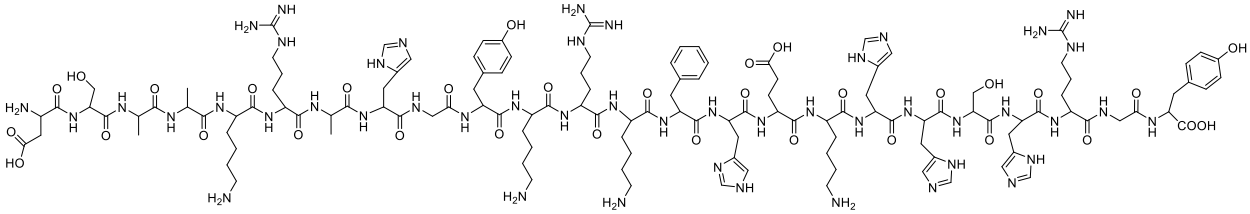

HPLC purification of the crude (80 min program, Section **6.2.6**) let to peptide **H3,7A** as a white solid (2.90 mg, 21%), HPLC R_t =10.3 min. HRMS *m*/*z* (ESI) calculated for $[M + 6H]^{6+}$ $C_{127}H_{191}N_{47}O_{33}^{+}$ = 484.9202. Found = 484.9110.

Histatin D1A; H7,8A: ASAAKRAAGY KRKFHEKHHS HRGY

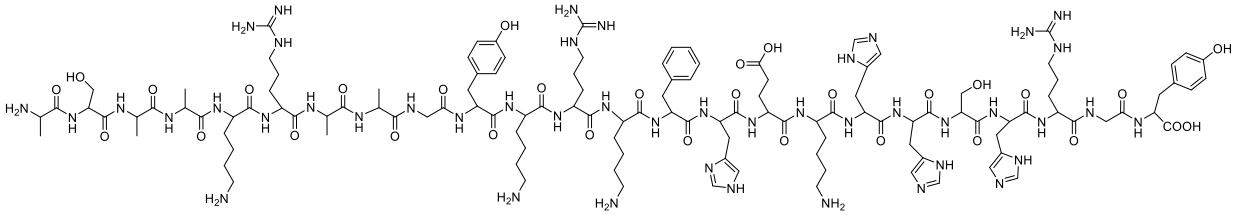

HPLC purification (80 min program, **Section 6.2.6**) let to peptide **D1A; H7,8A** as a white solid (4.50 mg, 27%), HPLC R_t = 10.4 min (procedure **6.2.5**), HRMS *m*/*z* (ESI) calculated for $[M + 3H]^{3+}$ $C_{123}H_{189}N_{45}O_{31}^{+}$ = 932.1619. Found = 932.1489.

Histatin D1A: ASAAKRHHGYKRKFHEKHHSHRGY

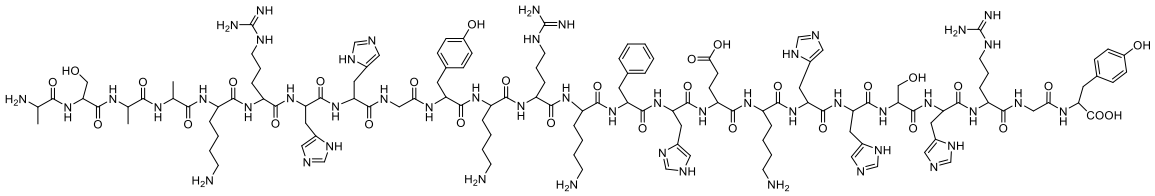

HPLC purification (60 min program, **Section 6.2.6**) let to peptide **D1A** as a white solid (4.1 mg, 27%), HPLC R_t = 9.6 min (procedure **6.2.5**)), HRMS *m*/*z* (ESI) calculated for $[M + 5H]^{5+}$ $C_{129}H_{198}N_{49}O_{31}^{+}$ 586.1090. Found = 586.0995.

Histatin H7,8A: DSHAKRAAGYKRKFHEKHHSHRGY

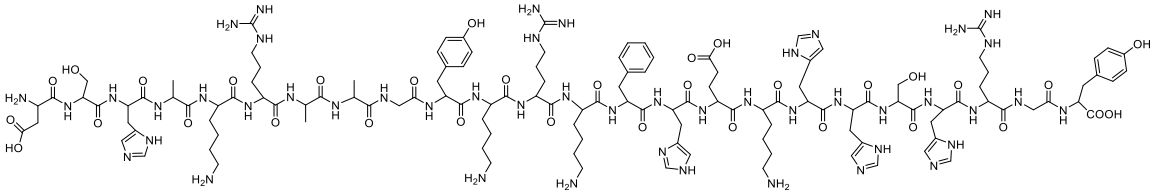

HPLC purification (60 min program, **Section 6.2.6**) let to peptide **D1A; H7,8A** as a white solid (2.50 mg, 17%), HPLC R_t = 9.4 min (procedure **6.2.5**), HRMS *m*/*z* (ESI) calculated for $[M + 5H]^{5+}$ $C_{127}H_{191}N_{47}O_{33}^{+}$ = 581.7026. Found = 581.7010.

6.5 Peptoids

6.5.1 General protocol for the Ugi reaction

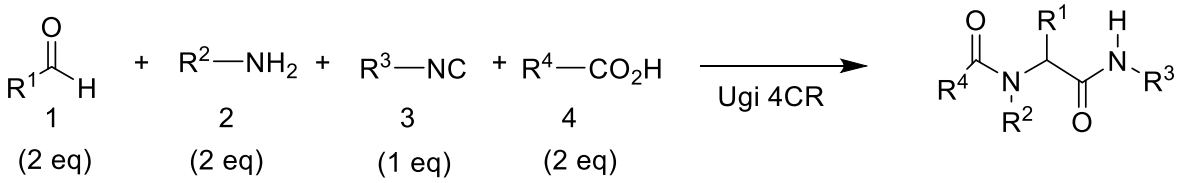

R^1,R^2,R^3,R^4= alkyl or aryl

Scheme 6.1 General scheme of Ugi 4CR.

Anhydrous $MgSO_4$ was added to a round bottom flask. It was sealed and flushed with N_2 to create an inert atmosphere. Aldehyde (2 equiv), amine (2 equiv), acid (2 equiv) and isocyanide (1 equiv) to the flask, using a syringe and leave stirring between 1-7 days. The reaction mixture was filtered and the solid was washed several times with methanol. This

solvent was removed under reduced pressure. The residue was purified by column chromatography on silica gel with dichloromethane/methanol (90:10, *v/v*) as eluent.

6.5.2 Optimised protocol for the Ugi reaction

Anhydrous $MgSO_4$ was added to the quick-thread glass reaction tube, sealed and flushed with N_2 to create an inert atmosphere. Aldehyde (2 equiv), amine (2 equiv), isocyanide (1 equiv) and carboxylic acid (2 equiv) are added to the flask sequentially, using a syringe. The reaction was left stirring for a minimum of 7 days. The reaction mixture was monitored by (TLC), filtered and the product washed with saturated sodium bicarbonate (3 x 25 ml). The solvent was removed in vacuo and depending on the residue, purified by column chromatography on silica gel with either dichloromethane/methanol (90:10, v/v) or ethyl acetate/hexane (50:50, v/v) as eluent. Repurifications with a dry loading were carried out using column chromatography on silica purchased from Fluorochem using hexane/ethyl acetate solvent systems or using a Combiflash Nextgen 100 equipped with a 12-24g redisep column, according to reaction scale, using hexane/ethyl acetate solvent systems.

6.5.3 Peptoid synthesis with MW assistance

To a solution of aldehyde, amine, and acid (0.914 equiv) in MeOH was added the corresponding isocyanate (0.457 equiv). A small amount of anhydrous $MgSO_4$ was added, and the solution was prestirred for 5 min then heated under microwave conditions at 60 °C for 1 h. The solution was filtered and washed with MeOH. The solvent was evaporated under reduced pressure to give the corresponding crude that was characterized by NMR and LC-MS to identify desire product. Purification was carried out with according to procedure **6.5.4**.

6.5.4 Reverse phase purification with Combiflash Nextgen 100

Compounds where prepared according to protocol **6.5.2**, unless specified. Samples were dissolved in ethyl acetate, followed by celite addition with an amount dependant to the reaction scale. Dry loading addition was carried out in a 5 g cartridge for sample injection. Loading cartridge was insert into a 15.5 g Reusable RediSep Rf Gold® C_{18} Reversed

Phase columns, 20–40 microns, attached to a Combiflash Nextgen 100. An isocratic gradient of 20% B (where A = H_2O; B = MeCN) for 2 minutes. Followed by a linear gradient of 20% -60% B over 50 minutes, then 60-100% B for 2 minutes. Finally, a 100% B isocratic hold for 7 mins at a flow rate of 30 mL/min was used for separations unless otherwise stated. Column was calibrated for storage conditions at 80% B. Absorbance data were collected at all wavelengths 200-300 nm. Selected fractions were analysed by LC-MS and analytical HPLC and peak fractions of interest were pooled and lyophilised.

6.5.5 Products obtained from the Ugi reactions

Peptoid library with a high purity (>90%) shown to be difficult. A summary table is shown in Table 6.2.

Table 6.2. Peptoids Summary table

Entry	Peptoid structure	1st generation library	2nd generation library	Pure peptoid	Crude peptoid
1	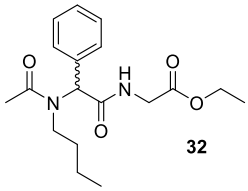 32		✓	✓	
2	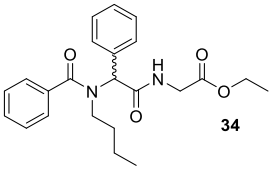 34	✓		✓	
3	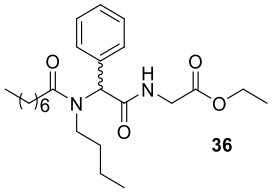 36	✓		✓	
4	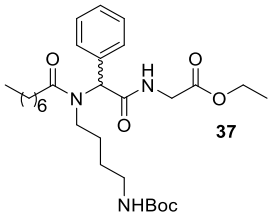 37	✓		✓	
5	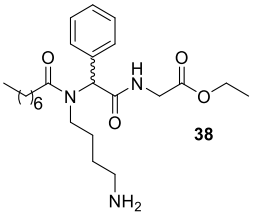 38	✓		✓	
6	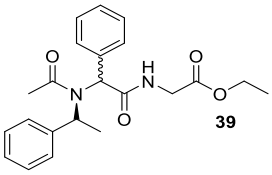 39	✓			✓

7	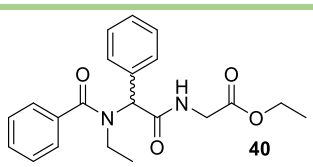 **40**	✓	✓	
8	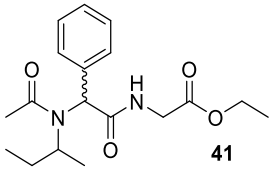 **41**	✓		✓
9	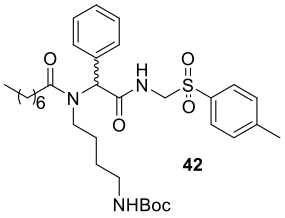 **42**	✓	✓	
10	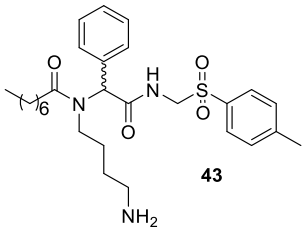 **43**	✓		✓
11	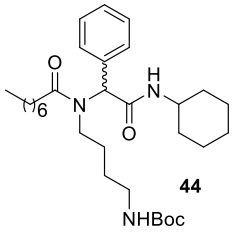 **44**	✓	✓	
12	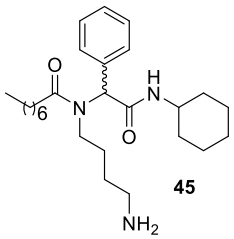 **45**	✓	✓	
13	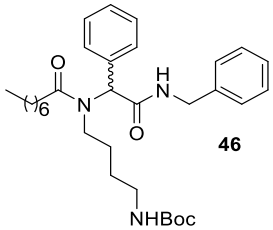 **46**	✓	✓	

14	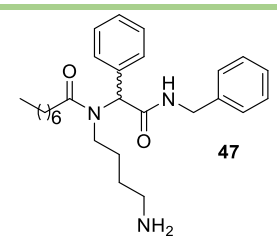 **47**	✓		✓	
15	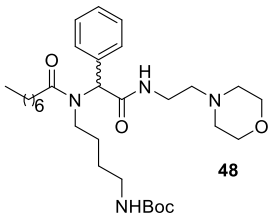 **48**	✓			✓
16	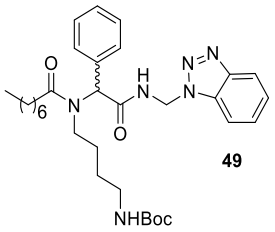 **49**	✓			✓
17	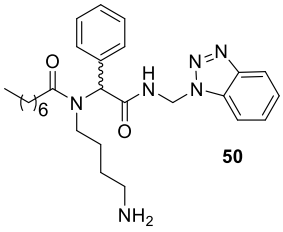 **50**	✓			✓
18	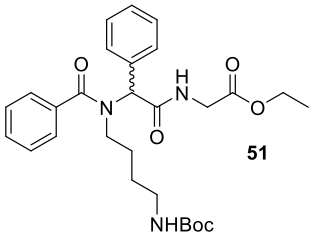 **51**		✓	✓	
19	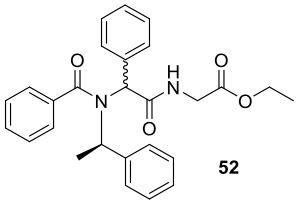 **52**		✓	✓	
20	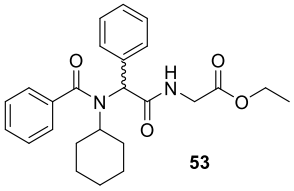 **53**		✓		✓
21	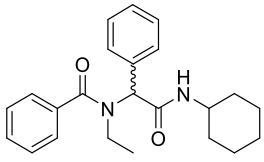 **54**		✓		✓

22	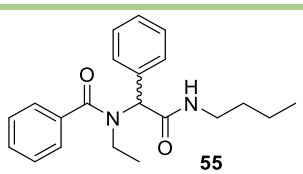 **55**	✓	✓	
23	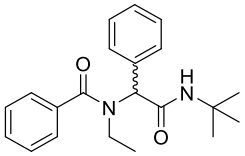 **56**	✓		✓
24	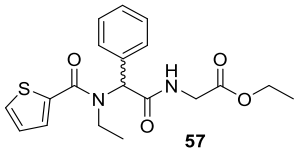 **57**	✓	✓	
25	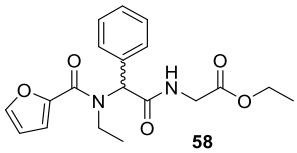 **58**	✓	✓	
26	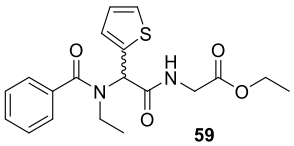 **59**	✓		✓
27	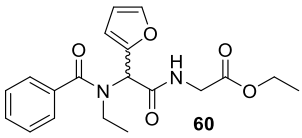 **60**	✓		✓
28	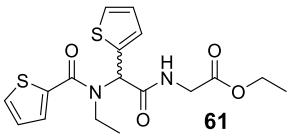 **61**	✓	✓	
29	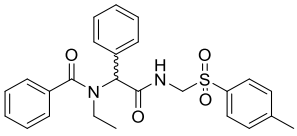 **66**	✓	✓	
30	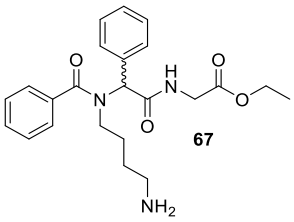 **67**	✓	✓	
31	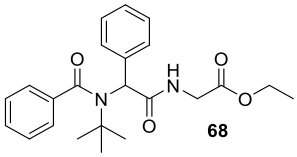 **68**	✓		✓
32	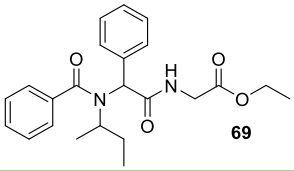 **69**	✓		✓

33	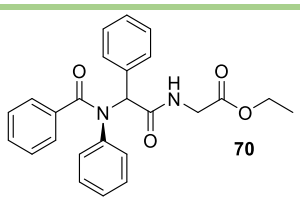 **70**	✓	✓
34	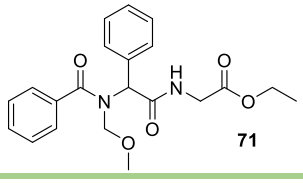 **71**	✓	✓

Synthesis of ethyl 2-[2-(N-butyl-1-phenylformamido)-2-phenylacetamido] acetate (34)

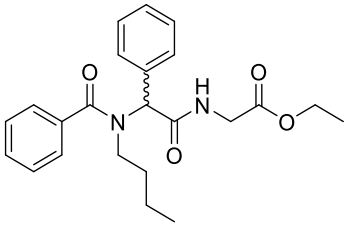

34 was synthesised according to the general procedure **6.5.3** and purified with protocol **6.5.4**. Accordingly, 0.457 mmol of ethyl isocyanoacetate was used and **34** was obtained as a brown oil (99 mg) in 87% yield.

^{1}H NMR (400 MHz, Chloroform-*d*) δ 7.62 – 7.50 (m, 5H, Ar*H*), 7.49 – 7.37 (m, 5H, Ar*H*), 6.78 (s, 1H, N*H*), 5.82 (s, 1H, C*H*), 4.23 (q, *J* = 7.1 Hz, 2H, CH_2),4.09 (d, *J* = 5.4 Hz, 2H, CH_2), 3.40 –3.21 (m, 2H, CH_2), 1.28 (t, *J* = 3.1 Hz, 3H, CH_3), 1.00 –0.90 (m, 4H, CH_2), 0.64 –0.62 (m, 3H, CH_3). ^{13}C NMR (176 MHz, Chloroform-*d*) δ 172.8, 170.0, 169.6, 136.5, 135.0, 129.6, 129.3, 128.8, 128.7, 128.6, 126.5, 61.7, 61.4, 41.5, 31.3, 19.8, 14.1, 13.3. HRMS ESI^{+} Calculated for [M+H] $^{+}$ $C_{23}H_{29}N_2O_4^{+}$ = 397.2127. Found = 397.2116.

Synthesis of ethyl 2-(2-(*N*-butyloctanamido)-2-phenylacetamido) acetate (36)

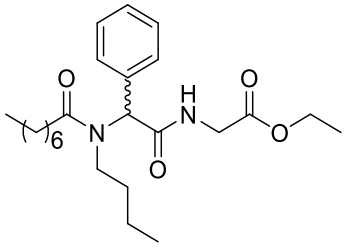

36 was synthesised according to the general procedure **6.5.3** and purified with protocol **6.5.4**. Accordingly, 0.457 mmol of ethyl isocyanoacetate was used and **36** was obtained as a brown oil (36.4 mg) in 19% yield.^{1}H NMR (400 MHz, Chloroform-*d*) δ 7.49 – 7.24 (m, 5H, Ar*H*), 6.51 (s, 1H, N*H*), 5.88 (s, 1H, C*H*), 4.17 (q, *J* = 7.1 Hz, 2H, CH_2),3.90 – 3.75 (m**,** 2H, CH_2), 3.33 – 3.26 (m, 2H, CH_2), 2.47 –2.34 (m, 2H, CH_2), 2.47 –2.34 (m, 2H, CH_2), 1.35 –1.27 (m, 14H, CH_2), 0.92 –0.89 (m, 6H, CH_3), 0.73 (t, *J* = 7.1 Hz, 3H, CH_3). ^{13}C NMR (176 MHz, Chloroform-*d*) *,$^{\#}$ δ 174.3, 170.3. 169.3, 135.1, 129.5, 128.8, 62.9, 61.4, 47.1, 41.5, 33.5, 31.7, 29.4, 29.1, 28.9, 25.4, 22.6, 19.9, 14.2 ,14.1, 13.5. HRMS ESI^{+} Calculated for [M+H] $^{+}$ $C_{24}H_{39}N_2O_4^{+}$ = 419.2910. Found = 419.2922.

*missing C_4Ar

$^{\#}$rotamers present

Synthesis of ethyl 2-{2-[N-(4-{[(tertbutoxy) carbonyl]amino}butyl)octanamido]-2-phenylacetamido}acetate (37)

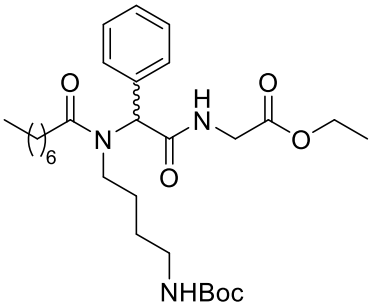

37 was synthesised according to the general procedure **6.5.1**. Accordingly, 0.457 mmol of ethyl isocyanoacetate was used and **37** was obtained as a brown oil (241.2 mg) in 9%

yield.[1]H NMR (400 MHz, Chloroform-*d*) δ 7.44 – 7.31 (m, 5H, Ar*H*), 6.61 (s, 1H, N*H*), 5.94 (s, 1H, C*H*), 4.23 – 4.17 (q, *J* = 7.2 Hz, 2H, CH_2), 4.09 – 4.03 (dd, *J* = 13.2, 7.5 Hz, 1H, CH_2), 3.91–3.86 (dd, *J* = 13.2, 7.5 Hz, 1H, CH_2), 3.31 –3.27 (m, 2H, CH_2), 2.96 –2.94 (m, 2H, CH_2), 2.43 –2.32 (m, 2H, CH_2), 1.71 –1.60 (m, 2H, CH_2), 1.45 (s, 9H, CH_3), 1.36 –1.29 (m, 15H, CH_2, CH_3), 0.94 –0.86 (m, 3H, CH_3). [13]C NMR (176 MHz, Chloroform-*d*) [#] δ 174.4, 170.2, 169.6, 156.2, 135.1, 129.4, 128.8, 126.0, 79.1, 61,3, 46.6, 41.5, 41.3, 39.7, 34.0, 33.5, 31.7, 29,4, 29.1, 28.4, 27.1, 26.8, 25.4, 22.6, 14.2,14.1. HRMS ESI$^+$ Calculated for [M+H] $^+$ $C_{29}H_{48}N_3O_6^+$ = 534.3543. Found = 534.3538.

[#]rotamers present

Synthesis of ethyl 2-{2-[N-(4-aminobutyl)octanamido]-2-phenylacetamido}acetate (38)

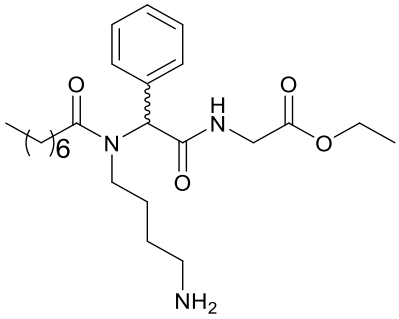

(24.7 mg, 0.046 mmol) of compound **37** were separated and dissolved in a 2 mL mixture with DCM and TFA (4:1, *v/v*). The mixture was stirred at room temperature for 2 h. The solvent was removed under reduced pressure. Several solvent additions with Et_2O (4 x 10 mL) were done in order to eliminate the TFA in vacuo. Unfortunately, this was not possible since there was some of it remaining. The obtained oil was dissolved in a mixture H_2O/MeCN and freeze dried for 48 h. The product, as a TFA salt, was identified as a brown oil (32 mg) in a 120% yield. [1]H NMR (400 MHz, MeOD) δ 7.55 –7.52 (m, 1H, Ar*H*), 7.51 – 7.35 (m, 4H, Ar*H*), 5.86 (s, 1H, C*H*), 4.31 (q, J = 7.1 Hz, 2H, CH_2), 3.40 – 3.22 (m, 2H, CH_2), 3.18 – 3.04 (m, 1H, CH_2), 2.98 – 2.89 (m, 1H, CH_2), 2.70 (t, J = 7.8 Hz, 2H, CH_2), 2.62 – 2.37 (m, 2H, CH_2), 1.76 – 1.57 (m, 2H, CH_2), 1.68 (m, 2H, CH_2), 1.55 – 1.45 (m, 1H, CH_2), 1.43 -1.28 (m, 11H, CH_2, CH_3), 1.24- 1.11(m, 1H, CH_2), 0.97 – 0.89 (m, 3H,

C*H*$_3$). ^{13}C NMR (176 MHz, MeOD)$^{\#}$ δ 174.9, 172.2, 167.1, 161.5, 134.7,129.5, 129.0, 126.0, 64.1, 62.3, 45.7, 45.6, 39.6, 33.6, 32.8, 31.5, 28.8, 26.3, 25.2, 24.3, 22.2, 13.0, 12.9. HRMS ESI$^+$ Calculated for [M+H] $^+$ $C_{24}H_{40}N_3O_4^+$ = 434.3019. Found = 434.3011.

$^{\#}$rotamers present

Ethyl 2-(2-phenyl-2-(*N*-(1-phenylethylacetamido)acetamido)acetate (39)

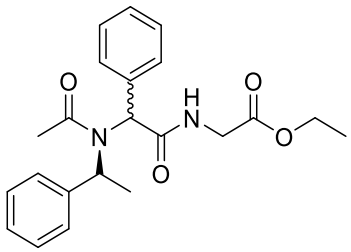

39 was synthesised according to the general procedure **6.5.1**. Accordingly,0.457 mmol of ethyl isocyanoacetate was used. The NMR showed acetic glacial was presented so the purified fraction was freeze dried. The compound was a mixture of inseparable compounds. HRMS ESI$^+$ Calculated for [M+H] $^+$ $C_{22}H_{27}N_2O_4^+$ = 383.1971. Found = 383.1951.

Synthesis of ethyl 2-[2-(N-ethyl-1-phenylformamido)-2- phenylacetamido]acetate (40)

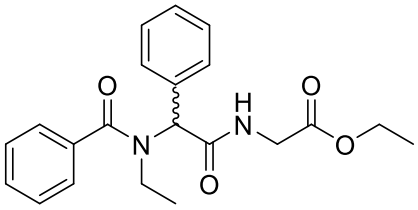

40 was synthesised according to the general procedure **6.5.1** and purified with protocol **6.5.4**. Accordingly,0.457 mmol of ethyl isocyanoacetate was used and **40** was obtained as a brown oil (13.0 mg) in 11% yield.^{1}H NMR (400 MHz, Chloroform-*d*) δ 8.16 – 8.10 (m, *J* = 8.12 Hz, 2H, Ar*H*), 7.63 – 7.58 (m, 3H, Ar*H),* 7.52 – 7.35 (m, 5H, Ar*H*) 6.90 (d, *J* = 5.2 Hz, 1H, N*H*), 6.42 (s, 1H, C*H*), 4.26 – 4.17 (m, 2H, C*H*$_2$), 4.14 – 4.07 (m, 4H, C*H*$_2$), 1.34 – 1.27 (m, 6H, C*H*$_3$). ^{13}C NMR (176 MHz, Chloroform-*d*) δ 172.8, 170.0, 169.6, 136.5, 133.2,

129.6, 129.3, 128.9, 128.6, 126,5, 126.0, 61.5, 58.9, 41.5, 31.6, 22.6, 14.1. HRMS ESI$^+$ Calculated for [M+H] $^+$ $C_{21}H_{25}N_2O_4^+$ = 369.1814. Found = 369.1800.

Synthesis of ethyl 2-(2-(N-(sec-butyl)acetamido)-2-phenylacetamido)acetate (41)

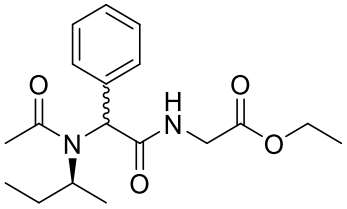

41 was synthesised according to the general procedure **6.5.1**. Accordingly,0.457 mmol of ethyl isocyanoacetate was used and **41** was obtained. The compound was a mixture of inseparable compounds. HRMS ESI$^+$ Calculated for [M+H] $^+$ $C_{18}H_{27}N_2O_4^+$ = 335.1971. Found = 335.1959.

Synthesis of tert-butyl N-{4-[N-({[(4- methylbenzenesulfonyl)methyl]carbamoyl} (phenyl)methyl)octanamido]butyl}carbamate (42)

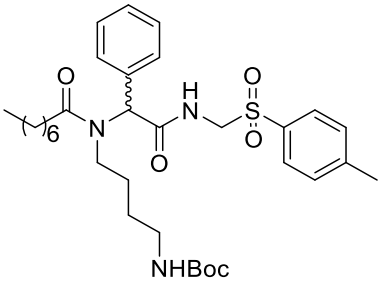

42 was synthesised according to the general procedure **6.5.2**. Accordingly,0.457 mmol of p-Toluenesulfonylmethyl isocyanide was used and **42** was obtained as a brown oil with a with solid (51 mg) in 18% yield. The compound was a mixture of inseparable compounds and was identified by LC-MS. ^{1}H NMR (400 MHz, $CDCl_3$) δ 7.72 (d, *J* = 8.1 Hz, 2H, Ar*H*), 7.38 – 7.28 (m, 5H, Ar*H*), 7.22 – 7.19 (m, 2H, Ar*H*), 7.07 (s, 1H, N*H*), 5.85 (s, 1H, C*H*), 4.76 (dd, *J* = 14.1, 6.9 Hz, 1H, CH_2), 4.63 (dd, *J* = 14.1, 6.5 Hz, 1H, CH_2), 4.44 (s, 1H, N*H*), 3.27 – 3.09 (m, 2H, CH_2), 2.90 (d, *J* = 7.1 Hz, 2H, CH_2), 2.46 (s, 3H, CH_3), 2.39 – 2.26 (m, 2H, CH_2), 1.63 (q, *J* = 9.5 Hz, 2H, CH_2), 1.44 (s, 9H, CH_3), 1.34 – 1.26 (m, 10H, CH_2), 1.16-1.09 (m, 2H, CH_2)), 0.94 – 0.86 (m, 3H, CH_3). ^{13}C NMR (151 MHz, Chloroform-

d)* δ 174.2, 169.7, 155.8, 145.1, 134.2, 134.0, 129.9, 129.4, 128.8,128.7, 79.1, 62.3, 60.3, 46.3, 39.6, 33.4, 31.7, 29.4, 29.1, 28.4, 27.2, 26.8, 25.3, 22.6, 21.7, 14.0. HRMS ESI$^+$ Calculated for [M+H] $^+$ $C_{33}H_{50}N_3O_6S^+$ = 616.3420. Found = 616.3407.

*missing C_4Ar

Synthesis of N-(4-aminobutyl)-N-({[(4- methylbenzenesulfonyl)methyl]carbamoyl} (phenyl)methyl)octanamide (43)

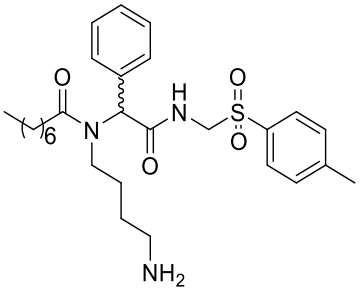

(24.7 mg, 0.040 mmol) of compound **42** were separated and dissolved in a 2 mL mixture with DCM and TFA (4:1, *v/v*). The mixture was stirred at room temperature for 2 h. The solvent was removed under reduced pressure. Several solvent additions with Et_2O (4 x 10 mL) were done in order to eliminate the TFA in vacuo. Unfortunately, this was not possible since there was some of it remaining. The obtained oil was dissolved in a mixture H_2O/MeCN and freeze dried for 48 h. The compound was a mixture of inseparable compounds because of the starting material used. Due to restrain times it was decided that the product should be used directly in the next step without further purification. This was to avoid accidental loss of product due to solubility issues. HRMS ESI$^+$ Calculated for [M+H] $^+$ $C_{28}H_{42}N_3O_6S^+$ = 516.2896. Found = 516.2891.

Synthesis of tert-butyl N-(4-{N-[(cyclohexylcarbamoyl) (phenyl) methyl] octanamido}butyl)carbamate (44)

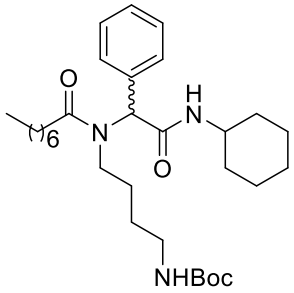

44 was synthesised according to the general **procedure 6.5.2**. Accordingly,0.457 mmol of cyclohexyl isocyanide was used and **44** was obtained as a white solid (119.3 mg) in 49% yield. ^{1}H NMR (^{1}H NMR (400 MHz, Chloroform-*d*) δ 7.36 - 7.26 (m, 5H, Ar*H*), 5.94 (d, *J* = 8.0 Hz, 1H, N*H*), 5.83 (s, 1H, C*H*), 4.49 (s, 1H, N*H*), 3.75 (m, 1H, C*H*), 3.25 (t, *J* = 8.1 Hz, 2H, CH_2), 2.90 (d, *J* = 6.5 Hz, 2H, CH_2), 2.38 – 2.25 (m,2H, CH_2), 1.85 (m, 2H, CH_2), 1.66 -1.58 (m, 4H, CH_2), 1.56 -1.50 (m, 1H, CH_2), 1.28 (s, 9H, CH_3), 1.25 - 1.22 (m, 13H, CH_2), 1.09 - 1.05 (m, 4H, CH_2), 0.84 (t, *J* = 6.9 Hz, 3H, CH_3). ^{13}C NMR (176 MHz, Chloroform-*d*) δ174.0, 168.9, 155.8, 135.8, 129.1, 128.7, 128.3, 78.9, 62.2, 48.4, 46.4, 44.8, 39.4, 33.9, 33.5, 32.8, 32.7, 31.7, 29.4, 29.1, 28.4, 27.1, 26.8, 25.5, 24.7, 22.6, 14.0. HRMS ESI^{+} Calculated for [M+H] $^{+}$ $C_{31}H_{52}N_3O_4^{+}$ = 530.3958. Found = 530.3934.

Synthesis of N-(4-aminobutyl)-N-[(cyclohexylcarbamoyl) (phenyl)methyl]octanamide (45)

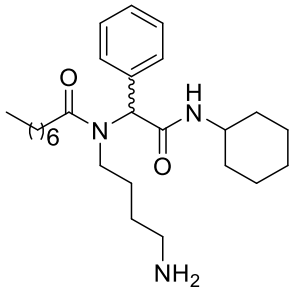

(22 mg, 0.042mmol) of compound **44** were separated and dissolved in a 1 mL mixture with DCM and TFA (1:1, *v/v*). The mixture was stirred at room temperature for 3 h. The solvent was removed under reduced pressure. Several solvent additions with Et_2O (4 x 10 mL) were done in order to eliminate the TFA in vacuo. Unfortunately, there was some of it remaining. The obtained brown oil was dissolved in a mixture H_2O/MeCN and freeze dried for 48 h. The product, as a TFA salt, was identified as a brown oil (28 mg) in a 122% yield. ^{1}H NMR (^{1}H NMR (400 MHz, MeOD) δ 7.36 - 7.25 (m, 5H, Ar*H*), 5.77 (s, 1H, C*H*), 3.68 - 3.57 (m, 1H, C*H*), 3.20 – 3.13 (m,2H, C*H*$_2$), 2.99 - 2.93 (m, 1H, C*H*$_2$), 2.61 - 2.52 (m,2H, C*H*$_2$), 2.47 - 2.29 (m,2H, C*H*$_2$), 1.95 – 1.86 (m, 1H, C*H*$_2$), 1.81 – 1.72 (m, 2H, C*H*$_2$), 1.60 - 1.49 (m, 4H, C*H*$_2$), 1.43 - 1.35 (m, 1H, C*H*$_2$), 1.33 - 1.17 (m, 13H, C*H*$_2$), 1.15 – 0.97 (m, 2H, C*H*$_2$), 0.84 – 0.80 (m, 3H, C*H*$_3$). ^{13}C NMR not available. HRMS ESI$^+$ Calculated for [M+H] $^+$ $C_{26}H_{44}N_3O_2^+$ = 430.3434. Found = 430.3430.

Synthesis of tert-butyl N-(4-{N-[(benzylcarbamoyl)(phenyl) methyl] octanamido} butyl) carbamate (46)

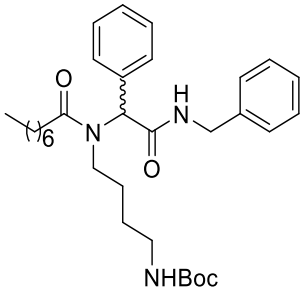

46 was synthesised according to the general procedure **6.5.1**. Accordingly, 0.457 mmol of benzyl isocyanide was used and **46** was obtained as a white solid (74.5 mg) in 30 % yield. ^{1}H NMR (700 MHz, $CDCl_3$) δ 7.32 – 7.15 (m, 10H, Ar*H*), 6.53 (s, 1H, N*H*), 5.87 (s, 1H, C*H*), 4.43 (s, 1H, N*H*), 4.37 (qd, *J* = 15.0, 5.9 Hz, 2H, CH_2), 3.22 (t, *J* = 8.2 Hz, 2H, CH_2), 2.84 -2.82 (m, 2H, CH_2), 2.42- 2.27 (m, 2H, CH_2), 1.56 (t, *J* = 7.5 Hz, 2H, CH_2), 1.35 (s, 9H, CH_3), 1.33 -1.30 (m, 1H, CH_2) 1.24 – 1.19 (m, 9H, CH_2), 1.15 – 1.11 (m, 2H, CH_2), 0.81 (t, *J* = 6.9 Hz, 3H, CH_3).^{13}C NMR (176 MHz, Chloroform-*d*) δ 174.2, 170.0, 155.9, 138.1, 135.5, 129.4, 128.8, 128.6, 128.5, 127.7, 127.3, 79.1, 62.2, 46.4, 43.6, 39.7, 33.5, 31.7, 29.4, 29.2, 27.1, 26.9, 25.4, 22.6,14.1. HRMS ESI$^+$ Calculated for [M+H] $^+$ $C_{32}H_{48}N_3O_4^+$ = 538.3645. Found = 538.3633.

Synthesis of N-(4-aminobutyl)-N- [(benzylcarbamoyl)(phenyl)methyl]octanamide (47)

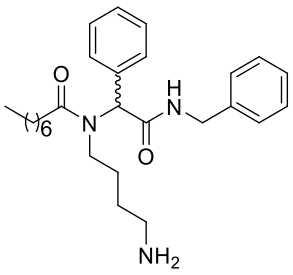

(27.9 mg, 0.052 mmol) of compound **47** were separated and dissolved in a 1 mL mixture with DCM and TFA (1:1, *v/v*). The mixture was stirred at room temperature for 3 h. The solvent was removed under reduced pressure. Several solvent additions with Et_2O (4 x 10 mL) were done in order to eliminate the TFA in vacuo. Unfortunately, this was not possible since there was some of it remaining. The obtained oil was dissolved in a mixture

H_2O/MeCN and freeze dried for 48 h. The product, as a TFA salt, was identified as a brown oil (25 mg) in a 90% yield. ^{1}H NMR (^{1}H NMR (400 MHz, MeOD) δ 7.45 – 7.40 (m, 2H, Ar*H*), 7.38 – 7.24 (m, 8H, Ar*H*), 5.75 (s, 1H, C*H*), 4.02 (s, 2H, CH_2), 3.01 -2.92 (m, 1H, CH_2), 2.87 -2.78 (m, 1H, CH_2), 2.61 -2.57 (m, 2H, CH_2), 2.48- 2.28 (m, 2H, CH_2), 1.72 – 1.67 (m, 1H, CH_2), 1.63 – 1.43 (m, 3H, CH_2), 1.44 -1.35 (m, 1H, CH_2), 1.33 -1.30 (m, 9H, CH_2) 1.36 – 1.19 (m, 9H, CH_2), 0.88 – 0.78 (m, 3H, CH_3). ^{13}C NMR not available.HRMS ESI$^+$ Calculated for [M+H] $^+$ $C_{27}H_{40}N_3O_4^+$ = 438.3121. Found = 438.3104.

Synthesis of tert-butyl N-{4-[N-({[2-(morpholin-4-yl) ethyl]carbamoyl} (phenyl) methyl)octanamido]butyl}carbamate (48)

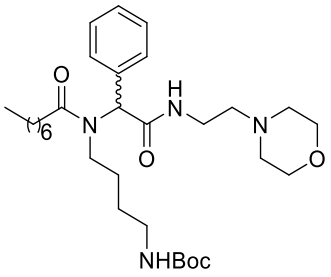

48 was synthesised according to the general procedure **6.5.1**. Accordingly,0.457 mmol of 2-Morpholinoethyl isocyanide was used and **48** was obtained. The compound was a mixture of inseparable compounds. HRMS ESI$^+$ Calculated for [M+H] $^+$ $C_{31}H_{53}N_4O_5^+$ = 561.4016. Found = 561.4010.

Synthesis of tert-butyl N-{4-[N-({[(1H-1,2,3-benzotriazol-1-yl) methyl] carbamoyl} (phenyl) methyl) octanamido]butyl}carbamate (49)

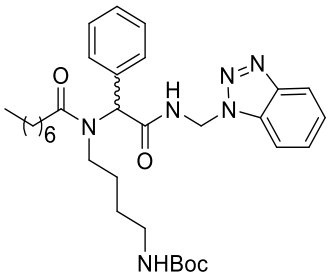

49 was synthesised according to the general procedure **6.5.1**. Accordingly,0.457 mmol of 1H-Benzotriazol-1-ylmethyl isocyanide was used. Compound **49** was repurified according to procedure **6.5.4** yielding a brown oil (5 mg) in 1% yield. The compound was identified by LC-MS. Due to restrain times it was decided that the product should be used directly in the next step without further purification. HRMS ESI$^+$ Calculated for [M+H] $^+$ $C_{32}H_{47}N_6O_4^+$ = 579.3659. Found = 579.3636.

Synthesis of N-(4-aminobutyl)-N-({[(1H-1,2,3-benzotriazol-1-yl) methyl] carbamoyl} (phenyl) methyl) octanamide (50)

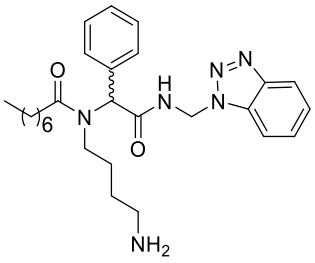

(22.2 mg, 0.041 mmol) of compound **49** were separated and dissolved in a 2 mL mixture with DCM and TFA (4:1, *v/v*). The mixture was stirred at room temperature for 3 h. The solvent was removed under reduced pressure. Several solvent additions with Et_2O (4 x 10 mL) were done in order to eliminate the TFA in vacuo. Unfortunately, this was not possible since there was some of it remaining. The obtained oil was dissolved in a mixture H_2O/MeCN and freeze dried for 48 h. The compound was a mixture of inseparable compounds and was identified by LC-MS. Due to restrain times it was decided that the product should be used directly in the next step without further purification. This was so

as to avoid accidental loss of product due to solubility issues. HRMS ESI$^+$ Calculated for [M+H] $^+$ $C_{27}H_{39}N_6O_2^+$ = 479.3134. Found = 479.3136.

Synthesis of ethyl 2-[2-(N-butylacetamido)-2-phenylacetamido] acetate (32)

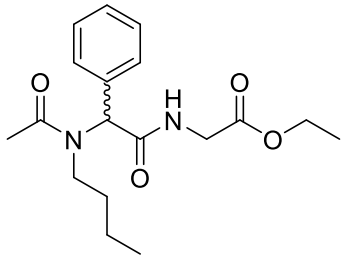

32 was synthesised according to procedure **6.5.3** and purified according to **protocol 6.5.4**. Accordingly,0.457 mmol of ethyl isocyanoacetate was used and **32** was obtained as a white solid (42.1 mg) in 28% yield. ^{1}H NMR (400 MHz, Chloroform-d) δ 7.48 – 7.32 (m, 5H, Ar*H*), 6.51 (t, J = 5.4 Hz, 1H, N*H*), 5.93 (s, 1H, C*H*), 4.20 (q, J = 7.1 Hz, 2H, CH_2), 4.14 – 3.97 (m, 2H, CH_2), 3.38 – 3.21 (m, 2H, CH_2), 2.20 (s, 3H, CH_3), 1.43 (m, 1H, CH_2), 1.28 (t, J = 7.1 Hz, 3H, CH_3), 1.18 – 1.05 (m, 2H, CH_2), 1.18 – 0.90 (m, 1H, CH_2), 0.75 (t, J = 7.3 Hz, 3H, CH_3). ^{13}C NMR (176 MHz, Chloroform-d)* δ 171.6, 170.2, 169.6, 135.1, 129.6, 128.8, 62.6, 61.5, 47.8, 41.5, 31.6, 21.8, 19.9, 14.2, 13.5. HRMS ESI$^+$ Calculated for [M+H] $^+$ $C_{18}H_{27}N_2O_4$ $^+$ = 335.1971. Found = 335.1989.

*missing C_4Ar

Synthesis of 2-(N-ethyl-1-phenylformamido)-N-[(4- methylbenzenesulfonyl)methyl]-2-phenylacetamide (66)

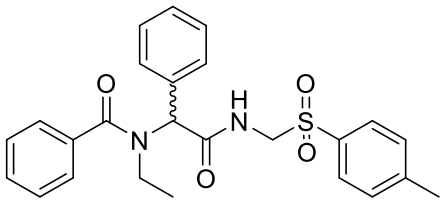

66 was synthesised according to the general procedure **6.5.2** and purified with **protocol 6.5.4**. Accordingly, 0.457 mmol of p-Toluenesulfonylmethyl isocyanide was used and **66** was obtained as a white solid (98.6 mg) in 48% yield. ^{1}H NMR (400 MHz, Chloroform-d) δ 7.81 – 7.74 (m, 2H, ArH), 7.52 – 7.37 (m, 10H, ArH), 7.33 (d, J = 8.0 Hz, 2H, ArH), 7.14 (s, 1H, NH), 5.76 (s, 1H, C*H*), 4.69- 4.63 (m, 2H, CH_2), 3.28 (m, 2H, CH_2), 2.46 (s, 3H, CH_3), 0.72 (t, J = 7.1 Hz, 3H, CH_3). ^{13}C NMR (176 MHz, $CDCl_3$)* δ 172.9, 169.6, 136.2, 134.2, 134.0, 130.0, 129.8, 129.2, 129.0, 128.9, 128.6, 126.5, 65.1, 60.4, 38.9, 21.7, 13.2. HRMS ESI$^+$ Calculated for $[M+H]^+$ $C_{25}H_{27}N_2O_4S^+$ = 451.1692. Found = 451.1698.

*missing two C_4Ar

Synthesis of ethyl 2-[2-{N-(4-{[(tertbutoxy) carbonyl]amino}butyl)-1-phenylformamido}-2- phenylacetamido] acetate (51)

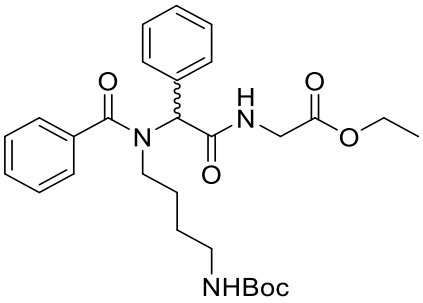

51 was synthesised according to the general procedure **6.5.2** with ethyl acetate/hexane (50:50, *v/v*) as eluent. Accordingly, 2.285 mmol of ethyl isocyanoacetate was used and **51** was obtained as an orange oil (276.2 mg) in a 38 % yield. ^{1}H NMR (400 MHz, Chloroform-d) δ 7.46 – 7.24 (m, 9H, Ar*H*), 7.21 – 7.10 (m, 1H, Ar*H*), 6.90 (s, 1H, N*H*), 5.89 (s, 1H, C*H*), 4.11 (q, J = 7.1 Hz, 2H, CH_2), 3.99 – 3.84 (m, 2H, CH_2), 3.27 – 3.15 (m, 2H, CH_2), 2.82 – 2.58 (m, 2H, CH_2), 1.33 (s, 9H, CH_3), 1.24 – 1.13 (m, 4H, CH_2, CH_3), 1.08 – 0.74 (m, 3H, CH_2). ^{13}C NMR (176 MHz, Chloroform-d) δ 171.2, 169.9, 169.6, 155.8, 136.4, 135.0, 129.7, 129.3, 128.9, 128.8, 128.6, 126.5, 78.9, 62.6, 61.4, 48.0, 45.0, 41.4, 39.5, 28.4, 26.9, 14.2. HRMS ESI$^+$ Calculated for $[M+H]^+$ $C_{28}H_{38}N_3O_6^+$ = 512.2761. Found = 512.2746.

Synthesis of ethyl 2-{2-[N-(3-aminopropyl)-1-phenylformamido]-2-phenylacetamido}acetate (67)

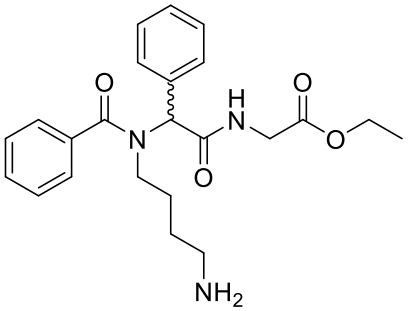

(24.7 mg, 0.048 mmol) of compound **51** were separated and dissolved in a 2 mL mixture with DCM and TFA (1:1, *v/v*). The mixture was stirred at room temperature for 2 h. The solvent was removed under reduced pressure. Several solvent additions with Et_2O (4 x 10

mL) were done in order to eliminate the TFA in vacuo. To eliminate any TFA traces, the obtained oil was dissolved in a mixture H_2O/MeCN and freeze dried for 48 h. The product, as a TFA salt, was identified as a brown oil (49 mg) in a 190% yield. ^{1}H NMR (400 MHz, MeOD) δ 7.56 – 7.35 (m, 10H, Ar*H*), 5.80 (s, 1H, C*H*), 4.31 (q, J = 7.1 Hz, 2H, CH_2), 4.25 – 4.21 (m, 2H, CH_2), 3.31 – 3.21 (m, 2H, CH_2), 2.96 – 2.91 (m, 2H, CH_2), 1.35– 1.28 (m, 4H, CH_2, CH_3), 1.13 – 0.98 (m, 3H, CH_2). ^{13}C NMR not available. HRMS ESI$^+$ Calculated for [M+H] $^+$ $C_{23}H_{30}N_3O_4^+$ = 412.2236. Found = 412.2241.

Synthesis of ethyl 2-[2-phenyl-2-(N-(1-phenylethylacetamido)formamido)-2-phenylacetamido] acetate (52)

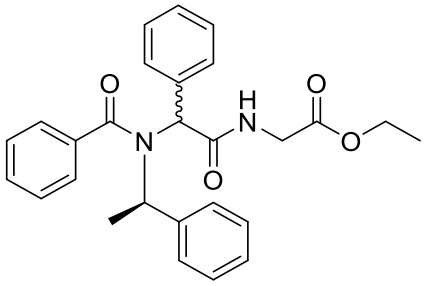

52 was synthesised according to procedure **6.5.4** and purified with protocol **6.5.5**. Accordingly, 0.941 mmol of ethyl isocyanoacetate was used and **52** was obtained as orange oil (104.0 mg) in a 77 % yield, diastereoisomeric mixture. ^{1}H NMR (400 MHz, Chloroform-d) δ 7.67 – 7.57 (m, 4H, Ar*H*), 7.56 – 7.45 (m, 9H, Ar*H*), 7.44 – 7.31 (m, 6H, Ar*H*), 7.25 – 7.20 (m, 3H, Ar*H*), 7.19 – 7.13 (m, 6H, Ar*H*), 7.13 – 7.08 (m, 2H, Ar*H*), 6.94 (s, 1H, N*H*), 6.66 (m, 1H, N*H*), 5.32 – 5.22 (m, 2H, C*H*), 4.81 – 4.74 (m, 2H, C*H*), 4.22 – 4.14 (m, 4H, CH_2), 4.11 – 4.08 (m, 2H, CH_2), 4.07 – 3.92 (m, 1H, CH_2), 3.82 (dd, *J* = 18.4, 4.7 Hz, 1H, CH_2), 1.76 (d, *J* = 7.0 Hz, 3H), 1.47 (d, *J* = 7.0 Hz, 3H), 1.29 – 1.24 (m, 6H, CH_3). ^{13}C NMR (176 MHz, Chloroform-d) diastereoisomeric mixture. δ 167.19, 167.10, 165.49, 164.47, 164.07, 133.73, 133.38, 131.89, 131.72, 131.35, 130.73, 124.61, 124.20, 123.7, 123.58, 123.57, 123.40, 123.15, 123.09, 123.05, 123.02, 123.0, 122.96, 122.75, 122.70, 122.49, 122.47, 121.11, 120.77, 72.08, 58.13, 57.82, 56.12, 56.06, 53.01, 52.85, 36.44, 36.39, 13.47. HRMS ESI$^+$ Calculated for [M+H] $^+$ $C_{27}H_{29}N_2O_4$ $^+$ = 445.2127. Found = 445.2123.

Synthesis of ethyl 2-[2-(N-cyclohexyl-1-phenylformamido)-2- phenylacetamido] acetate (53)

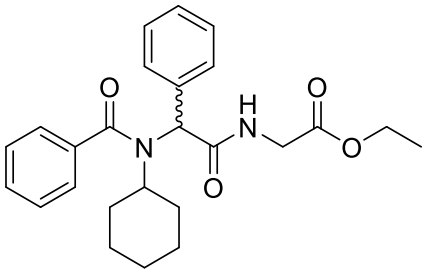

53 was synthesised with 0.457 mmol of ethyl isocyanoacetate according to the general procedure **6.5.2** with ethyl acetate/hexane (50:50, v/v) as eluent. The obtained oil resulted in an inseparable mixture of compounds. HRMS ESI$^+$ Calculated for $[M+H]^+$ $C_{25}H_{31}N_2O_4^+$ = 423.2284. Found = 423.2269.

Synthesis of N-cyclohexyl-2-(N-ethyl-1-phenylformamido)-2- phenylacetamide (54)

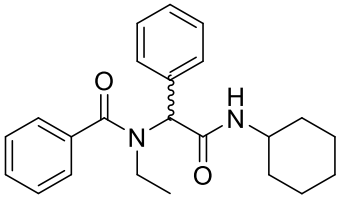

54 was synthesised according to the general procedure **6.5.1** with 0.121 mmol of ethylamine and 0.457 mmol of cyclohexyl isocyanide. The obtained oil resulted in a inseparable mixture of compounds. The presence of **54** was confirmed by LC-MS analysis ($C_{23}H_{29}N_2O_2$ $[M + H]^+$ *m/z* =365.356).

Synthesis of N-butylcarbamoyl-[2-(N-ethyl-1-phenylacetamido)-1-phenyl (55)

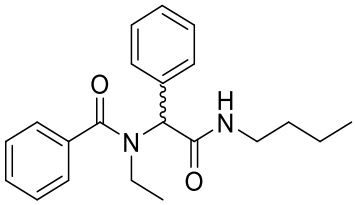

55 was synthesised according to the general procedure **6.5.2** with ethyl acetate/hexane (50:50, v/v) as eluent. Accordingly, 0.457 mmol of butyl isocyanide was used and **55** was obtained as a colourless oil (13.3 mg) in a 9 % yield. ^{1}H NMR (400 MHz, Chloroform-d) δ

7.51 – 7.33 (m, 10H, ArH), 6.37 (s, 1H, NH), 5.83 (s, 1H, C*H*), 3.45 – 3.35 (m, 2H, CH_2), 3.31 (q, J = 6.8 Hz, 2H, CH_2), 1.54 – 1.44 (m, 2H, CH_2), 1.38 – 1.26 (m, 2H, CH_2), 0.92 (t, J = 7.3 Hz, 3H, CH_3), 0.85 – 0.75 (m, 3H, CH_3). ^{13}C NMR (176 MHz, Chloroform-d) δ 172.7, 169.6, 136.7, 135.5, 129.5, 129.1, 128.8,128.5, 128.4,126.5, 63.2, 43.6,39.5, 31.5, 20.0, 14.8, 13.7. HRMS ESI$^+$ Calculated for [M+H] $^+$ $C_{21}H_{27}N_2O_2$ $^+$ = 339.2073. Found = 339.2067.

Synthesis of ethyl 2-[2-(N-(sec-butyl)-1-phenylformamido)-2- phenylacetamido] acetate (57)

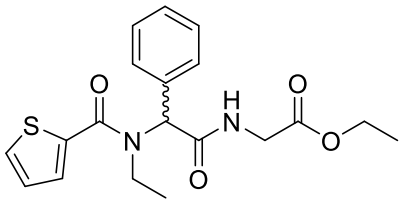

57 was synthesised according to the general procedure **6.5.2** and purified with **protocol 6.5.4**. Accordingly,0.457 mmol of ethyl isocyanoacetate was used and **57** was obtained as a yellow oil (133.4 mg) in 78% yield.^{1}H NMR (400 MHz, , Chloroform-d) δ 7.41 – 7.33 (m, 4H, ArH), 7.33 – 7.21 (m, 3H, ArH), 6.96 (dd, J = 5.0, 3.7 Hz, 1H, ArH), 6.89 (t, J = 5.5 Hz, 1H, NH), 5.87 (s, 1H, C*H*), 4.10 (q, J = 7.2 Hz, 2H, CH_2), 3.96 (dd, J = 5.5, 1.9 Hz, 2H, CH_2), 3.68 – 3.55 (m, 1H, CH_2), 3.53 – 3.45 (m, 1H, CH_2), 1.18 (t, J = 7.1 Hz, 3H, CH_3), 0.82 (t, J = 7.0 Hz, 3H, CH_3). ^{13}C NMR (176 MHz, Chloroform-d) δ 169.9, 169.6, 165.3, 137.6, 134.9, 129.4, 129.1, 128.9, 128.6, 127.5, 127.1, 64.6, 61.4, 42.9, 41.6, 14.8, 14.2. HRMS ESI$^+$ Calculated for [M+H] $^+$ $C_{19}H_{23}N_2O_4S$ $^+$ =375.1379. Found = 375.1375.

Synthesis of ethyl 2-[2-(N-ethyl-1-furanformamido)-2-phenylacetamido] acetate (58)

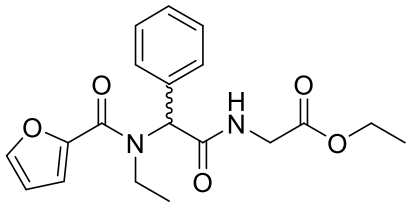

58 was synthesised according to the general procedure **6.5.1** with ethyl acetate/hexane (50:50, v/v) as eluent. Accordingly, 0.457 mmol of ethyl isocyanoacetate was used and 43 was obtained as a colourless oil (5.8 mg) in a 4 % yield. ^{1}H NMR (400 MHz, Chloroform-d) δ 7.58 – 7.55 (m, 1H, ArH), 7.51 – 7.45 (m, 2H, ArH), 7.34 – 7.29 (m, 3H, ArH), 7.27 – 7.25 (m, 1H, ArH), 6.74 – 6.64 (m, 1H, NH), 6.48 (dd, J = 3,5, 1.7 Hz, 1H, ArH), 5.91 (s, 1H, C*H*), 4.15 (q, J = 7.1 Hz, 2H, CH_2), 4.05 – 3.95 (m, 2H, CH_2), 3.79 – 3.55 (m, 4H, CH_2), 1.26 – 1.14 (m, 6H, CH_3). ^{13}C NMR (176 MHz, Chloroform-d)* δ 169.5, 168.2, 156.6, 147.1, 143.6, 135.0, 129.2, 128.8, 127.6, 119.4, 112.2, 75.4, 61.7, 41.3, 21.1, 14,2 14.1. HRMS ESI+ Calculated for $[M+H]^+$ $C_{19}H_{23}N_2O_5$ + = 359.1607. Found = 359.1598.

*missing C=O

Synthesis of ethyl 2-[2-(N-ethyl-1-phenylformamido)-2-(thiophen-2- yl) acetamido]acetate (59)

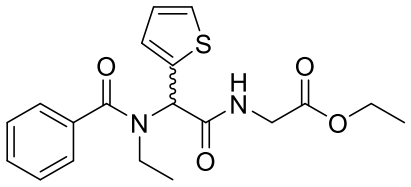

59 was synthesised according to the general procedure **6.5.1** with 0.121 mmol of ethylamine and 0.457 mmol of cyclohexyl isocyanide. The obtained oil resulted in an inseparable mixture of compounds. The presence of **59** was confirmed by LC-MS analysis ($C_{19}H_{22}N_2O_4S$ $[M + H]^+$ *m/z* =375.267).

Synthesis of ethyl 2-[2-(N-ethyl-1-phenylformamido)-2-(furan-2- yl)acetamido] acetate (60)

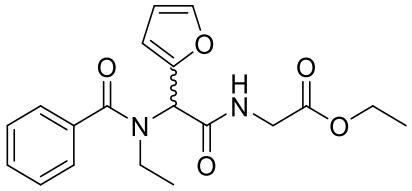

60 was synthesised according to the general procedure **6.5.1** with 0.121 mmol of ethylamine and 0.457 mmol of cyclohexyl isociyanide. The obtained oil resulted in an inseparable mixture of compounds. The presence of **60** was confirmed by LC-MS analysis ($C_{19}H_{23}N_2O_5$ $[M + H]^+$ *m/z* =359.305).

Synthesis of ethyl 2-[2-(N-ethyl-1-thiopheneformamido)-2- thiopheneacetamido] acetate (61)

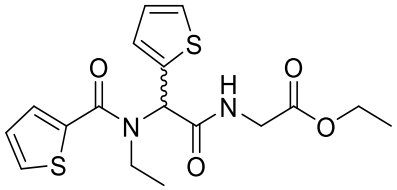

65 was synthesised according to the general procedure **6.5.1** with DCM/methanol (90:10, v/v) as eluent. Accordingly, 0.457 mmol of ethyl isocyanoacetate was used and **65** was obtained as dark red oil (116.2 mg) in a 67 % yield. ^{1}H NMR (400 MHz, Chloroform-d) δ 7.55 – 7.47 (m, 2H, ArH), 7.40 (dd, J = 5.1, 1.2 Hz, 1H, ArH), 7.32 (dt, J = 3.6, 1.0 Hz, 1H, ArH), 7.09 (dd, J = 5.0, 3.7 Hz, 1H, ArH), 7.06 (dd, J = 5.2, 3.6 Hz, 1H, ArH), 6.90 – 6.3 (s, 1H, NH), 6.05 (s, 1H, C*H*), 4.21 (q, J = 7.2 Hz, 2H, CH_2), 4.17 – 4.12 (m, 1H, CH_2), 4.04 (dd, J = 18.2, 5.1 Hz, 1H, CH_2), 3.75 – 3.64 (m, 2H, CH_2), 1.29 (t, J = 7.1 Hz, 3H, CH_3), 1.12 (t, J = 7.1 Hz, 3H, CH_3). ^{13}C NMR (176 MHz, Chloroform-d) δ 169.5, 168.9, 165.1, 137.2, 136.5, 129.7, 129.5, 129.4, 127.8, 127.1, 126.7, 61.5, 43.6, 43.3, 41.6, 14.9, 14.2. HRMS ESI$^+$ Calculated for $[M+H]^+$ $C_{17}H_{21}N_2O_4S_2^+$ = 381.0943. Found = 381.0948.

Synthesis of ethyl 2-[2-(N-tert-butyl-1-phenylformamido)-2- phenylacetamido] acetate (68)

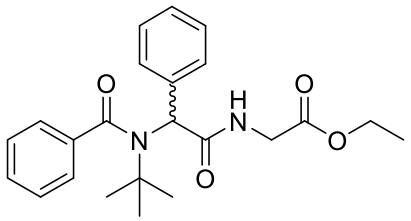

68 was synthesised according to the general procedure **6.5.1** with 0.121 mmol of ethylamine and 0.457 mmol of cyclohexyl isocyanide. The obtained oil resulted in an inseparable mixture of compounds. The presence of **68** was confirmed by LC-MS analysis ($C_{23}H_{29}N_2O_4$ $[M + H]^+$ *m/z* =395.543).

Synthesis of ethyl 2-[2-(N-(sec-butyl)-1-phenylformamido)-2- phenylacetamido] acetate (69)

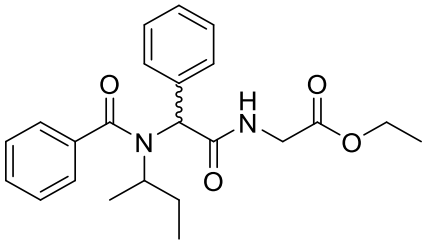

70 was synthesized with 0.457 mmol of ethyl isocyanoacetate according to the general procedure **6.5.1** with ethyl acetate/hexane (50:50, v/v) as eluent. The obtained oil resulted in an inseparable mixture of compounds. HRMS ESI$^+$ Calculated for $[M+H]^+$ $C_{23}H_{29}N_2O_4^+$ = 397.2112. Found = 397.2127.

Synthesis of ethyl 2-[2-(N,1-diphenylformamido)-2-phenylacetamido]acetate (70)

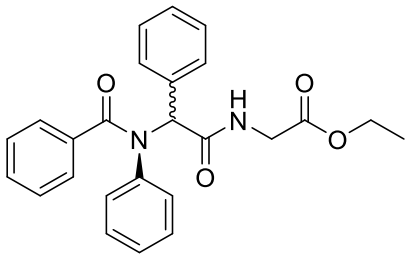

71 was synthesised according to the general procedure **6.5.2** with 0.457 mmol of ethyl isocyanoacetate. The obtained oil resulted in an inseparable mixture of compounds. The presence of **71** was confirmed by LC-MS analysis ($C_{25}H_{24}N_2O_4$ $[M + H]^+$ *m/z* =417.413).

Synthesis of ethyl 2-{2-[N-(methoxymethyl)-1-phenylformamido] -2-phenylacetamido} acetate (71)

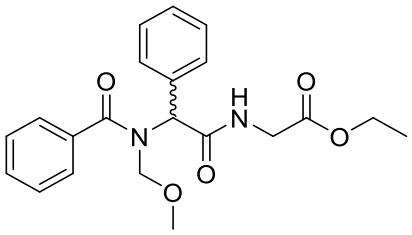

72 was synthesised according to the general procedure **6.5.1** with 0.457 mmol of ethyl isocyanoacetate. The obtained oil resulted in an inseparable mixture of compounds. The presence of **71** was confirmed by LC-MS analysis ($C_{21}H_{24}N_2O_5$ $[M + H]^+$ *m/z* =384.426).

6.6 Passerini compounds

Synthesis of ethyl 2-[2-(acetyloxy)-2-phenylacetamido] acetate (35)

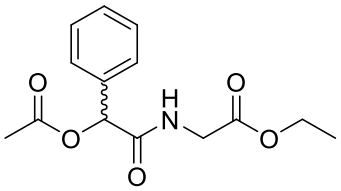

35 was synthesised according to the general procedure **6.5.1**. Accordingly, 0.457 mmol of ethyl isocyanoacetate was used and **35** was obtained as a white solid (165 mg) in a 97% yield.^{1}H NMR (400 MHz, Chloroform-*d*) δ 7.49 (dq, *J* = 6.6, 2.8, 2.4 Hz, 2H, Ar*H*), 7.43 – 7.36 (m, 3H, Ar*H*), 6.74 (s, 1H, N*H*), 6.16 (s, 1H, C*H*), 4.25 (q, *J* = 7.1 Hz, 2H, CH_2),4.14 – 4.03 (m, 2H, CH_2), 2.22 (s, 3H, CH_3), 1.30 (t, *J* = 7.2 Hz, 3H, CH_3).^{13}C NMR (176 MHz, Chloroform-*d*) δ 169.6, 169.1, 168.5, 135.3, 129.1, 128.8, 127.5, 75.4, 61.8, 41.3, 21.0, 14.1. HRMS ESI^{+} Calculated for [M+H] $^{+}$ $C_{14}H_{18}NO_5^{+}$ = 280.1185. Found = 280.1175

Synthesis of N-cyclohexylcarbamoyl-[1-(phenyl)-1-benzoate] (62)

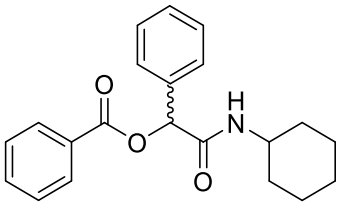

62 was synthesised according to the general protocol detailed in **Section 6.5.2** without the amine substituent, with DCM/methanol (90:10, v/v) as eluent. Accordingly, 0.457 mmol of cyclohexyl isocyanide was used and 49 was obtained as a white solid (115.6 mg) in a 74 % yield. ^{1}H NMR (400 MHz, Chloroform-d) δ 8.14 – 8.09 (m, 2H, ArH), 7.66 – 7.60 (m, 1H, ArH), 7.58 – 7.54 (m, 2H, ArH), 7.53 – 7.44 (m, 2H, ArH), 7.43 – 7.35 (m, 3H, ArH), 6.24 (s, 1H, CH), 5.98 (d, J = 8.2 Hz, 1H, NH), 3.81 - 3.71 (m, 1H, CH), 1.92 - 1.78 (m, 2H, CH_2), 1.67 - 1.47 (m, 3H, CH_2), 1.35 - 1.22 (m, 2H, CH_2), 1.17 - 1.00 (m, 3H, CH_2). ^{13}C NMR (176 MHz, Chloroform-d) δ 167.3, 164.9, 135.8, 133.7, 129.8, 129.3, 129.0, 128.8,

128.7, 127.4, 75.9, 48.2, 33.0, 32.9, 25.5, 24.8, 24.7. HRMS ESI$^+$ Calculated for [M+H] $^+$ $C_{21}H_{23}NO_3$ $^+$ = 338.1756. Found = 338.1760.

Synthesis of N-butylcarbamoyl-[1-(phenyl)-1-benzoate] (63)

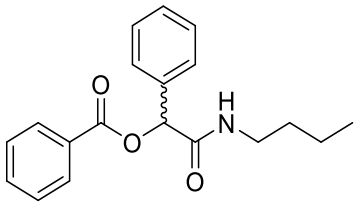

63 was synthesised according to the general procedure **6.5.1** with ethyl acetate/hexane (50:50, v/v) as eluent. Accordingly, 0.457 mmol of butyl isocyanide was used and **63** was obtained as a colourless oil (122.4 mg) in 86 % yield. ^{1}H NMR (400 MHz, Chloroform-d) δ 8.02 – 7.98 (m, 2H, ArH), 7.51 – 7.42 (m, 3H, ArH), 7.38 – 7.32 (m, 2H, ArH), 7.30 – 7.20 (m, 3H, ArH), 6.50 – 6.34 (m, 1H, NH), 6.21 (s, 1H, C*H*), 3.20 – 3.11 (m, 2H, C*H*$_2$), 1.41 – 1.34 (m, 2H, C*H*$_2$), 1.24 – 1.10 (m, 2H, C*H*$_2$), 0.82 – 0.72 (m, 3H, C*H*$_3$). ^{13}C NMR (176 MHz, Chloroform-d) δ 168.4, 165.1, 135.8, 135.7, 133.6, 129.9, 129.3, 129.0, 128.8, 128.6, 127.4, 76.0, 39.3, 31.5, 20.0, 13.7. HRMS ESI$^+$ Calculated for [M+H] $^+$ $C_{19}H_{22}NO_3$ $^+$ = 312.1600. Found = 312.1598

N-tert-butyl carbamoyl-[2-(phenyl)-2-benzoate] (64)

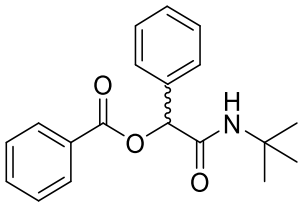

64 was synthesised according to the general procedure **6.5.1** with DCM/methanol (90:10, v/v) as eluent. Accordingly, 0.457 mmol of tert-butyl isocyanide was used and **64** was obtained as a white solid (131 mg) in a 92 % yield. ^{1}H NMR (400 MHz, Chloroform-d) δ 8.10 – 8.01 (m, 2H, ArH), 7.56 – 7.52 (m,1H, ArH), 7.46 – 7.39 (m, 4H, ArH), 7.35 – 7.29 (m, 3H, ArH) 6.25 (s, 1H, C*H*), 6.04 (s, 1H, NH), 1.39 (s, 9H, C*H*$_3$). ^{13}C NMR (176 MHz, Chloroform-d) δ 167.4, 164.9, 136.0, 133.6, 129.8, 129.4, 128.9, 128.8, 128.7, 127.5, 76.0, 51.6, 28.7. HRMS ESI$^+$ Calculated for [M+H] $^+$ $C_{19}H_{22}NO_3$ $^+$ = 312.1600. Found = 312.1597

Synthesis of ethyl 2-[2-(2-furoate)-2-phenylacetamido] acetate (65)

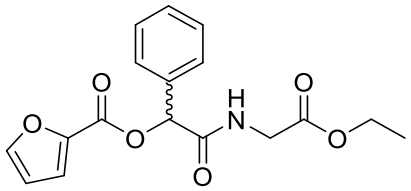

65 was synthesised according to the general procedure **6.5.1** with ethyl acetate/hexane (50:50, v/v) as eluent. Accordingly, 0.457 mmol of ethyl isocyanoacetate was used and **65** was obtained as a white solid (99.4 mg) in a 66 % yield. ^{1}H NMR (400 MHz, Chloroform-d) δ 7.56 (dd, J = 1.7, 0.8 Hz, 1H, ArH), 7.50 – 7.46 (m, 2H, ArH), 7.35 – 7.28 (m, 3H, ArH), 7.27 (dd, J = 3.5, 0.8 Hz, 1H, ArH), 6.86 (s, 1H, NH), 6.49 (dd, J = 3.5, 1.7 Hz, 1H, ArH), 6.29 (s, 1H, CH), 4.15 (q, J = 7.2 Hz, 2H, CH2), 4.07 (dd, J = 18.5, 5.3 Hz, 1H, CH_2), 3.98 (dd, J = 18.5, 5.0 Hz, 1H, CH_2), 1.21 (t, J = 7.1 Hz, 3H, CH_3). ^{13}C NMR (176 MHz, Chloroform-d) δ 169.5, 168.3, 156.6, 147.1, 143.7, 135.1, 129.2, 128.9, 127.6, 119.5, 112.3 75.4, 61.8, 41.3, 14.1. HRMS ESI^{+} Calculated for $[M+H]^{+}$ $C_{17}H_{18}NO_6^{+}$ = 332.1138 Found = 332.1134.

6.7 Biological assays

6.7.1 Promastigote parasite culture

Isolates of Leishmania mexicana (MNYC/BZ/62/M379*), L. major* (FV1) and *L. amazonensis* (MHOM/Br/75/JOSEFA) promastigotes were thawed at 37 °C and immediately transferred into Schneider's insect medium (Sigma-Aldrich) supplemented with 0.4 g/L $NaHCO_3$, 0.6 g/L anhydrous $CaCl_2$, 15% (v/v) heat-inactivated foetal bovine serum (FBS; Gibco) and 1% (v/v) Penicillin/Streptomycin solution (Gibco), pH 7. The cultures were incubated at 26 °C for 2-3 days until parasites were growing well and then inoculated into fresh media at a concentration of 5 x 10^5 cells/mL. Subsequently, parasites were maintained at the log phase by splitting to 5 x 10^5 cells/mL every 2-3 days. Cells were counted using a Neubauer Improved Haemocytometer.

6.7.2 Culturing of *Leishmania mexicana* axenic amastigotes

L. mexicana log phase promastigotes were differentiated to axenic amastigotes by transferring to Schneider's insect medium supplemented with 0.4 g/L $NaHCO_3$, 0.6 g/L anhydrous $CaCl_2$ 20% heat inactivated FBS, pH 5.5 and 1% (v/v) penicillin/streptomycin (Gibco) at 5 x 105 cells/mL and incubating at 26°C for 5-6 days until they reach the metacyclic stage. Parasites were then seeded at 5 x 10^5 cells/mL in the same medium and incubated at 33°C. After additional 5-7 days of incubation, parasites should be in the amastigote stage. *L. mexicana* axenic amastigotes were maintained at 33°C by subculturing at a 5 x 10^5 cells/mL concentration every 5-7 days.22

6.7.3 Preparation of frozen stocks

L. mexicana, L. major and *L. amazonensis* promastigotes were grown to log phase, then 500 µL of parasite culture (0.5-1 x 10^7 cells/mL) was added to 500 µL of freezing culture medium (10% DMSO, 60% Schneider's Insect medium, 30% heat-inactivated FBS). This was then transferred into cryovials (STARLAB) and frozen slowly by incubating serially at 4°C, -20°C and -80°C for 2 hours each before transferring to a labelled box for long-term storage at -150°C. All cells were frozen at a low passage number.

6.7.4 Preparation of test compounds and amphotericin B stock solutions

All the purified compounds, unless specified, and amphotericin B (Sigma-Aldrich) were prepared at 10 mM in DMSO (Sigma-Aldrich). The stocks were then stored at -20 ºC between uses and before each use stock was thoroughly defrosted, and vortexed. 1 mM stock solutions were freshly prepared with Schneider's insect media according to the parasite stage before testing.

6.7.5 Cell counting and concentration determination

Cells were counted using a Neubauer Improved Haemocytometer under a light microscope (×40 magnification). 10 µL of cell culture was loaded into each of the two counting chambers and for dense cultures, a dilution (1:10) of cells in the medium was required to allow a better cell separation. The medium-sized squares in the 1 mm^2 area at

the centre of the 3×3 grid was selected for counting (1×10^{-4} mL volume per square) (**Figure 6.1**).

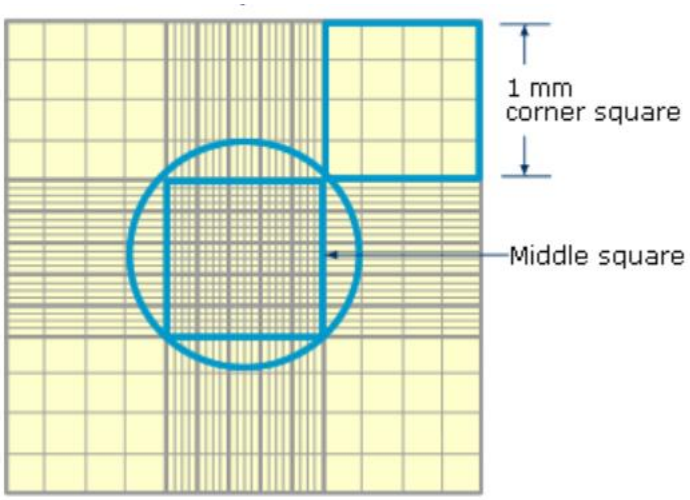

Figure 6.1 Standard Haemocytometer chamber (https://www.dlsweb.rmit.edu.au/Toolbox/Laboratory/laboratory/studynotes/SNHaemo.htm)

The number of cells per mL was counted as follows:

$$Cell\ density = \frac{(number\ of\ cells\ counted)(dilution\ factor)}{(number\ of\ squares\ counted)(volume\ of\ a\ square)}$$

6.7.6 Assay validation for *L. mexicana* promastigotes and axenic amastigotes

Two 96-well microtiter plates were set up by adding 100 µL of Schneider's Insect medium (pH 7.0, 15% FBS, 1% penicillin/streptomycin) containing *L. mexicana* promastigotes at the following concentrations: 2×10^6 cells/mL, 1×10^6 cells/mL, 5×10^5 cells/mL, 2.5×10^5 cells/mL, 1.25×10^5 cells/mL, 6.25×10^4 cells/mL, 3.125×10^4 cells/mL, and 1.562×10^4 cells/mL. These concentrations were achieved by carrying out a 2-fold serial dilution from a 2×10^6 cells/mL culture and each dilution was prepared in triplicate. 100 µL of culture media was added to all the empty wells to establish the background fluorescence. One plate was incubated for 20 hrs and the other plate for 44 hrs at 26 ºC. Then, 10 µL (10% v/v) of resazurin solution (5mg dissolved in 40mL of sterile PBS, 0.0125% w/v; Sigma-Aldrich) was added to each well and the plate incubated for a further 4 hrs at 26

ºC. Fluorescence was measured using the Biotek microplate reader (Biotek FLx800, λ_{ex} 560 nm, λ_{em} 600 nm).

Assay validation for *L. mexicana* axenic amastigotes was carried out using the same protocol as above, but instead using Schneider's insect medium (pH 5.5, 20% FBS, 1% penicillin/streptomycin) and an incubation temperature of 33 °C.

6.7.7 Assay validation for *L. major* and *L. amazonensis* promastigotes

Validation was carried out with optimised conditions from **protocol 6.7.7**. Both plates, containing different parasite species, were incubated for 20 hrs at 26 ºC. Then, 10 µL (10% v/v) of resazurin solution (0.0125% w/v; Sigma-Aldrich) was added to each well and incubated for a further 4 hrs at 26 ºC. Fluorescence was measured using the Biotek microplate reader (Biotek FLx800, λ_{ex} 560 nm, λ_{em} 600 nm).

6.7.8 Preliminary screening of histatin library at 50 and 100 µM concentration against *L. amazonensis, L. major and L. mexicana* species

Promastigotes at 1 x 10^6 cells/mL in Schneider's insect media (pH 7.0) were seeded into a 96-well microtiter plate (final volume of 200 ul per well). 10 ul and 20 ul of each test compound (1 mM in media) were added in triplicate to produce final concentrations of 50 and 100 µM, respectively. Controls (Schneider's insect media used as a negative control and amphotericin B used as a positive control) were added to the corresponding wells in triplicate. Promastigotes containing plates were incubated at 26 °C for 20 hrs. Then, 20 µL (10% v/v) of resazurin solution (0.0125% w/v; Sigma-Aldrich) was added to each well and the plates incubated for a further 4 hrs at respective temperature. Plates were read using the Biotek microplate reader (Biotek FLx800, λ_{ex} 560 nm, λ_{em} 600 nm). The percentage of cell viability was calculated using MS excel data sheets and bar charts were created to present the percentage of viable cells following treatment with each test compound at 50 and 100 µM.

The preliminary screen for *L. mexicana* axenic amastigotes was carried out using the same protocol as above, but instead using Schneider's insect medium (pH 5.5, 20% FBS, 1% penicillin/streptomycin) and an incubation time of 44 hrs with a temperature of 33 °C.

6.7.9 Preliminary screen for temporin library at 200 µM concentration against *L. major*, *L. amazonensis* and *L. mexicana* species

Schneider's insect media (pH 7.0) containing promastigotes at 1 x 10^6 cells/mL were seeded into a 96-well microtiter plate (final volume of 200 µL per well). Required volumes of each test compounds were added in a triplicate assay to produce a final concentration of 200 µM. Controls (DMSO used as a negative control and amphotericin B used as a positive control) were added to the corresponding wells, again in triplicate. Promastigote containing plates were incubated at 26 °C for 20 hrs. Subsequent steps were carried out according to **protocol 6.7.8**.

6.7.10 Preliminary screen of the peptoid library at 50 µM against *L. mexicana* promastigotes and axenic amastigotes

Schneider's insect medium (pH 7.0 or pH 5.5) with cells at 1 x 10^6 cells/mL were seeded into a 96-well microtiter plate (final volume of 200 µL per well). Required volumes of each test compounds were added in a triplicate assay to produce a final concentration of 50 µM. Controls (DMSO used as a negative control and amphotericin B used as a positive control) were also added to the corresponding wells in triplicate. Promastigote plates were incubated at 26 °C for 20 hrs and axenic amastigote plates at 33 °C for 44 hrs. Subsequent steps were carried out according to **protocol 6.7.8**.

6.7.11 Dose-response assays with *L. mexicana* promastigotes and axenic amastigotes

L. mexicana promastigotes at 1 x 10^6 cells/mL in Schneider's insect medium (pH 7.0, 15% FBS, 1% penicillin/streptomycin) (200 µL/well) were treated with a serial drug dilution and seeded into 96 well plates. Drug dilutions were of eight 3-fold dilution steps covering a range from 50 – 0.0228 µM, and were assayed in triplicate. Amphotericin B was used as a positive control (100 µM final concentration) and DMSO as the negative control (2% final

concentration). Plates were incubated at 26 °C for 20 hrs. Then, 20 µL (10% v/v) resazurin solution (0.0125% w/v; Sigma-Aldrich) was added to each well and the plates incubated for a further 4 hrs at the respective temperature. Plates were subsequently read using a plate reader (Biotek FLx800, λ_{ex} 560 nm, λ_{em} 600 nm).

Dose-response assays using *L. mexicana* axenic amastigotes were carried out using the same protocol as above, but instead using Schneider's insect medium (pH 5.5, 20% FBS, 1% Penicillin/Streptomycin) and incubating at 33 °C for 44 hrs before the addition of resazurin solution (0.0125% w/v; Sigma-Aldrich).

6.7.12 Data treatment and statistical analysis

Date was plotted, and curve adjustments, regressions and statistical analyses made, using the GraphPad Prism 7 package.

Appendix

A.1 Histatins as metal chelators

Antimicrobial peptides (AMPs) are an important part of the innate immune system. Some AMPs, including histatins (HSTs), are known to have metal binding properties, the extent and function of which remains largely unclear. HSTs are particularly interesting with regards to the development of new therapeutics, since they act on pathogens using an alternative mechanism to other AMPs, which typically induce cell membrane lysis.[1] HSTs and many of their variants, are also known to be non-toxic to humans, this combined with their specific and novel mode of action means that this class of peptide may provide a way to design compounds that could be used to tackle antibiotic resistant bacteria.[2]

A.1.1 The Effect of Zinc and Copper Binding by Histatin-5 Variants on Streptococcus pyogenes Growth.

Zinc (Zn) and copper (Cu) are essential metals for bacterial survival, however, in excess they can be toxic due to mis-metallation of bacterial enzymes.[3] Host proteins frequently sequester metals away from pathogens, in a process known as nutritional immunity. Several host AMPs are known to bind metals, and these include defensins, amyloid-β, psoriasins and histatins (HSTs). As part of a 4th year research project (collaboration between the Cobb group and Dr. Karrera Djoko, Department of Biosciences, Durham University), Ms. Isabel Holmes, under my supervision, studied the interactions of the salivary AMP histatin-5 (HST-5) with Zn(II) and Cu(II). This work also evaluated how the antibacterial activity of HST-5 is affected by metal binding.

A.1.2 The role of histatins in oral cavities

HSTs comprise a subset of more than 200 distinct salivary peptides present in saliva of humans.[1] They are present in saliva at concentrations in the range concentration 50–425

μM in healthy adults.[4] HSTs are His-rich, cationic proteins secreted from the salivary glands in higher primates. In humans, all of the HST proteins are derived from 2 genes on chromosome 4q13; htn1 and htn3, also known respectively as his1 and his2. The gene products are Pre-HST1 and Pre-HST3, which are proteolytically cleaved to give HST-1 and HST-3, respectively. However, there are at least 10 other HST peptides which are cleavage products (**Table 1**).[5] Transcriptional regulation of these genes is not fully understood, although the HTN27 box upstream of htn1 was shown to be a positive transcriptional element that is only highly stimulated in salivary gland cells.[6]

Table 1. Primary sequences of HST-1 and HST-3 and all of the proteolytic fragments produced from them, where p indicates phosphoserine, with the ATCUN motif (DSH) and the Zn binding motif (HEXXH) indicated; table modified from reference.[7]

Human Histatin	Sequence
Histatin 1	DSpHEKRHHGYRRKFHEKHHSHREFPFYGDYGSNYLYDN
Histatin 2	RKFHEKHHSHREFPFYGDYGSNYLYDN
Histatin 3	DSHAKRHHGYKRKFHEKHHSHRGYRSNYLYDN
Histatin 4	KFHEKHHSHRGYRSNYLYDN
Histatin 5	DSHAKRHHGYKRKFHEKHHSHRGY
Histatin 6	DSHAKRHHGYKRKFHEKHHSHRGYR
Histatin 7	RKFHEKHHSHRGY
Histatin 8	KFHEKHHSHRGY
Histatin 9	RKFHEKHHSHRGYR
Histatin 10	KFHEKHHSHRGYR
Histatin 11	KRHHGYKR
Histatin 12	KRHHGYK

HST-1, -3 and -5 are the most abundant, each making up 20-30% of total HST proteins within the oral cavity.[7] While less is known about their antibacterial activity, all three of these HSTs have antifungal activity.[2] This is enabled by the helix-to-coil transitions present, in order for HSTs to associate with and translocate through membranes.[2] HST-3 has been shown to kill up to 70% of *C. albicans* cells at concentrations present in the oral cavity(up to 12 μM). Although, HST-5, as the dominant HST, has the most potent fungicidal activity against pathogenic fungi, including *C. albicans*.[8,9] HSTs potent activity is comparable to currently used antifungals, and the additional lack of toxicity towards

human cells makes HSTs ideal candidates for the development of antimicrobial therapeutics. However, resistance to HSTs has been demonstrated in *C. albicans* for example by Fitzgerald *et al*., who showed that over time the *C. albicans* strain CA132A displayed a five-fold reduction in susceptibility to killing by HST-3, despite HST-3 being maintained at physiological concentrations.[10]

HSTs bind one Zn and/or two Cu ions through specific motifs indicated in **Table 1**; they have a His rich C-terminus which is used to bind Zn and they bind Cu via N-terminal HH and DSH motifs, the latter being the ATCUN motif.[7] When complexed with metal, HSTs become more resistant to proteolysis and these complexes are thought to be of functional importance, indicated by small unilamellar vesicle fusion catalysis by Zn(II)-HST-5 complexes *in vitro*.[11]

A.1.3 Histatin-5

Histatin-5 (**HST-5, Figure 1**) is a major proteolytic product of HST-3, whilst it is unstructured in aqueous solution; it displays an α-helical structure in organic solvents.[2] HST-5 is of particular interest due to it having the most potent anticandidal activity of all the HSTs *in vitro*; with a half maximal inhibitory concentration (IC_{50}) of 6.25 μg ml^{-1} against *C. albicans*.[2] Hence, HST-5 at 15 - 50 μM in saliva causes high non-viability in *Candida spp*.. However, as with other HSTs, *C. albicans* has been demonstrated to develop resistance to HST-5. Resistance is in part accredited to the Flu1 efflux pump which exports HST-5 from cells.[12] HST-5 is a cationic peptide, so it can form interactions with various proteins and lipids; such as with the anionic sialic acid components in all salivary mucins or the anionic teichoic acids that make bacterial cell walls negatively charged.[5,13] HST-5 has bactericidal and bacteriostatic activity on *Streptococcus* mutants at neutral pH. This is enhanced in buffers with low-ionic strength, which may be due to enhancing the aforementioned interactions.[14]

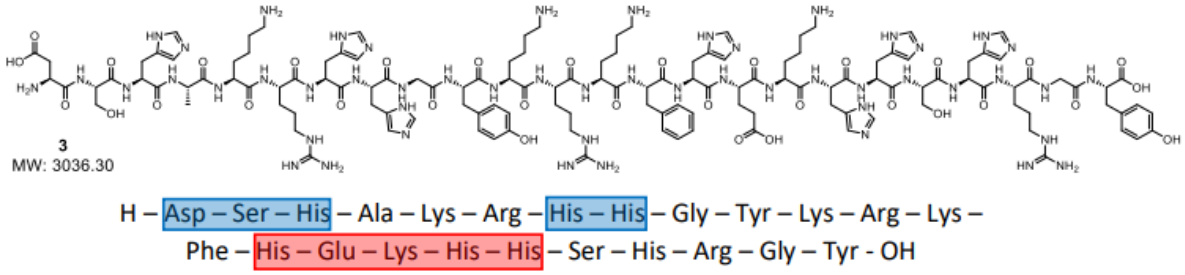

Figure 1. Primary structure of HST-, N- terminal Asp-Ser-His and His-His in blue are respectively important in Cu(II)/Ni(II) and Cu(I) binding and C-terminal His-Glu-Lys-His-His (HEXXH) in red binds Zn (II)

A.2. Project aims

The primary aim was to determine whether metal chelation by HST-5 has evolved to starve pathogens of metals. In particular, there was a drive to determine whether HST-5 starves oral bacteria of Zn, by testing whether the Zn(II)-HST-5 complex exerts a more potent antimicrobial activity than the apo-form. The potential role of HST-5 in nutritional immunity against bacteria, as an oral chelator of Zn, had also not yet been studied in detail. Therefore, the human pathogen Group A *Streptococcus*, also known as GAS, was to be used. GAS can infect many parts of the body including the nose, throat and skin. GAS is a Gram-positive bacterium which most frequently causes strep throats (pharyngitis) and impetigo, but it can also cause more serious infections such as pneumonia, scarlet fever, streptococcal toxic shock syndrome, necrotising fasciitis, septicaemia, endocarditis, and glomerulonephritis (kidney inflammation). Globally at least half a million deaths from these infections occur annually, and antibiotic resistance to this specific bacterium is an increasing problem.[15]

Secondly, in order to test above-mentioned hypothesis, the synthesis of HST-5 and six variants which lack certain metal-binding residues, was carried out using MW solid-phase peptide synthesis (SPPS) as detailed in **Chapter 3**, **Section 3.3.1**. The stoichiometries and affinities of wild type HST-5 and the HST-5 variants for Zn will be determined using spectrophotometric assays with colorimetric metal reporters. HST-5 and its analogues will

be tested against GAS to see the antibacterial effect of withholding metals. The background metal concentrations will be controlled with a metal-depleted, chemically defined medium. The growth in the presence or absence of HSTs of wild type (WT) GAS and mutant GAS was monitored; with mutant GAS lacking Zn efflux or import systems, to see if supplementation with Zn restored normal bacterial growth.

A.3 Use of the acetate or TFA salt of HST-5 does not influence metal binding.

In **Figure 2** WT HST-5 was used in two separate sets of experiments, after being produced by two different methods. The TFA salt of HST-5 (prepared in Durham) and the acetate salt of HST-5 (bought from GenScript), were found to perform in a similar manner with regards to Cu binding activity. Overlaying the competitive ligand titrations with Cu showed that the absorbances mapped onto each other nearly exactly. Hence, using a TFA salt as opposed to an acetate salt had no effect on Cu binding by the ATCUN motif (**Figure 2A**) and had no effect on Cu binding by NTA (**Figure 2B**).

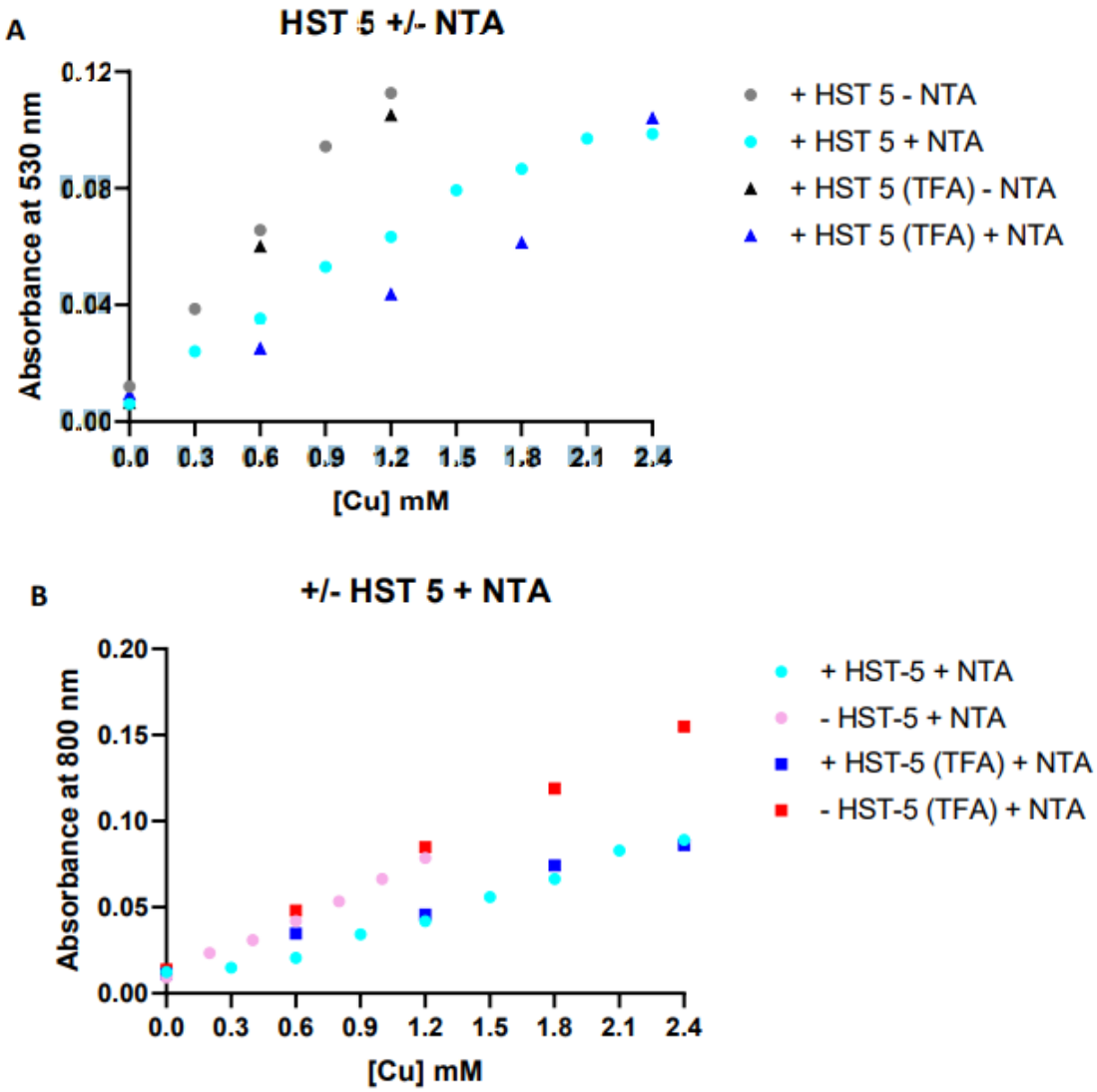

Figure 2. Comparison between HST-5 (3) (1 mM), as an acetate salt or a TFA salt, competing with NTA (1 mM) for Cu (0 to 2.4 mM). Monitoring A, absorbance due to the ATCUN motif of HST-5 complexing Cu(II) at 530 nm and B, absorbance due to NTA complexing Cu(II) at 800 nm.

A.4 Histatin work summary

Metal binding sites of well-known natural AMP HST-5 were further characterised as part of this study. Previous findings that HST-5 binds Cu with a K_d of approximately 2 x 10^{-11} M and that the N-terminal ATCUN motif is important in Cu binding were corroborated. HST-5 can rescue GAS growth in high concentrations of Zn suggesting that HST-5 does bind Zn. However, the affinity was insufficient to compete with Zincon (Zn·HST-5 K_d > 2.09 × 10^{-6} M). Hence, the HST-5 Zn binding activity cannot restrict Zn from GAS *in vivo* because the GAS Zn importer, AdcA, binds Zn more tightly than HST-5 (K_d of 2.7 x 10^{-8} M).[16] These results were found independently of use of the TFA salt or acetate salt of

HST-5 as detailed in **Section 3.6**. These findings mean HST-5 is unlikely to be involved in nutritional immunity. Together with results that HST-5 decreased GAS growth independently of Zn concentration, this indicates that HST-5 does not depend on influencing Zn uptake or export in GAS to cause an antibacterial effect. Rather than the antibacterial mechanism of HST-5 involving metal binding, alternative hypotheses need to be pursued.

A.5 References

1. Melino, S., Santone, C., Di Nardo, P. & Sarkar, B. Histatins: Salivaryx peptides with copper(II)- and zinc(II)-binding motifs Perspectives for biomedical applications. *FEBS Journal* **281**, 657–672 (2014).
2. Grogan, J., McKnight, C. J., Troxler, R. F. & Oppenheim, F. G. Zinc and copper bind to unique sites of histatin 5. *FEBS Lett* **491**, 76–80 (2001).
3. Djoko, K. Y., Y. Ong, C. L., Walker, M. J. & McEwan, A. G. The role of copper and zinc toxicity in innate immune defense against bacterial pathogens. *Journal of Biological Chemistry* **290**, 1854–1861 (2015).
4. Vinayak Patel, V. B., Bhagwathi, B. T., Vinayak, V. & Gupta, M. Histatins and their role in oral cavity. *International Journal Of Research In Dentistry* **4**, (2014).
5. Wang, G. Human antimicrobial peptides and proteins. *Pharmaceuticals* **7**, 545–594 (2014).
6. Fujigaki, Y. *et al.* Polymorphism of salivary histatin gene and periodontal disease in the Japanese population. *J Int Acad Periodontol* **11**, 220–5 (2009).
7. Khurshid, Z. *et al.* Histatin peptides: Pharmacological functions and their applications in dentistry. *Saudi Pharmaceutical Journal* **25**, 25–31 (2017).
8. Xu, Y. *et al.* Histatin 3-mediated killing of Candida albicans: Effect of extracellular salt concentration on binding and internalization. *Antimicrob Agents Chemother* **43**, 2256–2262 (1999).
9. Puri, S. & Edgerton, M. How does it kill?: Understanding the candidacidal mechanism of salivary histatin 5. *Eukaryot Cell* **13**, 958–964 (2014).
10. Fitzgerald, D. H., Coleman, D. C. & O'Connell, B. C. Binding, internalisation and degradation of histatin 3 in histatin-resistant derivatives of Candida albicans. *FEMS Microbiol Lett* **220**, 247–253 (2003).
11. Melino, S. *et al.* Zn2+ ions selectively induce antimicrobial salivary peptide histatin- 5 to fuse negatively charged vesicles. Identification and characterization of a zinc-binding motif present in the functional domain. *Biochemistry* **38**, 9626–9633 (1999).

12. Hampe, I. A. I., Friedman, J., Edgerton, M. & Morschhäuser, J. An acquired mechanism of antifungal drug resistance simultaneously enables Candida albicans to escape from intrinsic host defenses. *PLoS Pathog* **13**, 1–28 (2017).

13. Iontcheva, I., Oppenheim, F. G. & Troxler, R. F. Human salivary mucin MG1 selectively forms heterotypic complexes with amylase, proline-rich proteins, statherin, and histatins. *J Dent Res* **76**, 734–743 (1997).

14. Mackay, B. J., Denepitiya, L., Iacono, V. J., Krost, S. B. & Pollock, J. J. Growth-inhibitory and bactericidal effects of human parotid salivary histidine-rich polypeptides on Streptococcus mutans. *Infect Immun* **44**, 695–701 (1984).

15. Walker, M. J. *et al.* Disease manifestations and pathogenic mechanisms of group A Streptococcus. *Clin Microbiol Rev* **27**, 264–301 (2014).

16. Cao, K. *et al.* Two zinc-binding domains in the transporter AdcA from Streptococcus pyogenes facilitate high-affinity binding and fast transport of zinc. *Journal of Biological Chemistry* **293**, 6075–6089 (2018).

ACS Infectious Diseases

pubs.acs.org/journal/aidcbc

Article

Salivary Antimicrobial Peptide Histatin-5 Does Not Display Zn(II)-Dependent or -Independent Activity against Streptococci

Louisa J. Stewart,[⊥] YoungJin Hong,[⊥] Isabel R. Holmes, Samantha J. Firth, Yasmin Ahmed, Janet Quinn, Yazmin Santos, Steven L. Cobb, Nicholas S. Jakubovics, and Karrera Y. Djoko*

Cite This: *ACS Infect. Dis.* 2023, 9, 631−642

Read Online

ACCESS | Metrics & More | Article Recommendations | Supporting Information

ABSTRACT: Histatin-5 (Hst5) is a member of the histatin superfamily of cationic, His-rich, Zn(II)-binding peptides in human saliva. Hst5 displays antimicrobial activity against fungal and bacterial pathogens, often in a Zn(II)-dependent manner. In contrast, here we showed that under *in vitro* conditions that are characteristic of human saliva, Hst5 does not kill seven streptococcal species that normally colonize the human oral cavity and oropharynx. We further showed that Zn(II) does not influence this outcome. We then hypothesized that Hst5 exerts more subtle effects on streptococci by modulating Zn(II) availability. We initially proposed that Hst5 contributes to nutritional immunity by limiting nutrient Zn(II) availability and promoting bacterial Zn(II) starvation. By examining the interactions between Hst5 and *Streptococcus pyogenes* as a model *Streptococcus* species, we showed that Hst5 does not influence the expression of Zn(II) uptake genes. In addition, Hst5 did not suppress growth of a Δ*adcAI* mutant strain that is impaired in Zn(II) uptake. These observations establish that Hst5 does not promote Zn(II) starvation. Biochemical examination of purified peptides further confirmed that Hst5 binds Zn(II) with high micromolar affinities and does not compete with the AdcAI high-affinity Zn(II) uptake protein for binding nutrient Zn(II). Instead, we showed that Hst5 weakly limits the availability of *excess* Zn(II) and suppresses Zn(II) toxicity to a Δ*czcD* mutant strain that is impaired in Zn(II) efflux. Altogether, our findings led us to reconsider the function of Hst5 as a salivary antimicrobial agent and the role of Zn(II) in Hst5 function.

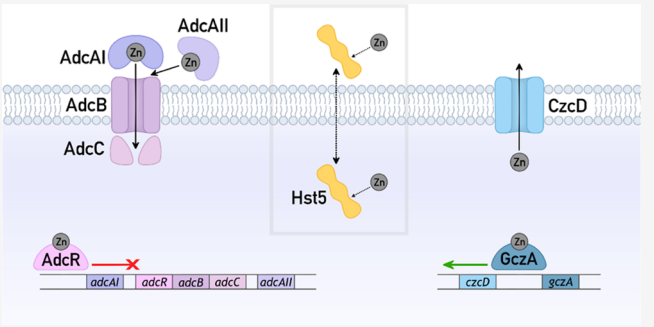

KEYWORDS: *antimicrobial peptide, histatin, zinc, nutritional immunity, Streptococcus*

Antimicrobial peptides are short, often cationic peptides that are secreted by diverse organisms from across the domains of life.[1] These peptides usually act as immune effectors that kill invading microbes as part of the host innate immune system, but many also play key functions in the normal biology of the host organism. A subfamily of antimicrobial peptides binds metals. Some of these metallo-peptides become activated upon metal binding,[2−4] for instance, by folding into an optimal conformation for disrupting microbial membranes or for acting on their targets (*e.g.*, clavanin A from tunicates[4] and piscidin from fish[2]). Other metallo-peptides bind metals and withhold these essential nutrients away from microbes, causing them to starve (*e.g.*, microplusin from cattle ticks[5]).

Histatins comprise a family of cationic, His-rich, metallo-peptides in the saliva and tears of humans and some higher primates.[6−8] These peptides are derived from two parent peptides, namely, Histatin-1 and Histatin-3.[6,9] Both parent histatins are expressed by the salivary and tear glands.[10,11] Upon secretion in saliva into the oral cavity, the parent histatins are rapidly processed into shorter fragments[12−14] by unidentified human salivary proteases or proteases from resident oral microbes. Whether the parent histatins are proteolytically degraded in tears is currently unknown. Of the various salivary fragments, Histatin-5 (Hst5; Table 1) is the best characterized *in vitro*.

Hst5 is noted for its ability to kill the fungus *Candida albicans*[15,16], and several pathogenic bacterial species, namely, *Pseudomonas aeruginosa*, *Staphylococcus aureus*, *Acinetobacter*

Table 1. Hst5 Peptides Used in This Work

Peptide	Sequence
	1 11 21
Hst5	DSHAKRHHGY KRKFHEKHHS HRGY
ΔH15,18,19	DSHAKRHHGY KRKFAEKAAS HRGY

Received: November 17, 2022
Published: February 24, 2023

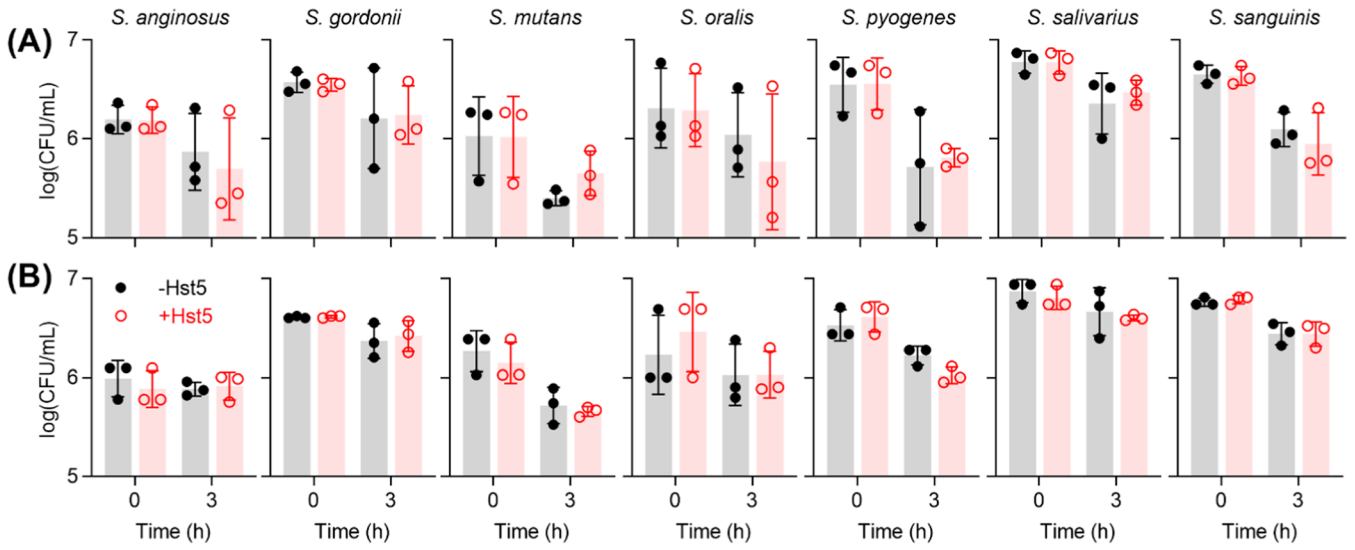

Figure 1. Effects of Hst5 on survival of streptococci in (A) phosphate buffer and (B) artificial saliva buffer. Bacteria were incubated in phosphate buffer (10 mM, pH 7.4; $N = 3$) or artificial saliva buffer (pH 7.2−7.4; $N = 3$), with (○) or without (●) Hst5 (50 μM), and sampled at $t = 0$ and 3 h for enumeration. Hst5 did not affect the survival of any species in either buffer ($P = 0.73$, 0.99, 0.57, 0.72, 0.85, 0.71, 0.50 in phosphate buffer, and 0.72, 0.71, 0.43, 0.56, 0.52, 0.48, and 0.86 in artificial saliva buffer, for *S. anginosus*, *S. gordonii*, *S. mutans*, *S. oralis*, *S. pyogenes*, *S. salivarius*, and *S. sanguinis*, respectively).

baumanii, *Enterococcus faecium*, and *Enterobacter cloacae*.[16] Unlike other antimicrobial peptides, Hst5 does not appear to permeabilize fungal membranes, although it does destabilize some bacterial membranes.[16] Beyond its direct action on membranes, the antimicrobial activity of Hst5 requires the peptide to be internalized into the cytoplasm, usually *via* energy-dependent pathways for peptide uptake.[16,17] Once in the cytoplasm, Hst5 is thought to encounter its targets, which in *C. albicans* include the mitochondria[18] but in bacteria remain unidentified, and causes toxicity *via* multiple pathways that are not fully elucidated.[15,18]

Hst5 contains a characteristic Zn(II)-binding motif, His-Glu-x-His-His (Table 1), but whether Hst5 associates with Zn(II) in saliva is unknown. Likewise, whether Zn(II) binding is essential for the antimicrobial activity of Hst5 is unclear. Synthetic Hst5 derivatives that lack one or all three putative Zn(II)-binding His residues remain active against *C. albicans*.[19] In addition, conflicting reports show that addition of Zn(II) can both enhance[20] and suppress[21] Hst5 activity against this fungus. However, a recent report indicates that the role of Zn(II) is concentration-dependent: low concentrations of added Zn(II) enhance the antimicrobial activity of Hst5 against *C. albicans* (compared with the control without any added Zn(II)), while high concentrations of added Zn(II) suppress it.[22]

Beyond histatins and Zn(II)-binding metallo-peptides, Zn(II)-dependent host innate immune responses are well described. In response to microbial infection, Zn(II) levels and those of Zn(II)-binding or Zn(II)-transporting proteins within a host organism can rise and fall, leading to fluctuations in Zn(II) availability within different niches in the infected host. Increases in Zn(II) availability promote microbial poisoning while decreases in Zn(II) availability promote microbial starvation. These antagonistic host responses, known as "nutritional immunity",[23] suppress microbial growth in the host and inhibit the progress of infectious disease. Although Zn(II) influences the activity of Hst5,[22] it is unclear whether histatins themselves participate in nutritional immunity by modulating Zn(II) availability to microbes.

The healthy human oral cavity and oropharynx are colonized by a mixture of microbial species, with *Streptococcus* as the most abundant taxon.[24−28] Some species, such as *S. gordonii* and *S. sanguinis*, are considered commensals. These species contribute to oral health, for example, by inhibiting colonization by competitor species.[29,30] Some streptococcal species are considered pathogenic. For example, *S. mutans* and *S. pyogenes* are associated with dental caries and pharyngitis,[31] respectively. Nevertheless, asymptomatic carriage of these pathogenic species is common[32] and these species are generally considered normal components of the healthy oral and oropharyngeal microflora. Importantly, all streptococci are opportunistic pathogens that can cause disseminated infections, such as bacterial infective endocarditis.[33]

The goals of this study were to determine the antibacterial activity of Hst5 against oral and oropharyngeal streptococci, and to investigate the potential role of this peptide in influencing Zn(II) availability to the streptococci as a component of nutritional immunity. Based on the established features of nutritional immunity, we specifically examined whether Hst5 limits Zn(II) availability (and promotes microbial Zn(II) starvation) and/or raises Zn(II) availability (and promotes Zn(II) poisoning).

RESULTS

Hst5 Does Not Kill Oral or Oropharyngeal Streptococci. There is little consensus regarding the antibacterial activity of Hst5 against streptococci—it varies depending on the species or experimental conditions,[34−40] but the chemical and molecular reasons for these discrepancies have not been identified. In this work, the ability of Hst5 to kill seven oral or oropharyngeal streptococci, namely, *S. anginosus*, *S. gordonii*, *S. mutans*, *S. oralis*, *S. pyogenes*, *S. salivarius*, and *S. sanguinis*, was examined in parallel. Following the approach used previously for *C. albicans* and ESKAPE pathogens, these kill assays were performed for several hours in dilute phosphate buffer (10

https://doi.org/10.1021/acsinfecdis.2c00578
ACS Infect. Dis. 2023, 9, 631−642

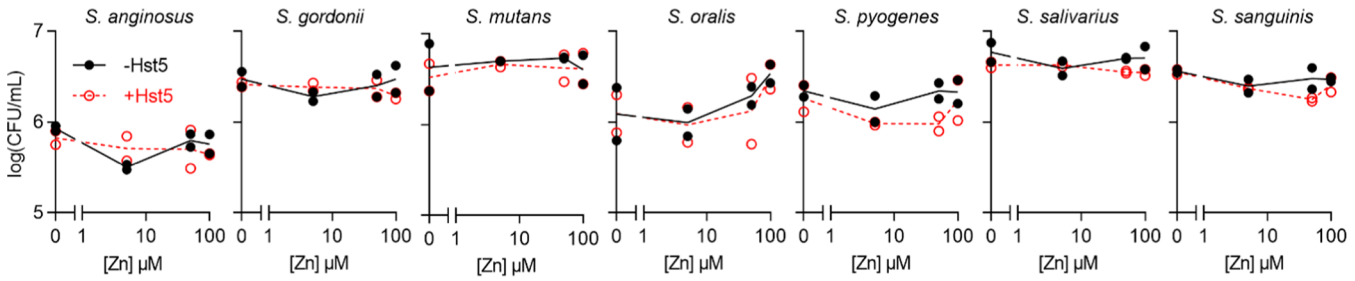

Figure 2. Effects of Zn(II) and Hst5 on survival of streptococci in artificial saliva buffer. Bacteria ($N = 2$) were incubated in artificial saliva buffer in the presence of added Zn(II) (0, 5, 50, or 100 μM), with (○) or without (●) Hst5 (50 μM), and sampled at $t = 3$ h for enumeration. Addition of Zn(II) did not influence the effects of Hst5 on the survival of any species (P values for the interaction between Zn(II) and Hst5 = 0.40, 0.46, 0.96, 0.98, 0.69, 0.45, and 0.09 for *S. anginosus*, *S. gordonii*, *S. mutans*, *S. oralis*, *S. pyogenes*, *S. salivarius*, and *S. sanguinis*, respectively).

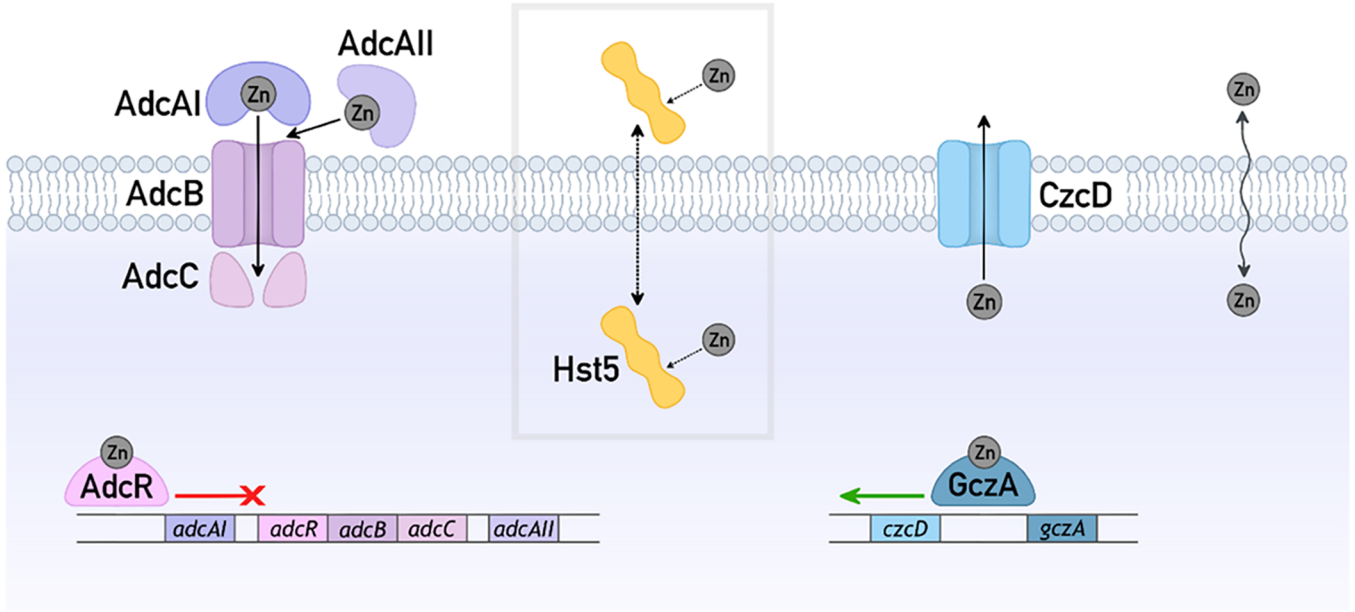

Figure 3. Zn(II) homeostasis in GAS and hypothesized actions of Hst5. Zn(II) uptake: AdcAI and AdcAII capture extracellular Zn(II) and transfer this metal to AdcBC for import into the cytoplasm. These proteins are transcriptionally upregulated in response to decreases in Zn(II) availability and Zn(II) starvation (and downregulated in response to increases in Zn(II) availability).[49] Alternatively, Zn(II) may enter the cytoplasm *via* nonspecific cation transporters (wavy arrow). Zn(II) efflux: CzcD exports excess Zn(II) out of the cytoplasm. It is transcriptionally upregulated by GczA in response to increases in Zn(II) availability and Zn(II) poisoning.[50] Alternatively, Zn(II) may exit the cytoplasm *via* nonspecific cation transporters (wavy arrow). Hypothesized actions of Hst5: Hst5 may bind extracellular Zn(II) and either remain extracellular to suppress Zn(II) availability or become internalized as the Zn(II)−Hst5 complex and increase Zn(II) availability. Alternatively, Hst5 may enter the cytoplasm (dotted arrow), bind intracellular Zn(II), and suppress intracellular Zn(II) availability.

mM).[16,20] Under these conditions, up to 50 μM Hst5 (*ca.* total histatin concentrations in fresh salivary secretions[13]) did not promote killing of the streptococcal species (Figure 1A), even when the assay was extended to 24 h (Figure S1). Consistent with a previous report,[16] parallel control experiments showed that Hst5 killed *P. aeruginosa* and *C. albicans* (Figure S2), confirming that our peptide preparations were active.

Like other cationic antimicrobial peptides, the antimicrobial activity of Hst5 is influenced by pH and ionic strength.[16,19,41−45] To better reflect the physiological context in which Hst5 plays a role, the kill assays were repeated in an artificial, synthetic "saliva buffer", whose pH and ionic composition approximate that of saliva (Table S1A). Again, Hst5 did not kill any of the streptococci (Figures 1B and S1). Interestingly, under these new conditions, Hst5 did not kill the control organisms *P. aeruginosa* and *C. albicans* (Figure S2). The high ionic strength of the saliva buffer likely interferes with electrostatic binding of the peptide to surface proteins or membranes of these control organisms,[16,46] and subsequent internalization and killing. To better understand the activity of Hst5 under conditions that are more characteristic of saliva, further kill assays below used the artificial saliva buffer.

Zn(II) Does Not Influence the Activity of Hst5 against Streptococci. Saliva typically contains low micromolar levels of total Zn(II) (between 0.2 and 3 μM have been reported[47]), although the speciation or bioavailability of this metal ion is poorly defined. Our artificial saliva buffer is Zn(II)-deplete (low nanomolar concentrations of Zn(II) are routinely detected by inductively coupled plasma mass spectrometry (ICP MS)). Thus, to determine if the activity of Hst5 against streptococci is Zn(II)-dependent, the kill assays were repeated in the presence of added Zn(II). The results showed that added Zn(II), whether substoichiometric (5 μM), stoichiometric (50 μM), or super-stoichiometric (100 μM) relative to Hst5 (50 μM), neither suppresses nor enhances killing of the seven streptococcal species by Hst5 (Figure 2).

https://doi.org/10.1021/acsinfecdis.2c00578
ACS Infect. Dis. 2023, 9, 631−642

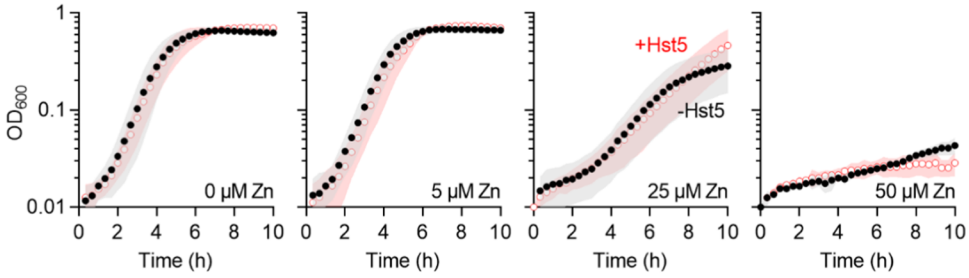

Figure 4. Effects of Zn(II) and Hst5 on growth of GAS. Bacteria (N = 3) were cultured in CDM in the presence of Zn(II) (0, 5, 25, or 50 μM), with (○) or without (●) Hst5 (50 μM), and sampled every 20 min for a total of 10 h. While addition of Zn(II) inhibited bacterial growth (P = 1.0, <0.0001, and <0.0001 for 5, 25, and 50 μM Zn(II), respectively), addition of Hst5 did not influence this effect (P = 0.88, 0.82, 0.83, and 0.56 for 0, 5, 25, and 50 μM Zn(II), respectively).

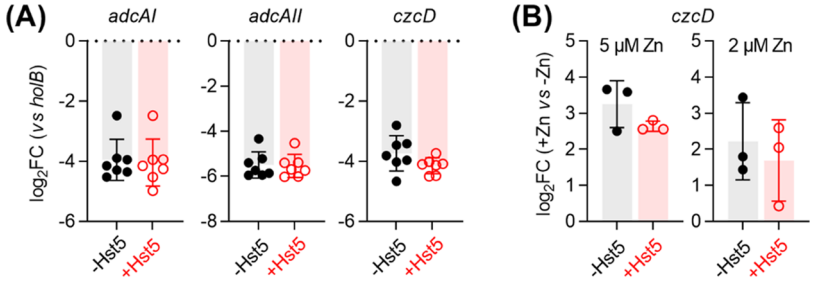

Figure 5. Effects of Hst5 on expression of Zn(II)-responsive genes in GAS. (A) Background expression of all genes. Bacteria (N = 7) were cultured in CDM with (○) or without (●) Hst5 (50 μM). Levels of *adcAI*, *adcAII*, and *czcD* mRNA were determined by quantitative real-time polymerase chain reaction (qRT-PCR) and normalized to *holB*. Addition of Hst5 did not affect the background expression of any of the three genes (P = 0.35, 0.74, and 0.08 for *adcAI*, *adcAII*, and *czcD*, respectively). (B) Zn(II)-dependent expression of *czcD*. Bacteria (N = 3) were cultured in CDM with or without added Zn(II) (2 or 5 μM), with (○) or without (●) Hst5 (50 μM). Levels of *czcD* mRNA were measured by qRT-PCR, normalized to *holB*, and compared with normalized mRNA levels of the corresponding untreated controls (0 μM added Zn(II)). Addition of Hst5 did not affect Zn(II)-dependent expression of *czcD* (P = 0.21 and 0.71 for 2 and 5 μM Zn(II), respectively).

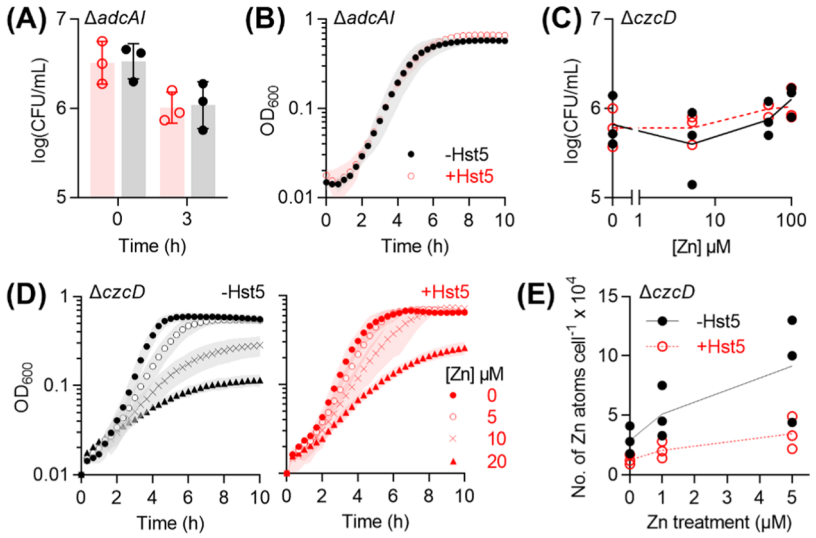

Figure 6. Effects of Hst5 on Zn(II) availability. (A) Survival of Δ*adcAI*. Bacteria (N = 3) were incubated in artificial saliva buffer, with (○) or without (●) Hst5 (50 μM), and sampled at t = 0 and 3 h for enumeration. Hst5 did not affect the time-dependent survival of the Δ*adcAI* mutant (P = 0.90). (B) Growth of Δ*adcAI*. Bacteria (N = 2) were cultured in CDM with or without Hst5 (50 μM). Hst5 did not affect the growth of the Δ*adcAI* mutant (P = 0.26). (C) Survival of Δ*czcD*. Bacteria (N = 3) were incubated in artificial saliva buffer, with or without added Zn(II) (0, 5, 50, or 100 μM), with (○) or without (●) Hst5 (50 μM). Hst5 did not affect the Zn(II)-dependent survival of the Δ*czcD* mutant (P value for the interaction between Hst5 and Zn(II) = 0.73). (D) Growth of Δ*czcD*. Bacteria (N = 3) were cultured in CDM in the presence of Zn(II) (0−20 μM), with (○) or without (●) Hst5 (50 μM). Hst5 did not affect the growth of the Δ*czcD* mutant in the absence of Zn(II) (P = 0.61) but it did affect growth in the presence of Zn(II) (P = 0.07, 0.02, and 0.01 for 5, 10, and 20 μM Zn(II), respectively). (E) Levels of cell-associated Zn(II) in Δ*czcD*. Bacteria (N = 3) were cultured in CDM in the presence of Zn(II) (0−5 μM), with (○) or without (●) Hst5 (50 μM), and sampled at t = 4 h. Levels of cell-associated Zn(II) were measured by ICP MS and normalized to colony counts. Addition of Hst5 had a negative effect on cellular Zn(II) levels (P = 0.005).

https://doi.org/10.1021/acsinfecdis.2c00578
ACS Infect. Dis. 2023, 9, 631−642

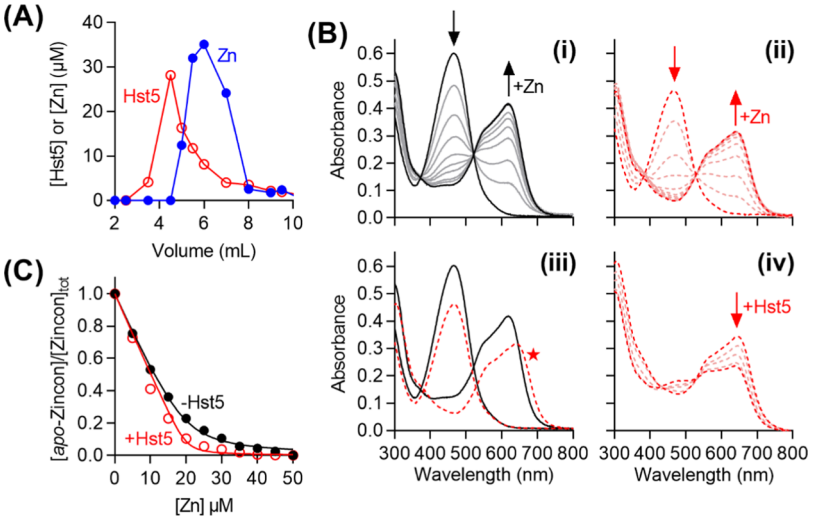

Figure 7. Zn(II) affinity of Hst5. (A) Separation of Hst5 (○) and Zn(II) (●) on a polyacrylamide desalting column. (B) Representative spectral changes upon addition of Zn(II) (0−50 μM) into *apo*-Zincon (20 μM): (i) in the absence (solid traces) or (ii) presence (dashed traces) of Hst5 (20 μM). (iii) Overlaid spectra for 0 and 50 μM Zn(II) from panels (i) and (ii). The new peak at 650 nm is indicated with a star. (iv) Representative spectral changes upon addition of excess Hst5 (0−200 μM) into a solution of Zn(II) (20 μM) and *apo*-Zincon (25 μM). (C) Normalized plot of the absorbance intensities of *apo*-Zincon at 467 nm upon addition of Zn(II), in the absence (●) or presence (○) of Hst5 (20 μM).

Hst5 Does Not Contribute to Zn(II)-Dependent Nutritional Immunity. To determine whether Hst5 contributes to Zn(II)-dependent nutritional immunity against streptococci, either by promoting Zn(II) starvation or Zn(II) poisoning, we examined the effects of Hst5 on transcription of Zn(II)-responsive genes. *S. pyogenes* (Group A *Streptococcus* or GAS) was used as a model *Streptococcus*, since the transcriptional responses of this species to varying Zn(II) availability is understood (Figure 3), mutant strains lacking key Zn(II) transport proteins are available in our laboratory, and the phenotypes of these mutant strains are known.[48]

In response to decreases in Zn(II) availability and Zn(II) starvation, GAS upregulates transcription of the AdcR regulon, including *adcAI* and *adcAII*. Conversely, in response to increases in Zn(II) availability and Zn(II) poisoning, GAS upregulates transcription of the GczA regulon, including *czcD*. Expression of *adcAI*, *adcAII*, and *czcD*, with and without Hst5, was thus examined here. However, poor RNA yields were obtained from the static (nongrowing) bacterial suspensions used in the kill assays. As an alternative approach, GAS was grown in a metal-deplete (low nanomolar concentrations of Zn(II) are routinely detected by ICP MS), chemically defined medium (CDM).[51] GAS displayed the same phenotypes in CDM and in artificial saliva buffer, *i.e.*, addition of up to 50 μM Hst5 did not affect the growth of this streptococcus and addition of Zn(II) did not influence this outcome (Figure 4), thus validating the approach.

In the control experiment, adding Zn(II) alone did not perturb transcription of *adcAI* and *adcAII* in wild-type GAS, but it did induce expression of *czcD* (Figure S3A), consistent with an increase in cellular Zn(II) availability or Zn(II) poisoning. Conversely, adding the Zn(II) chelator TPEN induced expression of *adcAI* and *adcAII*, consistent with a decrease in cellular Zn(II) availability or Zn(II) starvation, but it did not perturb transcription of *czcD* (Figure S3B). By contrast, adding Hst5 perturbed neither the basal expression of *adcAI* or *adcAII* (Figure 5A) nor the Zn(II)-dependent expression of *czcD* (Figure 5B). These results indicate that Hst5 promotes neither Zn(II) starvation nor Zn(II) poisoning to GAS and that Hst5 does not contribute to Zn(II)-dependent nutritional immunity against GAS.

Hst5 Weakly Suppresses Zn(II) Toxicity. To further explore the hypothesized role of Hst5 in modulating Zn(II) availability, the effects of Hst5 were examined using GAS Δ*adcAI* and Δ*czcD* mutant strains that are deficient in Zn(II) uptake and Zn(II) efflux, respectively (Figure 3). These mutant strains were validated to be sensitive to growth inhibition by the Zn(II) chelator TPEN[52,53] and added Zn(II),[50,53] respectively (Figure S4). Although additional Zn(II)-binding lipoproteins such as AdcAII contribute to Zn(II) uptake, AdcAI is thought to act as the primary Zn(II) uptake lipoprotein.[52,53] Therefore, only the Δ*adcAI* mutant was employed here.

The Δ*adcAI* mutant strain displayed wild-type survival and growth phenotypes in the presence of Hst5 (Figure 6A,B), strengthening our proposal that Hst5 does not starve GAS of nutrient Zn(II). Similarly, the Δ*czcD* mutant strain displayed wild-type survival phenotype (Figure 6C). However, mild differences between the Δ*czcD* mutant and wild-type strains were observed in growth experiments. While Hst5 did not influence the growth of Zn(II)-treated wild-type organism (see Figure 4), Hst5 weakly but reproducibly improved the growth of the Zn(II)-treated Δ*czcD* mutant strain (Figure 6D). This effect was observed most clearly upon comparing final culture densities after 10 h of growth since the exponential growth rates were unaffected (Figure S5). This growth-promoting effect of Hst5 appeared to require the predicted Zn(II)-binding ligands His15, His18, and His19[54,55] since the ΔH15,18,19 variant of Hst5 did not rescue the growth of the Zn(II)-treated Δ*czcD* mutant strain (Figure S6, see Table 1 for peptide sequences). These results suggest that Hst5 binds to Zn(II) and suppresses (instead of enhances) the toxicity of an excess of this metal ion to GAS.

Two mechanisms are plausible (see Figure 3): (i) Hst5 binds extracellular Zn(II) and suppresses accumulation of this metal ion in the cytoplasm, leading to less Zn(II) toxicity, or

https://doi.org/10.1021/acsinfecdis.2c00578
ACS Infect. Dis. 2023, 9, 631−642

(ii) Hst5 binds cellular Zn(II) and enables more Zn(II) to accumulate in the cytoplasm, but with less toxicity. To distinguish between these models, total cell-associated Zn(II) levels in the Δ*czcD* mutant strain were assessed by ICP MS. Only up to 5 μM Zn(II) was used, since adding 10 μM Zn(II) or more into the cultures inhibited the growth of the Δ*czcD* mutant and did not produce sufficient biomass for metal analyses. Only wild-type Hst5 peptide was used, owing to the large culture volumes required and the high cost of peptide synthesis. Figure 6E shows that Zn(II) treatment increased cell-associated Zn(II) levels in the Δ*czcD* mutant, but co-treatment with Hst5 suppressed this effect. These results are consistent with model (i) above, in which Hst5 binds extracellular Zn(II) and suppresses accumulation of Zn(II) in GAS.

Hst5 Binds Zn(II) with Micromolar Affinities. To understand how Hst5 weakly modulates Zn(II) availability to GAS and suppresses the toxicity of excess Zn(II) without promoting nutrient Zn(II) starvation, we examined the ability of this peptide to bind Zn(II). Hst5 is thought to bind up to three Zn(II) ions. Previous measurements by isothermal titration calorimetry (ITC) yielded log $K_{Zn(II)}$ values of 5.1, 5.0, and 4.0,[56] indicating that each Zn(II) ion binds to Hst5 with a high micromolar affinity. In agreement with this proposal, a high micromolar concentration of the Zn(II)−Hst5 complex readily dissociated upon passage through a desalting column (Figure 7A). The affinities of Hst5 to Zn(II) were further re-examined here by competing the peptide with the colorimetric Zn(II) indicator Zincon (log $K_{Zn(II)}$ ∼ 6.0) in (Mops) buffer and by monitoring solution absorbances of *apo*-Zincon (466 nm) and Zn(II)-Zincon (620 nm) (Figure 7B). The competition curve (in the presence of Hst5) was nearly indistinguishable from the control (in the absence of Hst5) (Figure 7C). Moreover, a new peak at 650 nm appeared in the presence of Hst5 (Figure 7B(iii)), indicating the formation of a new species, likely a ternary complex between Hst5, Zincon, and Zn(II). This peak did not disappear upon adding excess Hst5 (10 molar equiv; Figure 7B(iv)). These results indicate that Hst5 does not compete effectively with Zincon and that this peptide binds Zn(II) with high micromolar affinities, as previously estimated by ITC.[56]

The lack of competition between Hst5 and Zincon as shown in Figure 7 contrasts with a previous study showing an effective competition between Hst5 and Zincon in phosphate buffer, with Hst5 removing 2 molar equiv of Zn(II) from Zincon.[20] Here it is important to highlight that phosphate binds to Zn(II). Although the affinity of phosphate to Zn(II) is relatively low (log $K_{Zn(II)}$ ∼ 2.4),[57] when used at millimolar concentrations, phosphate can interfere with Zn(II) binding studies by competing for Zn(II). Addition of Zn(II) to *apo*-Zincon in phosphate buffer (50 mM) instead of Mops buffer led to incomplete formation of Zn(II)-Zincon (monitored at 620 nm), suggesting that Zn(II) partitioned between Zincon and phosphate (Figure S7A,B). Conversely, prolonged incubation (>10 min) of a pre-formed Zn(II)-Zincon complex in phosphate buffer led to a loss of the characteristic blue color (Figure S7C), indicating removal of Zn(II) from Zn(II)-Zincon by phosphate alone (without adding Hst5). Therefore, our studies of Zn(II) binding by Hst5 in Mops buffer are likely to be more reliable.

AdcAI from GAS Binds Zn(II) with Sub-Nanomolar Affinity. The low affinity of Hst5 to Zn(II) was clearly insufficient to starve wild-type GAS of nutrient Zn(II) (see Figure 5A), indicating that this peptide does not compete with the high-affinity, Zn(II)-specific uptake protein AdcAI (see Figure 3). Therefore, the Zn(II) affinities of AdcAI were examined here by competition with the colorimetric Zn(II) indicator Mag-fura2 (Mf2). The competition curve, generated by monitoring the solution absorbance of *apo*-Mf2 at 377 nm (Figure 8A(i)), clearly showed two Zn(II) binding sites in

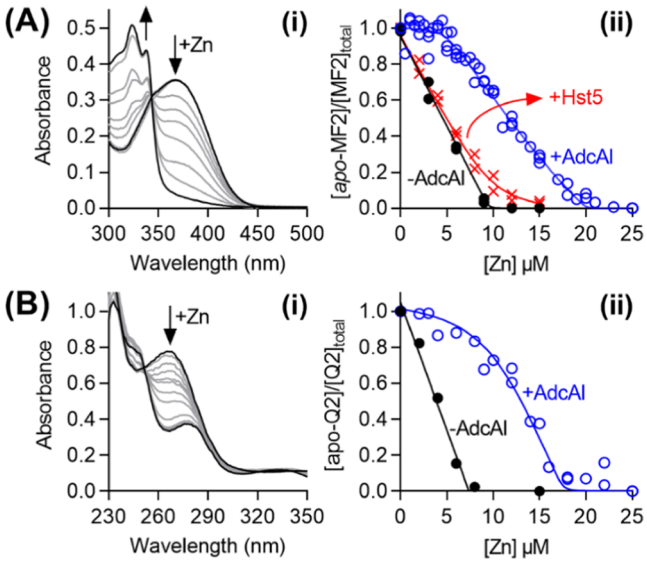

Figure 8. Zn(II) affinity of AdcAI. (A) Low-affinity site. (i) Representative spectral changes upon titration of Zn(II) (0−25 μM) into a mixture of *apo*-Mf2 (10 μM) and AdcAI (5 μM). (ii) Normalized plot of the absorbance intensities of *apo*-MF2 (10 μM) at 377 nm upon addition of Zn(II), in the absence (●) or presence (○) of AdcAI (5 μM). Competition with Hst5 (X; 10 μM) is shown for comparison. (B) High-affinity site. (i) Representative spectral changes upon titration of Zn(II) (0−25 μM) into a mixture of *apo*-Q2 (7.5 μM) and AdcAI (10 μM). (ii) Normalized plot of the absorbance intensities of *apo*-Q2 (7.5 μM) at 262 nm upon addition of Zn(II), in the absence (●) or presence (○) of AdcAI (10 μM).

AdcAI as anticipated.[58] The high-affinity Zn(II) binding site outcompeted Mf2, as evidenced by the lack of spectral changes upon adding up to 1 molar equiv of Zn(II) *vs* AdcAI (Figure 8A(ii)). The low-affinity site competed effectively with Mf2 with a log $K_{Zn(II)}$ = 8.5 (±0.2). The high-affinity site was better estimated using Quin-2 (Q2) as a competitor. By monitoring the absorbance of *apo*-Q2 at 266 nm, log $K_{Zn(II)}$ = 12.5 (±0.2) was obtained for this site (Figure 8B).

The log $K_{Zn(II)}$ values for AdcAI determined here were each ∼1000-fold higher than those determined previously by ITC.[58] ITC can underestimate high metal binding affinities due to lack of sensitivity.[59] Crucially, Hst5 did not compete with Mf2 for Zn(II) (Figure 8A(ii)). Thus, the relative affinities between Hst5 and AdcAI, determined using the same approach under the same conditions, support the hypothesis that Hst5 does not compete with AdcAI for binding Zn(II). These relative affinities also provide a molecular explanation for why Hst5 does not suppress the availability of nutrient Zn(II) to wild-type GAS.

Hst5 did not affect the growth of GAS even when AdcAI was deleted by mutagenesis (see Figure 6A,B), suggesting that this peptide does not compete with other high-affinity Zn(II) uptake proteins such as AdcAII (see Figure 3). AdcAII was also expressed here for measurements of Zn(II) affinity. However,

https://doi.org/10.1021/acsinfecdis.2c00578
ACS Infect. Dis. 2023, 9, 631−642

consistent with a previous report,[60] recombinant AdcAII co-purified with 1 molar equiv of bound Zn(II), which could not be removed without denaturing the protein. Nevertheless, the reported apparent affinity of the *S. pneumoniae* homologue to Zn(II) ($\log K_{Zn(II)}$ = 7.7; 67% identity, 81% similarity), determined *via* competition with Mf2,[61] is ∼100-fold higher than that of Hst5, consistent with our proposal that Hst5 does not compete effectively with AdcAII for binding Zn(II).

DISCUSSION

Role of Histatins as Salivary Antimicrobial Agents. The oral cavity is rich in saliva, and interactions between with the components of this host fluid are key for colonization, maintenance, infection, and subsequent transmission of streptococci.[62−64] For example, exposure to saliva promotes aggregation of some streptococci and blocks adherence to mucosal epithelia.[65,66] Saliva also contains polysaccharides and glycoproteins that may serve as sources of nutrients. Finally, antimicrobial peptides and enzymes such as lysozyme, lactoperoxidase, and chitinase directly inhibit or kill streptococci.[67]

Given the widely reported antimicrobial activity of Hst5, histatins are thought to function as salivary antimicrobial peptides. Yet, our work shows that Hst5 does not kill seven oral and oropharyngeal streptococcal species under *in vitro* experimental conditions that are characteristic of saliva. It is tempting to speculate that histatins help shape the microbial composition in the healthy oral cavity by suppressing the viability of some microbes (*e.g.*, *C. albicans*) but not others (*e.g.*, streptococci). Future work should carefully examine this potential for histatins to exert a selective antimicrobial activity, to verify that it is not associated only with low ionic strength conditions that are not characteristic of saliva. For example, our work showed that antimicrobial activity of Hst5 against *C. albicans* and *P. aeruginosa* disappears when examined in our artificial saliva buffer (see Figure S2).

To date, there is no consensus as to whether histatin levels in saliva correlate with infection levels in the oral cavity. Comparisons of children or adult patients with and without dental caries have found no variation in salivary histatin levels,[68,69] higher salivary histatin levels in patients with caries,[70,71] and lower salivary histatin levels in patients with caries.[72−74] Similarly, there is no clear correlation between histatin levels and the prevalence of oral *C. albicans* in healthy people[75] but high histatin levels do correlate with high prevalence of oral candidiasis in immunocompromised patients.[76] It is important to note that distinct ecological niches exist within the oral cavity. These niches differ in, among many variables, nutrient content, pH, and oxygen tension. Our work does not discount the possibility that histatins exert strong and selective antimicrobial activity in some niches.

Interactions between Zn(II) and Histatins. Systems for the uptake and efflux of metals such as Zn(II) are important for the survival of streptococci in the oral cavity and oropharynx since salivary concentrations of metals can fluctuate, for example, during and between meals, disease, or human hygiene and dental interventions. In addition, salivary components such as lactoferrin and calprotectin sequester metals and restrict microbial growth.

Our work showed that Hst5 does not contribute to Zn(II)-dependent nutritional immunity against streptococci, since this peptide neither starves our model *Streptococcus* (*S. pyogenes* or GAS) of nutrient Zn(II) nor enhances Zn(II) toxicity to this bacterium. These findings are consistent with results from a genome-wide screen of a GAS mutant library, which did not identify genes involved in Zn(II) uptake or Zn(II) efflux as essential for growth in saliva.[77] Given the general conservation of Zn(II) homeostasis mechanisms among the streptococci, we anticipate that Hst5 does not contribute to Zn(II)-dependent nutritional immunity against other streptococci.

The low affinity of Hst5 to Zn(II), particularly compared with the high affinities of the Zn(II) uptake lipoproteins AdcAI and AdcAII, explains why Hst5 does not starve GAS (and, presumably, other streptococci) of nutrient Zn(II). Here, the antimicrobial protein calprotectin provides a useful comparison. Calprotectin binds two Zn(II) ions with affinities ($\log K_{Zn(II)}$ > 11 and >9.6)[78] that are comparable to those of AdcAI and higher than that of AdcAII. Indeed, adding calprotectin induces a robust Zn(II) starvation response in streptococci,[79,80] consistent with its established role in nutritional immunity.

Its low affinity to Zn(II) also explains why Hst5 only weakly suppresses the availability of excess (toxic) Zn(II) to GAS *in vitro*. Like most culture media, our CDM[51] contains phosphate (∼6 mM) and amino acids (∼6 mM total), which would outcompete Hst5 (50 μM) for binding Zn(II).[57] However, if these competing ligands become depleted, for example as a result of bacterial growth, then Hst5 may become competitive and bind Zn(II), particularly when Zn(II) concentrations are high. Such shifts in Zn(II) speciation likely explain why the protective effect of Hst5 on the GAS Δ*czcD* mutant strain during conditions of Zn(II) stress became apparent only at the later stages of growth (see Figure S5). The increased binding of Zn(II) to Hst5 in these later stages of growth may suppress nonspecific Zn(II) import into the GAS cytoplasm, for instance by outcompeting promiscuous divalent metal transporters.

Unlike *in vitro* growth media, saliva and its components are continuously replenished *in vivo*. Saliva contains ∼10 mM phosphate[81,82] and proteinaceous components that also bind Zn(II).[83] Thus, *in vivo*, Hst5 is unlikely to be competitive for binding Zn(II). Nonetheless, synergistic effects between Zn(II) and Hst5 may occur *in vivo*, but likely *via* indirect mechanisms that do not rely on direct binding of Zn(II) to Hst5 and formation of a Zn(II)−Hst5 complex. Zn(II) and Hst5 may separately target the same cellular pathways in a microbe, leading to the enhancement of the antimicrobial activity of Hst5 by Zn(II). Alternatively, Zn(II) may disable cellular pathways that render the target microbe more susceptible to the separate action of Hst5 on a different cellular pathway (or *vice versa*), again leading to the enhancement of microbial killing. Indirect interactions between Zn(II) and Hst5 may also exert subtle effects on microbial physiology that do not lead to a direct antimicrobial action and thus are not captured by the assays described here. For example, a combination of Zn(II) and Hst5 at nonlethal doses is thought to reduce the virulence of *C. albicans*.[84] Whether Hst5 reduces the virulence of streptococci and subsequently enables these organisms to become the dominant commensal microorganisms in the oral cavity and oropharynx is an intriguing concept that warrants further investigation.

METHODS

Data Presentation. Except growth curves, individual replicates from microbiological experiments are plotted, with

https://doi.org/10.1021/acsinfecdis.2c00578
ACS Infect. Dis. 2023, 9, 631−642

shaded columns representing the means and error bars representing standard deviations. Growth curves show the means, with shaded regions representing standard deviations. The number of biological replicates (independent experiments, using different starter cultures and different medium or buffer preparations, performed on different days; N) is stated in figure legends. In the case of metal−protein and metal−peptide titrations, individual data points from two technical replicates (independent experiments performed on different days but using the same protein or peptide preparation) are plotted, but only representative spectra are shown for clarity of presentation.

Statistical Analyses. Descriptive statistics are displayed on all graphical plots. Inferential statistics have been computed for all data and the relevant P values are listed in figure legends. Unless otherwise stated, tests of significance used two-way analysis of variance using the statistical package in GraphPad Prism 8.0. All analyses were corrected for multiple comparisons.

Reagents. The nitrate salt of Zn(II) was used in experiments. Numerous additional tests did not identify any observable difference in the results when the chloride or sulfate salts of Zn(II) were used. Peptides were synthesized commercially with free N- and C-termini as the acetate salt, purified to >95% (GenScript), and confirmed to be metal-free by ICP MS. Concentrations of stock peptide solutions were estimated using solution absorbances at 280 nm in Mops buffer (50 mM, pH 7.4; ε_{280} = 2667 cm^{-1}). Concentrations of fluorometric and colorimetric metal indicators (Zincon, PAR, Mf2, Q2) were standardized using a commercial standard solution of copper chloride. Concentrations of optically silent chelators (NTA) were standardized by competition with a standardized solution of Zn(II)-Zincon.

Strains and Culture Conditions. All bacterial strains (Table S1B) were propagated from frozen glycerol stocks onto solid THY (Todd Hewitt + 0.2% yeast extract) medium without any antibiotics and incubated overnight in the presence of 5% v/v of atmospheric CO_2. Liquid cultures were prepared in THY or CDM.[51] All solid and liquid growth media contained catalase (50 μg/mL).

Streptococcal Kill Assays. Fresh colonies from an overnight THY agar were resuspended to 10^6−10^7 CFU/mL in either potassium phosphate buffer (10 mM, pH 7.4) or artificial saliva buffer (pH 7.2; Table S1A). The cultures were incubated at 37 °C with or without Hst5 and/or Zn(II) as required. At t = 0 and 3 h, cultures were sampled and serially diluted in CDM. Exactly 10 μL of each serial dilution was spotted onto THY agar. Colonies were enumerated after overnight incubation at 37 °C.

***C. albicans* Kill Assays.** Cells from a fresh YPD plate were harvested, washed three times in phosphate-buffered saline (PBS), and resuspended in either potassium phosphate buffer (10 mM, pH 7.4) or saliva salts (pH 7.2) to an OD_{600} of 0.4 (~5 × 10^6 CFU/mL). Cultures were incubated with or without Hst5 at 37 °C. Tubes were inverted every 20 min to maintain cell suspension. At t = 0, 1, and 3 h, samples were taken, serially diluted, and plated onto YPD agar. Colonies were numerated following overnight incubation at 30 °C.

Growth Assays. Colonies from an overnight THY agar were resuspended in CDM to an OD_{600} = 0.02 and dispensed into wells in flat-bottomed 96-well plates (200 μL per well) containing Hst5 and/or Zn(II) as required. Bacterial growth was monitored using an automated microplate shaker and reader. Each plate was sealed with a gas-permeable, optically clear membrane (Diversified Biotech). OD_{600} values were measured every 20 min for 10 h. The plates were shaken immediately before each reading (200 rpm, 1 min, double-orbital mode). OD_{600} values were not corrected for path length (*ca.* 0.58 cm for a 200 μL culture).

RNA Extraction. Colonies from an overnight THY agar were resuspended in CDM to an OD_{600} = 0.02 and incubated in 24-well plates (1.6 mL per well), with or without Hst5 or Zn(II) as required, without shaking, at 37 °C. Each plate was sealed with a gas-permeable, optically clear membrane (Diversified Biotech). At t = 4 h, cultures were centrifuged (4000g, 4 °C, 5 min) and the resulting bacterial pellets were resuspended immediately in RNAPro Solution (0.5 mL; MP Biomedicals). Bacteria were lysed in Lysing Matrix B and total RNA was extracted following the manufacturer's protocol (MP Biomedicals). Crude RNA extracts were treated with RNase-Free DNase I (New England Biolabs). Removal of gDNA was confirmed by PCR using gapA-check-F/R primers (Table S1C). gDNA-free RNA was purified using Monarch RNA Clean-up Kit (New England Biolabs) and visualized on an agarose gel.

qRT-PCR Analyses. cDNA was generated from RNA (1.6 μg) using SuperScript IV First-Strand Synthesis System (Invitrogen). Each qRT-PCR reaction (20 μL) contained cDNA (5 ng) as template and the appropriate primer pairs (0.4 μM; Table S1C). Samples were analyzed in technical duplicates. Amplicons were detected with Luna Universal qRT-PCR Master Mix (New England Biolabs) in a CFXConnect Real-Time PCR Instrument (Bio-Rad Laboratories). C_q values were calculated using LinRegPCR[85] after correcting for amplicon efficiency. C_q values of technical duplicates were typically within ±0.25 of each other. *holB*, which encodes DNA polymerase III, was used as reference gene. Its transcription levels were verified to remain constant in the experimental conditions tested here.

Cellular Metal Content. Colonies from an overnight THY agar were resuspended in CDM to an OD_{600} = 0.02 and incubated at 37 °C with or without Hst5 and/or Zn(II) as required. At t = 4 h, an aliquot was collected for the measurement of plating efficiency (colony counts). The remaining cultures were centrifuged (5000g, 4 °C, 10 min). The resulting bacterial pellets were washed once with ice-cold wash buffer (1 M D-sorbitol, 50 mM Tris−HCl, 10 mM $MgCl_2$, 1 mM ethylenediaminetetraacetic acid (EDTA), pH 7.4) and twice with ice-cold PBS. The final pellets were dissolved in concentrated nitric acid (100 μL), heated (85 °C, 1.5 h), and diluted to 3.5 mL with 2% nitric acid. Total metal levels were determined by ICP MS and normalized to colony counts.

Elution of Zn(II)−Hst5 on a Desalting Column. *Apo*-Hst5 (100 μM) was incubated with 1.5 molar equiv of Zn(II) for 15 min at the bench and loaded onto a polyacrylamide desalting column (1.8 kDa molecular weight cutoff, Thermo Scientific). Peptide and Zn(II) were eluted from the column using Mops buffer (50 mM, pH 7.4). The concentration of Hst5 in each fraction was determined using QuantiPro BCA Assay Kit (Merck) and known quantities of Hst5 as standards. The concentration of Zn(II) was determined using the colorimetric Zn(II) ligand PAR against a standard curve.

Equilibrium Competition Reactions. Our approach to determine metal-binding affinities followed that described by Young and Xiao.[59] For each competition (eq 1), a master stock was prepared to contain both competing ligands (L1 and L2)

https://doi.org/10.1021/acsinfecdis.2c00578
ACS Infect. Dis. 2023, 9, 631−642

in Mops buffer (50 mM, pH 7.4). Serial dilutions of the metal (M) were prepared separately in deionized water. Exactly 135 μL of the master stock was dispensed into an Eppendorf UVette and 15 μL of the appropriate metal stock was added. Solution absorbances were recorded and used to calculate concentrations of *apo*- and metalated forms of each ligand. These concentrations were plotted against metal concentrations and fitted in DynaFit[86] using binding models as described in the text. The known association or dissociation constants for all competitor ligands are listed in Table S1D

$$M{-}L1_n + mL2 \rightleftharpoons nL1 + M{-}L2_m \quad (1)$$

Overexpression and Purification of AdcAI and AdcAII. Nucleic acid sequences encoding the soluble domains of AdcAI (from Thr21) and AdcAII (from Thr31) from M1GAS strain 5448 were subcloned into vector pSAT1-LIC using primers listed in Table S1C. This vector generates N-terminal His6-SUMO fusions with the target proteins. The resulting plasmids were propagated in *Escherichia coli* Dh5α, confirmed by Sanger sequencing, and transformed into *E. coli* BL21 Rosetta 2(DE3).

To express the proteins, transformants were plated onto Lysogeny Broth (LB) agar. Fresh colonies were used to inoculate LB (1 L in 2 L baffled flasks) to an OD_{600} of 0.01. The culture medium contained ampicillin (100 μg/mL) and chloramphenicol (33 μg/mL). Cultures were shaken (200 rpm, 37 °C) until an OD_{600} of 0.6−0.8 was reached, and expression was induced by adding isopropyl β-D-1-thiogalactopyranoside (IPTG) (0.1 mM). After shaking for a further 16 h at 20 °C, the cultures were centrifuged (4000*g*, 4 °C) and the pellets were resuspended in buffer A500 (20 mM Tris−HCl, pH 7.9, 500 mM NaCl, 5 mM imidazole, 10% glycerol).

To purify proteins, bacteria were lysed by sonication (40 kpsi), centrifuged (20,000*g*, 4 °C), and filtered through a 0.45 μm poly(ether sulfone) (PES) membrane filtration unit. Clarified lysates were loaded onto a HisTrap HP column (Cytiva). The column was washed with 10 column volumes (CV) of buffer A500 followed by 10 CV of buffer A100 (20 mM Tris−HCl, pH 7.9, 100 mM NaCl, 10% w/v glycerol) containing imidazole (5 mM). Both AdcAI and AdcAII were bound to the column and subsequently eluted with 3 CV of buffer A100 containing 250 mM imidazole followed by 5 CV of 500 mM imidazole. Protein-containing fractions were loaded onto a Q HP column (Cytiva). The column was washed with 5 CV of buffer A100 and bound proteins were eluted using a step gradient of 0, 10, 15, and 20% buffer C1000 (20 mM Tris−HCl, pH 7.9, 1000 mM NaCl, 10% w/v glycerol). Eluted proteins were incubated overnight at 4 °C with hSENP2 SUMO protease to cleave the His6-SUMO tag from the target protein. Samples were passed through a second Q HP column and the flowthrough fractions containing untagged target protein were collected.

■ ASSOCIATED CONTENT

Supporting Information

The Supporting Information is available free of charge at https://pubs.acs.org/doi/10.1021/acsinfecdis.2c00578.

Recipe for artificial saliva buffer, generated by combining the known salt composition of human saliva (Table S1A); microbial strains used in this study (Table S1B); list of primers used in this study (Table S1C); and list of fluorometric and colourimetric metal indicators used in this study (Table S1C) (XLSX)

Effects of Hst5 on survival of streptococci after 24 h of exposure (Figure S1); effects of Hst5 on survival of control organisms *P. aeruginosa* and *C. albicans* (Figure S2); effects of Zn and TPEN on gene expression in wild-type GAS (Figure S3); characteristic phenotypes of the GAS Δ*adcAI* and Δ*czcD* mutant strains (Figure S4); effects of Hst5 on growth of GAS Δ*czcD* mutant strain (Figure S5); effects of Hst5 and the ΔH15,18,19 variant on the GAS Δ*czcD* mutant strain (Figure S6); and competition between phosphate and Zincon for binding Zn (Figure S7) (PDF)

■ AUTHOR INFORMATION

Corresponding Author

Karrera Y. Djoko − *Department of Biosciences, Durham University, Durham DH1 3LE, United Kingdom;* orcid.org/0000-0001-9814-6515; Email: karrera.djoko@durham.ac.uk

Authors

Louisa J. Stewart − *Department of Biosciences, Durham University, Durham DH1 3LE, United Kingdom*

YoungJin Hong − *Department of Biosciences, Durham University, Durham DH1 3LE, United Kingdom*

Isabel R. Holmes − *Department of Biosciences, Durham University, Durham DH1 3LE, United Kingdom*

Samantha J. Firth − *Department of Biosciences, Durham University, Durham DH1 3LE, United Kingdom*

Yasmin Ahmed − *Biosciences Institute, Newcastle University, Newcastle NE2 4HH, United Kingdom*

Janet Quinn − *Biosciences Institute, Newcastle University, Newcastle NE2 4HH, United Kingdom*

Yazmin Santos − *Department of Chemistry, Durham University, Durham DH1 3LE, United Kingdom*

Steven L. Cobb − *Department of Chemistry, Durham University, Durham DH1 3LE, United Kingdom;* orcid.org/0000-0002-3790-7023

Nicholas S. Jakubovics − *School of Dental Sciences, Newcastle University, Newcastle NE2 4BW, United Kingdom*

Complete contact information is available at: https://pubs.acs.org/10.1021/acsinfecdis.2c00578

Author Contributions

[⊥]L.J.S. and Y.H. contributed equally to the experimental work. L.J.S. is listed first to acknowledge greater involvement in manuscript preparation and editing. K.Y.D. conceived the project. Y.H., K.Y.D., L.J.S., and N.S.J. designed experiments. N.S.J. provided oral streptococci strains. I.R.H., S.L.C., and Y.S. synthesized peptides for preliminary studies. K.Y.D. and L.J.S. performed kill assays with streptococci. Y.A. and J.Q. performed kill assays with *C. albicans*. I.R.H., Y.H., K.Y.D., and L.J.S. performed growth assays. K.Y.D. measured gene expression by qRT-PCR. K.Y.D. and L.J.S. measured metal levels by ICP MS. I.R.H. and Y.H. measured affinities of peptides to Zn(II), with guidance from S.J.F. Y.H. produced AdcA and AdcAII proteins, and measured their affinities to Zn(II), with guidance from S.J.F. Y.H., K.Y.D., and L.J.S. prepared figures and drafted the manuscript. All authors contributed to editing the manuscript and approved its final form.

https://doi.org/10.1021/acsinfecdis.2c00578
ACS Infect. Dis. 2023, 9, 631−642

Notes

The authors declare no competing financial interest.

■ ACKNOWLEDGMENTS

This work was funded in part by the Wellcome Trust grant number 214930/Z/18/Z to K.Y.D and L.J.S., and 215599/Z/19/Z to J.Q. and Y.A. For the purpose of open access, the author has applied a CC BY public copyright licence to any Author Accepted Manuscript version arising from this submission. This project was also supported by a Flexible Funding Award from the Durham Biophysical Sciences Institute to K.Y.D. S.J.F. was supported by a studentship from the BBSRC Newcastle-Liverpool-Durham Doctoral Training Partnership. T Blower (Durham University) provided constructs and reagents for the production of AdcAI and AdcAII. GAS Δ*adcAI* and Δ*czcD* mutant strains were from C Ong, A McEwan, and M Walker (The University of Queensland). Quin2 was from T Young (Durham University). The authors thank R Borthwick and P Chivers (Durham University) for insightful discussions, and J Drury (Durham University) for help with statistical analyses.

■ REFERENCES

(1) Zhang, L. J.; Gallo, R. L. Antimicrobial peptides. *Curr. Biol.* **2016**, *26*, R14.
(2) Kim, S. Y.; Zhang, F.; Gong, W.; Chen, K.; Xia, K.; Liu, F.; Gross, R.; Wang, J. M.; Linhardt, R. J.; Cotten, M. L. Copper regulates the interactions of antimicrobial piscidin peptides from fish mast cells with formyl peptide receptors and heparin. *J. Biol. Chem.* **2018**, *293*, 15381.
(3) Portelinha, J.; Heilemann, K.; Jin, J.; Angeles-Boza, A. M. Unraveling the implications of multiple histidine residues in the potent antimicrobial peptide Gaduscidin-1. *J. Inorg. Biochem.* **2021**, *219*, No. 111391.
(4) Juliano, S. A.; Pierce, S.; deMayo, J. A.; Balunas, M. J.; Angeles-Boza, A. M. Exploration of the Innate Immune System of *Styela clava*: Zn(2+) Binding Enhances the Antimicrobial Activity of the Tunicate Peptide Clavanin A. *Biochemistry* **2017**, *56*, 1403.
(5) Silva, F. D.; Rezende, C. A.; Rossi, D. C.; Esteves, E.; Dyszy, F. H.; Schreier, S.; Gueiros-Filho, F.; Campos, C. B.; Pires, J. R.; Daffre, S. Structure and mode of action of microplusin, a copper II-chelating antimicrobial peptide from the cattle tick *Rhipicephalus (Boophilus) microplus*. *J. Biol. Chem.* **2009**, *284*, 34735.
(6) Sabatini, L. M.; Azen, E. A. Histatins, a family of salivary histidine-rich proteins, are encoded by at least two loci (HIS1 and HIS2). *Biochem. Biophys. Res. Commun.* **1989**, *160*, 495.
(7) Azen, E. A.; Leutenegger, W.; Peters, E. H. Evolutionary and dietary aspects of salivary basic (Pb) and post Pb (PPb) proteins in anthropod primates. *Nature* **1978**, *273*, 775.
(8) Kalmodia, S.; Son, K. N.; Cao, D.; Lee, B. S.; Surenkhuu, B.; Shah, D.; Ali, M.; Balasubramaniam, A.; Jain, S.; Aakalu, V. K. Presence of Histatin-1 in Human Tears and Association with Aqueous Deficient Dry Eye Diagnosis: A Preliminary Study. *Sci. Rep.* **2019**, *9*, No. 10304.
(9) Troxler, R. F.; Offner, G. D.; Xu, T.; Vanderspek, J. C.; Oppenheim, F. G. Structural relationship between human salivary histatins. *J. Dent. Res.* **1990**, *69*, 2.
(10) Shah, D.; Ali, M.; Pasha, Z.; Jaboori, A. J.; Jassim, S. H.; Jain, S.; Aakalu, V. K. Histatin-1 Expression in Human Lacrimal Epithelium. *PLoS One* **2016**, *11*, No. e0148018.
(11) Huang, L. C.; Jean, D.; Proske, R. J.; Reins, R. Y.; McDermott, A. M. Ocular surface expression and in vitro activity of antimicrobial peptides. *Curr. Eye Res.* **2007**, *32*, 595.
(12) Helmerhorst, E. J.; Alagl, A. S.; Siqueira, W. L.; Oppenheim, F. G. Oral fluid proteolytic effects on histatin 5 structure and function. *Arch. Oral Biol.* **2006**, *51*, 1061.
(13) Campese, M.; Sun, X.; Bosch, J. A.; Oppenheim, F. G.; Helmerhorst, E. J. Concentration and fate of histatins and acidic proline-rich proteins in the oral environment. *Arch. Oral Biol.* **2009**, *54*, 345.
(14) Baum, B. J.; Bird, J. L.; Millar, D. B.; Longton, R. W. Studies on histidine-rich polypeptides from human parotid saliva. *Arch. Biochem. Biophys.* **1976**, *177*, 427.
(15) Puri, S.; Edgerton, M. How does it kill?: understanding the candidacidal mechanism of salivary histatin 5. *Eukaryotic Cell* **2014**, *13*, 958.
(16) Du, H.; Puri, S.; McCall, A.; Norris, H. L.; Russo, T.; Edgerton, M. Human Salivary Protein Histatin 5 Has Potent Bactericidal Activity against ESKAPE Pathogens. *Front. Cell. Infect. Microbiol.* **2017**, *7*, No. 41.
(17) Mochon, A. B.; Liu, H. The antimicrobial peptide histatin-5 causes a spatially restricted disruption on the *Candida albicans* surface, allowing rapid entry of the peptide into the cytoplasm. *PLoS Pathog.* **2008**, *4*, No. e1000190.
(18) Helmerhorst, E. J.; Breeuwer, P.; van't Hof, W.; Walgreen-Weterings, E.; Oomen, L. C. J. M.; Veerman, E. C. I.; Nieuw Amerongen, A. V.; Abee, T. The cellular target of histatin 5 on *Candida albicans* is the energized mitochondrion. *J. Biol. Chem.* **1999**, *274*, 7286.
(19) Helmerhorst, E. J.; van't Hof, W.; Veerman, E. C. I.; Simoons-Smit, I.; Nieuw Amerongen, A. V. Synthetic histatin analogues with broad-spectrum antimicrobial activity. *Biochem. J.* **1997**, *326*, 39.
(20) Norris, H. L.; Kumar, R.; Ong, C. Y.; Xu, D.; Edgerton, M. Zinc Binding by Histatin 5 Promotes Fungicidal Membrane Disruption in *C. albicans* and *C. glabrata*. *J. Fungi* **2020**, *6*, No. 124.
(21) Puri, S.; Li, R.; Ruszaj, D.; Tati, S.; Edgerton, M. Iron binding modulates candidacidal properties of salivary histatin 5. *J. Dent. Res.* **2015**, *94*, 201.
(22) Campbell, J. X.; Gao, S.; Anand, K. S.; Franz, K. J. Zinc Binding Inhibits Cellular Uptake and Antifungal Activity of Histatin-5 in *Candida albicans*. *ACS Infect. Dis.* **2022**, *8*, 1920.
(23) Hood, M. I.; Skaar, E. P. Nutritional immunity: transition metals at the pathogen-host interface. *Nat. Rev. Microbiol.* **2012**, *10*, 525.
(24) Bik, E. M.; Long, C. D.; Armitage, G. C.; Loomer, P.; Emerson, J.; Mongodin, E. F.; Nelson, K. E.; Gill, S. R.; Fraser-Liggett, C. M.; Relman, D. A. Bacterial diversity in the oral cavity of 10 healthy individuals. *ISME J.* **2010**, *4*, 962.
(25) Zaura, E.; Keijser, B. J.; Huse, S. M.; Crielaard, W. Defining the healthy "core microbiome" of oral microbial communities. *BMC Microbiol.* **2009**, *9*, No. 259.
(26) Dewhirst, F. E.; Chen, T.; Izard, J.; Paster, B. J.; Tanner, A. C.; Yu, W. H.; Lakshmanan, A.; Wade, W. G. The human oral microbiome. *J. Bacteriol.* **2010**, *192*, 5002.
(27) Aas, J. A.; Paster, B. J.; Stokes, L. N.; Olsen, I.; Dewhirst, F. E. Defining the normal bacterial flora of the oral cavity. *J. Clin. Microbiol.* **2005**, *43*, 5721.
(28) Bach, L. L.; Ram, A.; Ijaz, U. Z.; Evans, T. J.; Lindström, J. A Longitudinal Study of the Human Oropharynx Microbiota Over Time Reveals a Common Core and Significant Variations With Self-Reported Disease. *Front. Microbiol.* **2021**, *11*, No. 573969.
(29) Herrero, E. R.; Slomka, V.; Bernaerts, K.; Boon, N.; Hernandez-Sanabria, E.; Passoni, B. B.; Quirynen, M.; Teughels, W. Antimicrobial effects of commensal oral species are regulated by environmental factors. *J. Dent.* **2016**, *47*, 23.
(30) Abranches, J.; Zeng, L.; Kajfasz, J. K.; Palmer, S. R.; Chakraborty, B.; Wen, Z. T.; Richards, V. P.; Brady, L. J.; Lemos, J. A. Biology of Oral Streptococci. *Microbiol. Spectrum* **2018**, *6*, 6.5.11.
(31) Carapetis, J. R.; Steer, A. C.; Mulholland, E. K.; Weber, M. The global burden of group A streptococcal diseases. *Lancet Infect. Dis.* **2005**, *5*, 685.
(32) Shaikh, N.; Leonard, E.; Martin, J. M. Prevalence of streptococcal pharyngitis and streptococcal carriage in children: a meta-analysis. *Pediatrics* **2010**, *126*, e557−e564.

https://doi.org/10.1021/acsinfecdis.2c00578
ACS Infect. Dis. 2023, 9, 631−642

(33) Pant, S.; Patel, N. J.; Deshmukh, A.; Golwala, H.; Patel, N.; Badheka, A.; Hirsch, G. A.; Mehta, J. L. Trends in infective endocarditis incidence, microbiology, and valve replacement in the United States from 2000 to 2011. *J. Am. Coll. Cardiol.* **2015**, *65*, 2070.
(34) Fernández-Presas, A.; Marquez Torres, Y.; Garcia Gonzalez, R.; Reyes Torres, A.; Becker Fauser, I.; Rodriguez Barrera, H.; Ruiz Garcia, B.; Toloza Medina, R.; Delgado Dominguez, J.; Molinari Soriano, J. L. Ultrastructural damage in *Streptococcus mutans* incubated with saliva and histatin 5. *Arch. Oral Biol.* **2018**, *87*, 226.
(35) MacKay, B. J.; Denepitiya, L.; Iacono, V. J.; Krost, S. B.; Pollock, J. J. Growth-inhibitory and bactericidal effects of human parotid salivary histidine-rich polypeptides on *Streptococcus mutans*. *Infect. Immun.* **1984**, *44*, 695.
(36) Tian, X. L.; Salim, H.; Dong, G.; Parcells, M.; Li, Y. H. The BceABRS four-component system that is essential for cell envelope stress response is involved in sensing and response to host defence peptides and is required for the biofilm formation and fitness of *Streptococcus mutans*. *J. Med. Microbiol.* **2018**, *67*, 874.
(37) Andrian, E.; Qi, G.; Wang, J.; Halperin, S. A.; Lee, S. F. Role of surface proteins SspA and SspB of *Streptococcus gordonii* in innate immunity. *Microbiology* **2012**, *158*, 2099.
(38) Krzyściak, W.; Jurczak, A.; Piątkowski, J.; Kościelniak, D.; Gregorczyk-Maga, I.; Kołodziej, I.; Papież, M. A.; Olczak-Kowalczyk, D. Effect of histatin-5 and lysozyme on the ability of *Streptococcus mutans* to form biofilms in *in vitro* conditions. *Postepy Hig Med. Dosw.* **2015**, *69*, 1056.
(39) Helmerhorst, E. J.; Hodgson, R.; van't Hof, W.; Veerman, E. C. I.; Allison, C.; Nieuw Amerongen, A. V. The Effects of Histatin-derived Basic Antimicrobial Peptides on Oral Biofilms. *J. Dent. Res.* **1999**, *78*, 1245.
(40) Moussa, D. G.; Siqueira, W. L. Bioinspired caries preventive strategy via customizable pellicles of saliva-derived protein/peptide constructs. *Sci. Rep.* **2021**, *11*, No. 17007.
(41) Jang, W. S.; Li, X. S.; Sun, J. N.; Edgerton, M. The P-113 fragment of histatin 5 requires a specific peptide sequence for intracellular translocation in *Candida albicans*, which is independent of cell wall binding. *Antimicrob. Agents Chemother.* **2008**, *52*, 497.
(42) Yu, H. Y.; Tu, C. H.; Yip, B. S.; Chen, H. L.; Cheng, H. T.; Huang, K. C.; Lo, H. J.; Cheng, J. W. Easy strategy to increase salt resistance of antimicrobial peptides. *Antimicrob. Agents Chemother.* **2011**, *55*, 4918.
(43) Han, J.; Jyoti, M. A.; Song, H. Y.; Jang, W. S. Antifungal Activity and Action Mechanism of Histatin 5-Halocidin Hybrid Peptides against Candida ssp. *PLoS One* **2016**, *11*, No. e0150196.
(44) Helmerhorst, E. J.; Flora, B.; Troxler, R. F.; Oppenheim, F. G. Dialysis unmasks the fungicidal properties of glandular salivary secretions. *Infect. Immun.* **2004**, *72*, 2703.
(45) Meurer, M.; O'Neil, D. A.; Lovie, E.; Simpson, L.; Torres, M. D. T.; de la Fuente-Nunez, C.; Angeles-Boza, A. M.; Kleinsorgen, C.; Mercer, D. K.; von Kockritz-Blickwede, M. Antimicrobial Susceptibility Testing of Antimicrobial Peptides Requires New and Standardized Testing Structures. *ACS Infect. Dis.* **2021**, *7*, 2205.
(46) Li, X. S.; Sun, J. N.; Okamoto-Shibayama, K.; Edgerton, M. *Candida albicans* cell wall ssa proteins bind and facilitate import of salivary histatin 5 required for toxicity. *J. Biol. Chem.* **2006**, *281*, 22453.
(47) Lynch, R. J. M. Zinc in the mouth, its interactions with dental enamel and possible effects on caries; a review of the literature. *Int. Dent. J.* **2011**, *61*, 46.
(48) Turner, A. G.; Ong, C. Y.; Walker, M. J.; Djoko, K. Y.; McEwan, A. G.Transition Metal Homeostasis in *Streptococcus pyogenes* and *Streptococcus pneumoniae*. In *Microbiology of Metal Ions*, Advances in Microbial Physiology; Elsevier B.V., 2017; Vol. *70*, p 123 DOI: 10.1016/bs.ampbs.2017.01.002.
(49) Sanson, M.; Makthal, N.; Flores, A. R.; Olsen, R. J.; Musser, J. M.; Kumaraswami, M. Adhesin competence repressor (AdcR) from *Streptococcus pyogenes* controls adaptive responses to zinc limitation and contributes to virulence. *Nucleic Acids Res.* **2015**, *43*, 418.
(50) Ong, C. L.; Gillen, C. M.; Barnett, T. C.; Walker, M. J.; McEwan, A. G. An antimicrobial role for zinc in innate immune defense against group A streptococcus. *J. Infect. Dis.* **2014**, *209*, 1500.
(51) Stewart, L. J.; Ong, C. L.; Zhang, M. M.; Brouwer, S.; McIntyre, L.; Davies, M. R.; Walker, M. J.; McEwan, A. G.; Waldron, K. J.; Djoko, K. Y. Role of Glutathione in Buffering Excess Intracellular Copper in *Streptococcus pyogenes*. *mBio* **2020**, *11*, No. e02804-20.
(52) Tedde, V.; Rosini, R.; Galeotti, C. L. Zn2+ Uptake in *Streptococcus pyogenes*: Characterization of adcA and lmb Null Mutants. *PLoS One* **2016**, *11*, No. e0152835.
(53) Ong, C. L.; Berking, O.; Walker, M. J.; McEwan, A. G. New Insights into the Role of Zinc Acquisition and Zinc Tolerance in Group A Streptococcal Infection. *Infect. Immun.* **2018**, *86*, No. e00048-18.
(54) Grogan, J.; McKnight, C. J.; Troxler, R. F.; Oppenheim, F. G. Zinc and copper bind to unique sites of histatin 5. *FEBS Lett.* **2001**, *491*, 76.
(55) Melino, S.; Stefano Rufini, S.; Sette, M.; Morero, R.; Grottesi, A.; Paci, M.; Petruzzelli, R. Zn(2+) ions Selectively Induce Antimicrobial Salivary Peptide Histatin-5 To Fuse Negatively Charged Vesicles. Identification and Characterization of a Zinc-Binding Motif Present in the Functional Domain. *Biochemistry* **1999**, *38*, 9626.
(56) Gusman, H.; Lendenmann, U.; Grogan, J.; Troxler, R. F.; Oppenheim, F. G. Is salivary histatin 5 a metallopeptide? *Biochim. Biophys. Acta, Protein Struct. Mol. Enzymol.* **2001**, *1545*, 86.
(57) Krężel, A.; Maret, W. The biological inorganic chemistry of zinc ions. *Arch. Biochem. Biophys.* **2016**, *611*, 3.
(58) Cao, K.; Li, N.; Wang, H.; Cao, X.; He, J.; Zhang, B.; He, Q. Y.; Zhang, G.; Sun, X. Two zinc-binding domains in the transporter AdcA from *Streptococcus pyogenes* facilitate high-affinity binding and fast transport of zinc. *J. Biol. Chem.* **2018**, *293*, 6075.
(59) Young, T. R.; Xiao, Z. Principles and practice of determining metal-protein affinities. *Biochem. J.* **2021**, *478*, 1085.
(60) Linke, C.; Caradoc-Davies, T. T.; Young, P. G.; Proft, T.; Baker, E. N. The laminin-binding protein Lbp from *Streptococcus pyogenes* is a zinc receptor. *J. Bacteriol.* **2009**, *191*, 5814.
(61) Župan, M. L.; Luo, Z.; Ganio, K.; Pederick, V. G.; Neville, S. L.; Deplazes, E.; Kobe, B.; McDevitt, C. A. Conformation of the Solute-Binding Protein AdcAII Influences Zinc Uptake in *Streptococcus pneumoniae*. *Front. Cell. Infect. Microbiol.* **2021**, *11*, No. 729981.
(62) Hamburger, M.; Robertson, O. H. Expulsion of group a hemolytic streptococci in droplets and droplet nuclei by sneezing, coughing and talking. *Am. J. Med.* **1948**, *4*, 690.
(63) Hamburger, M., Jr. Studies on the transmission of hemolytic streptococcus infections: II. Beta hemolytic streptococci in the saliva of persons with positive throat cultures. *J. Infect. Dis.* **1944**, 71.
(64) Courtney, H. S.; Hasty, D. L. Aggregation of group A streptococci by human saliva and effect of saliva on streptococcal adherence to host cells. *Infect. Immun.* **1991**, *59*, 1661.
(65) Courtney, H. S.; Hasty, D. Aggregation of group A streptococci by human saliva and effect of saliva on streptococcal adherence to host cells. *Infect. Immun.* **1991**, *59*, 1661.
(66) Wollein Waldetoft, K.; Mohanty, T.; Karlsson, C.; Morgelin, M.; Frick, I. M.; Malmstrom, J.; Bjorck, L. Saliva-Induced Clotting Captures Streptococci: Novel Roles for Coagulation and Fibrinolysis in Host Defense and Immune Evasion. *Infect. Immun.* **2016**, *84*, 2813.
(67) Amerongen, A. N.; Veerman, E. C. Saliva–the defender of the oral cavity. *Oral Dis.* **2002**, *8*, 12.
(68) Bhadbhade, S. J.; Acharya, A. B.; Thakur, S. L. Salivary and gingival crevicular fluid histatin in periodontal health and disease. *J. Clin. Exp. Dent.* **2013**, *5*, No. e174.
(69) Ribeiro, T. R.; Dria, K. J.; de Carvalho, C. B. M.; Monteiro, A. J.; Fonteles, M. C.; de Moraes Carvalho, K.; Fonteles, C. S. R. Salivary peptide profile and its association with early childhood caries. *Int. J. Paediatr. Dent.* **2013**, *23*, 225.
(70) Jurczak, A.; Koscielniak, D.; Papiez, M.; Vyhouskaya, P.; Krzysciak, W. A study on beta-defensin-2 and histatin-5 as a

diagnostic marker of early childhood caries progression. *Biol. Res.* **2015**, *48*, No. 61.
(71) Bielawski, K.; Tokajuk, G.; Bielawska, A.; Maciorkowska, E.; Jablonski, R.; Wojcicka, A.; Bielawski, K. The assessment of sIgA, histatin-5, and lactoperoxidase levels in saliva of adolescents with dental caries. *Med. Sci. Monit.* **2014**, *20*, 1095.
(72) Sun, X.; Huang, X.; Tan, X.; Si, Y.; Wang, X.; Chen, F.; Zheng, S. Salivary peptidome profiling for diagnosis of severe early childhood caries. *J. Transl. Med.* **2016**, *14*, No. 240.
(73) Munther, S. The impact of salivary lactoperoxidase and histatin-5 on early childhood caries severity in relation to nutritional status. *Saudi Dent. J.* **2020**, *32*, 410.
(74) Vitorino, R.; Lobo, M. J. C.; Duarte, J. R.; Ferrer-Correia, A. J.; Domingues, P. M.; Amado, F. M. L. The role of salivary peptides in dental caries. *Biomed. Chromatogr.* **2005**, *19*, 214.
(75) Jainkittivong, A.; Johnson, D. A.; Yeh, C. K. The relationship between salivary histatin levels and oral yeast carriage. *Oral Microbiol. Immunol.* **1998**, *13*, 181.
(76) Atkinson, J. C.; Yeh, C.; Oppenheim, F. G.; Bermudez, D.; Baum, B. J.; Fox, P. C. Elevation of salivary antimicrobial proteins following HIV-1 infection. *J. Acquired Immune Defic. Syndr.* **1990**, *3*, 41.
(77) Zhu, L.; Charbonneau, A. R. L.; Waller, A. S.; Olsen, R. J.; Beres, S. B.; Musser, J. M. Novel Genes Required for the Fitness of *Streptococcus pyogenes* in Human Saliva. *mSphere* **2017**, *2*, No. e00460.
(78) Brophy, M. B.; Hayden, J. A.; Nolan, E. M. Calcium ion gradients modulate the zinc affinity and antibacterial activity of human calprotectin. *J. Am. Chem. Soc.* **2012**, *134*, 18089.
(79) Makthal, N.; Nguyen, K.; Do, H.; Gavagan, M.; Chandrangsu, P.; Helmann, J. D.; Olsen, R. J.; Kumaraswami, M. A Critical Role of Zinc Importer AdcABC in Group A Streptococcus-Host Interactions During Infection and Its Implications for Vaccine Development. *EBioMedicine* **2017**, *21*, 131.
(80) Burcham, L. R.; Le Breton, Y.; Radin, J. N.; Spencer, B. L.; Deng, L.; Hiron, A.; Ransom, M. R.; Mendonca, J. D. C.; Belew, A. T.; El-Sayed, N. M.; McIver, K. S.; Kehl-Fie, T. E.; Doran, K. S. Identification of Zinc-Dependent Mechanisms Used by Group B Streptococcus To Overcome Calprotectin-Mediated Stress. *mBio* **2020**, *11*, No. e02302-20.
(81) Hartman, M. L.; Groppo, F.; Ohnishi, M.; Goodson, J. M.; Hasturk, H.; Tavares, M.; Yaskell, T.; Floros, C.; Behbehani, K.; Razzaque, M. S.Can Salivary Phosphate Levels Be an Early Biomarker to Monitor the Evolvement of Obesity? *Contributions to Nephrology*; Karger Publishers, 2013; Vol. *180*, p 138.
(82) Savica, V.; Calo, L. A.; Caldarera, R.; Cavaleri, A.; Granata, A.; Santoro, D.; Savica, R.; Muraca, U.; Mallamace, A.; Bellinghieri, G. Phosphate salivary secretion in hemodialysis patients: implications for the treatment of hyperphosphatemia. *Nephron Physiol.* **2007**, *105*, p52.
(83) Lynge Pedersen, A. M.; Belstrom, D. The role of natural salivary defences in maintaining a healthy oral microbiota. *J. Dent.* **2019**, *80*, S3.
(84) Norris, H. L.; Kumar, R.; Edgerton, M. A Novel Role for Histatin 5 in Combination with Zinc to Promote Commensalism in *C. albicans* Survivor Cells. *Pathogens* **2021**, No. 1609.
(85) Ramakers, C.; Ruijter, J. M.; Deprez, R. H.; Moorman, A. F. Assumption-free analysis of quantitative real-time polymerase chain reaction (PCR) data. *Neurosci. Lett.* **2003**, *339*, 62.
(86) Kuzmič, P.DynaFit--A Software Package for Enzymology. *Methods in Enzymology*; Elsevier B.V., 2009; Vol. *467*, p 247.

https://doi.org/10.1021/acsinfecdis.2c00578
ACS Infect. Dis. 2023, 9, 631−642